

Generation and effect of photo-induced radicals on cross-linking, color change, and isomerization in formulations of peptides and proteins

By

Indira Prajapati

Copyright 2020

Submitted to the graduate degree program in Pharmaceutical Chemistry and the Graduate Faculty of the University of Kansas in partial fulfillment of the requirements for the degree of Doctor of Philosophy.

Chair: Dr. Christian Schöneich

Dr. John F. Stobaugh

Dr. Teruna Siahaan

Dr. Thomas Tolbert

Dr. Prajna Dhar

Date Approved: July 02, 2020

The Dissertation Committee for Indira Prajapati

certifies that this is the approved version of the following dissertation:

Generation and effect of photo-induced radicals on cross-linking, color change, and isomerization in formulations of peptides and proteins

Chair: Dr. Christian Schöneich

Date Approved: July 02, 2020

Abstract

Protein biotherapeutics, especially monoclonal antibodies (mAbs), have been on the rise due to their high efficacy, potency, and low toxicity. They are mainly used for the treatment of cancer, autoimmune diseases, infectious diseases, and organ transplantation. While mAbs are well-tolerated by patients and have fewer adverse effects, their stability can be challenged by physical and chemical degradation. Hence, they are formulated with buffers and other excipients such as polysorbate 80 (PS80), which help to maintain the pH of the formulation and prevent aggregation, respectively. However, when the drug product is exposed to light, heat, or contains metal impurities, they are likely to undergo degradation. Some of the reactive amino acids of the proteins such as Trp, Tyr, His, Met, and Cys residues are more prone to photooxidation. Thus, we have investigated the effect of both UV and visible light on peptides, and proteins and further looked into the role of protein- and buffer-derived radicals on degradation of PS80.

We explored the role of methionine sulfur cation, generated by photosensitization of 4-carboxybenzophenone in the Met- X_n -His-containing peptides ($n = 0 - 2$), a common sequence present in the biotherapeutics such as mAb and human parathyroid hormone. Here, we report on the formation of novel photo-oxidation products and cross-links between Met oxidation product(s) and a neighboring histidine residue. Mechanisms for the formation of these products will be proposed. Specifically, the formation of cross-links is hypothesized to involve photo-oxidation of Met to an aspartate semialdehyde, followed by reaction with the imidazole side chain of His, and elimination of water.

When a full mAbZ (mAb obtained from AstraZeneca) was exposed to visible light, discoloration of the solution was observed. The chromophoric product responsible for the color change was identified using a model Trp-containing compound, N-acetyl-L-tryptophan amide (NATA). The

product was identified as NATA-33, a conjugated product formed after loss of 33 Da from NATA, by mass spectrometry and NMR. The mAbZ formulation contains polysorbate 80 (PS80) that has unsaturated fatty acids such as oleic acid and linoleic acid. Hence, we address the question of how protein-derived radicals may affect the composition of PS80. Isobaric products of PS80 were identified by means of mass spectrometry, suggesting cis/trans isomerization of unsaturated fatty acids of PS80. This mechanism was confirmed by the analysis of isolated fatty acids, demonstrating, e.g., the conversion of oleic acid to elaidic acid. Another commonly used excipient in mAb biotherapeutics is citrate buffer. In the presence of metal impurities such as iron, citrate buffer and iron can generate citrate-derived degradants such as carbon dioxide radical anion after exposure to UV-A light. Such radical anion can donate an electron to a disulfide bond and form a thiyl radical, which can also induce cis/trans isomerization of unsaturated fatty acids of PS80. Therefore, photo-induced radicals and radical ions may lead to cross-linking of amino acids, color change in concentrated mAbs, and cis/trans isomerization of PS80.

*To my late uncle, Ram Krishna Prajapati, for instilling in me the value of education and teaching
me to dream big*

Acknowledgments

I am grateful to my family, mentors, and friends for always supporting, guiding, and encouraging me prior to and during my PhD journey. Here, I attempt to thank everyone in this brief acknowledgment section.

First of all, I want to acknowledge my PhD advisor, Dr. Christian Schöneich, for nourishing my scientific queries and guiding me throughout my graduate work. I greatly appreciate his time and advice in advancing my scientific career. I thank him for polishing my scientific writing and presentation skills and encouraging me to present my research in both national and international conferences. He has supported me in obtaining an internship in Genentech during my PhD, which has been a critical point for me to advance my career in the pharmaceutical industry. After years of rigorous trainings, I find myself thinking critically before approaching a problem. I have grown to be a confident scientist and I am better at communicating my ideas because of the discussions we have during our 1:1 interaction, group meetings, and during our meetings with internal and external collaborators.

I would also want to thank my dissertation committee members: Dr. John F. Stobaugh, Dr. Teruna Siahaan, Dr. Thomas Tolbert, and Dr. Prajna Dhar for their constructive feedbacks and scientific discussions. I would especially like to thank Dr. John F. Stobaugh and Dr. Teruna Siahaan for reviewing my dissertation chapters and providing comments and suggestions.

My PhD work would not be possible without the funding source from Wanda Waugh Fellowship, Goetsch scholarship, funding from AstraZeneca, and department of Pharmaceutical Chemistry at the University of Kansas. I want to thank all of the Pharmaceutical Chemistry department staff:

Nancy Helm, Michelle Huslig, Ann Heptig, Karen Hall, Nicole Brooks, and André Faucher, without whom our research work would not be possible.

I am extremely thankful to the previous and present members of Schöneich's lab in creating a good work environment where we could bounce ideas, discuss data, and collaborate on projects. I want to start off by thanking Olivier Mozziconacci in helping me to kick-start my first project. I have always learned from his passion for science, work ethics, enthusiasm, and plethora of knowledge. I also want to thank Asha Hewarathna, Christopher Asmus, and Lin Zhang for their help in getting me started in the lab. I want to specially thank Jessica Bane and Rupesh Bommana for always encouraging me, helping me with my work, and for their friendship. Their positive attitudes and high spirit have always made work fun. I also want to thank Hasitha Rathnayaka and Natalia Subelzu for their friendship, scientific discussion, and always having my back. I will definitely miss our coffee breaks. I want to also thank rest of the Schoneich's group members for their help and support: Bjorn Peters, Huan Kang, Yaqi Wu, and Yilue Zhang.

My graduate work was in collaboration with internal and external scientists. I also want to thank Bryan Kopec, Mario Moral, and Kavisha Ulapane from Dr. Siahaan's lab for teaching me to synthesize the model peptides discussed in chapter 1 of my dissertation. I want to thank Dr. Russ Middaugh, Nick Larson, Yangjie Wei, Reza Esfandiary, Sueshkumar Chaudhary, Cavan Kalonia, and Suzanne Hudak for their scientific contributions on chapters 3 and 4 of my dissertation. I would also like to thank Solomon Okbazghi and Derek White for providing me with IgG1-Fc, a project which is not addressed in my dissertation. Likewise, I want to thank our collaborators in Genentech, Inc.: Sandeep Yadav and Anthony Timlinson for their scientific input.

I had a great opportunity to work with John Wang during my internship in Genentech, Inc. I got a chance to learn about surfactants and their degradation pathways, which helped me in exploring other aspects of surfactant degradation during my PhD work.

My research on polysorbates and proteins would be difficult without help from the mass spectrometry and NMR core labs. I would like to thank Todd Williams, Larry Seib, Sarah Neuenswander, Minli Xing, and Justin Douglas for their help in setting up the instruments and scientific discussions.

I also learned from my fellow graduate students especially during our first two years of course work. I always enjoyed our group studies and discussions. I want to thank my classmates: Sanjeev Agarwal, Ninad Varkhede, Yangjie Wei, Martin Hu, Mei Feng, Melissa Presnall, Laura Drbohlav, and Matthew Christopher. Getting to experience skydiving and getting drinks together are always the highlight of graduate life. Many thanks to Laura Drbohlav and Jake Doyle for being wonderful roommates and cooking together was always relaxing. It was always fun watching movies and chit-chatting.

My stay in Lawrence was enhanced by the Nepalese community members. After four years I was able to celebrate Nepalese festivals and eat proper Nepali food. I want to thank Prem Thapa and Jhunu Thapa for their hospitality, love and support. I always enjoyed great company of Bibek Gautam, Smriti Gautam, Abhigna and Saleen. Thank you for making me feel at home. I also want to thank Isha, Dipin, Soham, Anmesh, Anjana, Manjish, Ashwin, Apurba, Poonam, Biswas, Pratik, and Alok for great times, laughter, good food, and overall, their friendship. I also want to thank all the members of Nepalese Student Association for inviting me during festivals and also for organizing fun events.

This list would not be complete without thanking my best friends Bivek Adhikari, Vivek Raj Karki, and Aakriti Gautam. I want to thank them for being there when I needed them the most. I have always looked forward to our road trips, camping, adventures, or simply staying home and relaxing. I want to thank them for giving me best advice, encouragement, and sometimes pampering me. I also want to thank my best friends from high school: Prerana and Pradip for always checking on me and for lots of cute and funny videos and pictures.

I want to thank Christopher family for embracing me as a part of their family. I have always enjoyed our holidays together. Thank you, Mary, for spoiling me with gifts. I want to thank Lauren and Alex for great company, laughter, and game times. I want to thank Michael, Holly, and baby Grant (whose cute videos have always uplifted me) for your company.

I want to thank each and every member of my family. First, I want to thank my late grandfather and late grandmother for sponsoring my education, and for their love and support. I want to thank my parents, Nazar and Karna Prajapati, for always believing in me and letting me come to the United States to pursue my education. I want to thank my siblings (best friends) Ishwori, Kavita, Indra Kumari, and Arij Prajapati for always checking on me and for daily dose of laughter. I also want to thank my aunt, Suprava, for supporting me. I want to thank all of my uncles, aunties, and cousins for always supporting me and for great times whenever we get to meet.

Last but not the least, I want to thank Matthew Christopher for his love, support, and encouragement. Thank you for always giving me positive suggestions when I was frustrated and pushing me to finish my dissertation on time. His delicious food, jokes, and light-heartedness always kept my morale high. Thank you very much for taking time to edit my dissertation, helping me to improve my writing skills, and moving to Maryland with me to begin the next chapter of our life.

Contents

| | |
|--|----|
| Chapter 1: Introduction | 1 |
| 1.1. Monoclonal Antibody as Therapeutics | 2 |
| 1.2. Structure of mAbs | 3 |
| 1.3. Routes of administration of mAbs | 4 |
| 1.4. Degradation of antibodies | 5 |
| 1.5. ICH Q1B guideline and photostability testing of biotherapeutics | 7 |
| 1.6. Case studies of highly concentrated mAbs degraded by UV-A and visible light | 8 |
| 1.7. Use of excipients for stabilizing mAbs | 10 |
| 1.8. Overview of this dissertation | 12 |
| 1.9. References | 14 |
| 1.10. Figures | 20 |
| Chapter 2: One-electron photo-oxidation of Met-X _n -His-containing peptides: Formation of novel cross-links | 22 |
| 2.1. Introduction | 23 |
| 2.2. Materials and Methods | 25 |
| 2.2.1. Materials | 25 |
| 2.2.2. Synthesis of model peptides and purification | 26 |
| 2.2.3. Photo-irradiation | 26 |
| 2.2.4. Reversed Phase-High Performance Liquid Chromatography (RP-HPLC) analysis | 27 |
| 2.2.5. NanoAcquity LC Electrospray Ionization Q-tof MS and LC-MS/MS analysis | 28 |
| 2.3. Results | 29 |
| 2.3.1. Identification of photoproducts | 29 |
| 2.3.2. Comparison of photoproducts at pH 3.30, 7.23, and 9.88 by LC-MS | 30 |
| 2.3.3. The photoproducts M1P1a and M1P1b | 31 |
| 2.3.4. Generation of M1P1a/M1P1b from peptide M1 containing ¹³ C-Met | 33 |
| 2.3.5. Generation of M1P1a/M1P1b-(¹⁵ N ₃) from peptide M3 containing ¹⁵ N-labeled His | 33 |
| 2.3.6. Effect of spacing on cross-link formation | 34 |
| 2.3.7. Formation of aspartic acid (M1P2) | 35 |
| 2.3.8. Formation of homocysteine (M1P3) and homocysteine sulfonic acid (M1P3-SO ₃ H) | 36 |
| 2.3.9. Formation of thioesters (M1P4a and M1P4b) | 37 |

| | | |
|--|---|----|
| 2.3.10. | 4-CB adducts on Met (M1P5a-d)..... | 38 |
| 2.3.11. | Formation of Met sulfoxide (M1P6a/M1P6b) and sulfone (M1P7)..... | 38 |
| 2.3.12. | Formation of His oxidation products (M1P8 and M1P9)..... | 39 |
| 2.4. | Discussion | 40 |
| 2.4.1. | Formation of M1P1a/M1P1b..... | 41 |
| 2.5. | Conclusions | 43 |
| 2.6. | References | 44 |
| 2.7. | Charts and Figures..... | 49 |
| 2.8. | Schemes..... | 66 |
| 2.9. | Supplementary Information..... | 69 |
| Chapter 3: Visible light degradation of a monoclonal antibody in a high concentration formulation: characterization of a tryptophan-derived chromophoric photoproduct by comparison to photodegradation of N-acetyl-L-tryptophan amide | | |
| | | 81 |
| 3.1. | Introduction | 82 |
| 3.2. | Materials and Methods..... | 84 |
| 3.2.1. | Sample preparation | 85 |
| 3.2.2. | Photo-irradiation | 85 |
| 3.2.3. | Photo-irradiation of mAbZ and NATA..... | 86 |
| 3.2.4. | Reducing and Non-reducing SDS-PAGE | 86 |
| 3.2.5. | Size Exclusion Chromatography (SEC)..... | 87 |
| 3.2.6. | Differential Scanning Calorimetry (DSC) | 87 |
| 3.2.7. | Proteolytic Digestion | 88 |
| 3.2.8. | UV-Visible Absorption Spectroscopy | 88 |
| 3.2.9. | Reverse Phase-High-Performance Liquid Chromatography | 88 |
| 3.2.10. | NanoAcquity HPLC Electrospray ionization Q-tof MS and HPLC-MS/MS analysis | 89 |
| 3.2.11. | Nuclear Magnetic Resonance | 90 |
| 3.3. | Results | 90 |
| 3.3.1. | Physical stability: studies on conformation and aggregation of mAbZ..... | 91 |
| 3.3.2. | Oxidation of Met and Trp | 92 |
| 3.3.3. | Formation of chromophoric photoproducts in mAbZ and NATA..... | 93 |
| 3.4. | Discussion | 95 |
| 3.4.1. | Aggregation, conformational changes, and oxidation of mAbZ..... | 95 |

| | | |
|---|---|-----|
| 3.4.2. | Formation of chromophoric photoproducts from mAbZ and NATA | 95 |
| 3.5. | References | 98 |
| 3.6. | Chart and Figures | 101 |
| 3.7. | Table and Scheme | 114 |
| 3.8. | Supplementary Information..... | 116 |
| Chapter 4: Cis/trans isomerization of unsaturated fatty acids in polysorbate 80 during light exposure of a monoclonal antibody-containing formulation | | 123 |
| 4.1. | Introduction | 124 |
| 4.2. | Materials and Methods..... | 127 |
| 4.2.1. | Materials | 127 |
| 4.2.2. | Photo-irradiation | 127 |
| 4.2.3. | Photo-irradiation of mAbZ formulations containing 0.01% PS80 | 128 |
| 4.2.4. | Photo-irradiation of spiked mAbZ formulations containing 0.2% PS80..... | 129 |
| 4.2.5. | Photo-irradiation of model peptide formulations containing 0.01% and 0.2% PS80 129 | |
| 4.2.6. | Photo-irradiation of PS80 in the absence of mAbZ and model peptides..... | 130 |
| 4.2.7. | Generation of FFAs from 0.01% and 0.2% PS80 with porcine esterase | 130 |
| 4.2.8. | HPLC-MS analysis of PS80 | 131 |
| 4.2.9. | HPLC-MS analysis of FFAs..... | 132 |
| 4.2.10. | Sample preparation for Raman Fourier transform infrared (FTIR) spectroscopy | 133 |
| 4.2.11. | Raman and FTIR Spectroscopy | 134 |
| 4.3. | Results | 134 |
| 4.3.1. | Oleic acid | 134 |
| 4.3.2. | Linoleic acid..... | 137 |
| 4.3.3. | Oxidation products..... | 139 |
| 4.3.4. | The model system containing PS80, GSSG, and NATA..... | 140 |
| 4.3.5. | Raman and FTIR Spectroscopy | 140 |
| 4.4. | Discussion | 142 |
| 4.5. | Footnotes | 147 |
| 4.6. | References | 148 |
| 4.7. | Figures..... | 152 |
| 4.8. | Supplementary Figures..... | 162 |

| | |
|--|-----|
| Chapter 5: Oxidation and Cis/trans Isomerization of Unsaturated Fatty Acids in Polysorbate 80 via photo-induced degradation of citrate buffer..... | 167 |
| 5.1. Introduction | 168 |
| 5.2. Materials and Methods | 170 |
| 5.2.1. Photo-irradiation | 170 |
| 5.2.2. Sample preparation | 170 |
| 5.2.3. Mass spectrometry | 171 |
| 5.3. Results | 172 |
| 5.3.1. Oxidation products..... | 172 |
| 5.3.2. Cis/trans isomerization..... | 174 |
| 5.4. Discussion | 177 |
| 5.4.1. Oxidation products..... | 178 |
| 5.4.2. Cis/trans isomerization..... | 179 |
| 5.5. References | 182 |
| 5.6. Charts and Figures..... | 187 |
| 5.7. Schemes..... | 198 |
| Chapter 6: Conclusions and Future Directions | 200 |
| 6.1. Summary and conclusions..... | 201 |
| 6.2. Future works..... | 203 |

Chapter 1: Introduction

1.1. Monoclonal Antibody as Therapeutics

Murine monoclonal antibody (mAb) was first produced in 1975 by César Milstein and Georges Köhler by using groundbreaking hybridoma technology, which opened a door for antibodies to be used as therapeutics.¹⁻² After a decade, in 1986 the first murine mAb, Orthoclone OKT3, was approved by the US Food and Drug Administration (FDA).³ In the early development of murine mAbs, immunogenicity and short half-lives of these mAbs were of concern due to the presence of anti-murine antibody in patients.⁴ This response was significantly reduced through the implementation of technologies such as chimeric, humanized, and full human mAbs. Since then, mAbs have emerged as an important class of drugs because of their potency, low toxicity, and high efficacy. Furthermore, mAbs are well-tolerated by patients, have fewer adverse effects, and are highly specific in comparison to small molecules.⁵ Thus, 79 FDA approved mAbs are in the market for the treatment of cancers, autoimmune diseases, infectious diseases, and organ transplantations.^{4, 6} Whilst mAbs have become less immunogenic with the transition away from mouse mAb sequences, degradation due to intrinsic and extrinsic factors remains.

Various factors such as protein formulations, container closure, manufacturing processes, and environmental factors (light and temperature) need to be considered to improve the stability of mAbs.⁷ Moreover, factors such as metal contaminants, pH, and ionic strength can also influence the stability of drugs.⁷⁻¹⁰ As a result of temperature and light stress and/or the presence of metal contaminants, mAbs can experience oxidation,¹¹⁻¹⁴ aggregation,¹⁵⁻¹⁶ fragmentation,¹⁷⁻¹⁸ cross-link formation,¹⁹⁻²⁰ and color change.^{16, 21-22} These degradation products may induce product immunogenicity risking patient's health. To mitigate the degradation of mAbs during long-term storage conditions, a robust formulation should be implemented that can be corroborated with

forced-stability studies. Formulation for each mAb should be addressed as a “case by case” basis because of the structural differences in the complementary determining regions (CDRs) and glycosylation.²³

1.2. Structure of mAbs

Most of the marketed mAbs are γ -immunoglobins (IgG) isotypes and are mainly comprised of IgG1, IgG2, and IgG4. These mAbs are tetrameric glycoproteins with molecular weights (MW) of approximately 150 kDa.²⁴⁻²⁵ As shown in Fig. 1, they consist of two identical heavy chains (HC), each with a MW of about 50 kDa, and two identical light chains (LC), each with a MW of about 25 kDa. These roughly Y-shaped proteins consist of three HC constant domains (C_{H1} , C_{H2} , and C_{H3}), one HC variable domain (V_H), one LC constant domain (C_L), and one LC variable domain (V_L). The C_{H2} and C_{H3} domains are part of the fragment crystallizable (Fc), which binds to cell surface receptors including the Fc γ receptors and the neonatal Fc receptor (FcRn). The V_L - V_H and C_L - C_{H1} domains make up the antigen binding fragment (Fab) region containing the highly variable complementary determining region (CDR) responsible for binding to target antigen. Due to these complexities in antibody structure, identification of degradation hotspots has become a key area of research.

Certain structural motifs have been identified that are susceptible to degradation throughout the stages of mAb production.²⁶⁻²⁸ For instance, the sequences Gly-Asn or Asn-Gly are more prone to deamidation. Yang *et al.* changed two degradation hotspots, LC-Asn30 and HC-Asp102 into LC-Gln30 and HC-Glu102, which decreased the rate of deamidation and isomerization, and retained the biological activity.²⁹ Kumar *et al.* has carried out single point (V44K, E59S, E59T and E59Y) and double mutations (V44KE59S, V44KE59T and V44KE59Y) in the light chain of mAb1 that

improved the biological activity, protein solubility, and viscosity of the protein.²⁶ Such mutations can also disrupt aggregation and oxidation prone hotspots.

1.3. Routes of administration of mAbs

Traditionally, mAbs are administered via the intravenous route in the hospital settings. mAbs are infused based on the patient's weight, so the diluted mAbs, though more stable, take several hours of infusion time.³⁰ This requires trained personnel to prepare, administer, and monitor the drug product (DP) and the lengthy process also compromises patient's compliance. As such, other routes of administration such as intramuscular (IM) and subcutaneous (SC) injections are being explored. SC injection requires administration of highly concentrated mAb solutions (≥ 100 mg/ml) in small volumes. For SC injections, pre-filled syringes, pens and auto-injectors are used, enabling patients to use them at home and reducing injection time to minutes. Thus, SC administration is becoming increasingly popular due to its user convenience, better therapy compliance, and economic impacts.³¹ Whilst SC injections have many advantages over IV injections, concerns of reduced volume, back-pressure, and pain at the site of injection remain. To overcome such concerns, mAbs such as rituximab and trastuzumab took advantage of an excipient such as recombinant hyaluronidase (rHuPH20)^{5, 32-33} and were approved for tumor therapy. rHuPH20 is an enzyme that temporarily degrades hyaluronan at the injection site, facilitating delivery of ~5-10 ml via SC injection.

The stability of a highly concentrated DP in an SC formulation is crucial for its success; however, the highly concentrated mAb makes it challenging because of protein-protein interactions, which lead to high viscosity and aggregation. Self-association of the protein may be mainly attributed to electrostatic interactions,³⁴ in particular Fab-Fab interactions.³⁵ By changing the charged residues in the CDR of a mAb, Yadav *et al.* were able to reduce its viscosity.³⁶ Additionally, when exposed

to UV and visible light, heat, and/or metal contaminants, highly concentrated mAbs are reported to aggregate or undergo color change due to greater protein-protein interactions and reduced volume.^{16, 21-22}

1.4. Degradation of antibodies

The stability of mAbs can be compromised during manufacturing and administration, mainly via interfacial stress, mechanical stress, light exposure, and metal-catalyzed oxidation (MCO). These stresses and reactions may degrade mAbs, causing physical and chemical instability.^{8-9, 37} Physical instability is defined as structural changes of proteins without formation or breakage of the chemical bonds. For example, physical instability of the protein may be caused by hydrophobic interactions between two or more molecules, leading to protein aggregation because of shear forces and cavitation-induced spikes in pressure and temperature.^{8, 38} Alternatively, chemical instability is defined by change in covalent bonds, i.e. hydrolysis of the existing bonds or the formation of new bonds. Thus, deamidation, β -elimination, fragmentation, aggregation, oxidation, and cross-link formation fall under chemical instability. Physical and chemical instabilities are interrelated as one can influence the other. For instance, aggregation in proteins can also occur via chemical instability by disulfide scrambling and cross-links between various amino acids.

Oxidation occurs mainly via (i) peroxides, (ii) metal-catalyzed oxidation (MCO), and (iii) light exposure. Peroxides may be introduced into the drug substance (DS) as contaminants from excipients. Iron can be present in the solution as contaminant from manufacturing and storage containers, and excipients, which promotes MCO and can generate ROS such as the hydroxyl radical (\bullet OH) by Fenton reaction.³⁹ Peroxides and other oxidants generated by MCO and light exposure may react with numerous amino acids including: methionine (Met), cysteine (Cys), tryptophan (Trp), histidine (His), tyrosine (Tyr), and phenylalanine (Phe).^{13, 40-41} These ROS can

result in the generation of oxidation products such as methionine sulfoxide (MetO) that can, for example, modify the biological activity of a protein and alter the binding affinity of IgGs.⁴²⁻⁴³ MCO has also been reported to play a role in the hydrolysis between Met and His residues in human parathyroid hormone and IgG1.¹⁷⁻¹⁸ Therefore, it is important to carefully monitor contaminants that may be introduced into the formulation to avoid degradation of the proteins.

The exposure of the DP to light during manufacturing, storage, or administration can result in degradation, altering the protein irreversibly. The aromatic residues of proteins can undergo photoexcitation that may result in either type I or type II photooxidation (Scheme 1).⁴⁴ In the type I mechanism, light is directly absorbed by chromophores such as aromatic amino acids (e.g. Trp, Tyr), giving an excited triplet state.⁴⁵⁻⁴⁷ This is followed by the transfer of an electron to a suitable acceptor, such as molecular oxygen (O₂) or disulfide bonds, leading to the formation of radical cations (e.g. Trp radical cation) and radical anions; O₂ will form superoxide⁴⁸ or disulfide will form a disulfide radical anion, which exists in equilibrium with thiolate and thiyl radical.^{14, 49-50} Thiyl radicals can undergo a cascade of reactions such as disulfide scrambling,⁵¹⁻⁵² thioether formation,⁵³ abstraction of either an electron, hydrogen, or both from other amino acids,^{50, 54} and involvement in cis/trans isomerization.⁵⁵⁻⁵⁶ The latter topic is discussed in detail in Chapters 4 and 5. On the other hand, the formation of a Trp radical cation can lead to the loss of the side chain of Trp⁵⁷⁻⁵⁸ and Tyr⁵⁹ after UV light exposure. For instance, a Trp radical cation can abstract an electron from Tyr, forming a Tyr radical cation, which can then eliminate a protonated quinone methide. Other amino acids may also undergo light-induced oxidation, including Met, which primarily degrades into MetO. Photosensitizers such as 4-carboxybenzophenone (4-CB) have widely been used to study the oxidation of Met via the type I mechanism, which gives a sulfur radical cation (Met>S⁺).⁶⁰ We have employed this technique to generate Met>S⁺, which led to

the identification of novel cross-links between Met oxidation product(s) and a His residue, discussed in Chapter 2.

In the type II mechanism, energy is transferred from an excited triplet state to O₂, generating singlet oxygen (¹O₂). This reactive oxygen species can react with Met and His, forming MetO¹¹⁻¹² and peroxide derivatives of His, respectively.⁶¹ In addition, ¹O₂ may react with Trp, generating photoproducts such as N-formyl kynurenine (NFK) and kynurenine (Kyn). These photoproducts can further act as photosensitizers, resulting in the degradation of proteins upon exposure to UV-A and visible light.⁶²⁻⁶⁶ Therefore, the International Conference on Harmonization (ICH) has provided guidelines for drug product exposure to UV-A and visible light stresses, which are outlined in section 1.5 and 1.6.

1.5. ICH Q1B guideline and photostability testing of biotherapeutics

According to the ICH guidelines for photostability testing of DS(s) and DP(s) (Q1B), “light testing should be an integral part of stress testing”.⁶⁷ For forced degradation and confirmatory testing, ICH requires the DS and DP to be tested using light sources with output similar to D65/ID65. The ICH guideline defines D65 and ID65 as follows: “D65 is the internationally recognized standard for outdoor daylight as defined in The International Standards Organization (ISO) 10977 (1993). ID65 is the equivalent indoor indirect daylight standard.” D65 and ID65 can be accomplished by using artificial daylight fluorescent lamps, xenon lamps, or metal halide lamps. However, if cool white fluorescent lamps are used, it has to be accompanied by near UV lamps. All of these light source options should emit no less than 1.2 million lux hours of visible light and no less than 200 Watt hour per square meters (W.h/m²) of integrated near UV light. In addition, a dark control wrapped in aluminum should be tested alongside the authentic sample in the same environment. Dark control samples can also indicate the effect of heat generated on DP during light exposure.

1.6. Case studies of highly concentrated mAbs degraded by UV-A and visible light

When Qi *et al.* exposed a mAb (100 mg/ml formulated in histidine buffer, sorbitol and PS80 at pH 5.5) to the light intensity recommended by ICH Q1B guideline, it underwent significant physical and chemical changes depicted by covalent aggregates, fragmentation, oxidation of Met, His, and Trp, and deamidation of Asn.¹⁶ After light exposure, the colorless mAb solution turned yellow, a result which was also observed in our study (discussed in Chapter 3) on highly concentrated mAb after exposure to visible light. Additionally, in the same study by Qi *et al.*, a significant loss in biological activity of the mAb was observed due to Trp94 oxidation and Asn93 deamidation in the CDR region. Another study on 100 mg/ml mAb (MEDI-493) (in 10 mM His and 1.6 mM Gly buffer, pH 6.0) by Wei *et al.* also showed oxidation of Met and Trp after exposure to light emitting wavelengths between 300-700 nm for up to 7 days.⁶⁸ However, one single Trp 105 residing in the CDR of the heavy chain was responsible for the loss of binding and biological activity. These two Trp residues are solvent-exposed, which explains their readily oxidizable nature. Apart from Trp, Met and His residues also undergo oxidation and may negatively impact the efficacy of the drug.⁴²

Commonly, the light exposure experienced by DS and DP is far less harsh than those outlined in the ICH Q1B guideline.^{22, 69-70} Sreedhara *et al.*²² have done an extensive internal survey in normal laboratories and GMP processing areas and found a small UV-A light source emitting from 350 to 400 nm with an irradiance ranging from 0.05 to 0.3 W/m². Areas that used fluorescent lamps with plastic canopies, however, emitted wavelengths above 400 nm (commonly termed as ambient and mild light conditions). This indicates DS and DP may not see such extreme conditions mentioned in the ICH Q1B guideline.²² In the same study, under ambient light, mAb1 showed a site-specific oxidation of Trp resulting in potency loss and mAb2 (at 100 mg/ml) showed higher aggregation

and a color change of the solution; however, mAb3-5 were not impacted by ambient and mild light exposure.

Similarly, the study by Qi *et al.*¹⁶ concluded that the mAb underwent oxidation (of Trp and Met), deamidation, fragmentation, and aggregation formation during light exposure according to the ICH Q1B guideline, but was stable under ambient light conditions. Because ambient light may still contain a UV quotient, it is ambiguous which wavelengths cause the degradation of mAbs. Du *et al.*⁷¹ gave some insights into which part of the visible light is responsible for the color change of a mAb formulation and degradation of the mAb. The visible light was divided into multiple color spectra by using either colored filters or by using blue and red LED lamps. The mAbs exposed to blue light, filtered from visible light, and emitted from blue LED lamps displayed a brown color with maximum absorbance at 450 nm. Additionally, these mAb solutions displayed an increase in high molecular weight species and charge variant species. If possible, while handling highly photosensitive mAbs, such filters should be used to protect the proteins from degrading. It has also been suggested to fill the head space of the vials with N₂ to protect the DS and DP from rapid degradation.⁷²

The ICH Q1B guideline does not specify the light exposed during drug preparation and patient administration; however, some DP requires pharmacy preparation and long hours of administration time, where the DP is further exposed to light. As shown by Du *et al.* certain wavelengths of visible light can degrade the DP and impose concerns for the drug's efficacy and safety.^{71, 73} Therefore, the effect of light on mAbs highly depends on the photosensitivity of mAbs under study and light exposure time. The exposure to light during drug preparation and administration should also be considered when labelling the DP with "protect from light". Moreover, providing detailed

instructions on protecting the DP from light and including protective sleeves as part of the product kit will ensure the protection of the drug.⁷³

Apart from the Active Pharmaceutical Ingredient (API), excipients added to the final formulations can also undergo physical and chemical changes when exposed to light. For example, polysorbate, a commonly used surfactant to protect biotherapeutics, is susceptible to degradation forming peroxides, formic acid, formaldehyde, hydrogen peroxide, etc. when exposed to light.⁷⁴ Likewise, His buffer, a commonly used buffer, is also photosensitive. His degradation can form products that are photosensitizers, which can further oxidize other amino acid residues such as Met and Trp. Monoclonal antibodies formulated in His buffer are shown to suffer Trp oxidation in the CDR region, leading to reduced binding affinity for target proteins.⁷⁵⁻⁷⁶ Other excipients, such as Met and the Trp-derivative N-acetyl tryptophan (NAT), are used as antioxidants in the final DP formulation to reduce or prevent oxidation of proteins.⁷⁷ However, the oxidation products of NAT are also photosensitizers and should be carefully monitored as they can further oxidize proteins.⁷⁸ Our study on another Trp-containing compound, N-acetyl-L-tryptophan amide (NATA), also revealed oxidation upon exposure to visible light giving products such as NFK, Kyn, OH-Trp and other chromophoric products, which is discussed in Chapter 3.

1.7. Use of excipients for stabilizing mAbs

Since the production and administration of mAbs requires many steps, keeping them stable is important not just to meet the critical quality attributes but also for the safety and efficacy of the drug.⁸ Thus, formulation conditions should be optimized to achieve a longer shelf life by minimizing both physical and chemical instabilities. Excipients such as buffers, surfactants, salts, antioxidants, and chelators are chosen for an ideal formulation condition to lower viscosity,

aggregation rate, oxidation, and other unwanted reactions. A library of generally regarded as safe (GRAS) excipients can be used for initial screening to avoid extra regulatory requirements.⁷⁹

Buffers are used to maintain the pH and stability of the drug solution. Detailed reviews regarding the role of buffers on protein stability are provided by Zbacnik *et al.*⁸⁰ and Ugwu *et al.*⁸¹ The commonly used buffers for mAbs include His, phosphate, acetate, and citrate,⁸²⁻⁸⁵ where most of the concentrated mAbs are formulated in His buffer. Because most antibodies are formulated between pH 5.0 to 7.0, the use of His buffer is logical as its pKa is at 6.0. His buffer is also shown to decrease the viscosity of the high-concentration mAbs⁸⁶ and inhibit aggregation of a mAb.⁷⁵ Despite its advantages, His can be affected by heat⁸⁷ and light,⁸⁸⁻⁸⁹ so the DP has to be monitored carefully.

Another commonly used buffer, citrate buffer has four distinct pKas at 3.13, 4.76, 5.80, and 6.40,⁹⁰ making it suitable for protein formulation across a large range of pHs.⁸⁰ Some mAbs are shown to be more stable in citrate buffer via ligand binding. For example, Harinarayan *et al.* have shown binding of citrate buffer to the Fab region resulted in greater stability.⁹¹ Citrate, on the other hand, is also known to degrade or form adducts, resulting in acetonation of proteins⁹² or citrate can add to serine and threonine residues as adducts.⁹³ The citrate-phosphate formulation of Humira® was changed in pre-filled syringes and pen injectors due to pain at injection site associated with citrate.⁹⁴ In addition, our study discussed in Chapter 5 and a study by Subelzu *et al.*⁹⁵ indicated a role of citrate in generating ROS via the photo-Fenton reaction, which can degrade amino acids and surfactants

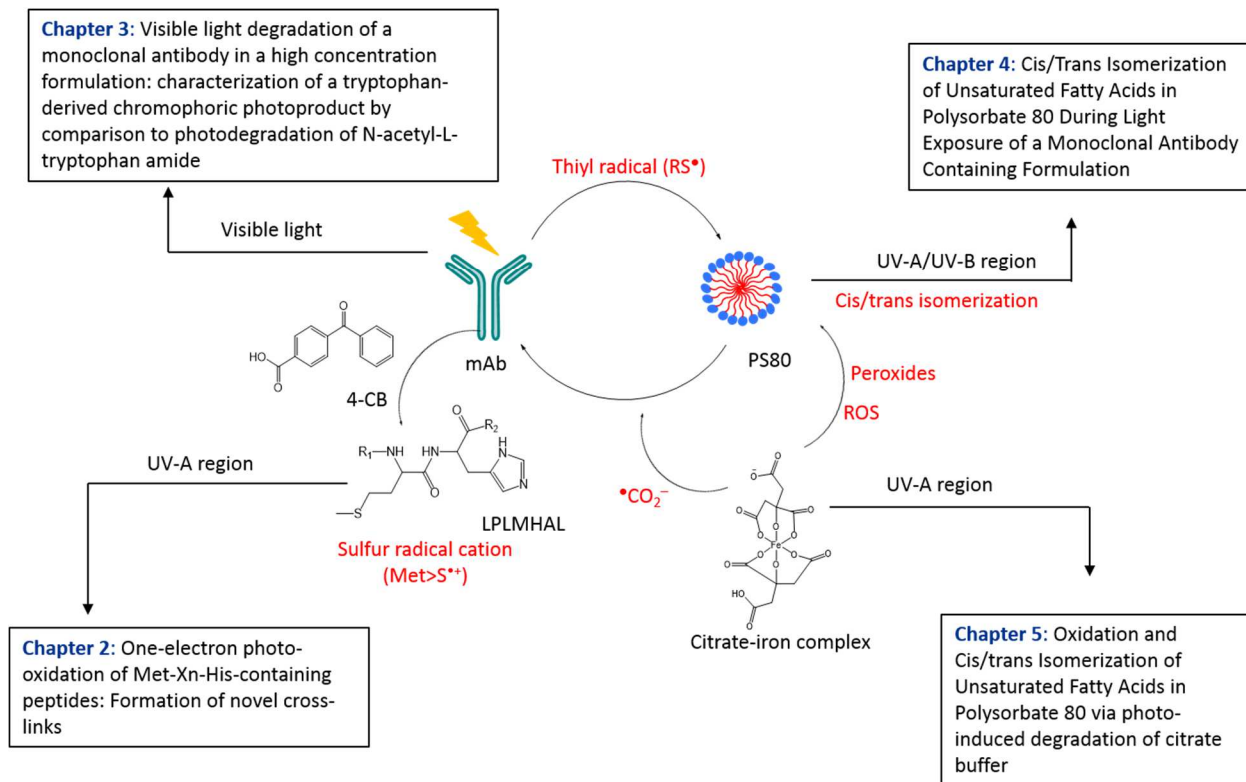
Excipients such as Met and Trp are used as sacrificial antioxidants, which maintain the stability of the protein by reacting with ROS instead of the amino acids in the protein. Other amino acids such

as His, Arg, and Lys are also added especially to highly concentrated mAb formulations to reduce viscosity and aggregation. These amino acids work either by interaction with aromatic acids or by electrostatic interaction.⁹⁶ Likewise, salts are added to the formulation to maintain the ionic strength and surfactants such as polysorbates and poloxamers are added to reduce the aggregation of protein via surface interfaces. However, one has to monitor the quality of a neat surfactant as it may contain peroxides, which can degrade proteins. Furthermore, surfactants can undergo oxidation in presence of heat, light, and metal contaminants.⁷⁴ They can also undergo hydrolysis in presence of host cell proteins, which are co-purified with desired proteins,⁹⁷⁻¹⁰⁰ forming unwanted particles in the DP formulations.

1.8. Overview of this dissertation

In this dissertation, the photo-degradation of model peptides, mAb, and surfactants are explored upon exposure to either UV or visible light. Both amino acid residues and surfactants, which are used to protect biotherapeutic proteins, are susceptible to degradation. The ingredients in the final formulation, such as mAb and surfactants, can have negative effect on each other. For example, the degradants of surfactants such as peroxides and aldehydes can oxidize reactive amino acids (Met and His) and react with Lys and Arg to form a Schiff base, respectively. In addition, free fatty acids generated from hydrolysis of ester bonds of polysorbate can form particles in the formulation raising concerns for patient safety. On the other hand, protein- (and citrate-) derived radical ions can generate ROS or thiyl radicals. These radicals can degrade surfactants or convert cis isomer of unsaturated fatty acids of PS80 to trans isomer,⁵⁶ as presented in Chapters 4 and 5. The role of sulfur radical cations, specifically, on cross-link formation in the Met-X_n-His (n = 0-2) sequence of model peptides is presented in Chapter 2. Finally, the formation of a chromophoric product in mAbZ formulations after exposure to visible light is discussed in Chapter 3. For these

studies RP-HPLC, HPLC-MS/MS, NMR, Raman spectroscopy, and FTIR were used to identify the photoproducts of amino acids and structural changes in PS80.



1.9. References

1. Reichert, J. M.; Rosensweig, C. J.; Faden, L. B.; Dewitz, M. C., Monoclonal antibody successes in the clinic. *Nat. Biotechnol.* **2005**, *23* (9), 1073-8.
2. Buss, N. A. P. S.; Henderson, S. J.; McFarlane, M.; Shenton, J. M.; de Haan, L., Monoclonal antibody therapeutics: history and future. *Curr. Opin. Pharmacol.* **2012**, *12* (5), 615-622.
3. Kroon, D. J.; Baldwin-Ferro, A.; Lalan, P., Identification of sites of degradation in a therapeutic monoclonal antibody by peptide mapping. *Pharm. Res.* **1992**, *9* (11), 1386-1393.
4. Carter, P. J., Potent antibody therapeutics by design. *Nat. Rev. Immunol.* **2006**, *6* (5), 343-357.
5. Cui, Y.; Cui, P.; Chen, B.; Li, S.; Guan, H., Monoclonal antibodies: formulations of marketed products and recent advances in novel delivery system. *Drug Dev. Ind. Pharm.* **2017**, *43* (4), 519-530.
6. Lu, R.-M.; Hwang, Y.-C.; Liu, I.-J.; Lee, C.-C.; Tsai, H.-Z.; Li, H.-J.; Wu, H.-C., Development of therapeutic antibodies for the treatment of diseases. *J. Biomed. Sci.* **2020**, *27* (1), 1-30.
7. Wang, W.; Ohtake, S., Science and art of protein formulation development. *Int. J. Pharm.* **2019**, 118505.
8. Krause, M. E.; Sahin, E., Chemical and physical instabilities in manufacturing and storage of therapeutic proteins. *Curr. Opin. Biotechnol.* **2019**, *60*, 159-167.
9. Manning, M. C.; Chou, D. K.; Murphy, B. M.; Payne, R. W.; Katayama, D. S., Stability of protein pharmaceuticals: an update. *Pharm. Res.* **2010**, *27* (4), 544-575.
10. Van Buren, N.; Rehder, D.; Gadgil, H.; Matsumura, M.; Jacob, J., Elucidation of Two Major Aggregation Pathways in an IgG2 Antibody. *J. Pharm. Sci.* **2009**, *98* (9), 3013-3030.
11. Davies, M. J., Singlet oxygen-mediated damage to proteins and its consequences. *Biochem. Biophys. Res. Commun.* **2003**, *305* (3), 761-770.
12. Davies, M. J., Reactive species formed on proteins exposed to singlet oxygen. *Photochemical & Photobiological Sciences* **2004**, *3* (1), 17-25.
13. Davies, M. J., The oxidative environment and protein damage. *Biochim. Biophys. Acta* **2005**, *1703* (2), 93-109.
14. Grassi, L.; Cabrele, C., Susceptibility of protein therapeutics to spontaneous chemical modifications by oxidation, cyclization, and elimination reactions. *Amino Acids* **2019**, 1-23.
15. Zheng, J. Y.; Janis, L. J., Influence of pH, buffer species, and storage temperature on physicochemical stability of a humanized monoclonal antibody LA298. *Int. J. Pharm.* **2006**, *308* (1), 46-51.
16. Qi, P.; Volkin, D. B.; Zhao, H.; Nedved, M. L.; Hughes, R.; Bass, R.; Yi, S. C.; Panek, M. E.; Wang, D.; DalMonte, P., Characterization of the photodegradation of a human IgG1 monoclonal antibody formulated as a high-concentration liquid dosage form. *J. Pharm. Sci.* **2009**, *98* (9), 3117-3130.
17. Mozziconacci, O.; Arora, J.; Toth, R. T. t.; Joshi, S. B.; Zhou, S.; Volkin, D. B.; Schoneich, C., Site-Specific Hydrolysis Reaction C-Terminal of Methionine in Met-His during Metal-Catalyzed Oxidation of IgG-1. *Mol. Pharm.* **2016**, *13* (4), 1317-28.
18. Mozziconacci, O.; Ji, J. A.; Wang, Y. J.; Schoneich, C., Metal-catalyzed oxidation of protein methionine residues in human parathyroid hormone (1-34): formation of homocysteine and a novel methionine-dependent hydrolysis reaction. *Mol. Pharm.* **2013**, *10* (2), 739-55.
19. Liu, M.; Zhang, Z.; Cheetham, J.; Ren, D.; Zhou, Z. S., Discovery and Characterization of a Photo-Oxidative Histidine-Histidine Cross-Link in IgG1 Antibody Utilizing 18O-Labeling and Mass Spectrometry. *Anal. Chem.* **2014**, *86* (10), 4940-4948.

20. Shen, H.-R.; Spikes, J. D.; Smith, C. J.; Kopeček, J., Photodynamic cross-linking of proteins: IV. Nature of the His–His bond (s) formed in the rose bengal-photosensitized cross-linking of N-benzoyl-L-histidine. *J. Photochem. Photobiol. A: Chem.* **2000**, *130* (1), 1-6.
21. Li, Y.; Polozova, A.; Gruia, F.; Feng, J., Characterization of the degradation products of a color-changed monoclonal antibody: tryptophan-derived chromophores. *Anal. Chem.* **2014**, *86* (14), 6850-6857.
22. Sreedhara, A.; Yin, J.; Joyce, M.; Lau, K.; Weckler, A. T.; Deperalta, G.; Yi, L.; John Wang, Y.; Kabakoff, B.; Kishore, R. S. K., Effect of ambient light on IgG1 monoclonal antibodies during drug product processing and development. *Eur. J. Pharm. Biopharm.* **2016**, *100*, 38-46.
23. Beck, A.; Wagner-Rousset, E.; Ayoub, D.; Van Dorsselaer, A.; Sanglier-Cianferani, S., Characterization of therapeutic antibodies and related products. *Anal. Chem.* **2013**, *85* (2), 715-736.
24. Wang, W.; Singh, S.; Zeng, D. L.; King, K.; Nema, S., Antibody structure, instability, and formulation. *J. Pharm. Sci.* **2007**, *96* (1), 1-26.
25. Schroeder Jr, H. W.; Cavacini, L., Structure and function of immunoglobulins. *J. Allergy Clin. Immunol.* **2010**, *125* (2), S41-S52.
26. Kumar, S.; Roffi, K.; Tomar, D. S.; Cirelli, D.; Luksha, N.; Meyer, D.; Mitchell, J.; Allen, M. J.; Li, L., Rational optimization of a monoclonal antibody for simultaneous improvements in its solution properties and biological activity. *Protein Engineering, Design and Selection* **2018**, *31* (7-8), 313-325.
27. Agrawal, N. J.; Dykstra, A.; Yang, J.; Yue, H.; Nguyen, X.; Kolvenbach, C.; Angell, N., Prediction of the Hydrogen Peroxide–Induced Methionine Oxidation Propensity in Monoclonal Antibodies. *J. Pharm. Sci.* **2018**, *107* (5), 1282-1289.
28. Jia, L.; Sun, Y., Protein asparagine deamidation prediction based on structures with machine learning methods. *PLoS One* **2017**, *12* (7).
29. Yang, Y.; Zhao, J.; Geng, S.; Hou, C.; Li, X.; Lang, X.; Qiao, C.; Li, Y.; Feng, J.; Lv, M., Improving trastuzumab's stability profile by removing the two degradation hotspots. *J. Pharm. Sci.* **2015**, *104* (6), 1960-1970.
30. Shire, S. J.; Shahrokh, Z.; Liu, J., Challenges in the development of high protein concentration formulations. *J. Pharm. Sci.* **2004**, *93* (6), 1390-1402.
31. Bodier-Montagutelli, E.; Respaud, R.; Watier, H.; Guillon-Munos, A. In *MABdelivery: administration routes for antibody therapy Third LabEx MABImprove industrial workshop, July 2, 2015 Tours, France*, MABs, Taylor & Francis: 2017; pp 579-585.
32. Ismael, G.; Hegg, R.; Muehlbauer, S.; Heinzmann, D.; Lum, B.; Kim, S.-B.; Pienkowski, T.; Lichinitser, M.; Semiglazov, V.; Melichar, B., Subcutaneous versus intravenous administration of (neo) adjuvant trastuzumab in patients with HER2-positive, clinical stage I–III breast cancer (HannaH study): a phase 3, open-label, multicentre, randomised trial. *Lancet Oncol.* **2012**, *13* (9), 869-878.
33. Rosengren, S.; Dychter, S. S.; Printz, M. A.; Huang, L.; Schiff, R. I.; Schwarz, H.-P.; McVey, J. K.; Drake, F. H.; Maneval, D. C.; Kennard, D. A., Clinical immunogenicity of rHuPH20, a hyaluronidase enabling subcutaneous drug administration. *The AAPS journal* **2015**, *17* (5), 1144-1156.
34. Liu, J.; Nguyen, M. D.; Andya, J. D.; Shire, S. J., Reversible self-association increases the viscosity of a concentrated monoclonal antibody in aqueous solution. *J. Pharm. Sci.* **2005**, *94* (9), 1928-1940.

35. Kanai, S.; Liu, J.; Patapoff, T. W.; Shire, S. J., Reversible self-association of a concentrated monoclonal antibody solution mediated by Fab–Fab interaction that impacts solution viscosity. *J. Pharm. Sci.* **2008**, *97* (10), 4219-4227.
36. Yadav, S.; Sreedhara, A.; Kanai, S.; Liu, J.; Lien, S.; Lowman, H.; Kalonia, D. S.; Shire, S. J., Establishing a link between amino acid sequences and self-associating and viscoelastic behavior of two closely related monoclonal antibodies. *Pharm. Res.* **2011**, *28* (7), 1750-1764.
37. Manning, M. C.; Patel, K.; Borchardt, R. T., Stability of protein pharmaceuticals. *Pharm. Res.* **1989**, *6* (11), 903-918.
38. Luo, Q.; Joubert, M. K.; Stevenson, R.; Ketchum, R. R.; Narhi, L. O.; Wypych, J., Chemical modifications in therapeutic protein aggregates generated under different stress conditions. *J. Biol. Chem.* **2011**, *286* (28), 25134-44.
39. Stadtman, E. R., Metal ion-catalyzed oxidation of proteins: Biochemical mechanism and biological consequences. *Free Radic. Biol. Med.* **1990**, *9* (4), 315-325.
40. Li, S.; Schoneich, C.; Borchardt, R. T., Chemical instability of protein pharmaceuticals: Mechanisms of oxidation and strategies for stabilization. *Biotechnol. Bioeng.* **1995**, *48* (5), 490-500.
41. Torosantucci, R.; Schöneich, C.; Jiskoot, W., Oxidation of Therapeutic Proteins and Peptides: Structural and Biological Consequences. *Pharm. Res.* **2014**, *31* (3), 541-553.
42. Gao, X.; Ji, J. A.; Veeravalli, K.; Wang, Y. J.; Zhang, T.; McGreevy, W.; Zheng, K.; Kelley, R. F.; Laird, M. W.; Liu, J.; Cromwell, M., Effect of individual Fc methionine oxidation on FcRn binding: Met252 oxidation impairs FcRn binding more profoundly than Met428 oxidation. *J. Pharm. Sci.* **2015**, *104* (2), 368-77.
43. Bertolotti-Ciarlet, A.; Wang, W.; Lownes, R.; Pristatsky, P.; Fang, Y.; McKelvey, T.; Li, Y.; Li, Y.; Drummond, J.; Prueksaritanont, T.; Vlasak, J., Impact of methionine oxidation on the binding of human IgG1 to Fc Rn and Fc gamma receptors. *Mol. Immunol.* **2009**, *46* (8-9), 1878-82.
44. Baptista, M. S.; Cadet, J.; Di Mascio, P.; Ghogare, A. A.; Greer, A.; Hamblin, M. R.; Lorente, C.; Nunez, S. C.; Ribeiro, M. S.; Thomas, A. H.; Vignoni, M.; Yoshimura, T. M., Type I and Type II Photosensitized Oxidation Reactions: Guidelines and Mechanistic Pathways. *Photochem. Photobiol.* **2017**, *93* (4), 912-919.
45. Bent, D.; Hayon, E., Excited state chemistry of aromatic amino acids and related peptides. III. Tryptophan. *JACS* **1975**, *97* (10), 2612-2619.
46. Bent, D.; Hayon, E., Excited state chemistry of aromatic amino acids and related peptides. I. Tyrosine. *JACS* **1975**, *97* (10), 2599-2606.
47. Creed, D., The photophysics and photochemistry of the near-UV absorbing amino acids–II. Tyrosine and its simple derivatives. *Photochem. Photobiol.* **1984**, *39* (4), 563-575.
48. Bensasson, R. V.; Land, E. J.; Truscott, T. G., *Flash photolysis and pulse radiolysis: contributions to the chemistry of biology and medicine*. Elsevier: 2013.
49. Schöneich, C., Radical-Based Damage of Sulfur-Containing Amino Acid Residues. *Encyclopedia of Radicals in Chemistry, Biology and Materials* **2012**.
50. Schöneich, C., Thiyl radicals and induction of protein degradation. *Free Radical Res.* **2016**, *50* (2), 143-149.
51. Wang, Y.; Lu, Q.; Wu, S.-L.; Karger, B. L.; Hancock, W. S., Characterization and comparison of disulfide linkages and scrambling patterns in therapeutic monoclonal antibodies: using LC-MS with electron transfer dissociation. *Anal. Chem.* **2011**, *83* (8), 3133-3140.

52. Wecksler, A. T.; Yin, J.; Lee Tao, P.; Kabakoff, B.; Sreedhara, A.; Deperalta, G., Photodisruption of the Structurally Conserved Cys-Cys-Trp Triads Leads to Reduction-Resistant Scrambled Intrachain Disulfides in an IgG1 Monoclonal Antibody. *Mol. Pharm.* **2018**, *15* (4), 1598-1606.
53. Steinmann, D.; Mozziconacci, O.; Bommana, R.; Stobaugh, J. F.; Wang, Y. J.; Schöneich, C., Photodegradation pathways of protein disulfides: human growth hormone. *Pharm. Res.* **2017**, *34* (12), 2756-2778.
54. Zhao, R.; Lind, J.; Merenyi, G.; Eriksen, T. E., Kinetics of one-electron oxidation of thiols and hydrogen abstraction by thiyl radicals from. alpha.-amino CH bonds. *JACS* **1994**, *116* (26), 12010-12015.
55. Chatgililoglu, C.; Ferreri, C.; Ballestri, M.; Mulazzani, Q. G.; Landi, L., Cis– trans isomerization of monounsaturated fatty acid residues in phospholipids by thiyl radicals. *JACS* **2000**, *122* (19), 4593-4601.
56. Prajapati, I.; Peters, B.-H.; Larson, N. R.; Wei, Y.; Choudhary, S.; Kalonia, C.; Hudak, S.; Esfandiary, R.; Middaugh, C. R.; Schöneich, C., Cis/Trans Isomerization of Unsaturated Fatty Acids in Polysorbate 80 During Light Exposure of a Monoclonal Antibody–Containing Formulation. *J. Pharm. Sci.* **2020**, *109* (1), 603-613.
57. Haywood, J.; Mozziconacci, O.; Allegre, K. M.; Kerwin, B. A.; Schöneich, C., Light-induced conversion of Trp to Gly and Gly hydroperoxide in IgG1. *Mol. Pharm.* **2013**, *10* (3), 1146-1150.
58. Mozziconacci, O.; Schöneich, C., Effect of conformation on the photodegradation of Trp-and cystine-containing cyclic peptides: octreotide and somatostatin. *Mol. Pharm.* **2014**, *11* (10), 3537-3546.
59. Kang, H.; Tolbert, T. J.; Schöneich, C., Photoinduced Tyrosine Side Chain Fragmentation in IgG4-Fc: Mechanisms and Solvent Isotope Effects. *Mol. Pharm.* **2019**, *16* (1), 258-272.
60. Dormán, G.; Nakamura, H.; Pulsipher, A.; Prestwich, G. D., The Life of Pi Star: Exploring the Exciting and Forbidden Worlds of the Benzophenone Photophore. *Chem. Rev.* **2016**, *116* (24), 15284-15398.
61. Lei, M.; Carcelen, T.; Walters, B. T.; Zamiri, C.; Quan, C.; Hu, Y.; Nishihara, J.; Yip, H.; Woon, N.; Zhang, T., Structure-based correlation of light-induced histidine reactivity in a model protein. *Anal. Chem.* **2017**, *89* (13), 7225-7231.
62. Schöneich, C., Photo-Degradation of Therapeutic Proteins: Mechanistic Aspects. *Pharm. Res.* **2020**, *37* (3), 45.
63. Parker, N. R.; Jamie, J. F.; Davies, M. J.; Truscott, R. J. W., Protein-bound kynurenine is a photosensitizer of oxidative damage. *Free Radic. Biol. Med.* **2004**, *37* (9), 1479-1489.
64. Mizdrak, J.; Hains, P. G.; Truscott, R. J.; Jamie, J. F.; Davies, M. J., Tryptophan-derived ultraviolet filter compounds covalently bound to lens proteins are photosensitizers of oxidative damage. *Free Radic. Biol. Med.* **2008**, *44* (6), 1108-1119.
65. Dreaden, T. M.; Chen, J.; Rexroth, S.; Barry, B. A., N-formylkynurenine as a marker of high light stress in photosynthesis. *J. Biol. Chem.* **2011**, *286* (25), 22632-22641.
66. Creed, D., The photophysics and photochemistry of the near-UV absorbing amino acids–i. Tryptophan and its simple derivatives. *Photochem. Photobiol.* **1984**, *39* (4), 537-562.
67. Guideline, I. H. T., Photostability testing of new drug substance and products. *Fed. Register* **1996**, *62*, 27115-27122.
68. Wei, Z.; Feng, J.; Lin, H. Y.; Mullapudi, S.; Bishop, E.; Tous, G. I.; Casas-Finet, J.; Hakki, F.; Strouse, R.; Schenerman, M. A., Identification of a single tryptophan residue as critical for

- binding activity in a humanized monoclonal antibody against respiratory syncytial virus. *Anal. Chem.* **2007**, *79* (7), 2797-805.
69. Baertschi, S. W.; Alsante, K. M.; Tønnesen, H. H., A critical assessment of the ICH guideline on photostability testing of new drug substances and products (Q1B): Recommendation for revision. *J. Pharm. Sci.* **2010**, *99* (7), 2934-2940.
 70. Mallaney, M.; Wang, S. h.; Sreedhara, A., Effect of ambient light on monoclonal antibody product quality during small-scale mammalian cell culture process in clear glass bioreactors. *Biotechnol. Progr.* **2014**, *30* (3), 562-570.
 71. Du, C.; Barnett, G.; Borwankar, A.; Lewandowski, A.; Singh, N.; Ghose, S.; Borys, M.; Li, Z. J., Protection of therapeutic antibodies from visible light induced degradation: Use safe light in manufacturing and storage. *Eur. J. Pharm. Biopharm.* **2018**, *127*, 37-43.
 72. Kerwin, B. A.; Remmele, R. L., Jr., Protect from light: photodegradation and protein biologics. *J. Pharm. Sci.* **2007**, *96* (6), 1468-79.
 73. Baertschi, S. W.; Clapham, D.; Foti, C.; Jansen, P. J.; Kristensen, S.; Reed, R.; Templeton, A. C.; Tonnesen, H. H., Implications of In-Use Photostability: Proposed Guidance for Photostability Testing and Labeling to Support the Administration of Photosensitive Pharmaceutical Products, Part 1: Drug Products Administered by Injection. *J. Pharm. Sci.* **2013**, *102* (11), 3888-3899.
 74. Kerwin, B. A., Polysorbates 20 and 80 used in the formulation of protein biotherapeutics: structure and degradation pathways. *J. Pharm. Sci.* **2008**, *97* (8), 2924-35.
 75. Chen, B.; Bautista, R.; Yu, K.; Zapata, G. A.; Mulkerrin, M. G.; Chamow, S. M., Influence of histidine on the stability and physical properties of a fully human antibody in aqueous and solid forms. *Pharm. Res.* **2003**, *20* (12), 1952-1960.
 76. Stroop, S. D.; Conca, D. M.; Lundgard, R. P.; Renz, M. E.; Peabody, L. M.; Leigh, S. D., Photosensitizers form in histidine buffer and mediate the photodegradation of a monoclonal antibody. *J. Pharm. Sci.* **2011**, *100* (12), 5142-5155.
 77. Dion, M. Z.; Leiske, D.; Sharma, V. K.; de Zafra, C. L. Z.; Salisbury, C. M., Mitigation of oxidation in therapeutic antibody formulations: a biochemical efficacy and safety evaluation of N-acetyl-tryptophan and L-methionine. *Pharm. Res.* **2018**, *35* (11), 222.
 78. Hogan, K. L.; Leiske, D.; Salisbury, C. M., Characterization of N-acetyl-tryptophan degradation in protein therapeutic formulations. *J. Pharm. Sci.* **2017**, *106* (12), 3499-3506.
 79. Bhambhani, A.; Kissmann, J. M.; Joshi, S. B.; Volkin, D. B.; Kashi, R. S.; Middaugh, C. R., Formulation design and high-throughput excipient selection based on structural integrity and conformational stability of dilute and highly concentrated IgG1 monoclonal antibody solutions. *J. Pharm. Sci.* **2012**, *101* (3), 1120-1135.
 80. Zbacnik, T. J.; Holcomb, R. E.; Katayama, D. S.; Murphy, B. M.; Payne, R. W.; Coccaro, R. C.; Evans, G. J.; Matsuura, J. E.; Henry, C. S.; Manning, M. C., Role of Buffers in Protein Formulations. *J. Pharm. Sci.* **2017**, *106* (3), 713-733.
 81. Ugwu, S. O.; Apte, S. P., The effect of buffers on protein conformational stability. *Pharm. Technol.* **2004**, *28* (3), 86-109.
 82. Nema, S.; Washkuhn, R.; Brendel, R., Excipients and their use in injectable products. *PDA J. Pharm. Sci. Technol.* **1997**, *51* (4), 166-171.
 83. Jeong, S. H., Analytical methods and formulation factors to enhance protein stability in solution. *Arch. Pharmacol. Res.* **2012**, *35* (11), 1871-1886.
 84. Uchiyama, S., Liquid formulation for antibody drugs. *Biochimica et Biophysica Acta (BBA)-Proteins and Proteomics* **2014**, *1844* (11), 2041-2052.

85. Kang, J.; Lin, X.; Penera, J., Rapid formulation development for monoclonal antibodies. *BioProcess Int* **2016**, *14* (4), 40.
86. Liu, J.; Shire, S. J., Reduced-viscosity concentrated protein formulations. Google Patents: 2014.
87. Fraenkel-Conrat, H.; Olcott, H. S., Reaction of formaldehyde with proteins VI. cross-linking of amino groups with phenol, imidazole, or indole groups. *J. Biol. Chem.* **1948**, *174* (3), 827-843.
88. Tomita, M.; Irie, M.; Ukita, T., Sensitized photooxidation of histidine and its derivatives. Products and mechanism of the reaction. *Biochemistry* **1969**, *8* (12), 5149-5160.
89. Bane, J.; Mozziconacci, O.; Yi, L.; Wang, Y. J.; Sreedhara, A.; Schoneich, C., Photo-oxidation of IgG1 and Model Peptides: Detection and Analysis of Triply Oxidized His and Trp Side Chain Cleavage Products. *Pharm. Res.* **2017**, *34* (1), 229-242.
90. Falconer, R. J., Advances in liquid formulations of parenteral therapeutic proteins. *Biotechnol. Adv.* **2019**.
91. Harinarayan, C.; Skidmore, K.; Kao, Y.; Zydney, A.; Van Reis, R., Small molecule clearance in ultrafiltration/diafiltration in relation to protein interactions: Study of citrate binding to a Fab. *Biotechnol. Bioeng.* **2009**, *102* (6), 1718-1722.
92. Valliere-Douglass, J. F.; Connell-Crowley, L.; Jensen, R.; Schnier, P. D.; Trilisky, E.; Leith, M.; Follstad, B. D.; Kerr, J.; Lewis, N.; Vunnum, S.; Treuheit, M. J.; Balland, A.; Wallace, A., Photochemical degradation of citrate buffers leads to covalent acetonation of recombinant protein therapeutics. *Protein Sci.* **2010**, *19* (11), 2152-63.
93. Valliere-Douglass, J. F.; Lewis, P.; Salas-Solano, O.; Jiang, S., Solid-state mAbs and ADCs subjected to heat-stress stability conditions can be covalently modified with buffer and excipient molecules. *J. Pharm. Sci.* **2015**, *104* (2), 652-665.
94. Houlton, S., Benefits and drawbacks of moving to biosimilar medicines. *Prescriber* **2019**, *30* (7), 13-15.
95. Subelzu, N.; Schoneich, C., Near UV and visible light induce iron-dependent photo-degradation reactions in pharmaceutical buffers: mechanistic and product studies
96. Dear, B. J.; Hung, J. J.; Truskett, T. M.; Johnston, K. P., Contrasting the influence of cationic amino acids on the viscosity and stability of a highly concentrated monoclonal antibody. *Pharm. Res.* **2017**, *34* (1), 193-207.
97. Labrenz, S. R., Ester hydrolysis of polysorbate 80 in mAb drug product: evidence in support of the hypothesized risk after the observation of visible particulate in mAb formulations. *J. Pharm. Sci.* **2014**, *103* (8), 2268-77.
98. Park, J. H.; Jin, J. H.; Lim, M. S.; An, H. J.; Kim, J. W.; Lee, G. M., Proteomic Analysis of Host Cell Protein Dynamics in the Culture Supernatants of Antibody-Producing CHO Cells. *Sci. Rep.* **2017**, *7*, 44246.
99. Kranz, W.; Wuchner, K.; Corradini, E.; Berger, M.; Hawe, A., Factors Influencing Polysorbate's Sensitivity Against Enzymatic Hydrolysis and Oxidative Degradation. *J. Pharm. Sci.* **2019**, *108* (6), 2022-2032.
100. Hall, T.; Sandefur, S. L.; Frye, C. C.; Tuley, T. L.; Huang, L., Polysorbates 20 and 80 Degradation by Group XV Lysosomal Phospholipase A2 Isomer X1 in Monoclonal Antibody Formulations. *J. Pharm. Sci.* **2016**, *105* (5), 1633-1642.

1.10. Figures

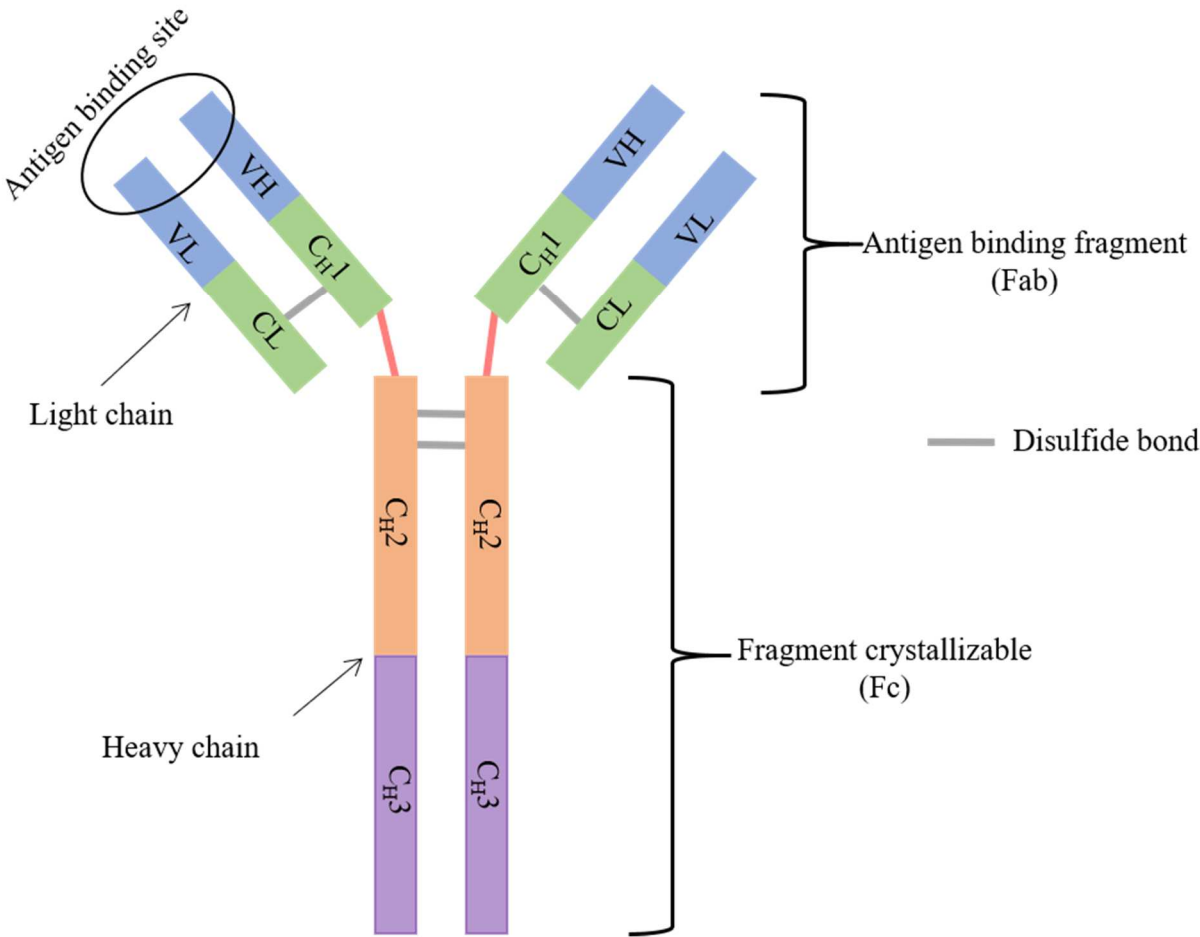
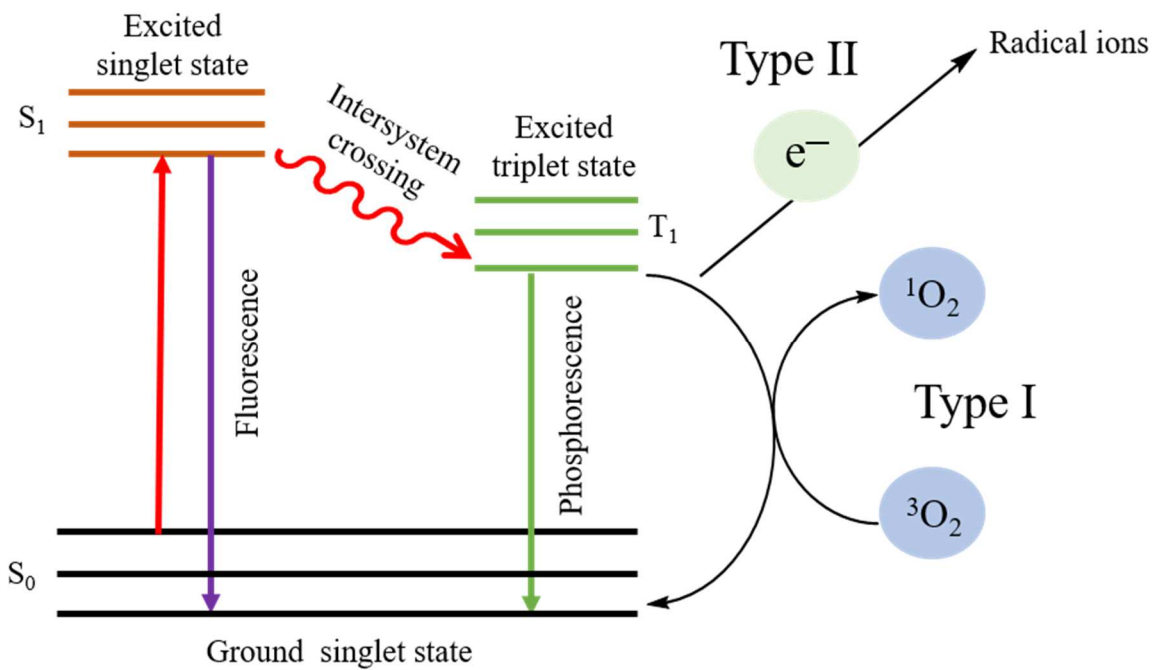


Figure 1: Structure of an antibody



Scheme 1: Jablonski's diagram showing Type I and Type II photosensitization.

**Chapter 2: One-electron photo-oxidation of Met-X_n-
His-containing peptides: Formation of novel cross-
links**

2.1. Introduction

Protein oxidation can target any amino acid depending on the oxidant; however, the aromatic (tryptophan, tyrosine, phenylalanine, and histidine) and sulfur-containing amino acids (cysteine (Cys), and methionine (Met)) are generally more susceptible to oxidation.¹⁻³ In particular, the oxidation of Met to Met sulfoxide (MetO) can have consequences for protein stability, structure and biological activity.⁴ For example, upon Met oxidation to MetO calmodulin undergoes structural changes, which destabilize the protein.⁵⁻⁶ In another case, the oxidation of Met in actin reduced actin polymerization.^{4, 7-13} Met oxidation also affects the interactions of Met with tryptophan (Trp),¹⁴⁻¹⁵ lysine (Lys),¹⁶ and histidine (His).¹⁷ In biological systems, methionine sulfoxide reductase (Msr) isoforms are present to reduce MetO back to Met.¹⁸⁻¹⁹ However, the enzymatic reduction of MetO to Met is not possible in biotherapeutics, which are usually formulated for long time storage. Therefore, Met oxidation in biotherapeutics is carefully monitored. One issue of concern is the oxidation of Met residues in monoclonal antibodies, which can affect binding to the neonatal fragment crystallizable receptor (FcRn), leading to a decrease in receptor binding and potentially affecting the pharmacokinetics of the antibodies.^{17, 20-21}

Met oxidation can occur through one or two-electron processes. The one-electron oxidation usually involves a strong one-electron oxidant such as a hydroxyl radical (HO•),²²⁻²⁶ or an alkoxy radical (RO•),²⁷ even to a certain extent peroxyxynitrite, ONOO•.²⁸⁻³⁰ One-electron transfer from Met yields a Met sulfur radical cation (Met>S^{•+}), which can form a 2 centers – 3 electrons (2c-3e) bond with a nearby heteroatom (oxygen, nitrogen, sulfur); such 2c-3e bonds were identified by their absorption spectra during time-resolved pulse radiolysis or flash photolysis experiments.³¹⁻³² On the other hand, the two-electron oxidation of Met can be achieved with hydrogen peroxide (H₂O₂),^{20, 27} organic peroxides (ROOH),³³ ONOO⁻,²⁸⁻²⁹ and singlet oxygen (¹O₂)²⁷. Recent studies

on the Fenton oxidation via $[\text{Fe}^{\text{II}}(\text{EDTA})]^{2-}/\text{H}_2\text{O}_2$ of parathyroid hormone 1-34 (PTH (1-34)) and a monoclonal antibody suggest that the intermediary generation of peptide and protein $\text{Met}>\text{S}^{*+}$ can lead to the hydrolysis of the peptide bond C-terminal of $\text{Met}>\text{S}^{*+}$ specifically in the subsequence -Met-His-.²⁴⁻²⁵ In the proposed mechanism,²⁴⁻²⁵ the His residue served to bind an $[\text{Fe}^{\text{II}}(\text{EDTA})]^{2-}$ complex to promote generation of an oxidant in the immediate vicinity of Met.

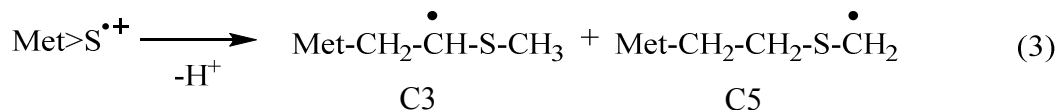
The experiments described in the current chapter were undertaken in order to evaluate whether the generation of $\text{Met}>\text{S}^{*+}$ in the absence of $[\text{Fe}^{\text{II}}(\text{EDTA})]^{2-}$ would lead to hydrolysis of C-terminal of $\text{Met}>\text{S}^{*+}$. For this purpose, we subjected Met-His-containing peptides to one-electron photo-oxidation by triplet 4-carboxybenzophenone (*4-CB) according to the reactions 1 and 2.



Earlier studies have elucidated reaction of *4-CB with Met and Met-containing peptides, where the additive quantum yield for the generation of $\text{Met}>\text{S}^{*+}$ via reaction (2) was on the order of 0.08-0.27.³⁴⁻³⁵ Importantly, upon one-electron photo-oxidation of the Met- X_n -His ($n = 0-2$) sequences subjected to photo-oxidation in the current chapter we did not observe subsequent hydrolysis indicating the formation of $\text{Met}>\text{S}^{*+}$ in the absence of $[\text{Fe}^{\text{II}}(\text{EDTA})]^{2-}$ was not sufficient for hydrolysis.

However, the generation of $\text{Met}>\text{S}^{*+}$ in our peptide sequence resulted in the formation of a series of (novel) photoproducts including covalent cross-link, possibly related to carbon-centered radical generated via deprotonation of $\text{Met}>\text{S}^{*+}$ according to reaction (3). The formation of covalent cross-

links is of great significance for protein oxidation during conditions of oxidative stress and aging.³⁶⁻⁴² In addition cross-link formation is stability concern for the formulation and



administration of protein biotherapeutics, where cross-links correlate with the loss of biological activity and the formation of aggregates and particles, which may be immunogenic.⁴³⁻⁴⁶ Frequently, the mechanisms and structures of cross-links in protein biotherapeutics are unknown, and the current chapter adds some mechanistic insight into cross-link formation relevant for the semaphorin-6A and monoclonal antibodies and , which contain at least one, and some cases more than one Met-His subsequence in their structure.⁴⁷⁻⁴⁹

2.2. Materials and Methods

2.2.1. Materials

The model peptide M1 and LPLAHAL (A1) were purchased either from GenScript (Piscataway, NJ), or was synthesized in-house. All other model peptides, LPLM(¹³C5)HAL (M2), LPLMH(¹⁵N₃)AL (M3), LPLMGHAL (M4), and LPLMGGHAL (M5) were synthesized in-house. All amino acids for peptide synthesis were from Gyros Protein Technologies AB (Tucson, AZ). The Fmoc stable isotope-labeled Met and His residues were purchased from Cambridge Isotope laboratories Inc (Tewksbury, MA). Triisopropylsilane (TIPS), trifluoroacetic acid (TFA), 4-CB, Girard's reagent T (GRT), N-ethylmaleimide (NEM), and sodium borohydride (NaBH₄) were from Sigma-Aldrich (St. Louis, MO) at the highest commercially available grade. Acetonitrile (ACN), Optima® water with FA, and Optima® ACN with FA were purchased from Fisher Scientific

(Hampton, NH). The ultra-pure quality water (dH₂O) (18.2 MΩ) was produced fresh daily by a WaterPro PS Polishing System (Labconco, Kansas City, MO).

2.2.2. Synthesis of model peptides and purification

Model peptides (Chart 1) were synthesized using Fmoc-chemistry on a Tribute® solid-phase peptide synthesizer (Gyros Protein Technologies AB, Tucson, AZ). After synthesis, the protection groups and resin in the peptidyl-resin were deprotected using an Fmoc-cleavage mixture containing 94% TFA, 3% TIPS and 3% water by stirring for 2 h at room temperature.⁵⁰ The cleaved peptide and resin were separated using a filter with 70-170 μm pore size, and the filtrate containing the cleaved peptide was evaporated using a rotary evaporator. The dried peptide was reconstituted in 10 ml of 1:1 of acetonitrile: mobile phase A (95%water, 5%ACN and 0.1% TFA) and filtered using a 0.2 μm filter before injecting onto a semi preparative HPLC column (Waters XBridge C18 column, 19 mm × 250 mm, 5 μm particle size; Waters Corporation, Milford, MA). The peptide was eluted at a flow rate of 15 ml/min and dried by lyophilization. The purified peptides were analysed for purity in a Waters Micromass LCT Premier Mass Spectrometer (Micromass Ltd., Manchester, U.K.).

2.2.3. Photo-irradiation

Solutions of 1 mM peptide and 100 μM 4-CB were prepared in 10 mM phosphate buffer and the pH adjusted to 3.30, 7.23, or 9.88 using HCl and/or NaOH. These solutions were saturated with either air or Ar, and photo-irradiated for 0-90 min at room temperature in borosilicate test tubes. The photo-irradiation was performed in a Rayonet photoreactor (RPR200, The Southern New England Ultraviolet Company, Branford, CT) equipped with four lamps (Southern New England, Branford, CT, RMA-500) that emit UV-A light between 310 nm and 410 nm, with $\lambda_{\text{max}} = 350$ nm.

Actinometry was done with the ferrioxalate actinometer⁵¹⁻⁵³, which gave a flux of $\sim 3 \times 10^{-8}$ Einstein.s⁻¹ and an irradiance of ~ 6.3 W.h/m². The solutions in our experimental conditions was exposed to irradiances of 0-9.45 W.h/m². The latter value is significantly below 200 W.h/m² for photostability testing with UV light, recommended by the ICH Q1B guideline of the International Conference of Harmonization (ICH).⁵⁴ Control solutions were placed in the dark at room temperature for 1 h or wrapped with aluminum foil and placed in the Rayonet photoreactor for 1 h during photo-irradiation. All solutions were analyzed by HPLC and mass spectrometry.

2.2.4. Reversed Phase-High Performance Liquid Chromatography (RP-HPLC) analysis

Control and photo-irradiated solutions were analyzed in a RP-HPLC equipped with a PDA detector (Shimadzu Corporation, Kyoto, Japan). The unmodified peptides, photoproducts, and 4-CB were monitored at 214 nm. The separation was achieved at a flow rate of 1ml/min on a Vydac® 218TP54 protein and peptide C18 column (4.6 mm i.d. x 250 mm, 5 μ m particle size, and 300 Å pore size) (Alltech Associates Inc, Deerfield, IL), maintained at 35 °C in a column heater. Mobile phase A and B consisted of water with 0.1% TFA and ACN with 0.1% TFA, respectively. Resolution of unmodified peptides, photoproducts, and 4-CB was achieved with the following gradient program: 97% A and 3% B was held for 7 min, changed to 85% A and 15% B at 7.1 min, and linearly changed to 45% A and 55 % B within 14 min. Then, the composition of solvents was changed to 30% A and 70% B over 6 min and maintained for 1 min before re-equilibration to 3% A and 97% B for 7 min. The data were collected and analyzed with the Shimadzu LabSolutions software, and plotted with the GraphPad Prism 7 software.

2.2.5. NanoAcquity LC Electrospray Ionization Q-tof MS and LC-MS/MS analysis

The photo-irradiated solutions were analyzed on a nanoAcquity Ultra Performance Liquid Chromatography system connected to a Xevo-G2 Qtof tandem mass spectrometer (LC-MS) (Waters Corporation, Milford, MA). The instrument was operated in the positive and data-dependent mode at a mass range of 150-2000 Da. The capillary voltage and sampling cone voltage were set to 2.7 kV and 45 V, respectively. The electrospray ionization (ESI) source temperature was maintained at 100 °C. Four microliters of 20 µM control or photo-irradiated solutions were injected onto a Symmetry® C18 Waters trap column (2G-V/M Trap) with a dimension of 180 µm x 200 mm, 5 µm particle size, and 100 Å pore size, connected to an analytical nanoAcquity ultra performance Waters peptide CSH™ C18 column with a dimension of 75 µm x 250 mm, 1.7 µm particle size, and 130 Å pore size. The analytical column temperature was maintained at 40 °C. Mobile phase A consisted of Optima® water with 0.1% formic acid (FA) and mobile phase B consisted of acetonitrile containing 0.1% FA. The solutions were injected onto the trapping column for 2 min at a flow rate of 4 µl/min. After 2 min, the solutions were directed to the analytical column with a flow rate of 0.3 µl/min. The peptide and the photoproducts were separated using the following gradient: the initial composition was 97% A and 3% B mobile phases, which was changed linearly to 65% A and 35% B within 50 min, held for 20 min, changed to 5% A and 95% B at 70 min and held for another 3 min. Subsequently, the composition was reverted to 97% A and 3% B to re-equilibrate the column and held for 10 min. The mass spectrometer was operated and the obtained data analyzed with the Masslynx v.4.1 software. The data were plotted with the GraphPad Prism 7 software.

2.3. Results

2.3.1. Identification of photoproducts

The solutions containing peptide M1 and 4-CB in 10 mM phosphate buffer were exposed to UV-A light for 0-90 min; representative data for 60 min will be discussed in detail. When the solution at pH 7.23 was photo-irradiated under air or Ar with $\lambda_{\text{max}} = 350$ nm for 60 min, several photoproducts were resolved and characterized by LC-MS analysis (Fig. 1, red trace). The photoproducts with their names, abbreviations, m/z value, and charge state are provided in Table S1. The control solution only showed the unmodified peptide M1 ($t_{\text{R}} = 21.20$ min) displaying a molecular ion with m/z 397.73 ($z = 2$), and a small amount of oxidation products M1P6a and M1P6b with m/z 405.70 ($z = 2$), eluting at 20.96 min and 21.23 min, respectively (Fig. 1, black trace).

When M1 was photo-irradiated at pH 7.23 under air (red trace), ~30% of the unmodified M1 were lost (Table S2), leading to the formation of several photoproducts that eluted before and after the peak of unmodified M1. LC-MS analysis revealed that the photoproducts M1P6a and M1P6b, eluting at $t_{\text{R}} = 20.96$ and 21.23 min display a molecular ion with m/z 405.70 ($z = 2$), an increase of 16 Da relative to M1. At $t_{\text{R}} = 21.84$ and 22.04 min, isobaric photoproducts (M1P1a and M1P1b) nearly co-eluted, displaying molecular ions with m/z 381.70 ($z = 2$), representing a loss of 32 Da from M1 (more details in section 3.3). At $t_{\text{R}} = 22.84$ min, a photoproduct (M1P2) displaying a molecular ion with m/z 389.70 ($z = 2$) was observed and characterized by the loss of 16 Da from unmodified M1 (more detail in section 3.7). Another photoproduct that elutes before unmodified M1, at $t_{\text{R}} = 23.82$ min, is M1P3, displaying a molecular ion with m/z 390.70 ($z = 2$), which is more prominent at pH 3.30 shown in Fig. 2 (green trace). The photoproducts that elute at $t_{\text{R}} = 26.80$ and 27.17 min showed increase by 34 Da (M1P3-SO₃H) and 32 Da (M1P7) relative to M1, respectively

(more detail in sections 3.8 and 3.11). Photoproducts M1P5a-d, eluting at $t_R = 28.55, 29.05, 30.01,$ and 30.75 min, all display a molecular ion m/z 510.72 ($z = 2$). These isobaric products reveal an increase by 226 Da relative to M1, corresponding to the molecular weight of 4-CB. Therefore, products M1P5a-d are likely generated by reaction between peptide-derived radicals and a ketyl radical derived from 4-CB (more detail in section 3.10). The extracted ion chromatogram (XIC) of a photo-irradiated solution also revealed His oxidation products (more detail in section 3.12). All observed products are discussed in detail below. In contrast to air-saturated solutions, the photo-irradiation of Ar saturated solutions M1 and 4-CB (Fig. 1, blue trace) showed a significant lower conversion of M1 (7%), generating small yields of M1P1a/M1P1b, and products M1P5a-d. The structures of photoproducts from peptide M1 is shown in Chart 2. As a control, the solution containing peptide A1 with 4-CB was photo-irradiated in the similar conditions as M1 and 4-CB. As expected, the products generated from the original Met were not observed, including M1P1a and M1P1b (Fig. S1).

2.3.2. Comparison of photoproducts at pH 3.30, 7.23, and 9.88 by LC-MS

Control and photo-irradiated solutions of M1 and 4-CB in 10 mM phosphate buffer, at pH 3.30, 7.23, or 9.88 (under air) were analyzed by LC-MS (Fig. 2). The control solutions were wrapped in aluminum foil and placed in Rayonet reactor during photo-irradiation. The control solutions contained <3% of oxidation products M1P6a and M1P6b, characterized by an increase of 16 Da on the Met residue. In general, photo-irradiation at pH 3.30 generated higher yield of photoproducts as compared to pH 7.23 and 9.88 (Table S2). At pH 3.30, M1 was converted into M1P6a/ M1P6b ($t_R = 20.96$ and 21.23 min), M1P1a/M1P1b ($t_R = 21.81$ and 22.04 min), M1P2 ($t_R = 22.84$ min), M1P3 ($t_R = 23.82$ min), M1P4 ($t_R = 23.91$ min), M1P3+SO₃H ($t_R = 26.80$ min), M1P7 ($t_R = 27.17$ min), and M1P5a-d ($t_R = 28.55, 29.05, 30.01,$ and 30.75 min). At pH 7.23

M1P4a/M1P4b was not observed and at pH 9.88, only 0.11% of M1P4a/M1P4b was formed, which is ~4% less in comparison to pH 3.30 (Table S2). The percentages of M1P3 formed at pH 7.23 and at pH 9.88 were 0.03 and 0.05, respectively, whereas at pH 3.30, 0.48% of M1P3 was formed. Similar observations were made when photoproducts at pH 3.30, 7.23, and 9.88 were analyzed by HPLC coupled to UV-detection (Fig. S2).

2.3.3. The photoproducts M1P1a and M1P1b

At $t_R = 21.84$ and 22.04 min (Fig. 1, red trace), two isobaric photoproducts (M1P1a and M1P1b) were identified by LC-MS analysis, displaying molecular ion with m/z 381.72 ($z = 2$). These ions indicate a loss of 32 Da from M1. The LC-MS/MS spectrum of M1P1a/M1P1b was compared with that of unmodified M1 (Fig. 3) to elucidate structural changes leading to M1P1a/M1P1b. The LC-MS/MS spectrum of unmodified M1 revealed all the y-ions (y1-y6), a b2 ion, and several internal fragments such as HA, MH, LMH, LMHA, PLMH, and PLMHA, confirming that the amino acids in M1 were not modified (Fig. 3A). In contrast, the LC-MS/MS spectrum of M1P1a/M1P1b showed the y1 ion, and multiple y ions undergoing loss of water such as y4-H₂O, y5-H₂O, y5-H₂O, and y6-H₂O. Additionally, it displays internal fragments characterized by neutral water loss or neutral CO loss. All internal fragments are present with cross-link between oxidized Met and His. Importantly, prominent ions such as y3 and the internal fragment HA, which are present in LC-MS/MS spectrum of unmodified M1, are absent in the LC-MS/MS spectrum of M1P1a/M1P1b. Moreover, the intensity of immonium ion of His is decreased significantly in the LC-MS/MS spectrum of M1P1a/M1P1b. These data suggest a cross-link formation between the original residues Met and His after the loss of 32 Da. Another important observation is that M1P1a/M1P1b loses a water molecule during LC-MS/MS analysis, resulting in a product M1P1a/M1P1b-H₂O, displaying a molecular ion with 372.72 ($z = 2$). M1P1a/M1P1b and

M1P1a/M1P1b-H₂O have identical fragmentation patterns (Fig. S3) indicating that they are related to each other. Based on the LC-MS/MS spectrum of M1P1a/M1P1b, we propose a mechanism in Scheme 1, according to which M1P1a/M1P1b is derived from aspartate semialdehyde M1P1 (reaction 8). M1P1 is also isobaric to M1P1a/M1P1b; however, the LC-MS/MS spectrum of m/z 381.72 ($z = 2$) did not show fragmentation pattern for open chain aldehyde. M1P1a/M1P1b must be in equilibrium with M1P1 as shown in reaction 8 Scheme 1. In order to prove the existence of the aspartate semialdehyde M1P1, the photo-irradiation samples were subjected to reduction by NaBH₄ and derivatization with GRT, as described below.

2.3.3.1. Reduction by NaBH₄

When a photo-irradiated solution was incubated with 20 mM NaBH₄ at 37 °C for 15 min at pH 12.00 and analysed by LC-MS (Fig. 4), the peaks with m/z 381.72 ($z = 2$), representing M1P1a/M1P1b disappeared and a new peak at $t_R = 21.23$ min appeared. This new peak contained a product with a molecular ion with m/z 382.70 ($z = 2$), indicating an increase of 2 Da relative to M1P1a/M1P1b. As M1P1a/M1P1b are connected to M1P1 via equilibrium 8 Scheme 1, reduction process converts aspartate semialdehyde M1P1 into an alcohol as shown in Scheme 3.

2.3.3.2. Derivatization by GRT

The photo-irradiated solution was subjected to derivatization with GRT, which forms a hydrazone derivative of aldehydes. A photo-irradiated solution was incubated with 20 mM GRT at 37 °C and pH 3.30 for 19 h and analysed by LC-MS. This reaction resulted in the reduction of peak area of the signal representing M1P1a/M1P1b and the formation of a new peak at $t_R = 17.52$ min containing a product with a molecular ion with m/z 438.23 ($z = 2$) (Fig. 5, insert). This peak contains the hydrazone derived from M1P1 (M1P1-GRT) shown in Scheme 4. The LC-MS/MS spectrum of M1P1-GRT contained the ions y_3 - y_6 and an internal fragment u_1H , where $u_1 =$

hydrazone, depicting a chemical modification of the original Met residue (Fig. S4), further indicating that M1P1a/M1P1b are in equilibrium with M1P1.

2.3.4. Generation of M1P1a/M1P1b from peptide M1 containing ^{13}C -Met

The LC-MS/MS spectrum of M1P1a/M1P1b suggests a cross-link between the original residues Met and His after the loss of 32 Da. In order to evaluate whether the loss of 32 Da originates from Met and His, peptide M1 was synthesized with stable isotope-labeled Met (ϵ - ^{13}C) (M2) or His ($^{15}\text{N}_3$; section 3.5) (M3). One pathway to the loss of 32 Da would be oxidation of Met to aspartate semialdehyde (M1P1), accounting for a net loss of 32 Da. A solution containing 1 mM peptide M2 and 100 μM 4-CB was photo-irradiated at pH 7.20 under the same conditions as outlined in section 2.3. The LC-MS chromatogram of the photo-irradiated solution shows that unmodified M2 and several photoproducts are higher in mass by 1 Da; however, the cross-link M1P1a/M1P1b derived from peptide M2 shows an identical molecular ion (m/z 381.70, $z = 2$) as M1P1a/M1P1b derived from peptide M1, indicating that the original Met residue had lost the ϵ - CH_3 group, consistent with a loss of $^{13}\text{CH}_3\text{SH}$ to form aspartate semialdehyde, M1P1.

2.3.5. Generation of M1P1a/M1P1b-($^{15}\text{N}_3$) from peptide M3 containing ^{15}N -labeled His

Theoretically, a loss of 32 Da from M1 would also be consistent with a loss of hydrazine ($\text{H}_2\text{N}-\text{NH}_2$), which could originate from His. Therefore, peptide M3 (Chart 1) was synthesized and subjected to photo-oxidation and LC-MS/MS analysis. The LC-MS chromatogram showed formation of M1P1a/M1P1b-($^{15}\text{N}_3$) with an increase of 3 Da in comparison to M1P1a/M1P1b derived from peptide M1. The LC-MS/MS spectrum of M1P1a/M1P1b-($^{15}\text{N}_3$) (Fig. 6) revealed the presence of y4-y6 including their neutral loss of H_2O and absence of y2 and y3. The internal fragment $\text{H}(^{15}\text{N}_3)\text{A}$ is not observed, and all other internal fragments display cross-link between

oxidized Met and His(¹⁵N₃) characterized by neutral water loss or neutral CO loss. The LC-MS/MS spectrum indicates the side chain of the His residue is intact, and Met and His(¹⁵N₃) are cross-linked after the loss of 32 Da and a water molecule, like M1P1a/M1P1b. Hence, the experiments with M2 and M3 are consistent with the structural assignment of product M1P1a/M1P1b derived from peptide M1.

2.3.6. Effect of spacing on cross-link formation

Two model peptides M4 and M5 containing one Gly and two Gly, respectively, between Met and His were synthesized to observe the effect of spacing between Met and His in cross-link formation. Solutions containing either M4 or M5 and 4-CB were photo-irradiated under the conditions outlined in section 2.3 and the products were analysed by LC-MS/MS. The cross-link product formed from M4 (M4P1a/M4P1b) displays a molecular ion with m/z 410.27 ($z = 2$) corresponding to the loss of 32 Da from M4. The LC-MS/MS spectrum of M4P1a/M4P1b (Fig. 7) displays the characteristic ions y_2 , y_5-H_2O , y_6-H_2O , and y_7-H_2O . All internal fragments contained cross-linked oxidized Met, Gly, and His, characterized by loss of neutral H₂O loss or neutral loss of CO. Together with the absence of y_3 and y_4 ions and of the internal fragments that would contain either Met or His, these data are consistent with cross-link formation between Met and His across a bridging Gly residue. It is interesting that the LC-MS/MS spectrum in Fig. 7 shows a small signal for the His immonium ion, suggesting that the cross-link may be sensitive to dissociation during electrospray LC-MS analysis, consistent with equilibrium 8 (Scheme 1).

The cross-link product M5P1a/M5P1b formed from peptide M5 was analyzed by LC-MS/MS. The LC-MS/MS spectrum of M5P1a/M5P1b (Fig. 8) displayed the ions y_2 , y_3 , y_6-H_2O , y_7-H_2O , and y_8-H_2O . However, the ions y_4 and y_5 are not present in the LC-MS/MS spectrum. Importantly, an

ion y3 and the internal fragment HA are observed at low intensity, which indicates that the cross-link with a Gly-Gly bridge may not be stable during electrospray LC-MS analysis. However, like M1P1a/M1P1b and M1P1a/M1P1b-(¹⁵N₃), we observed loss of water from the molecular ion during gas-phase fragmentation from M4P1a/M4P1b and M5P1a/M5P1b, analogous to the formation of M1P1a/M1P1b-H₂O from M1 according to reaction 9.

2.3.7. Formation of aspartic acid (M1P2)

The photoproduct M1P2 is characterized by the loss of 16 Da from M1, with m/z 389.72 (*z* = 2). In Fig. 1, M1P2 eluted at *t_R* = 22.84 min and the y ion series (y1-y6) in the LC-MS/MS analysis (Fig. 9) indicated that the loss of 16 Da is derived from the Met residue of M1. This is confirmed by the fragments such as HA, MH-16, LMH-16, PLMHA-16, and the immonium ions of His, Pro and Leu. A net loss of 16 Da from Met would be consistent with the formation of thioaldehyde, vinyl homocysteine, or aspartic acid; all these proposed structures are isobaric. In order to test whether M1P2 was a thioaldehyde, the photo-irradiated solution was incubated with GRT, which would convert the thioaldehyde in a hydrazone, analogous to the derivatization of aspartic semialdehyde (section 3.3.2). However, the incubation with GRT did not change the peak intensity of M1P2, suggesting that this product is not a thioaldehyde. This was confirmed by reaction with NaBH₄, which did not result in any reduction product.

The second possible structure is vinyl homocysteine that contains a free thiol group. When photo-irradiated sample was incubated with the alkylating agent NEM at 37 °C for 1 h at pH 9.20, the peak intensity of M1P2 did not change, indicating that M1P2 does not contain a free thiol. Therefore, we propose that the structure of M1P2 contain aspartic acid, generated via reaction 10

(Scheme 1). M1P2 can also form after oxidation of aspartate semialdehyde (M1P1) via reaction 11 Scheme 1.

2.3.8. Formation of homocysteine (M1P3) and homocysteine sulfonic acid (M1P3-SO₃H)

The photoproduct M1P3 eluting at $t_R = 23.82$ min (Fig. 1), displays a molecular ion with m/z 390.70 ($z = 2$), corresponding to the loss of 14 Da from M1. The LC-MS/MS spectrum of M1P3 (Fig. 10) showed the presence of ion series y_1 - y_6 , indicating the loss of 14 Da from the Met residue. Moreover, the LC-MS/MS spectrum also displayed the immonium ions of Pro, Leu, and His, and internal fragments such as HA, MH-14, LMH-14, and PLMHA-14, indicating that modification of the Met residue is responsible for the formation of M1P3. A loss of 14 Da from Met would be consistent with the formation of homocysteine, which has been observed before as a product of Met \rightarrow S⁺.²⁵ Since homocysteine contains a free thiol group, the photo-irradiated solution was incubated with NEM at 37 °C for 1 h at pH 9.20. This incubation led to a new product with m/z 453.26 ($z = 2$), indicating the alkylation of M1P3 with NEM (Scheme 5). LC-MS/MS analysis of this NEM alkylated product (Fig. S5) displayed the expected ion series y_2 - y_6 , showing the addition of NEM to homocysteine (M1P3-NEM). In addition, the presence of internal fragments such as HA and u_2 H (where $u_2 = \text{homocysteine} + \text{NEM}$) indicate the formation of homocysteine.

The photo-oxidation of M1 in the presence of 4-CB led to a peak eluting at $t_R = 26.80$ min (Fig. 1, red trace), which displays a molecular ion with 414.72 ($z = 2$), corresponding to an addition of either 34 Da to M1 or 48 Da to M1P3. LC-MS/MS analysis (Fig. S6) of this peak reveals the ion series y_1 - y_6 , consistent with the oxidation of M1P3 to homocysteine sulfonic acid (product M1P3-SO₃H). This is further corroborated by the presence of immonium ions of Pro, Leu, and His, and

internal fragments such as HA and u_3H (where u_3 = homocysteine + 48). Interestingly, based on the relative signal intensities the yield of M1P3-SO₃H is four-fold and ~seven-fold higher at pH 3.30, compared to oxidation at pH 7.23 and 9.88, respectively (Fig. 2 and Table S2).

2.3.9. Formation of thioesters (M1P4a and M1P4b)

A photoproduct of M1 eluting at $t_R = 23.91$ min (Fig. 2, green trace) displays a molecular ion with m/z 404.72 ($z = 2$). This m/z may correspond to either M1P4a or M1P4b isomers. This photoproduct was only observed at pH 3.30, but not at pH 7.23 and 9.88. The molecular ion indicates an increase of 14 Da relative to M1. The LC-MS/MS spectrum of M1P4a/M1P4b (Fig. 11) displays immonium ions of Pro, Leu, and His, several internal fragments such as HA and LPLMH+14 and all the y -ions except for y_4 , which indicates that the chemical transformation targeted the Met residue. The molecular weight of M1P4a/M1P4b is consistent with the formation of a thioester, likely via reactions 6 (Scheme 1) and 14 (Scheme 2), respectively.

In order to confirm the formation of thioester from peptide M1, the photo-irradiated solution was incubated with NaBH₄ (Fig. 4), where the C=O of thioester may be reduced to an alcohol, similar to mechanism shown in Scheme 3. The reduced product will increase by 2 Da compared to M1P4 and give a molecular ion of 405.72 ($z = 2$), which is isobaric to MetO. After incubation, the peak corresponding to M1P4a/M1P4b disappeared. Since the reduced product is isobaric to MetO, it was difficult to identify it. Therefore, a separate derivatization experiment was carried out with GRT for 19 h at 37 °C in acidic pH, where C=O may form a hydrazone with GRT. However, we did not observe the derivatized product, instead higher yield of M1P3 was observed (Fig. 5). Because GRT derivatization was carried in acidic pH, M1P4b can undergo acid hydrolysis to give

M1P3 (reaction 16 Scheme 2). Similarly, M1P4a can also undergo acid hydrolysis to give M1P2 but our data did not indicate increase in M1P2.

2.3.10. 4-CB adducts on Met (M1P5a-d)

The photoproducts displaying molecular ions with m/z 510.72 ($z = 2$) (Fig. 1) are present in at least four distinct peaks referred to as (M1P5a-d) and correspond to an increase of 226 Da (mass of 4-CB) relative to M1. They elute at $t_R = 28.55, 29.05, 30.01,$ and 30.75 min. These peaks collectively represent 4-CB adducts either on the C3 or the C5 carbon of Met, which can be generated as various epimers. Such 4-CB adduct on Met have been reported previously.⁵⁵ Theoretically, we expected to observe four on the C3 carbon and two on the C5 carbon; as we can resolve only four distinct epimers, two of these epimer either do not form or co-elute with other epimers. Representative LC-MS/MS spectrum of M1P5b (Fig. 12) eluting at $t_R = 30.01$ min reveals the ions $y_1, y_2, y_3, y_4-H_2O, y_5-H_2O, y_6-H_2O,$ immonium ions of Pro, Leu, and His, and internal fragments such as HA, $MH+226-H_2O$; all of these ions indicate that the addition of 226 Da occurred on the Met residue of M1.

2.3.11. Formation of Met sulfoxide (M1P6a/M1P6b) and sulfone (M1P7)

The LC-MS chromatograms (Fig. 1) of control and photo-irradiated solutions of M1 and 4-CB displayed two peaks eluting at $t_R = 20.96$ and 21.23 min containing molecular ions with m/z 405.72 ($z = 2$), corresponding to an increase of 16 Da on M1. However, the photo-irradiated sample contained a higher intensity of these isobaric products. The LC-MS/MS spectra of these isobaric products (Fig. S7) were identical and revealed the ion series y_1 - y_6 , immonium ions of Pro, Leu, and His, and the internal fragments such as HA and $MH+16$, indicating an increase of 16 Da on the Met residue of M1. These isobaric products likely represent two MetO diastereomers.

In addition, the photo-irradiated solution also revealed a peak eluting at $t_R = 27.17$ min displaying a molecular ion with m/z 413.72 ($z = 2$), which corresponds to addition of 32 Da relative to peptide M1. The LC-MS/MS spectrum (Fig. S8) of this peak displays the ion series y_1 - y_6 , indicating that the increase of 32 Da occurred on the Met residue of M1. In addition, the presence of immonium ions of Pro, Leu, and His residue indicates that these residues are not modified, and the presence of internal fragments such as HA and MH+32 further solidifies our observation that the Met residue is modified. The increase in 32 Da is consistent with the formation of M1P7.

2.3.12. Formation of His oxidation products (M1P8 and M1P9)

The photo-irradiation of M1 and 4-CB leads to two peaks eluting at $t_R = 28.04$ and 29.27 min, displaying isobaric molecular ions with m/z 826.37 ($z = 1$), corresponding to an increase of 32 Da relative to M1. The LC-MS/MS spectra of these peaks (Fig. S9) are identical and display the ion series b_2 - b_6 and the b_5 - H_2O , indicating an addition of 32 Da to the His residue. This is corroborated by the absence of a His immonium ion, and the presence of immonium ions of Pro, Leu and Met. The two isobaric products (M1P18a and M1P8b) likely represent a 2,4-dihydroxy derivative of His and/or an endoperoxide, likely generated through the addition of singlet oxygen to His.⁵⁶ Singlet oxygen can be generated under our experimental condition through reaction of *4-CB with O_2 .⁵⁷⁻⁵⁸

Additional photoproduct (M1P7), eluting at $t_R = 45.85$ min, displays a molecular ion with m/z 808.4 ($z = 1$), corresponding to an increase of 14 Da relative to peptide M1. The LC-MS/MS spectrum (Fig. S10) of this peak displays the ion series b_2 - b_5 , which indicate that the increase of 14 Da occurred on the His residue. This is corroborated by absence of a His immonium ion and of

the internal fragment HA. The mass increase of 14 on M1P9 is consistent with the formation of 4-alkyl-2H-imidazol-2-one (see Chart 2), a commonly observed His oxidation product.

2.4. Discussion

The photo-irradiation of M1 and 4-CB formed a series of photoproducts that were identified by LC-MS/MS analysis. Peptide M1 contains two reactive amino acids (Met and His) in its sequence and we detected the photoproducts of Met were in higher yield compared to photoproducts of His. While generation of most of the Met photoproducts were proposed via $\text{Met}^{\bullet}\text{S}^{\bullet+}$, photoproducts in His may be generated via singlet oxygen. This is explained by the two types of photo-oxidation of 4-CB, where type I generates $\text{Met}^{\bullet}\text{S}^{\bullet+}$ after abstraction of an electron by 4-CB and in type II photo-oxidation triplet state 4-CB transfers energy to a molecular oxygen generating singlet oxygen.⁵⁹ The formation of $\text{Met}^{\bullet}\text{S}^{\bullet+}$, a key intermediate in our study, can be stabilized by nearby heteroatoms (N, O or S) forming 2c-3e bond, identified by pulse radiolysis.³¹⁻³²

The hydrogen on C3 or C5 carbons of $\text{Met}^{\bullet}\text{S}^{\bullet+}$ is deprotonated forming a carbon-centered radical, which can react readily with oxygen under air. These stable intermediates are important for the transformation of Met to photoproducts. However, under Ar these carbon-centered radicals do not react with oxygen to give oxidation products. As such, these carbon-centered radicals react more readily with 4-CB to give M1P5(a-d) photoproducts (Fig. 12). We have observed that the intensities of 4-CB adduct on Met residues are higher under Ar than under air. Apart from the role of oxygen to form these photoproducts of Met and His, we also looked into the effect of pH on the products formation at pH 3.30, 7.23, and 9.88. We detected a higher yield of photoproducts and new peaks at pH 3.30 compared to pH 7.23 and 9.88 (Table S2). This is likely because of the initial formation of 4-CB radical anion is protonated and back electron transfer is prohibited, therefore

generating more Met>S•+ and subsequently more photoproducts. One of the photoproducts detected was a cross-link product, M1P1a/M1P1b, which has not been reported previously.

2.4.1. Formation of M1P1a/M1P1b

Among many Met photoproducts observed, formation of the cross-link product M1P1a/M1P1b was the most notable product detected after photo-irradiation. M1P1a/M1P1b is characterized by the loss of CH₃SH from Met residue, formation of aldehyde on C3 carbon of oxidized Met, and attack by nitrogen of imidazole on aldehyde forming a cross-link. While there are studies on hydrolysis between Met and His in hGH and IgG1 as well as the effects of Met oxidation in IgG1 on binding ability of His with FcRn, no direct cross-link formation between Met and His side chains was reported previously. Considering the frequency of Met-His sequence in proteins, a mechanistic study for M1P1a/M1P1b formation is thoroughly studied.

The LC-MS/MS spectrum of M1P1a/M1P1b (Fig. 3B) indicates the formation of a cross-link product (section. 3.3). M1P1a/M1P1b formation involves multistep pathways and is initiated after the diffusion-controlled reaction between carbon-centered radical at C3 position of Met residue and a molecular oxygen forming a peroxy radical (reaction 4, Scheme 1). Two of these peroxy radicals combine and undergo Russell mechanism to give M1P4, a molecular oxygen, and an alcohol product, one of the intermediates of M1P1a/M1P1b (reactions 5 and 6, Scheme 1). We detected M1P4 in the LC-MS chromatogram at pH 3.30. At higher pHs, M1P4 may have hydrolyzed faster to give aspartic acid (M1P2), which was observed in all pHs. The detection of these two products in LC-MS chromatogram solidifies our proposed mechanism. Further, to form M1P1a/M1P1b, the alcohol intermediate forms an aspartate semialdehyde (M1P1) after loss of CH₃SH (reaction 7, Scheme 1). The emission of CH₃SH from Met has been studied earlier.⁶⁰ A

nucleophilic reaction occurs when nitrogen of imidazole attacks M1P1 forming a cross-link product, M1P1a/M1P1b (reaction 8, Scheme 1). The formation of M1P1a/M1P1b is also corroborated by our studies on isotopically labelled peptides M2 and M3. When C5 on Met was labelled with ^{13}C in M2, a cross-link product was observed with no change in m/z in comparison to M1P1a/M1P1b depicting loss of this carbon during the formation of the product as we have proposed in our mechanism. In addition, three nitrogen on His were isotopically labelled in M3, and after photo-irradiation a cross-link product with increase in 3 Da was observed (Fig. 6) indicating no loss of mass from His. Notably, M1P1a/M1P1b also undergoes loss of a water molecule in LC-MS (reaction 9, Scheme 1), which seems to be a common phenomenon on our MS settings as we also observed loss of water in the LC-MS/MS spectrum of 4-CB adducts on Met (Fig. 12) when an alcohol group was formed.

Few cross-links in proteins have been reported in the literature, mainly due to difficulty in identifying them without prior knowledge of mechanisms of formation, sites of cross-linking, and lack of MS data search engines.⁴⁶ Covalent chemical cross-linking is of major concern in biotherapeutics as it can lead to non-reducible aggregates and result in loss of biological activity and increase immunogenicity.⁴³⁻⁴⁵ This can affect the product quality, safety, and clinical efficacy. For example, previous studies reported on cross-linking formation of His-His cross-link, which may have resulted in a non-reducible aggregate.⁴⁶ His is also known to cross-link with other amino acids, such as Lys and Cys.⁶¹ Identification of cross-links may provide insight into the pathogenesis of conditions such as Alzheimer⁶²⁻⁶³ and cataract⁶³⁻⁶⁴ as protein aggregation is known to be a key factor in their development. Therefore, it is crucial to identify these non-reducible cross-links and understand their underlying mechanism; also, development of the cross-link identifying software from MS data can ease the process of identifying novel cross-links.

2.5. Conclusions

This chapter reports on the formation of a novel cross-link product between modified Met and His in a model peptide along with other Met and His oxidation products after photo-irradiation with 4-CB. The mechanism and supporting experiments for the cross-link formation are provided in detail. The mechanism primarily involves the formation of sulfur radical cation on Met residue leading to a radical on C3 carbon, loss of methanethiol (CH_3SH), and formation of an aldehyde, which is attacked by nitrogen on imidazole to form the cross-link product. Such modification on Met is irreversible and can change the structure and functionality of proteins. The prevalence of Met and His sequence in therapeutic proteins and their importance in protein efficacy make this sequence interesting and important.

2.6. References

1. Davies, M. J., The oxidative environment and protein damage. *Biochim. Biophys. Acta* **2005**, *1703* (2), 93-109.
2. Li, S.; Schoneich, C.; Borchardt, R. T., Chemical instability of protein pharmaceuticals: Mechanisms of oxidation and strategies for stabilization. *Biotechnol. Bioeng.* **1995**, *48* (5), 490-500.
3. Torosantucci, R.; Schöneich, C.; Jiskoot, W., Oxidation of Therapeutic Proteins and Peptides: Structural and Biological Consequences. *Pharm. Res.* **2014**, *31* (3), 541-553.
4. Chumsae, C.; Gaza-Bulseco, G.; Sun, J.; Liu, H., Comparison of methionine oxidation in thermal stability and chemically stressed samples of a fully human monoclonal antibody. *J. Chromatogr. B* **2007**, *850* (1-2), 285-294.
5. Anbanandam, A.; Bieber Urbauer, R. J.; Bartlett, R. K.; Smallwood, H. S.; Squier, T. C.; Urbauer, J. L., Mediating molecular recognition by methionine oxidation: conformational switching by oxidation of methionine in the carboxyl-terminal domain of calmodulin. *Biochemistry* **2005**, *44* (27), 9486-96.
6. Gao, J.; Yin, D. H.; Yao, Y.; Sun, H.; Qin, Z.; Schöneich, C.; Williams, T. D.; Squier, T. C., Loss of conformational stability in calmodulin upon methionine oxidation. *Biophys. J.* **1998**, *74* (3), 1115-1134.
7. Dalle-Donne, I.; Rossi, R.; Giustarini, D.; Gagliano, N.; Di Simplicio, P.; Colombo, R.; Milzani, A., Methionine oxidation as a major cause of the functional impairment of oxidized actin. *Free Radic. Biol. Med.* **2002**, *32* (9), 927-37.
8. Dow, L. K.; Changela, A.; Hefner, H. E.; Churchill, M. E., Oxidation of a critical methionine modulates DNA binding of the Drosophila melanogaster high mobility group protein, HMG-D. *FEBS Lett.* **1997**, *414* (3), 514-20.
9. Glaser, C. B.; Morser, J.; Clarke, J. H.; Blasko, E.; McLean, K.; Kuhn, I.; Chang, R. J.; Lin, J. H.; Vilander, L.; Andrews, W. H.; Light, D. R., Oxidation of a specific methionine in thrombomodulin by activated neutrophil products blocks cofactor activity. A potential rapid mechanism for modulation of coagulation. *J. Clin. Invest.* **1992**, *90* (6), 2565-73.
10. Lu, H. S.; Fausset, P. R.; Narhi, L. O.; Horan, T.; Shinagawa, K.; Shimamoto, G.; Boone, T. C., Chemical modification and site-directed mutagenesis of methionine residues in recombinant human granulocyte colony-stimulating factor: effect on stability and biological activity. *Arch. Biochem. Biophys.* **1999**, *362* (1), 1-11.
11. Teh, L. C.; Murphy, L. J.; Huq, N. L.; Surus, A. S.; Friesen, H. G.; Lazarus, L.; Chapman, G. E., Methionine oxidation in human growth hormone and human chorionic somatomammotropin. Effects on receptor binding and biological activities. *J. Biol. Chem.* **1987**, *262* (14), 6472-7.
12. Uversky, V. N.; Yamin, G.; Souillac, P. O.; Goers, J.; Glaser, C. B.; Fink, A. L., Methionine oxidation inhibits fibrillation of human alpha-synuclein in vitro. *FEBS Lett.* **2002**, *517* (1-3), 239-44.

13. Wood, M. J.; Becvar, L. A.; Prieto, J. H.; Melacini, G.; Komives, E. A., NMR structures reveal how oxidation inactivates thrombomodulin. *Biochemistry* **2003**, *42* (41), 11932-42.
14. Valley, C. C.; Cembran, A.; Perlmutter, J. D.; Lewis, A. K.; Labello, N. P.; Gao, J.; Sachs, J. N., The methionine-aromatic motif plays a unique role in stabilizing protein structure. *J. Biol. Chem.* **2012**, *287* (42), 34979-91.
15. Reid, K. S. C.; Lindley, P. F.; Thornton, J. M., Sulphur-aromatic interactions in proteins. *FEBS Lett.* **1985**, *190* (2), 209-213.
16. Vanacore, R.; Ham, A. J.; Voehler, M.; Sanders, C. R.; Conrads, T. P.; Veenstra, T. D.; Sharpless, K. B.; Dawson, P. E.; Hudson, B. G., A sulfilimine bond identified in collagen IV. *Science* **2009**, *325* (5945), 1230-4.
17. Bertolotti-Ciarlet, A.; Wang, W.; Lownes, R.; Pristatsky, P.; Fang, Y.; McKelvey, T.; Li, Y.; Li, Y.; Drummond, J.; Prueksaritanont, T.; Vlasak, J., Impact of methionine oxidation on the binding of human IgG1 to Fc Rn and Fc gamma receptors. *Mol. Immunol.* **2009**, *46* (8-9), 1878-82.
18. Brot, N.; Weissbach, H., Biochemistry and physiological role of methionine sulfoxide residues in proteins. *Arch Biochem Biophys* **1983**, *223* (1), 271-81.
19. Zhang, X. H.; Weissbach, H., Origin and evolution of the protein-repairing enzymes methionine sulfoxide reductases. *Biol. Rev. Camb. Philos. Soc.* **2008**, *83* (3), 249-57.
20. Gao, X.; Ji, J. A.; Veeravalli, K.; Wang, Y. J.; Zhang, T.; McGreevy, W.; Zheng, K.; Kelley, R. F.; Laird, M. W.; Liu, J.; Cromwell, M., Effect of individual Fc methionine oxidation on FcRn binding: Met252 oxidation impairs FcRn binding more profoundly than Met428 oxidation. *J. Pharm. Sci.* **2015**, *104* (2), 368-77.
21. Pan, H.; Chen, K.; Chu, L.; Kinderman, F.; Apostol, I.; Huang, G., Methionine oxidation in human IgG2 Fc decreases binding affinities to protein A and FcRn. *Protein Sci.* **2009**, *18* (2), 424-33.
22. Bobrowski, K.; Holcman, J., Formation and stability of intramolecular three-electron SN, SS, and SO bonds in one-electron-oxidized simple methionine peptides. Pulse radiolysis. *J. Phys. Chem.* **1989**, *93* (17), 6381-6387.
23. Hiller, K.; Masloch, B.; Goebel, M.; Asmus, K., Mechanism of the hydroxyl radical induced oxidation of methionine in aqueous solution. *J. Am. Chem. Soc.* **1981**, *103* (10), 2734-2743.
24. Mozziconacci, O.; Arora, J.; Toth, R. T. t.; Joshi, S. B.; Zhou, S.; Volkin, D. B.; Schoneich, C., Site-Specific Hydrolysis Reaction C-Terminal of Methionine in Met-His during Metal-Catalyzed Oxidation of IgG-1. *Mol. Pharm.* **2016**, *13* (4), 1317-28.
25. Mozziconacci, O.; Ji, J. A.; Wang, Y. J.; Schoneich, C., Metal-catalyzed oxidation of protein methionine residues in human parathyroid hormone (1-34): formation of homocysteine and a novel methionine-dependent hydrolysis reaction. *Mol. Pharm.* **2013**, *10* (2), 739-55.
26. Schoeneich, C.; Aced, A.; Asmus, K. D., Mechanism of oxidation of aliphatic thioethers to sulfoxides by hydroxyl radicals. The importance of molecular oxygen. *J. Am. Chem. Soc.* **1993**, *115* (24), 11376-11383.
27. Davies, M. J., Protein oxidation and peroxidation. *Biochem. J.* **2016**, *473* (7), 805-825.

28. Jensen, J. L.; Miller, B. L.; Zhang, X.; Hug, G. L.; Schöneich, C., Oxidation of Threonylmethionine by Peroxynitrite. Quantification of the One-Electron Transfer Pathway by Comparison to One-Electron Photooxidation. *J. Am. Chem. Soc.* **1997**, *119* (20), 4749-4757.
29. Lobachev, V. L.; Rudakov, E. S., The chemistry of peroxynitrite. Reaction mechanisms and kinetics. *Russ. Chem. Rev.* **2006**, *75* (5), 375.
30. Pryor, W. A.; Jin, X.; Squadrito, G. L., One-and two-electron oxidations of methionine by peroxynitrite. *Proceedings of the National Academy of Sciences* **1994**, *91* (23), 11173-11177.
31. Asmus, K.-D., Heteroatom-centered free radicals some selected contributions by radiation chemistry. In *StPTC*, Jonah, C. D.; Rao, B. S. M., Eds. Elsevier: 2001; Vol. 87, pp 341-393.
32. Asmus, K. D., Stabilization of oxidized sulfur centers in organic sulfides. Radical cations and odd-electron sulfur-sulfur bonds. *Acc. Chem. Res.* **1979**, *12* (12), 436-442.
33. Keck, R. G., The use of t-butyl hydroperoxide as a probe for methionine oxidation in proteins. *Anal. Biochem.* **1996**, *236* (1), 56-62.
34. Hug, G. L.; Bobrowski, K.; Kozubek, H.; Marciniak, B., Photo-oxidation of methionine-containing peptides by the 4-carboxybenzophenone triplet state in aqueous solution. Competition between intramolecular two-centered three-electron bonded (S...S)⁺ and (S...N)⁺ formation. *Photochem. Photobiol.* **2000**, *72* (1), 1-9.
35. Marciniak, B.; Hug, G. L.; Bobrowski, K.; Kozubek, H., Mechanism of 4-carboxybenzophenone-sensitized photooxidation of methionine-containing dipeptides and tripeptides in aqueous solution. *J. Phys. Chem.* **1995**, *99* (36), 13560-13568.
36. Wells-Knecht, M. C.; Lyons, T. J.; McCance, D. R.; Thorpe, S. R.; Baynes, J. W., Age-dependent increase in ortho-tyrosine and methionine sulfoxide in human skin collagen is not accelerated in diabetes. Evidence against a generalized increase in oxidative stress in diabetes. *J. Clin. Invest.* **1997**, *100* (4), 839-846.
37. Schey, K.; Patat, S.; Chignell, C.; Datillo, M.; Wang, R.; Roberts, J., Photooxidation of Lens α -Crystallin by Hypericin (Active Ingredient in St. John's Wort). *Photochem. Photobiol.* **2000**, *72* (2), 200-203.
38. Smith, J. B.; Jiang, X.; Abraham, E., Identification of hydrogen peroxide oxidation sites of α A- and α B-crystallins. *Free Radical Res.* **1997**, *26* (2), 103-111.
39. Finley, E. L.; Dillon, J.; Crouch, R. K.; Schey, K. L., Radiolysis-Induced Oxidation of Bovine α -Crystallin. *Photochem. Photobiol.* **1998**, *68* (1), 9-15.
40. Seppi, C.; Castellana, M. A.; Minetti, G.; Piccinini, G.; Balduini, C.; Brovelli, A., Evidence for membrane protein oxidation during in vivo aging of human erythrocytes. *Mech. Ageing Dev.* **1991**, *57* (3), 247-258.
41. Schöneich, C., Redox Processes of Methionine Relevant to β -Amyloid Oxidation and Alzheimer's Disease. *Arch. Biochem. Biophys.* **2002**, *397* (2), 370-376.
42. Vogt, W., Oxidation of methionyl residues in proteins: Tools, targets, and reversal. *Free Radical Biol. Med.* **1995**, *18* (1), 93-105.
43. Liu, H.; Gaza-Bulsecu, G.; Faldu, D.; Chumsae, C.; Sun, J., Heterogeneity of monoclonal antibodies. *J. Pharm. Sci.* **2008**, *97* (7), 2426-2447.

44. Beck, A.; Wagner-Rousset, E.; Ayoub, D.; Van Dorsselaer, A.; Sanglier-Cianferani, S., Characterization of therapeutic antibodies and related products. *Anal. Chem.* **2013**, *85* (2), 715-736.
45. Lispi, M.; Datola, A.; Bierau, H.; Ceccarelli, D.; Crisci, C.; Minari, K.; Mendola, D.; Regine, A.; Ciampolillo, C.; Rossi, M., Heterogeneity of commercial recombinant human growth hormone (r-hGH) preparations containing a thioether variant. *J. Pharm. Sci.* **2009**, *98* (12), 4511-4524.
46. Liu, M.; Zhang, Z.; Cheetham, J.; Ren, D.; Zhou, Z. S., Discovery and Characterization of a Photo-Oxidative Histidine-Histidine Cross-Link in IgG1 Antibody Utilizing 18O-Labeling and Mass Spectrometry. *Anal. Chem.* **2014**, *86* (10), 4940-4948.
47. Uniprot UniProtKB - Q9H2E6 (SEM6A_HUMAN).
<https://www.uniprot.org/uniprot/Q9H2E6>.
48. UniProt UniProtKB - A0A097PUH2 (A0A097PUH2_MOUSE).
<https://www.uniprot.org/uniprot/A0A097PUH2>.
49. UniProt UniProtKB - Q7Z351 (Q7Z351_HUMAN).
<https://www.uniprot.org/uniprot/Q7Z351>.
50. His, T., Cleavage, Deprotection, and Isolation of Peptides after Fmoc Synthesis.
51. Hatchard, C.; Parker, C. A., A new sensitive chemical actinometer-II. Potassium ferrioxalate as a standard chemical actinometer. *Proc. R. Soc. London, Ser. A* **1956**, *235* (1203), 518-536.
52. Lee, J.; Seliger, H., Quantum yield of the ferrioxalate actinometer. *J. Chem. Phys.* **1964**, *40* (2), 519-523.
53. Pozdnyakov, I. P.; Kel, O. V.; Plyusnin, V. F.; Grivin, V. P.; Bazhin, N. M., New insight into photochemistry of ferrioxalate. *J. Phys. Chem. A* **2008**, *112* (36), 8316-8322.
54. Guideline, I. H. T., Photostability testing of new drug substance and products. *Fed. Register* **1996**, *62*, 27115-27122.
55. Ignasiak, M. T.; Pedzinski, T.; Rusconi, F.; Filipiak, P.; Bobrowski, K.; Houée-Levin, C.; Marciniak, B., Photosensitized Oxidation of Methionine-Containing Dipeptides. From the Transients to the Final Products. *J. Phys. Chem. B* **2014**, *118* (29), 8549-8558.
56. Agon, V. V.; Bubb, W. A.; Wright, A.; Hawkins, C. L.; Davies, M. J., Sensitizer-mediated photooxidation of histidine residues: evidence for the formation of reactive side-chain peroxides. *Free Radic. Biol. Med.* **2006**, *40* (4), 698-710.
57. Miller, B. L.; Kuczera, K.; Schöneich, C., One-electron photooxidation of N-methionyl peptides. Mechanism of sulfoxide and azasulfonium diastereomer formation through reaction of sulfide radical cation complexes with oxygen or superoxide. *J. Am. Chem. Soc.* **1998**, *120* (14), 3345-3356.
58. Miller, B. L.; Williams, T. D.; Schöneich, C., Mechanism of sulfoxide formation through reaction of sulfur radical cation complexes with superoxide or hydroxide ion in oxygenated aqueous solution. *J. Am. Chem. Soc.* **1996**, *118* (45), 11014-11025.
59. Baptista, M. S.; Cadet, J.; Di Mascio, P.; Ghogare, A. A.; Greer, A.; Hamblin, M. R.; Lorente, C.; Nunez, S. C.; Ribeiro, M. S.; Thomas, A. H.; Vignoni, M.; Yoshimura, T. M., Type I and

Type II Photosensitized Oxidation Reactions: Guidelines and Mechanistic Pathways. *Photochem. Photobiol.* **2017**, *93* (4), 912-919.

60. Spasojevic, I.; Bogdanovic Pristov, J.; Vujisic, L.; Spasic, M., The reaction of methionine with hydroxyl radical: reactive intermediates and methanethiol production. *Amino Acids* **2012**, *42* (6), 2439-45.
61. Xu, C.-F.; Chen, Y.; Yi, L.; Brantley, T.; Stanley, B.; Sosic, Z.; Zang, L., Discovery and characterization of histidine oxidation initiated cross-links in an IgG1 monoclonal antibody. *Anal. Chem.* **2017**, *89* (15), 7915-7923.
62. Nemes, Z.; Devreese, B.; Steinert, P. M.; Van Beeumen, J.; Fesus, L., Cross-linking of ubiquitin, HSP27, parkin, and α -synuclein by γ -glutamyl- ϵ -lysine bonds in Alzheimer's neurofibrillary tangles. *FASEB J.* **2004**, *18* (10), 1135-1137.
63. Wang, S. S. S.; Wu, J. W.; Yamamoto, S.; Liu, H. S., Diseases of protein aggregation and the hunt for potential pharmacological agents. *Biotechnol. J.* **2008**, *3* (2), 165-192.
64. Balasubramanian, D.; Du, X.; Zigler Jr, J., The reaction of singlet oxygen with proteins, with special reference to crystallins. *Photochem. Photobiol.* **1990**, *52* (4), 761-768.

2.7. Charts and Figures

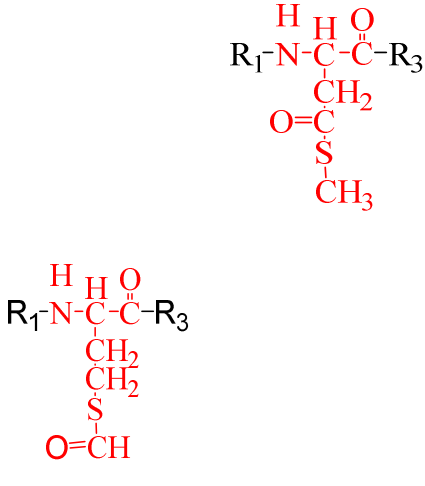
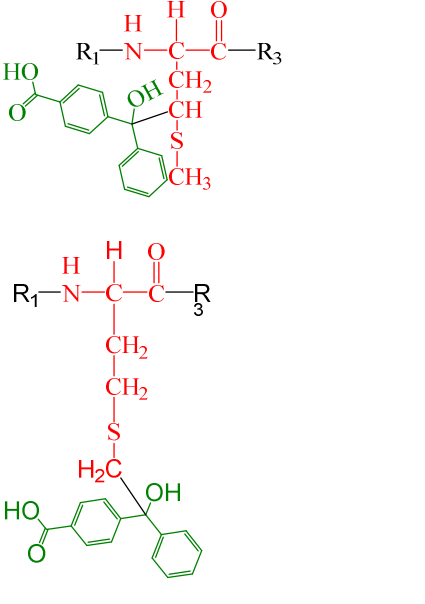
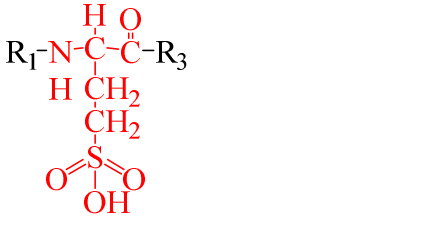
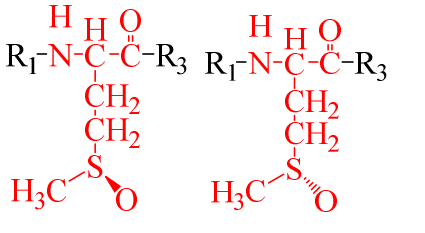
Chart 1: The structures and abbreviations of the model peptides synthesized to study the effect of photosensitization of 4-CB on Met and His containing peptides. R₁=LPL and R₂=AL

| Peptides Sequence | Abbreviation | Structure |
|----------------------------|--------------|-----------|
| LPLMHAL | M1 | |
| LPLM(¹³ C5)HAL | M2 | |
| LPLMH(¹⁵ N3)AL | M3 | |
| LPLMGHAL | M4 | |

| | | |
|-----------|----|--|
| LPLMGGHAL | M5 | |
|-----------|----|--|

Chart 2: The proposed structures of photoproducts generated after irradiation of M1 with 4-CB at $\lambda_{\max} = 350\text{nm}$ for 1 h. $R_1 = \text{LPL}$, $R_2 = \text{AL}$, and $R_3 = \text{HAL}$. P3a, P5a, P7a and P9a have similar structure as P1a and P3b, P5b, P7b and P9b have similar structure as P1b. P5a and 5b products contains three isotopically labelled nitrogen in His, P7a and P7b contains one Gly between Met and His, and P9a and P9b contains two Gly between Met and His (structures not shown).

| Photoproducts | Abbreviation | Proposed Structures | LC-MS/MS |
|---|------------------------------|---------------------|----------|
| Aspartate semialdehyde | M1P1 | | |
| Met-His cross-link | M1P1a/ M1P1b | | Fig. 3B |
| Loss of H ₂ O from M1P1a/M1P1b | M1P1a/M1P1b-H ₂ O | | Fig. S3A |
| Aspartic acid | M1P2 | | Fig. 9 |
| Homocysteine | M1P3 | | Fig. 10 |

| | | | |
|----------------------------|------------------------|--|---------|
| Thioester | M1P4a/ M1P4b |  | Fig. 11 |
| 4-CB adduct on Met | M1P5(a-d) |  | Fig. 12 |
| Homocysteine sulfonic acid | M1P3-SO ₃ H |  | Fig. S6 |
| Methionine sulfoxide | M1P6a/ M1P6b |  | Fig. S7 |

| | | | |
|---|------|---|----------|
| Methionine sulfone | M1P7 | $ \begin{array}{c} \text{H} \quad \text{H} \quad \text{O} \\ \quad \quad // \\ \text{R}_1\text{-N-C-C-R}_3 \\ \\ \text{CH}_2 \\ \\ \text{CH}_2 \\ \\ \text{O}=\text{S}=\text{O} \\ \\ \text{CH}_3 \end{array} $ | Fig. S8 |
| Histidine +32 | M1P8 | $ \begin{array}{c} \text{H} \quad \text{H} \quad \text{O} \quad \quad \text{O} \\ \quad \quad // \quad \quad // \\ \text{R}_1\text{-N-C-C-N-H-C-C-R}_2 \\ \quad \quad \quad \\ \text{CH}_2 \quad \quad \quad \text{CH}_2 \\ \quad \quad \quad \\ \text{CH}_2 \quad \quad \quad \text{OH} \\ \quad \quad \quad // \quad \quad \backslash \\ \text{S} \quad \quad \quad \text{N} \quad \quad \quad \text{NH} \\ \quad \quad \quad \backslash \quad \quad // \\ \text{CH}_3 \quad \quad \quad \text{O} \end{array} $ | Fig. S9 |
| 4-alkyl-2H-imidazol-2-one (Histidine+14) | M1P9 | $ \begin{array}{c} \text{H} \quad \text{H} \quad \text{O} \quad \quad \text{O} \\ \quad \quad // \quad \quad // \\ \text{R}_1\text{-N-C-C-N-H-C-C-R}_2 \\ \quad \quad \quad \\ \text{CH}_2 \quad \quad \quad \text{CH}_2 \\ \quad \quad \quad \\ \text{CH}_2 \quad \quad \quad \text{O} \\ \quad \quad \quad // \quad \quad \backslash \\ \text{S} \quad \quad \quad \text{N} \quad \quad \quad \text{N} \\ \quad \quad \quad \backslash \quad \quad // \\ \text{CH}_3 \quad \quad \quad \text{O} \end{array} $ | Fig. S10 |

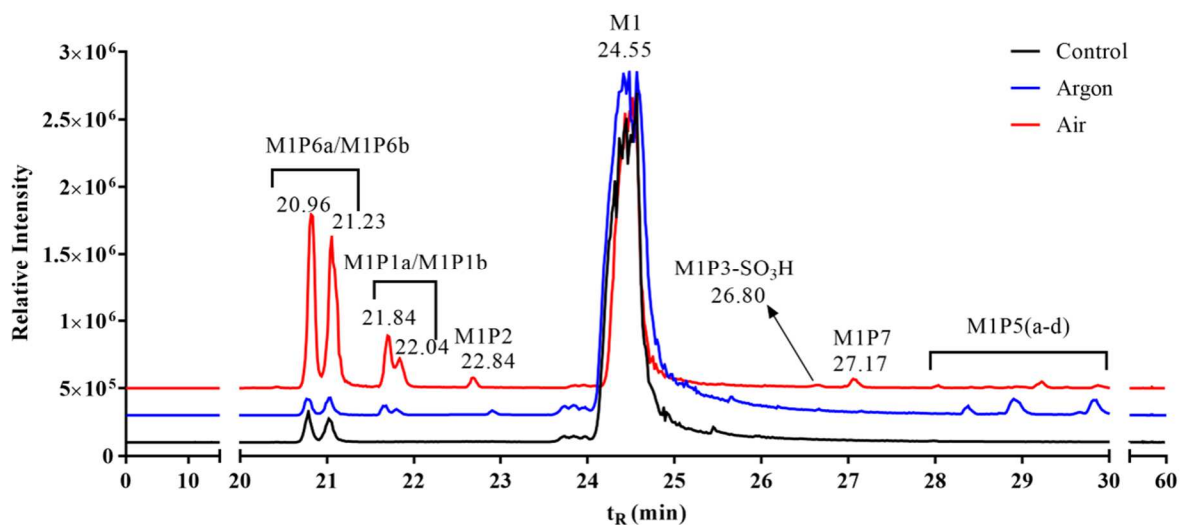


Figure 1: Full LC-MS chromatograms of photoproducts of peptide M1 and 4-CB in 10 mM phosphate buffer, pH 7.23 upon exposure to UV-A light with $\lambda_{\text{max}} = 350 \text{ nm}$ for 1 h under air (red-trace), argon (blue-trace) and aluminum wrapped control under air (black-trace). (Note: Refer to Chart 2 for the structures and names of the photoproducts).

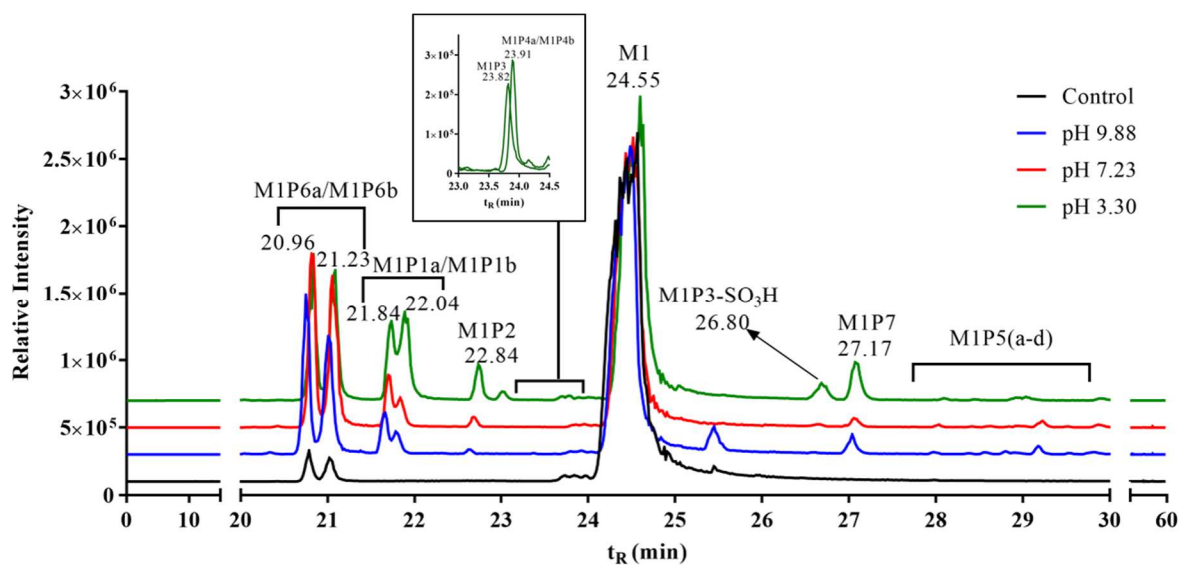


Figure 2: Full LC-MS chromatograms of photoproducts of peptide M1 and 4-CB in 10 mM phosphate buffer upon exposure to UVA light with $\lambda_{\max} = 350 \text{ nm}$ for 1 h under air at pH 3.30 (red-trace), pH 7.23 (blue-trace), pH 9.88 (red-trace), and aluminum wrapped control-at pH 3.30 (black-trace). Insert: XICs of M1P3 and M1P4a/m1P4b.

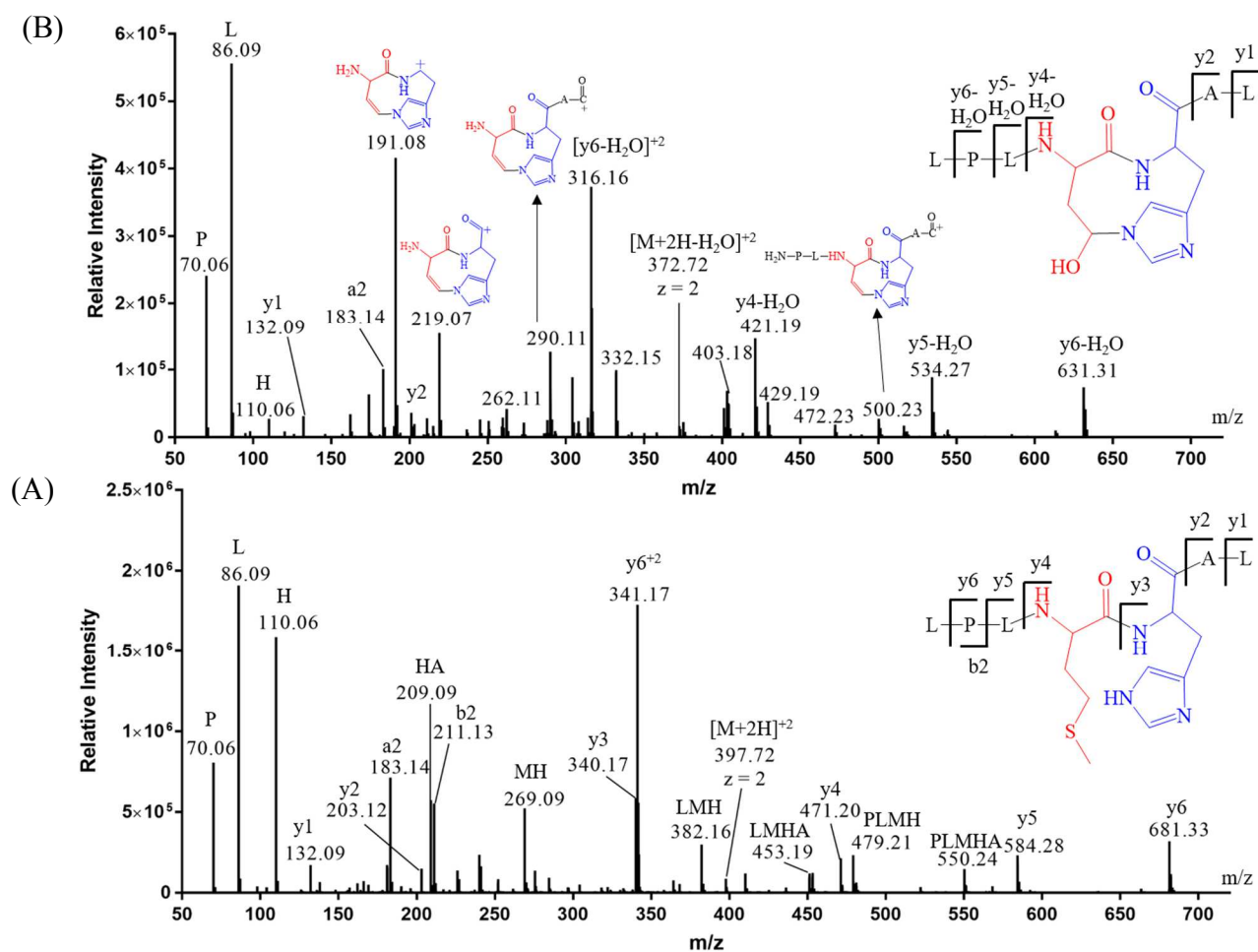


Figure 3: LC-MS/MS spectra of (A) unmodified M1 and (B) cross-link product, M1P1a/M1P1b, formed from peptide M1.

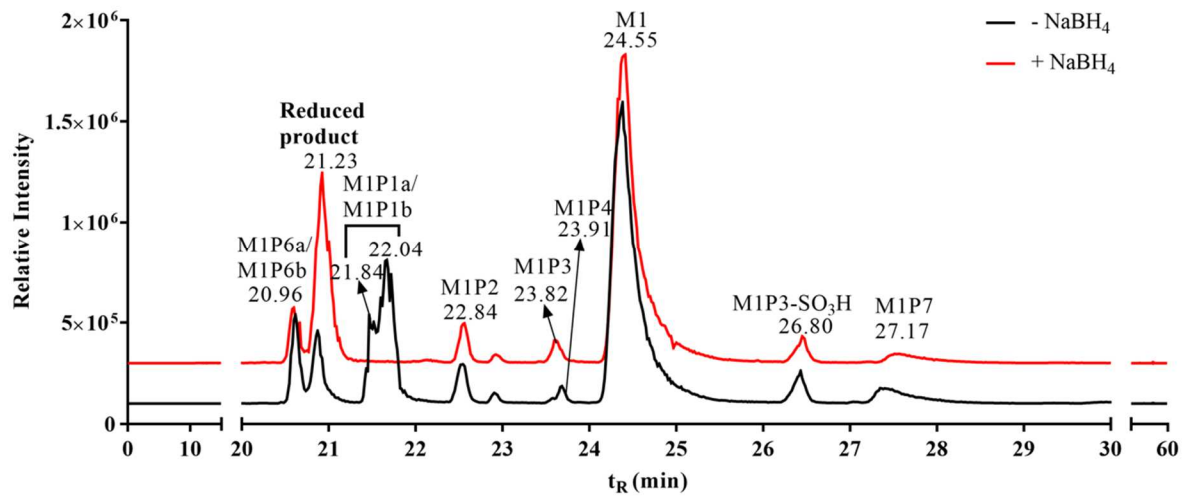


Figure 4: LC-MS full chromatograms of photo-irradiated M1: without NaBH₄ (black-trace) and with NaBH₄ (red-trace).

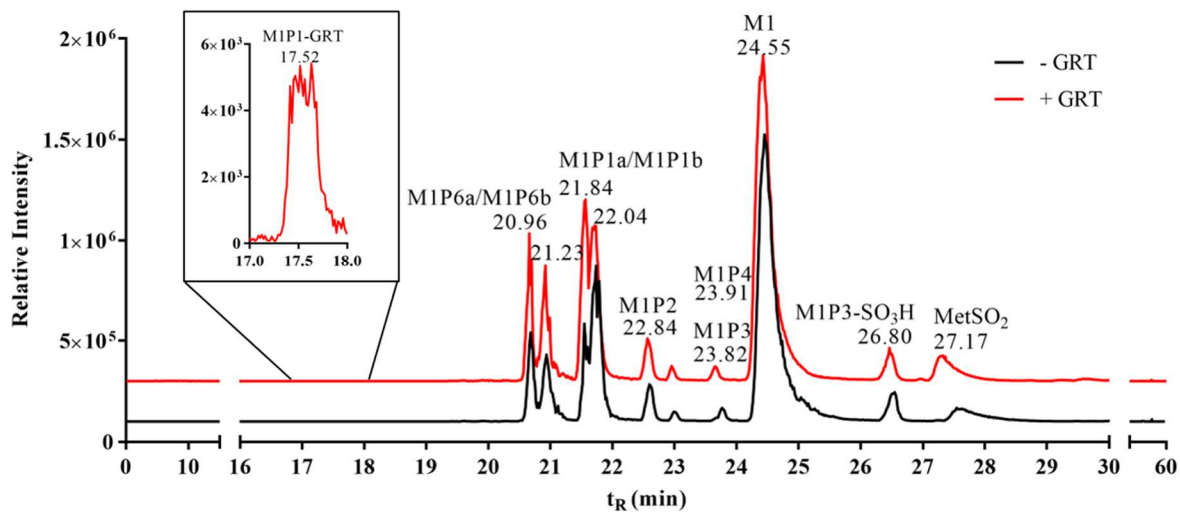


Figure 5: LC-MS full chromatograms of photo-irradiated M1: without GRT (black-trace) and with GRT (red-trace). Insert: XIC of a hydrazone formation between MIP1 and GRT.

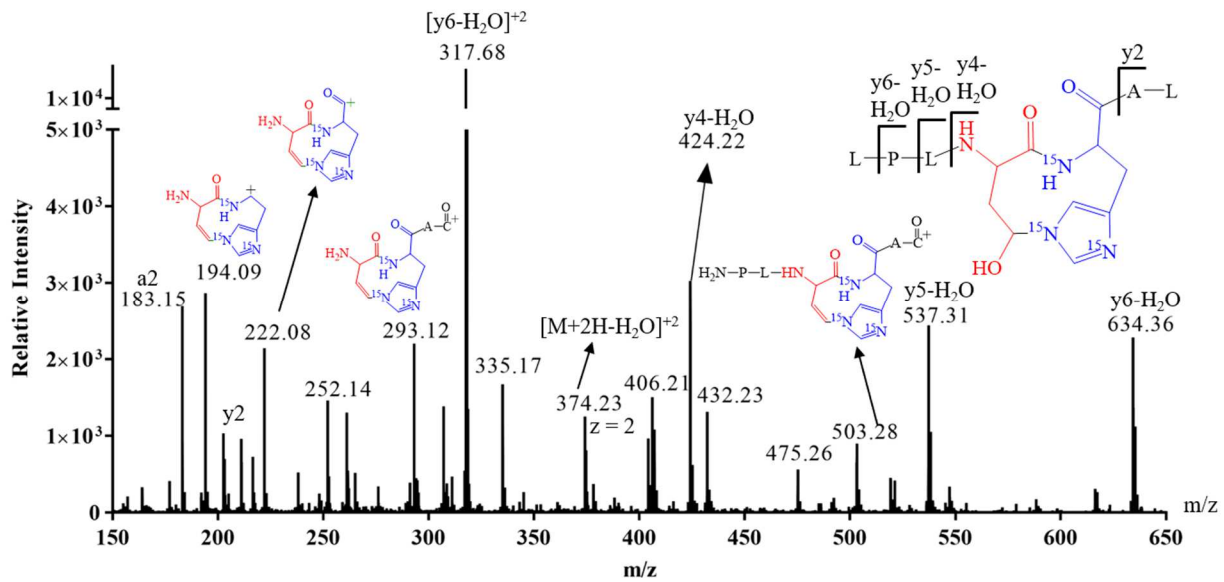


Figure 6: LC-MS/MS spectrum of M1P1a/M1P2-(¹⁵N₃), a cross-link with three isotopically labelled nitrogen in His, generated from M3 peptide.

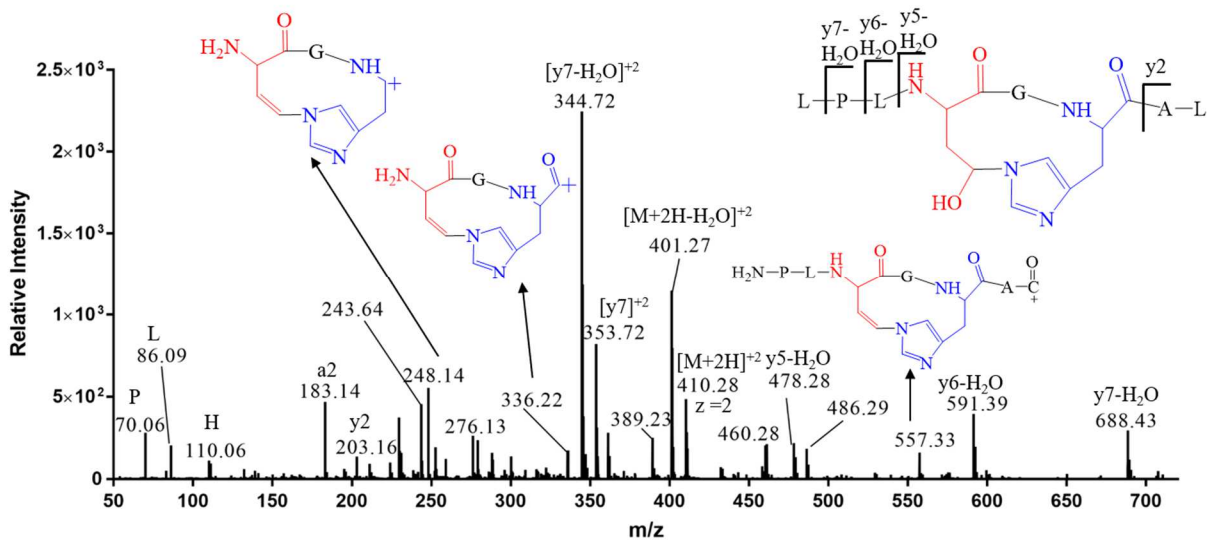


Figure 7: LC-MS/MS spectrum of M4P1a/M4P1b, a cross-link photoproduct formed from M4 peptide.

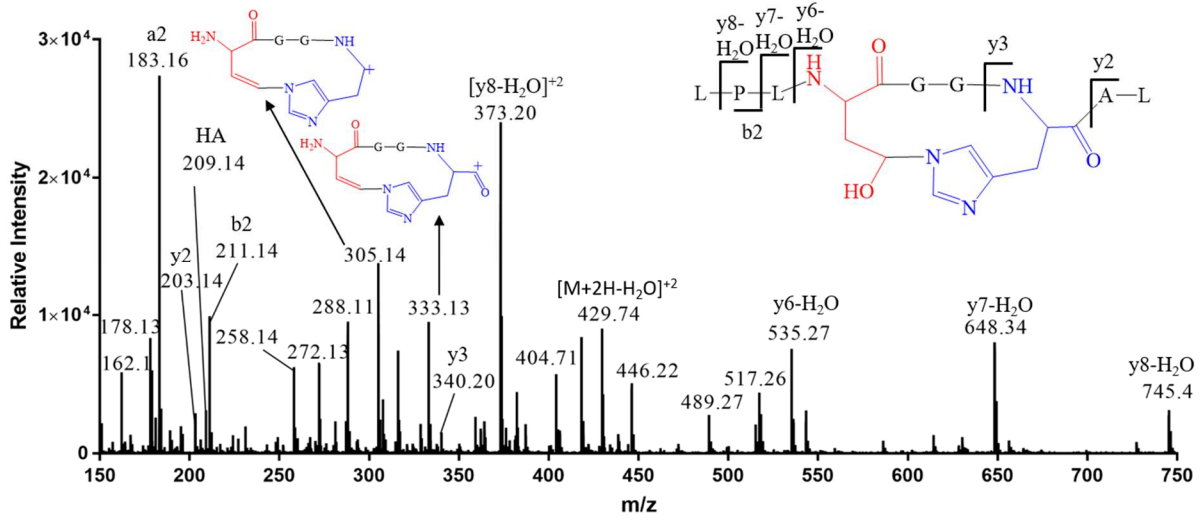


Figure 8: LC-MS/MS spectrum of M5P1a/M5P1b, a cross-link, formed from M5 peptide.

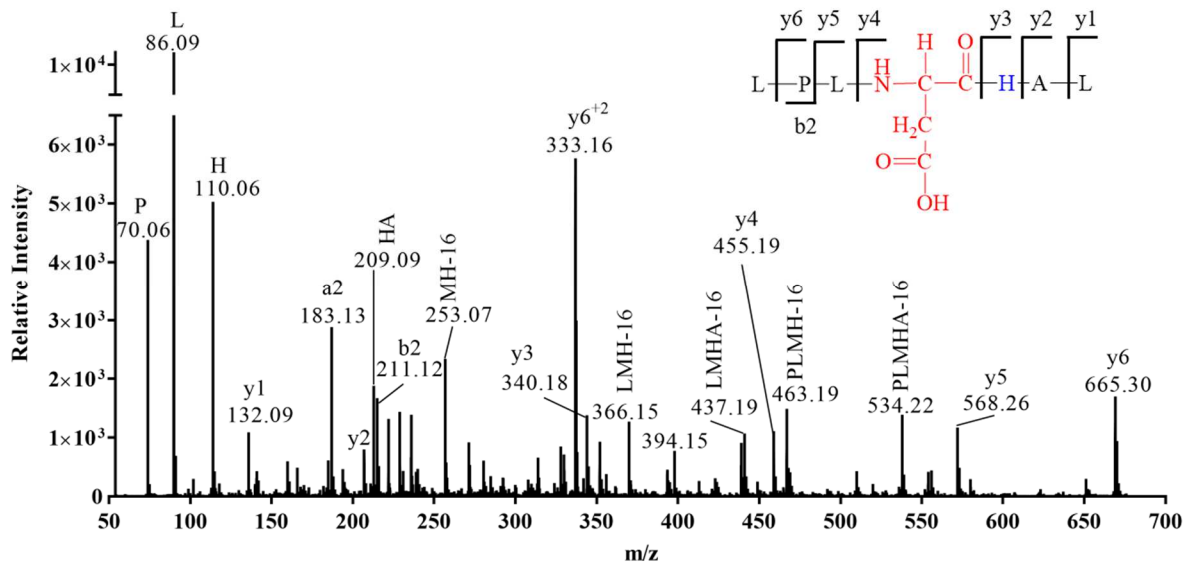


Figure 9: LC-MS/MS spectrum of M1P2.

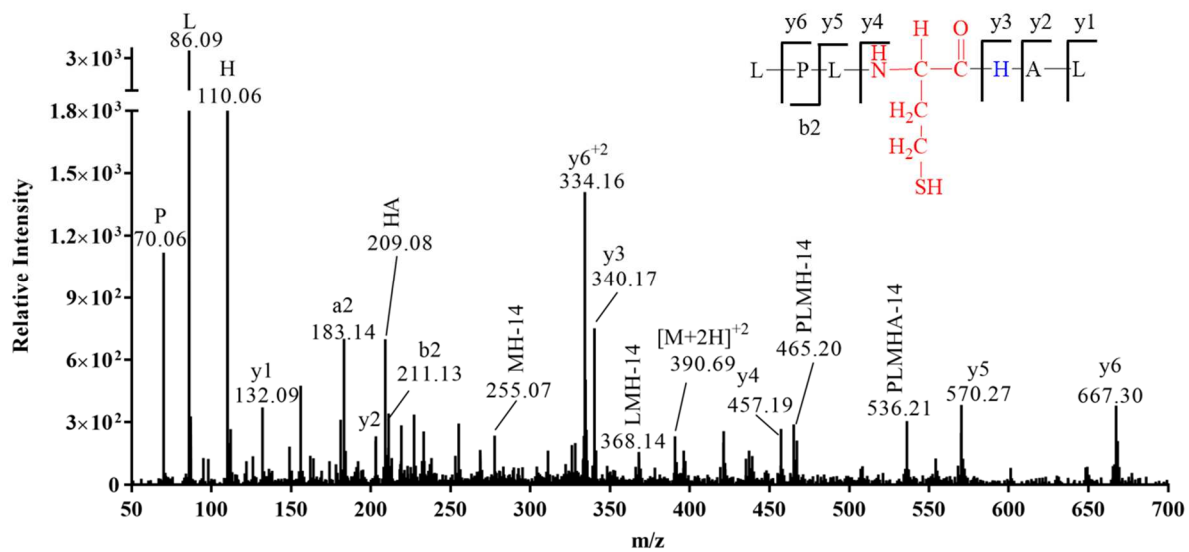


Figure 10: LC-MS/MS spectrum of M1P3.

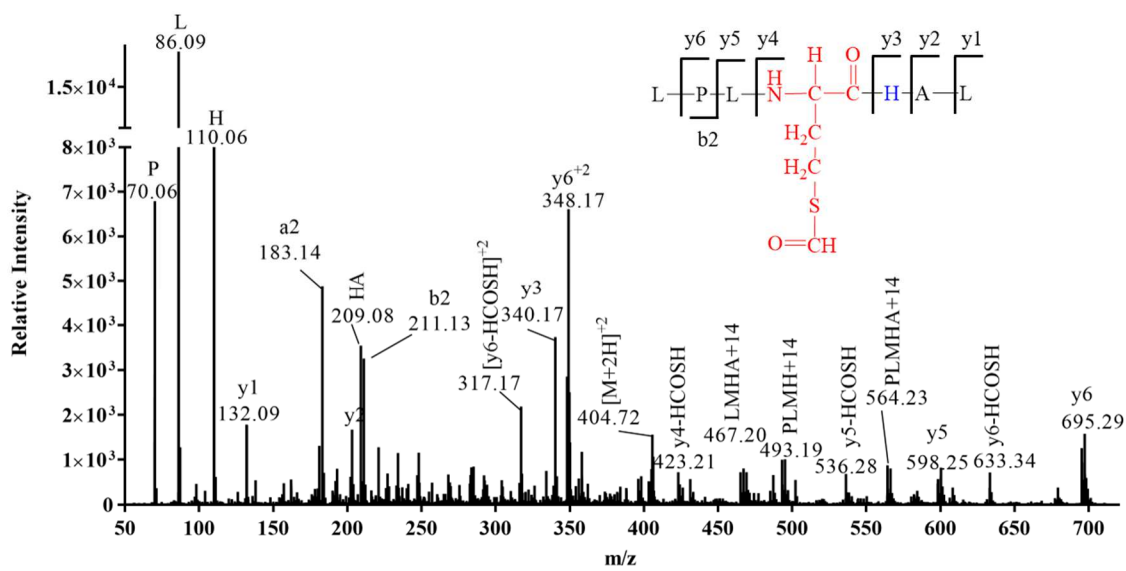


Figure 11: Representative LC-MS/MS spectrum of thioester (M1P4b).

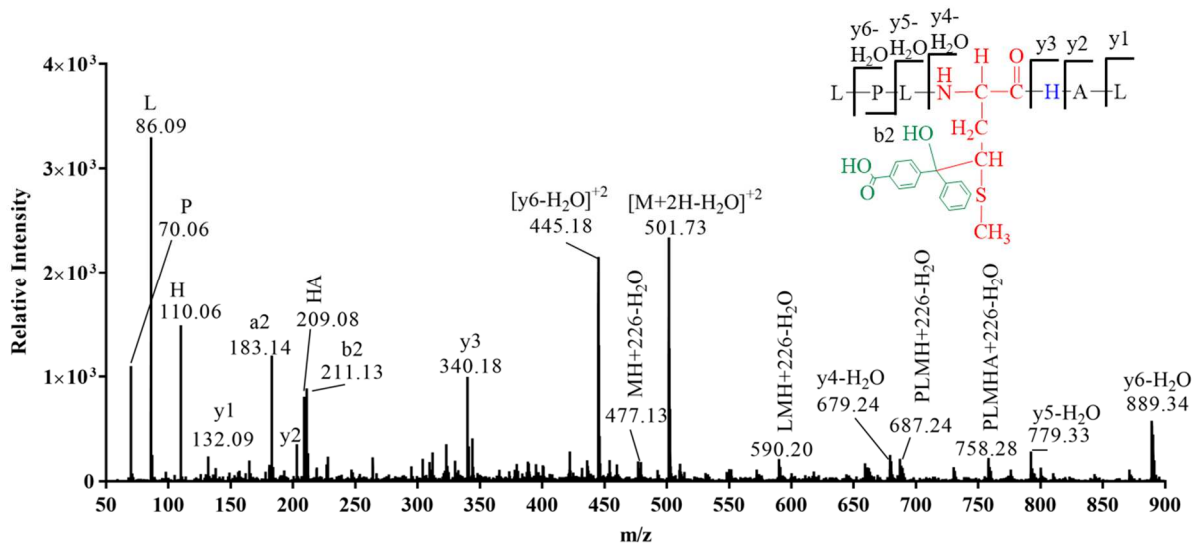
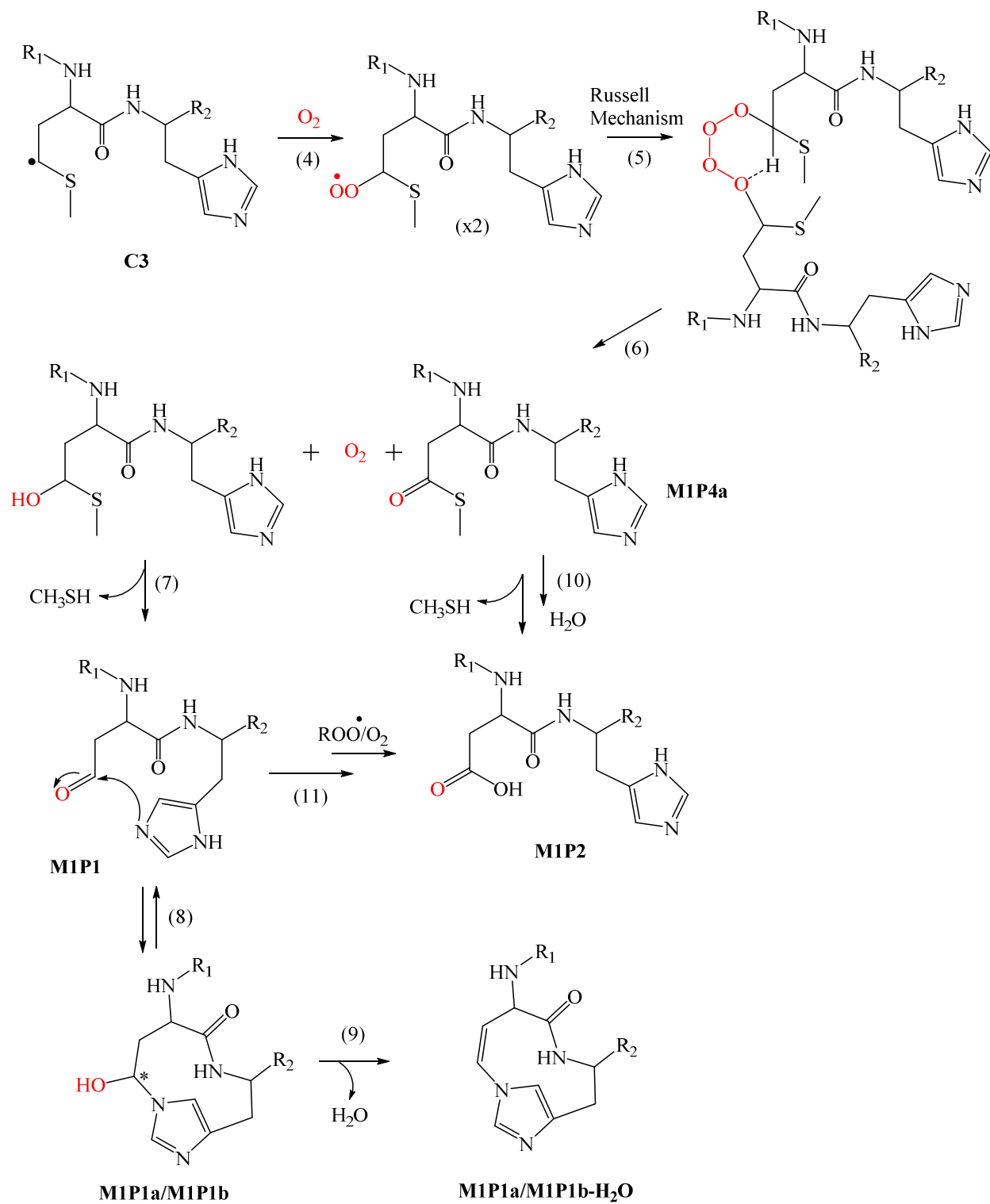
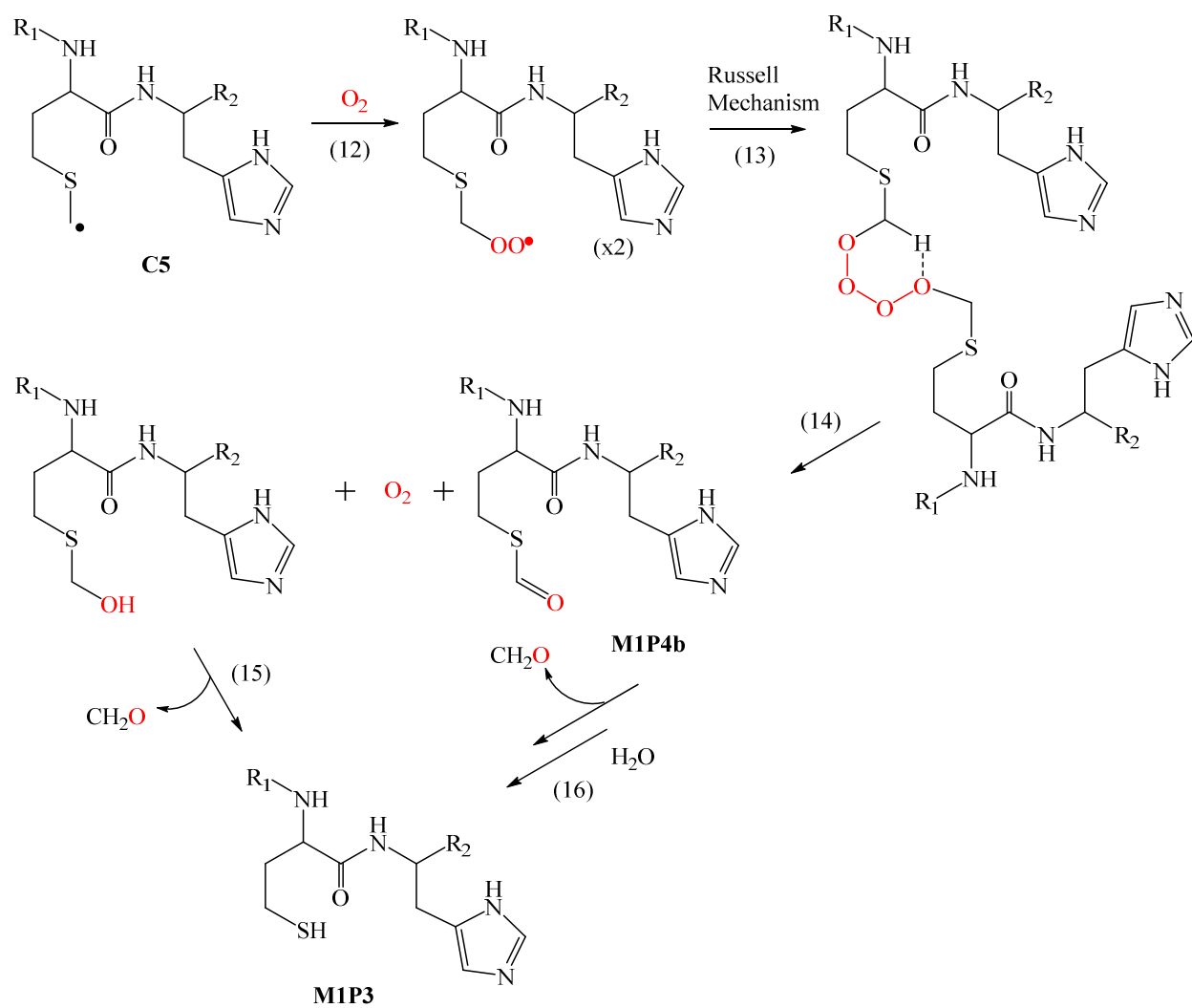


Figure 12: Representative LC-MS/MS spectrum of M1P5 at C3 position. This LC-MS/MS may also correspond to M1P5 at C3 position with other 3 different isomers and at C5 position.

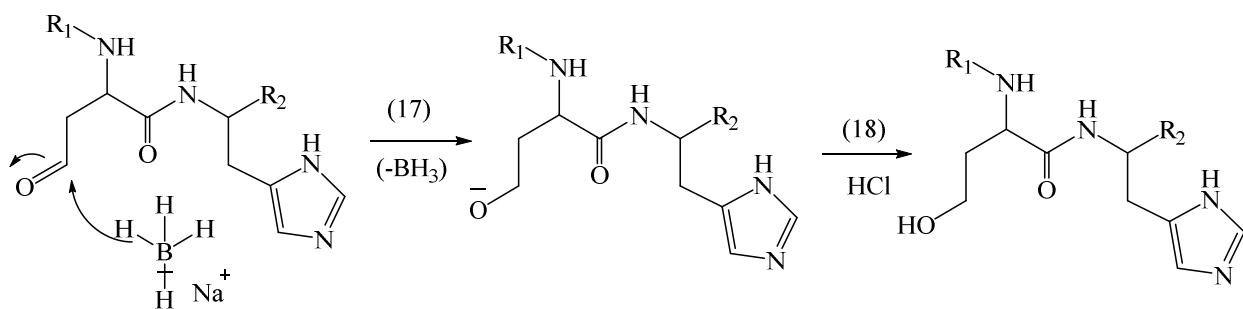
2.8. Schemes



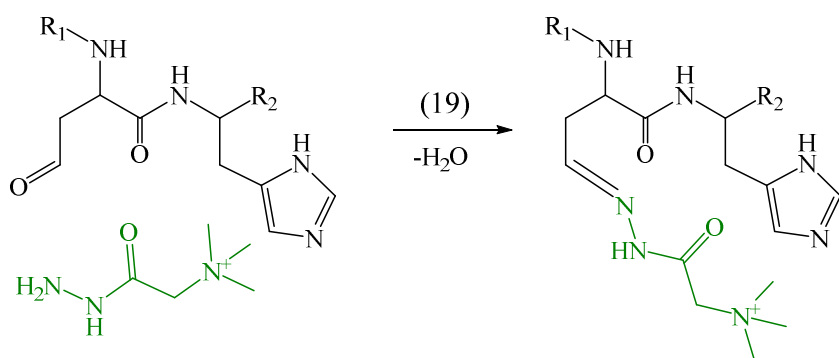
Scheme 1: Proposed mechanism of product formation: M1P1a, M1P1b, and M1P2. R₁ = LPL and R₂ = AL amino acids. Asterisk (*) represents chiral center.



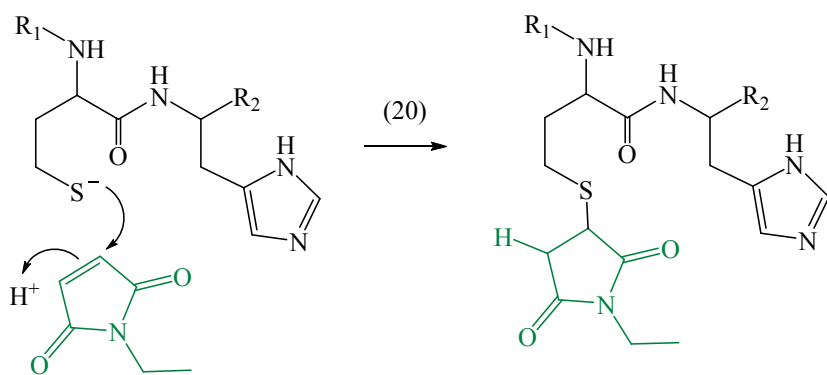
Scheme 2: Proposed mechanism of product formation: M1P4b and M1P3. $R_1 = \text{LPL}$ and $R_2 = \text{AL}$ amino acids.



Scheme 3: Proposed mechanism for the reduction of M1P1 with NaBH₄. R₁ = LPL and R₂ = AL amino acids.



Scheme 4: Proposed mechanism of derivatization of M1P1 with GRT. R₁ = LPL and R₂ = AL amino acids.



Scheme 5: Proposed mechanism of M1P3 derivatized with NEM. R₁ = LPL and R₂ = AL amino acids.

2.9. Supplementary Information

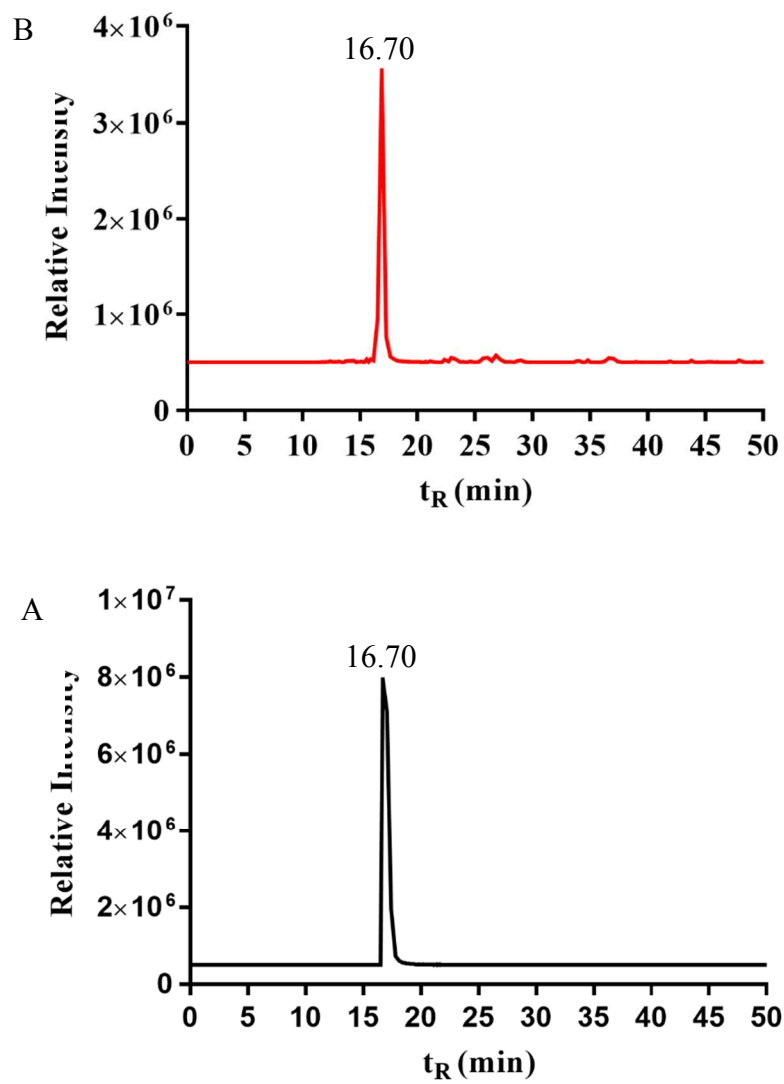


Figure S1: LC-MS chromatograms of (A) aluminum wrapped control LPLAHAL with 4-CB and (B) photo-irradiated LPLAHAL with 4-CB for 1 h at $\lambda_{\max} = 350$ nm.

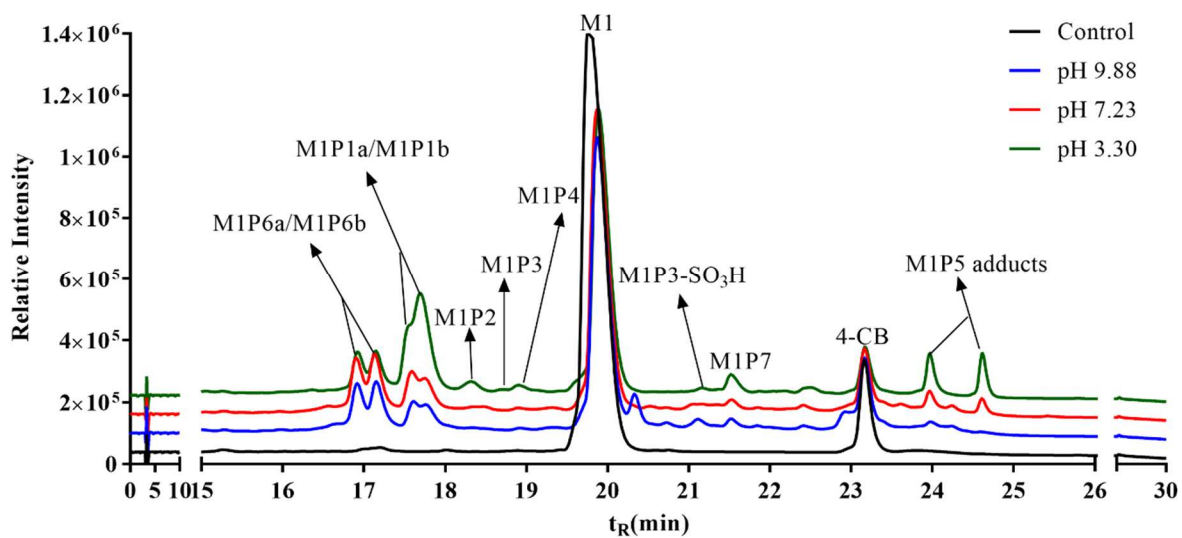


Figure S2: RP-HPLC chromatograms of photoproducts of peptide M1 and 4-CB in 10 mM phosphate buffer upon exposure to UV-A light with $\lambda_{\text{max}} = 350 \text{ nm}$ for 1 h under air at pH 3.30 (red-trace), pH 7.23 (blue-trace), pH 9.88 (red-trace), and aluminum wrapped control-at pH 3.30 (black-trace).

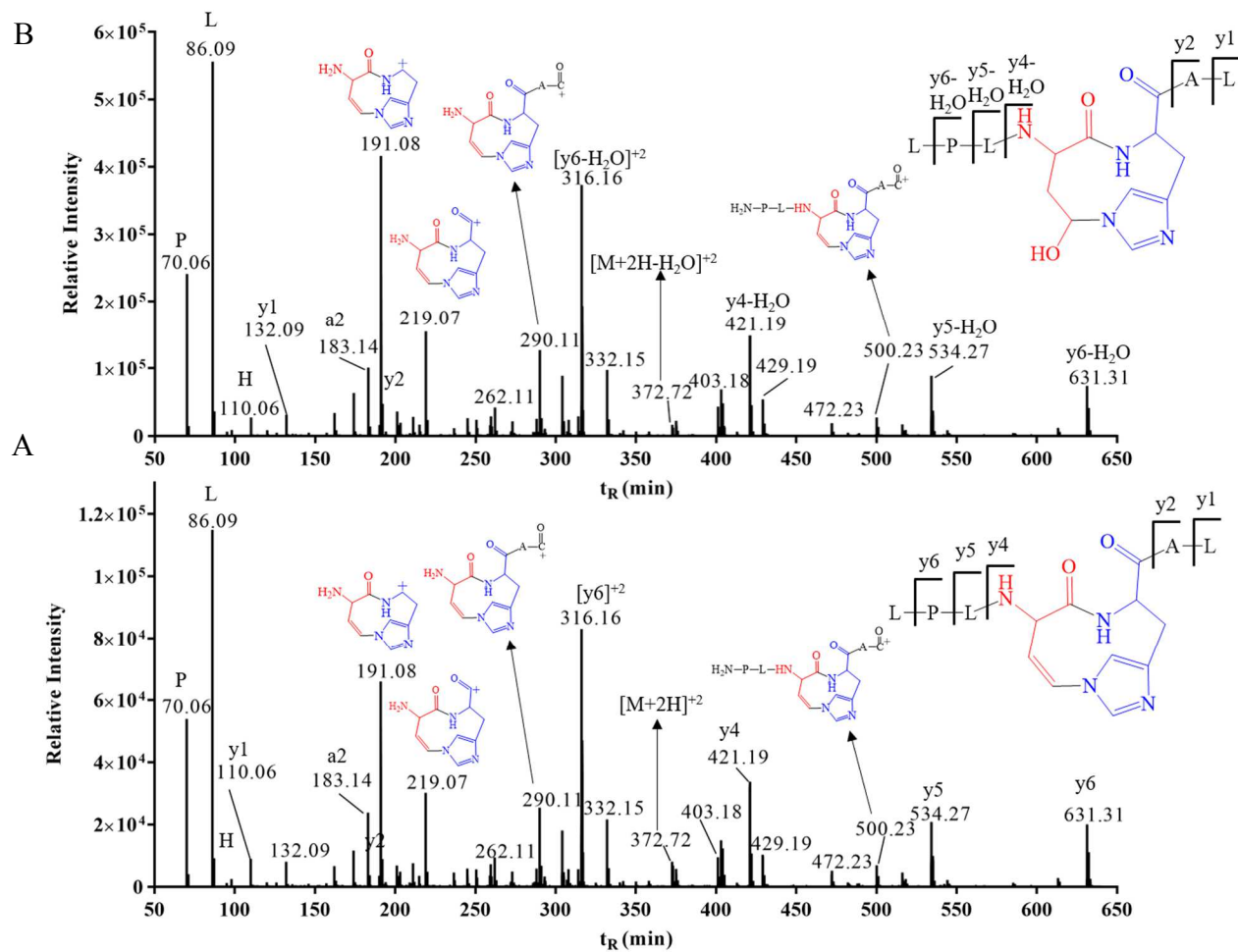


Figure S3: Comparison of LC-MS/MS spectra of (A) M1P1a/M1P1b-H₂O and (B) M1P1a/M1P1b.

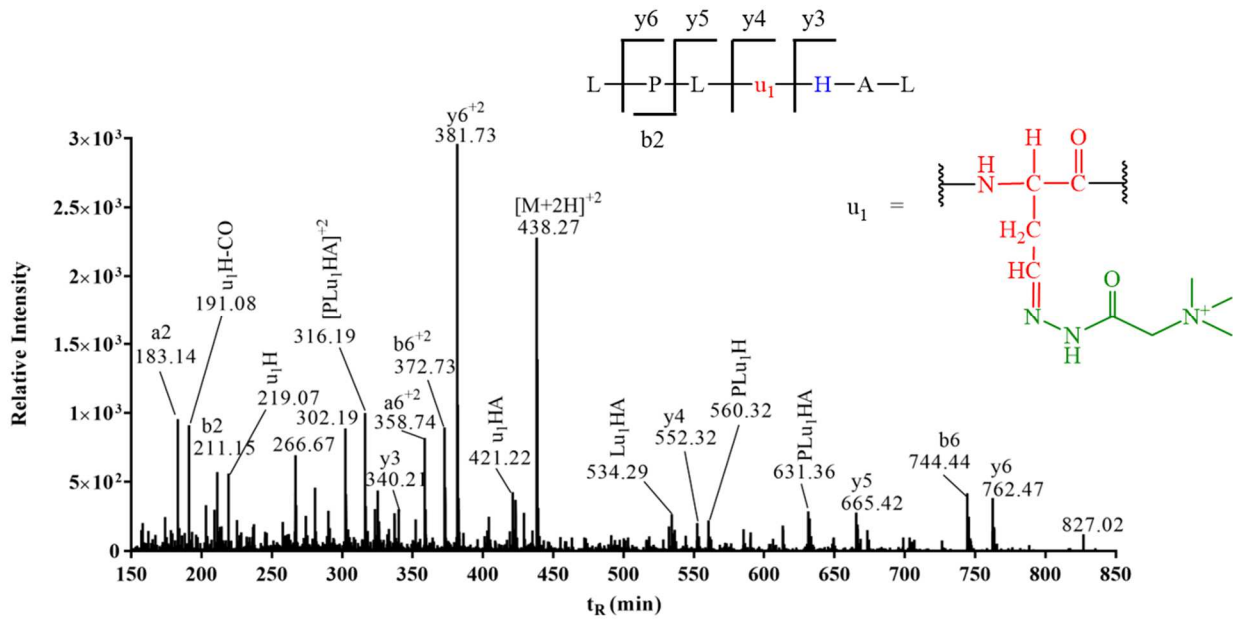


Figure S4: LC-MS/MS of M1P1-GRT derivatized product with m/z 438.27 ($z=2$), where u_1 = aspartate semialdehyde derivatized with GRT.

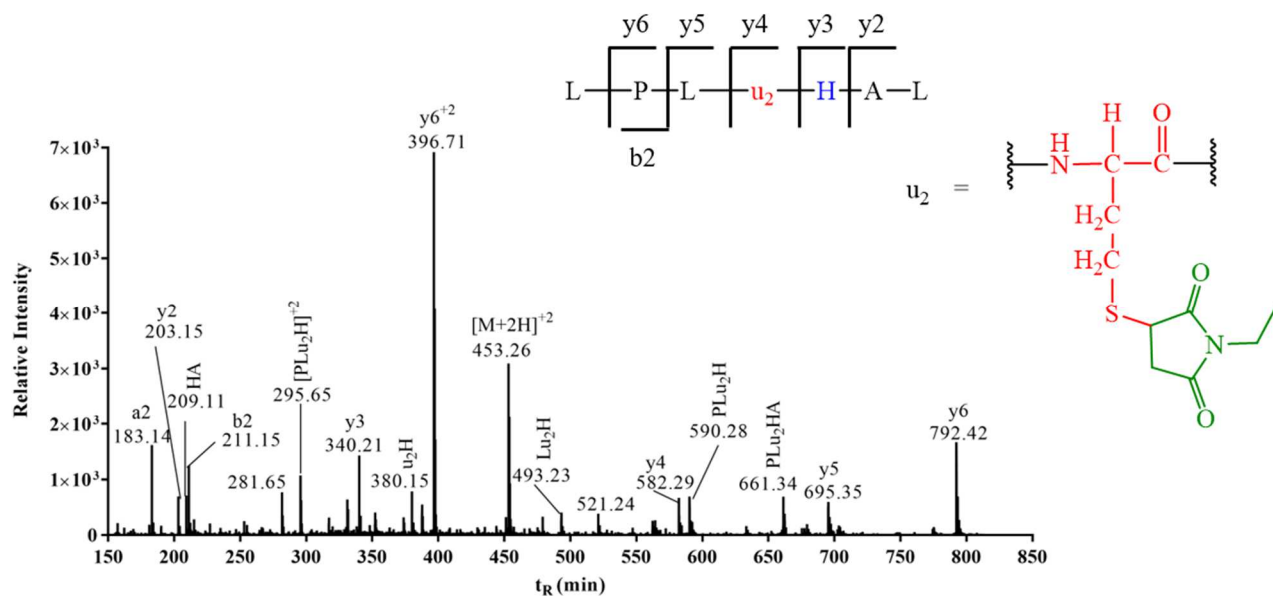


Figure S5: LC-MS/MS spectrum of M1P3-NEM alkylated product with m/z 453.26 ($z = 2$), where $u_2 =$ homocysteine alkylated with NEM.

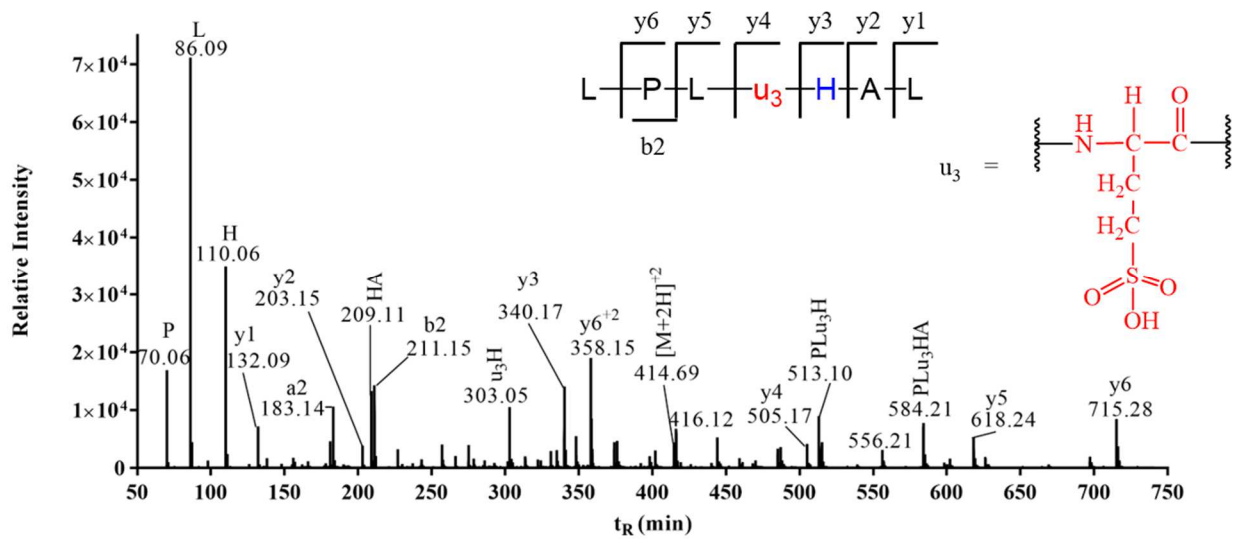


Figure S6: LC-MS/MS spectrum of M1P3-SO₃H with m/z 414.69 (z = 2), where u₃ = homocysteine sulfonic acid.

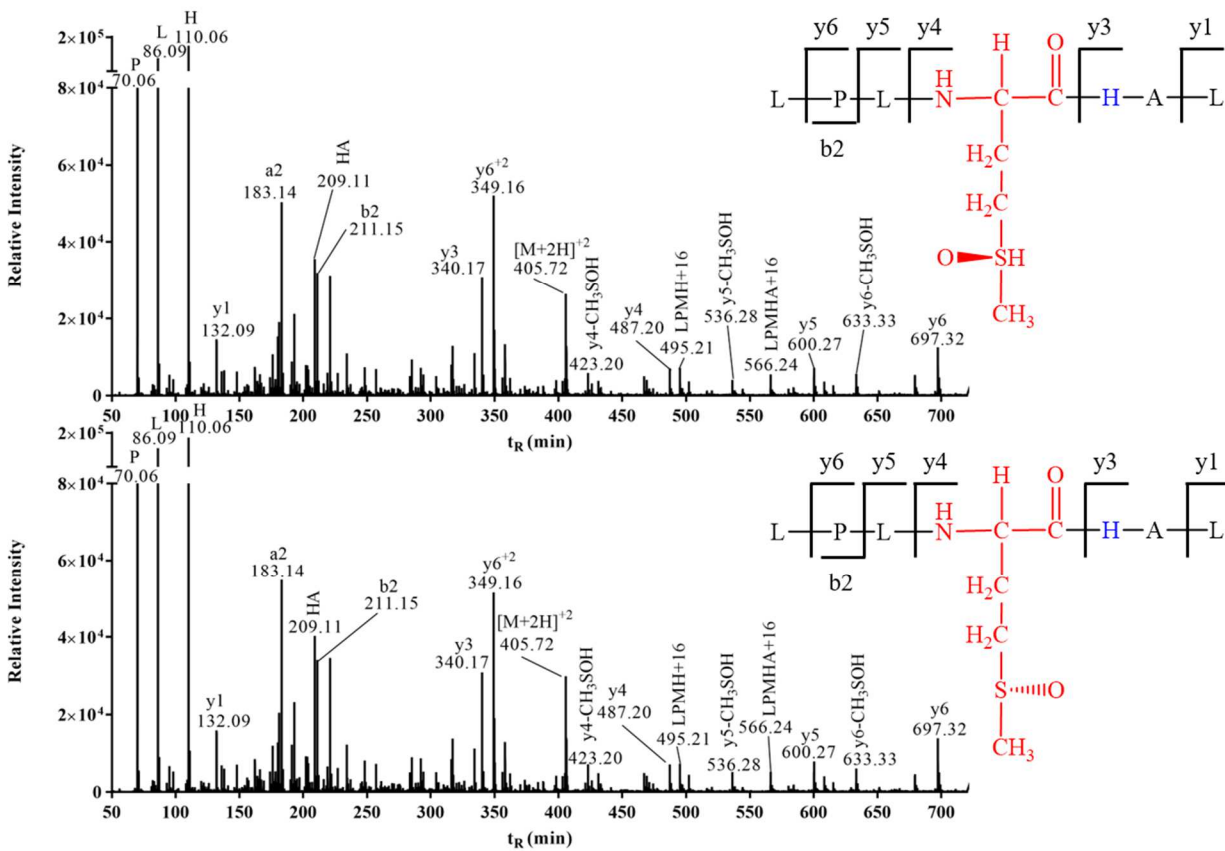


Figure S7: LC-MS/MS spectra of M1P6a/M1P6b diastereomers with m/z 405.72 ($z = 2$).

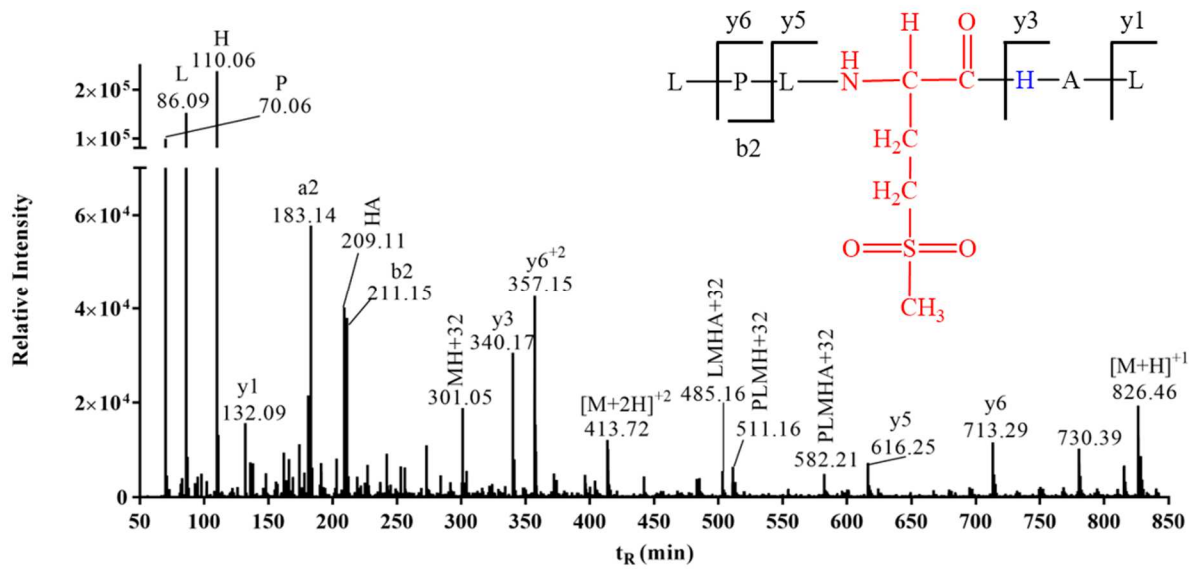


Figure S8: LC-MS/MS spectrum of M1P7 with m/z 413.72 ($z = 2$)

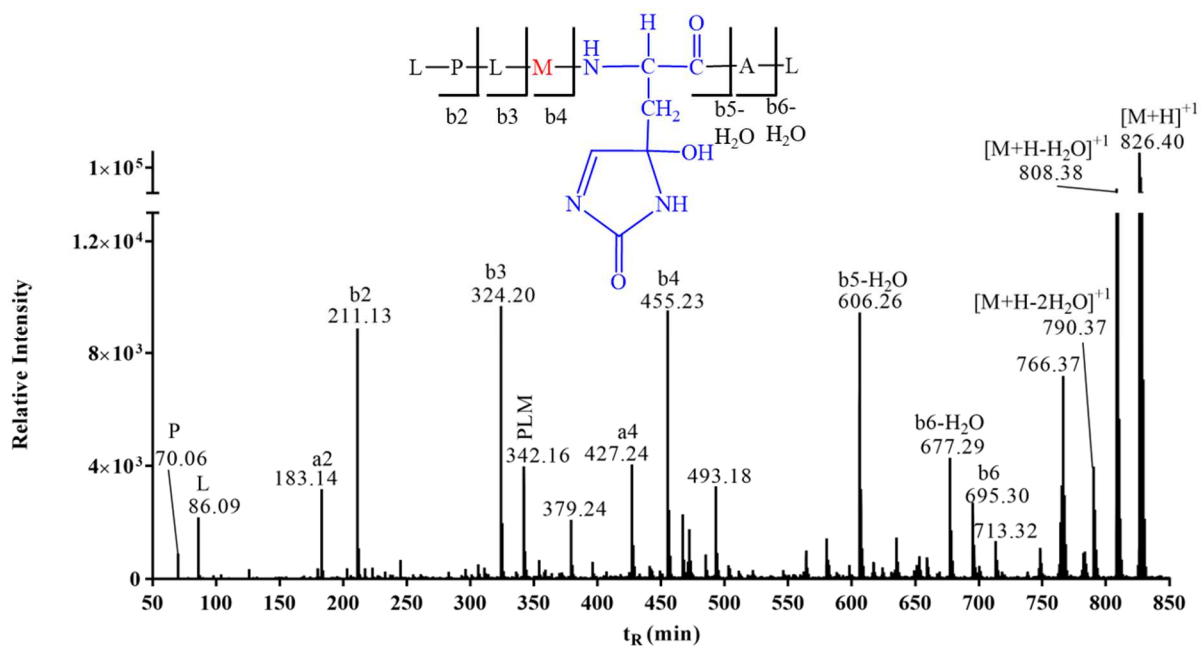


Figure S9: LC-MS/MS spectrum of M1P8 with m/z 826.40 ($z = 1$).

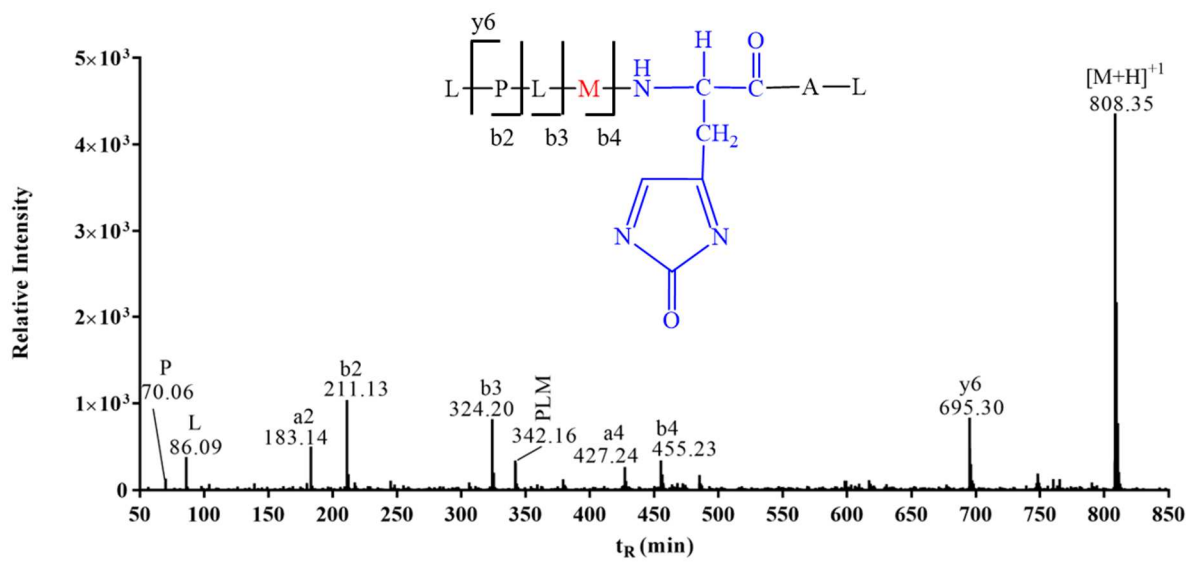


Table S1: The proposed photoproducts generated after photo-irradiation of M1 and 4-CB at λ_{max} = 350 nm for 1 h.

| Names of M1 photoproducts | Abbreviation | m/z | z |
|-----------------------------------|------------------------|------------|----------|
| Aspartate semialdehyde | M1P1a | 381.72 | 2 |
| Met-His cross-link | M1P1b | 381.72 | 2 |
| Aspartic acid | M1P2 | 389.72 | 2 |
| Homocysteine | M1P3 | 390.70 | 2 |
| Homocysteine sulfonic acid | M1P3-SO ₃ H | 414.72 | 2 |
| Thioester | M1P4a/M1P4b | 404.72 | 2 |
| 4-CB adducts | M1P5(a-d) | 510.72 | 2 |
| Methionine sulfoxide | M1P6a/M1P6b | 405.72 | 2 |
| Methionine sulfone | M1P7 | 413.72 | 2 |
| 2,4-dihydroxy-His or endoperoxide | M1P8 | 826.37 | 1 |
| 4-alkyl-2H-imidazole-2-one | M1P9 | 808.40 | 1 |

Table S2: Relative percent yield of unmodified peptide M1 remained and photoproducts formed after photo-irradiation of M1 and 4-CB at $\lambda_{\text{max}} = 350 \text{ nm}$ for 1 h.

| | pH 3.3 | pH 7.23 | pH 9.88 |
|------------------------|--------|---------|---------|
| M1 | 61.00 | 70.92 | 56.14 |
| M1P1a | 2.36 | 3.08 | 1.17 |
| M1P1b | 8.81 | 1.40 | 1.80 |
| M1P2 | 2.72 | 0.97 | 0.37 |
| M1P3 | 0.48 | 0.03 | 0.05 |
| M1P3-SO ₃ H | 1.83 | 0.47 | 0.28 |
| M1P4a/M1P4b | 0.43 | 0.00 | 0.11 |
| M1P5a | 0.11 | 0.10 | 0.11 |
| M1P5b | 0.19 | 0.24 | 0.26 |
| M1P5c | 0.32 | 0.48 | 0.32 |
| M1P5d | 0.16 | 0.22 | 0.17 |
| M1P6a | 8.43 | 9.78 | 9.83 |
| M1P6b | 9.33 | 10.76 | 9.58 |
| M1P7 | 3.84 | 0.93 | 1.45 |
| M1P8a | 0.00 | 0.16 | 0.17 |
| M1P8b | 0.00 | 0.40 | 18.10 |
| M1P9 | 0.00 | 0.07 | 0.10 |

Chapter 3: Visible light degradation of a monoclonal antibody in a high concentration formulation: characterization of a tryptophan-derived chromophoric photoproduct by comparison to photodegradation of N-acetyl-L-tryptophan amide

3.1. Introduction

The development and approval of biotherapeutics, especially monoclonal antibodies (mAbs), has been on the rise because of the high specificity and efficacy leading to enhanced patient safety.¹ Most commonly, mAbs are used for the treatment of cancer, autoimmune diseases, allergic diseases, asthma, and for organ transplants.²⁻⁴ mAbs have been formulated at low concentrations for intravenous infusion. Since this is time-consuming and requires the patient to be in a hospital setting, biopharmaceutical companies have been exploring other routes of administration such as subcutaneous (SC) injections, which can be administered by patients at home and require only a few minutes of injection time; as mAbs are formulated based on mg/kg and SC injections necessitate a small volume (<1.5 ml), mAbs for this route have to be formulated at concentrations above 100 mg/ml.⁵ At such high concentrations, viscosity problems are prominent and can complicate the injection process due to greater syringe back pressure and pain at the injection site.⁶⁻

⁷ The viscosity of mAbs can be overcome by the addition of salts (such as NaCl) and amino acids such as lysine (Lys), arginine (Arg), and histidine (His).⁸ This is accomplished either by electrostatic interactions or by interaction with aromatic amino acids. In particular, His has been used in marketed formulation of mAbs, as this can act as a buffer and simultaneously reduce viscosity.⁹ Other potential problems associated with high mAb concentrations are aggregation, oxidation, and color change.¹⁰ According to the International Conference on Harmonization (ICH) Q6B, color change is a critical quality attribute for drug release¹¹ and the protein formulation is expected to be clear to slightly yellow.¹² This is because an atypical color may indicate the presence of impurities, contaminants, degradation of the protein, and/or excipients, which may negatively impact patient health. Therefore, it is important to investigate the root cause of such atypical solution color and the mechanisms of color formation. Some of the color changes observed

so far are associated either with the components added to the culture media during manufacturing, or with degradation products generated after exposure to light or elevated temperature during storage.

During manufacturing, color changes in the culture fluid have been attributed mainly to three sources: (i) glucose (ii) B vitamins, and (iii) iron.¹³ When a high concentration of glucose is present in the culture media, glycation can occur, which may proceed to generate advanced glycation end products (AGEs).¹⁴ These can give rise to a yellow color to the solution.¹⁵ In addition, such AGEs may reduce the efficacy of a mAb or activate proinflammatory responses.¹⁶ The cell culture media also contains B vitamins, such as B₁₂ (cobalamine) and B₆ to increase antibody production. These vitamins can directly react with proteins or act as photosensitizers when exposed to light, leading to pink colored products.^{13, 17} The combination of iron with B vitamins can give a brown or brown-yellow color under aerobic cell culture conditions. This is likely due to reactive oxygen species (ROS), generated via Fenton reaction¹⁷⁻¹⁹ or photo-Fenton reaction,²⁰ which can oxidize proteins to chromophoric products. Specially the hydroxyl radical (HO•), a powerful oxidant, can convert tryptophan (Trp) to colored products such as N-formyl kynurenine (NFK) and kynurenine (Kyn).¹⁷⁻
¹⁸ More importantly, NFK and protein-bound Kyn are photosensitizers which can lead to secondary photooxidation.²¹⁻²⁵

During storage, previously colorless protein solutions may develop a yellow to brown-yellow color; such coloration is also observed after photostability testing to the recommendation of the ICH Q1B guideline (1.2 million lux hours of visible light and ≥ 200 Wh/m² of UV light).^{4, 10} Interestingly, such color change was also observed in highly concentrated mAb formulation during exposure to ambient light, at doses far below of that recommended by the ICH guideline.²⁶ This is an important observation as the essential aromatic acids or cystine will not absorb UV-A and

visible light; however, photoproducts such as Kyn can absorb light along with the B vitamins such as vitamins B₂ (riboflavin), B₆, B₉ (folic acid) and B₁₂ (cobalamine).²¹ The latter can act as photosensitizers via type I and type II reactions.²⁷ Apart from commonly known photoproducts of His and Trp, other products with chromophoric properties may be responsible for color in the formulation exposed to heat or light. One such product generated by the loss of 2 Da from Trp during storage at 25 °C for 12 months, displaying an absorption maximum at 335 nm.⁴ In addition, tyrosine derived photoproducts such as dihydroxyphenylalanine (DOPA)²⁸ may lead to the coloration of light exposed formulation. Studies on the yellowing of sheep wool²⁸ and lens proteins²⁹⁻³¹ have led to the identification of several Trp and Tyr-derived oxidation products such as carbolines, hydroxykynurenine, and DOPA.

In this chapter, we describe the formation of a chromophoric photoproduct of Trp during visible light exposure of a mAb in formulation containing sodium acetate (NaAc) or His/Lys buffer, and physical and chemical modifications accompanying yellow color formation. For structural characterization of the chromophoric photoproduct, we exposed a model compound, N-acetyl-L-tryptophan amide (NATA), to visible light photo-irradiation in sodium acetate buffer, followed by HPLC-mass spectrometry (MS) and nuclear magnetic resonance (NMR) analysis.

3.2. Materials and Methods

The mAb (mAbZ) for this study was obtained from AstraZenaca. NaAc, L-His monohydrochloride, L-Lys monohydrochloride, NATA, formic acid (FA), bis(2-mercaptoethyl)sulfone (BMS), iodoacetamide (IAA), and β -mercaptoethanol (β -ME) were purchased from Millipore Sigma (Burlington, MA). Borosilicate glass tubes, acetonitrile (ACN), Optima® water with FA, Optima® ACN with FA, acetic acid, and methanol were purchased from Fisher Scientific (Hampton, NH). All solutions were prepared using ultra-pure quality (18.2

MΩ) water, which was prepared freshly with a WaterPro PS Polishing System (Labconco, Kansas City, MO).

3.2.1. Sample preparation

The mAbZ formulation contained 0.01% PS80, 85 mM NaCl and was buffered in 50 mM NaAc at pH 5.5 (NaAc buffer). In order to prepare a formulation of mAbZ in His/Lys buffer, buffer exchange was performed with D-Tube™ Dialyzer Maxi (MWCO 3.5 kDa) in a container containing 2 L of 20 mM HisCl and 75 mM Lys at pH 5.50 (His/Lys buffer) for 2 h at 4 °C. Then, the dialyzer containing mAbZ was transferred into a 5 L container of His/Lys buffer, pH 5.5, and was dialyzed overnight at 4 °C. The samples were frozen at -80 °C until further experiments were performed. Solutions of 10 mM NATA either in NaAc, pH 5.5, or in His/Lys buffer, pH 5.5, were freshly prepared before the experiments.

3.2.2. Photo-irradiation

Solutions of mAbZ or NATA were photo-irradiated using eight RPR-4190A visible lamps (The Southern New England Ultraviolet Company, Branford, CT; $\lambda_{\text{max}} = 419 \text{ nm}$, emission spectrum between 390 and 475 nm), which were placed in a Rayonet Photoreactor (RPR200, The Southern New England Ultraviolet Company, Branford, CT). Photo-irradiation of the solutions were performed under air in borosilicate tubes. The lamps provided a flux of 6.44×10^{-8} Einstein/sec and an irradiance of $<25 \text{ W.h/m}^2$ for a 1 h photo-irradiation, based on ferrioxalate actinometry.³²⁻

3.2.3. Photo-irradiation of mAbZ and NATA

Solutions containing 500 μ l of 150 mg/ml mAbZ formulated either in NaAc or His/Lys buffer were photo-irradiated for 0-8 h under air. The control and photo-irradiated samples were either diluted as needed for further analysis or were digested for mass spectrometry analysis. Control samples were wrapped in aluminum foil and exposed to light for 8 h.

NATA is a suitable model to study the degradation pathways of Trp under the same experimental conditions as mAbZ. Solutions of NATA formulated either in NaAc or in His/Lys buffer were exposed to visible light for 0-24 h. The samples were analyzed by reverse phase-high-performance liquid chromatography (RP-HPLC), HPLC-MS, and NMR to identify photoproducts. Specially a photoproduct with the same UV/Vis spectroscopic properties as observed for mAbZ was fraction collected, lyophilized, and re-concentrated in DMSO. The concentrated sample was analyzed by HPLC-MS and ^1H - and ^{13}C -NMR.

3.2.4. Reducing and Non-reducing SDS-PAGE

Control and photo-irradiated mAbZ solutions were diluted to 1 mg/ml and combined with Laemmli buffer in a 1:1 ratio. Forty μ l of the mixture was loaded onto each polyacrylamide gel well (4-20% Mini-Protean® TGX™ Precast Gels, Bio-Rad, Hercules, CA), and molecular weight markers were used for molecular weight calibration. For reducing gels, 50 μ l of 13 M β -ME was added to the Laemmli buffer with the protein and incubated for 1 h at 50 °C before running the gels at 200 V. Both gels were stained with Coomassie Brilliant Blue R-250 (Amersham Pharmacia Biotech AB, Uppsala, Sweden) and destained using 50% MeOH and 10% acetic acid in water for visualization of the protein bands.

3.2.5. Size Exclusion Chromatography (SEC)

Control and photo-irradiated mAbZ were diluted from 150 mg/ml to 1 mg/ml either in NaAc or His/Lys buffer. SEC chromatography was run on a HPLC instrument (Shimadzu, Kyoto, Japan). Fifty μg of mAbZ were injected onto a TSK-Gel SWXL guard column (6.0 mm x 40 mm) and directed to a TSK-Gel G3000SWXL SEC column (7.8 mm x 300 mm) at a flow rate of 0.7 ml/min. The column temperature was maintained at 30 °C in a column heater, and monomer and higher molecular weight species (HMWS) eluted with 200 mM phosphate buffer, pH 6.8. Detection was achieved at 220 nm with a diode array detector (Shimadzu, Kyoto, Japan). The percentage of monomers and HMWS were calculated relative to the total peak areas detected in the SEC chromatograms.

3.2.6. Differential Scanning Calorimetry (DSC)

Differential scanning calorimetry (DSC) was performed on a MicroCal VP-Capillary calorimeter (Malvern Instruments, Malvern, UK) equipped with an autosampler. Samples of 300 μl volume containing 1 mg/ml mAbZ were stored in a sealed 96-well plate in an autosampler, kept at 4 °C. Temperature ramps were from 10 to 90 °C at a scan rate of 2 °C/min. A 15 min equilibration period at 10 °C was performed prior to each run. All thermograms were buffer subtracted, baseline corrected, and normalized for protein concentration. Apparent melting temperatures were calculated by fitting thermograms to a non-two-state equilibrium model in Origin 7.0 (OriginLab). Onset melting temperatures, T_{onset} , were designated as the temperature at which the heat capacity first reaches five percent of its maximum value.

3.2.7. Proteolytic Digestion

Control and photo-irradiated mAbZ were diluted to 10 mg/ml in 50 mM $\text{NH}_4^+\text{CO}_3^-$, pH 8.2. The diluted protein solutions were denatured with 3 M guanidine hydrochloride (in 50 mM $\text{NH}_4^+\text{CO}_3^-$), and disulfide bonds were reduced with 5 mM BMS (in ACN) at 37 °C for 1 h. The reduced samples were then alkylated with 25 mM IAA and further incubated at 37 °C for 1 h, diluted with 100 μl of 50 mM $\text{NH}_4^+\text{CO}_3^-$, and dialyzed in 50 mM $\text{NH}_4^+\text{CO}_3^-$ for 1 h in a D-Tube™ Dialyzer Maxi (MWCO 3.5 kDa) at room temperature. The reduced and alkylated protein solutions were digested with 9 μl of 0.1 mg/ml trypsin/LysC overnight at 37 °C. The digestion of protein was stopped by addition of 10 μl of FA:H₂O (0.1:0.9, v:v). The solution of the tryptic peptides was stored at -80 °C until further HPLC-MS analysis.

3.2.8. UV-Visible Absorption Spectroscopy

The absorbance spectra of control and photo-irradiated samples were collected on an Agilent 8453 UV-visible spectrophotometer (Agilent Technologies, Santa Clara, CA) equipped with a photodiode array detector. The initial concentrated samples of 150 mg/ml mAbZ were diluted to 10 mg/ml in either NaAc or His/Lys buffer. The samples were placed in 1 cm path length quartz cuvettes. UV-visible absorbance spectra of the samples were collected from 200 nm to 800 nm and the corresponding buffers were used as blanks. Second derivative spectra were obtained using a second order Savitzky-Golay smoothing filter.

3.2.9. Reverse Phase-High-Performance Liquid Chromatography

In order to fraction collect a specific photoproduct of NATA (i.e., NATA-33), we employed RP-HPLC (Shimadzu Corporation, Kyoto, Japan) equipped with a PDA detector. NATA and its

photoproduct were separated using a Vydac® 218TP54 protein and peptide C18 column (4.6 mm i.d. x 250 mm, 5 µm particle size, and 300 Å pore size) (Alltech Associates Inc, Deerfield, IL), which was maintained at 35 °C in a column heater. Aliquots of 10 µl of photo-irradiated NATA samples were injected onto the column and eluted with the following gradient of mobile phase A, (water with 0.1% TFA) and B (acetonitrile with 0.1% TFA) at a flow rate of 1 ml/min: composition of 97% A and 3% B was held for 5 min; the composition ranged linearly to 70% A and 30% B within 2 min, and subsequently changed linearly to 50% A and 50 % B within 3 min. To wash the column, 5% A and 95% B were employed for 2 min before the column was re-equilibrated to 97% A and 3% B for 6 min. The total run time was 20 min.

3.2.10. NanoAcquity HPLC Electrospray ionization Q-tof MS and HPLC-MS/MS analysis

The proteolytic peptides of mAbZ and NATA and its photoproducts were analyzed on a Xevo-G2 Qtof tandem mass spectrometer (Waters Corporation, Milford, MA), equipped with nanoAcquity Ultra Performance Liquid Chromatography system (Waters Corporation, Milford, MA). The proteolytic peptides (2.5 µl) were injected onto a Symmetry® C18 Waters trap column (2G-V/M Trap; 180 µm x 200 mm, 5 µm particle size, and 100 Å pore size) at a flow rate of 4 µl/min for 3 min with the mobile phase composed of 97% A and 3% B. Mobile phase A and mobile phase B containing Optima® water with 0.1% FA and Optima® ACN with 0.1% FA, respectively. After 3 min, the samples were directed to an analytical nanoAcquity ultra performance Waters peptide CSH™ C18 column, (75 µm x 250 mm, 1.7 µm particle size, and 130 Å pore size) at a flow rate of 0.3 µl/min, maintained at 40 °C in a column heater. The initial gradient started with 97% mobile phase A and 3% mobile phase B, and the composition to 65% A and 35% B within 50 min. Subsequently, the solvent composition was changed to 5% A and 95% B within 20 min and kept

at this composition for an additional 10 min to wash the column. The solvent composition was reverted to the initial composition of 97% A and 3% B, and re-equilibrated for 32 min.

For electrospray MS the source temperature was set at 100 °C. The instrument was operated in a positive mode and the mass analyzer allowed the mass range from 150-2000 Da. The capillary voltage was set at 2.7 kV. The non-fragmented peptides were passed through a collision cell at 5 eV, and the peptides were fragmented by ramping the collision cell energies between 18 eV and 45 eV. The data were collected in the MS^E mode. The HPLC-MS was operated, and data analyses were done with the Masslynx v.4.1 software. The data were plotted with the GraphPad Prism 7 software.

3.2.11. Nuclear Magnetic Resonance

NATA and NATA-33 were dissolved in DMSO-d₆ and transferred to a 5 mm Shigemi® tube (Wilma Lab Glass, Vineland, NJ). NMR spectra were collected on a Bruker AVIII 500 MHz instrument, equipped with a dual carbon/proton (CPBBFO) cryoprobe, at a sample temperature of 25° C. All data were recorded with DMSO as the reference standard. The ¹H-NMR spectrum was acquired with 256 scans at a spectrometer frequency of 500.19 MHz. The ¹³C-NMR spectrum was acquired with 66k scans at a spectrometer frequency of 125.79 MHz. The HSQC experiment was acquired with 32 scans, with 1024 points in the ¹H dimension and 256 increments in the ¹³C dimension. The spectral width was 14 and 180 for the ¹H and ¹³C dimensions, respectively. The relaxation delay was 2 seconds.

3.3. Results

Following exposure to visible light up to 8 h (1.44 W.h/m²) in NaAc or His/Lys buffer, mAbZ was analyzed for physical and chemical degradation.

3.3.1. Physical stability: studies on conformation and aggregation of mAbZ

The aggregation propensity of control and photo-irradiated mAbZ was monitored by SDS-PAGE and SEC. Non-reducing SDS-PAGE shows a major band at around 150 kDa for mAbZ in both NaAc and His/Lys buffer (Fig. 1A). A low intensity band around 75 kDa suggests some half antibody formation, likely via cleavage of interchain disulfide bridges. Photo-irradiation with visible light for up to 8 h results in the formation of a higher molecular band in NaAc buffer, but to a significantly lower extent in His/Lys buffer (e.g., lanes 5 and 10, Fig. 1A). A higher molecular weight band (between 100 and 150 kDa) is also visible after 8 h photo-irradiation with visible light in NaAc when analyzed with reducing SDS-PAGE (Fig. 1B, lane 5). This suggests that some higher molecular weight species are generated via covalent bond formation, but not disulfides.

These observations were corroborated by SEC (Fig. 2). Photo-irradiation with visible light induced the formation of dimers and HMWS in both buffers, where the yields of dimers and HMWS was two-fold higher in NaAc as compared to His/Lys buffer, ~7% of monomer was lost and ~3.5% dimer and ~3.5% HMWS were formed after 8 h light exposure (Fig. 2B). In comparison, in NaAc buffer, 15% of monomer was lost after 8 h of light exposure, which was accompanied by 6% dimer and 9% HMWS (Fig. 2B).

In order to evaluate whether transition of metals played a role in the aggregation of mAbZ, a mAbZ formulation in NaAc buffer was spiked with 5 mM EDTA and photo-irradiated for 4 h. The yields of monomer loss and aggregates (dimers and HMWS) were similar for mAbZ formulated in NaAc buffer in the absence and presence of EDTA (Fig. S1). This indicates metals do not play a role in aggregation formation. On the other hand, when 10 mM His were added to mAbZ formulated in NaAc buffer, a lower yield of aggregates was detected after 4 h visible light exposure (Fig. S1B).

Because of the significant aggregation of mAbZ especially in NaAc buffer, we monitored the conformation stability of control and photo-irradiated mAbZ in both NaAc and His/Lys buffer by differential scanning calorimetry (DSC) (Fig. 3). The thermograms (Fig. 3A) of all samples were deconvoluted to provide T_{m1} , T_{m2} , and T_{onset} . Control mAbZ in both buffers displayed similar T_{m1} , whereas the T_{m1} of mAbZ photo-irradiated in NaAc buffer decreased by about 0.5 °C after 8 h exposure to visible light (Fig. 3BI). Instead, the T_{m1} of mAbZ photo-irradiated in His/Lys buffer did not change upon light exposure (Fig. 3BI). For control, the T_{m2} of mAbZ was higher in His/Lys buffer as compared to NaAc buffer (Fig. 3BII). We observed no significant change of T_{m2} after light exposure for 8 h. However, T_{onset} decreased by 1 °C in NaAc buffer, whereas it decreased by 2 °C after 8 h visible light exposure in His/Lys buffer (Fig. 3BIII). However, as we did not observe large changes of the T_{m1} and T_{m2} values as a result of photo-irradiation, these data indicate that the tertiary structure of mAbZ did not undergo major changes.

3.3.2. Oxidation of Met and Trp

The proteolytic digests of control and photo-irradiated mAbZ were analyzed by HPLC-MS. The peak areas containing oxidized Met and Trp residues were calculated, and normalized by use of the proteolytic peptide, SLSLSLGK, which remained stable under our experimental conditions. There are six Met residues present in the heavy chain and none in the light chain of mAbZ. We observed the light-induced oxidation of Met to methionine sulfoxide (MetO) at positions 254, 360, and 430, where the yield of MetO increased with the duration of light exposure in both buffers, NaAc and His/Lys (Fig. 4A and 4C); however, higher yields of MetO were observed in NaAc buffer. The light chain of mAbZ contains four Trp residues, out of which only the Trp at position 90 (W90) was oxidized forming hydroxy tryptophan (OH-Trp) (Fig. 4B and 4D). The yields of OH-Trp were higher in NaAc as compared to His/Lys buffer, except for the longest photo-

irradiation time of 8 h. We also observed NFK formation at position 90, but only by MS analysis; the yields were too low for MS/MS identification.

3.3.3. Formation of chromophoric photoproducts in mAbZ and NATA

After light exposure of up to 8 h, mAbZ formulated in NaAc buffer exhibited a color change from clear to yellow (Fig. 5A). In contrast, mAbZ formulated in His/Lys buffer did not display a significant color change after visible light exposure (Fig. 5B). By comparison of the UV-visible absorption spectra of control and photo-irradiated mAbZ in NaAc buffer, we observed an increase of the absorbance in the visible region with a $\lambda_{\text{max}} = \sim 450$ nm (Fig. 6A). Importantly, visible light photo-irradiation of NATA in NaAc buffer (50 mM, pH 5.50) for 6 h resulted in a similar absorbance around $\lambda_{\text{max}} = \sim 450$ nm (Fig. 6B). Second derivative UV/Vis spectroscopy of mAbZ and NATA confirmed that indeed identical product was generated in both experiments (Fig. 6C). When we expanded the light exposure of NATA in NaAc buffer to 24 h, a yellow color was observed (Fig. 7). Instead, when NATA was photo-irradiated in His/Lys buffer, a light brown color was observed, which could originate from degradation product of either His³⁶ or Trp¹⁷, or both.

Control and NATA photo-irradiated in both NaAc and His/Lys buffers were analyzed by RP-HPLC and monitored at 300 or 400 nm. When exposed to visible light for up to 24 h, NATA converted into a number of products, monitored at 300 nm (Fig. 8AI and 8BI), where the individual yields increased with the duration of photo-irradiation; in general higher yields of photoproduct were observed in NaAc as compared to His/Lys buffer. We detected the formation of OH-Trp, NATA+14, Kyn, and NFK, eluting at $t_{\text{R}} = 6.95, 7.35, 7.70,$ and 7.85 min, respectively, before the unmodified NATA ($t_{\text{R}} = 8.75$ min) (Fig. 8A-I and 8B-I). In addition, when the photoproducts were monitored at 400 nm, two major peaks appeared for NATA photo-irradiated in NaAc buffer (Fig.

8A-II), and one peak for NATA photo-irradiated in His/Lys buffer (Fig. 8B-II). At $t_R = 7.85$ min, we detected the formation of Kyn; however, a peak at $t_R = 11.7$ min, containing NATA-33 was only observed in NaAc buffer. This peak was fraction-collected and analyzed by HPLC-MS. The HPLC-MS analysis revealed a molecular ion with m/z 213.09 ($z = 1$) (Fig. S2), corresponding to a loss of 33 Da from NATA (m/z 246.15, $z = 1$).

The ^{13}C -NMR spectrum of NATA-33 in DMSO- d_6 (Fig. 9A) displayed 15 peaks with chemical shift at 1.25, 29.11, 40.00, 98.49, 103.57, 116.10, 125.48, 128.08, 129.03, 133.80, 142.06, 147.5, 148.36, 149.06, and 180.39 ppm. The peaks at 1.25 and 116.10 ppm may correspond to the residual ACN left after drying, and the peak at 40.00 ppm corresponds to the carbons on DMSO- d_6 . The remainder of the signal were utilized for structural elucidation of NATA-33. A proposed structure, **P1**, is shown in Chart 1. The ^1H -NMR of NATA-33 is shown in Fig. 9B. Predictions for chemical shifts were made with MesoNova, nmrd.org, and ChemDraw software for structure **P1**, shown in Table 1, ^1H - ^{13}C Heteronuclear Single Quantum Correlation (HSQC) correlations are shown in Fig. S3, carbons at 98.49, 103.57, 116.1, 125.48, 128.08, and 129.03 correlate to 6.37, 6.38, 7.50, 7.40, 7.47, and 7.71, respectively.

HPLC-MS/MS analysis of NATA-33 was performed in the data dependent acquisition (DDA) mode (Fig. 10). The proposed structure **P1** would be consistent with the fragmentation pattern as in Fig. 10, displaying a molecular ion with m/z 213.09 ($z = 1$), which corresponds to the parent ion of **P1**. The loss of -CO gives the fragment with m/z 185.09 ($z = 1$). Either the ion with m/z 185.09 can lose -27 Da (H_3NO), or the molecular ion of **P1** can lose 55 Da (C_2HNO) to give a fragment with m/z 158.08 ($z = 1$). The loss of H_2O and CO from m/z 158.08 give an ion with m/z 144.06 and 130.08, respectively. A fragment containing an indole ring is observed with m/z 118.08 ($z = 1$), which indicates that the indole ring is intact in the structure of **P1**. By comparison to the HPLC-

MS/MS analysis of unmodified NATA, NATA-33 does not contain m/z 201.12 ($z = 1$), which corresponds to an intact N-terminus of NATA (Fig. S4), suggesting that NATA-33 may be generated through loss of the N-terminus of NATA. The combination of NMR and HPLC-NMR data fits structure **P1**. However, we also considered other possible structures of NATA-33 (**P2** and **P3a** or its isomers) shown in Chart 1, which will be discussed below.

3.4. Discussion

3.4.1. Aggregation, conformational changes, and oxidation of mAbZ

Highly concentrated mAbZ was formulated either in NaAc and His/Lys buffer at pH 5.50. For photostability testing, mAbZ formulated in either buffer was exposed to visible light up to 8 h, resulting in the formation of dimers and HMWS (Fig. 1). Notably, mAbZ in NaAc buffer (containing NaCl) generated more aggregates as compared to His/Lys buffer. The addition of EDTA had no effect on aggregation. On the other hand, the addition of His reduced HMWS formation. His residue can interact with aromatic residues⁸ and minimize self-association. The mAbZ formulation in His/Lys buffer contains additional Lys, which also reduces viscosity or self-association of mAbs via electrostatic interactions.^{8, 37-38} The overall extent of light-induced oxidation rate of Met (254), Met (360), and Met (430) in the heavy chain and W(90) in the light chain of mAbZ was higher in NaAc buffer as compared to His/Lys buffer. While degradation products of His can act as photosensitizer,³⁶ His also acts as a scavenger for reactive oxygen species such as singlet oxygen or hydroxyl radical.³⁹

3.4.2. Formation of chromophoric photoproducts from mAbZ and NATA

Interestingly, when the colorless mAbZ in either NaAc or His/Lys formulation was exposed to visible light, only the mAbZ in NaAc buffer turned yellow (Fig. 5), characterized by an absorption

spectrum with $\lambda_{\text{max}} = \sim 450$ nm (Fig. 6). Li *et al.* reported that photoproducts of Trp residues such as OH-Trp, NFK, and Kyn, in the variable domain of mAbZ are sources of color change.⁴ However, these photoproducts have absorbance maxima at 300 nm, 318 nm, and 360 nm, respectively,^{23,40-41} and cannot rationalize the absorption maximum around 450 nm. Therefore, we hypothesized that the absorption around 450 nm originated from a different tryptophan-derived oxidation product, and selected a Trp-containing model compound (NATA) for further characterization of this product.

When NATA was exposed to visible light in NaAc buffer, a comparable chromophoric photoproduct was detected, and RP-HPLC analysis revealed a new product, NATA-33. After fraction collection and concentration of NATA-33, a brown color was observed (Fig. 8), similar to the color of a mAb exposed for 14 days to UV-visible light.⁴ Therefore, NATA and mAbZ may form similar chromophoric photoproduct even in the absence of PS80. The concentrated atypical peak generated from NATA was analyzed by HPLC-MS/MS and contained a product generated by loss of 33 Da from unmodified NATA. ¹H- and ¹³C-NMR spectra were collected to elucidate the structure. Previous study by Dyer *et al.* on the photo-irradiation of wool proteins showed the formation of yellow β -carbolines (1,5-dihydro- β -carboline) from Trp after through reaction with formaldehyde or α -keto acids.²⁸ An analogous 1, 5-dihydro- β -carboline derivative derived from NATA is shown in the structure of product **P2** (Chart 1). This proposed structure has chemical formula $\text{C}_{13}\text{H}_{13}\text{N}_2\text{O}^+$, displaying a molecular ion with m/z 213.09 ($z = 1$); however, the predictions of ¹H- and ¹³C-NMR analysis of **P2** do not correlate well with the actual ¹H- and ¹³C-NMR spectra obtained for the chemical shift of NATA-33. Therefore, we evaluated alternative structures. The third proposed structure **P3a** may form via the mechanism shown in Scheme 1. Along with **P3a**, isomers such as **P3b**, **P3c**, and **P3d** may also be present (Chart 1). It is possible that ¹H- and ¹³C-

NMR spectra show a combination of these structures. The ^1H - and ^{13}C -NMR predictions for all isobaric species (Table S1 and S2) were calculated with the MesoNova, nmrd.org, and ChemDraw software, and were correlated to the NMR spectra obtained from NATA-33 (Fig. 9). In the ^{13}C -NMR predictions (Table S1), carbon at the position 5, 6, 7, and 8 may belong to the benzene ring and also correlate well with the observed peaks at 116.10, 125.48, 128.08, and 129.03 ppm (Fig. 9A). Likewise, the carbons at position 14 and 15 may correspond to the carbonyl (180.39 ppm) and methyl group (29.11 ppm), respectively. When predictor peaks of all the isobaric species are combined, further peaks in the obtained NMR can be assigned, such as the carbon at the position 9, which can be assigned to 133.80 ppm and carbons at positions 1, 2, 4, and 11, which can be assigned to 142.06, 147.5, 148.36, and 149.06 ppm. Similarly, carbons at positions 10 and 12 can be also be assigned to observed peaks at 98.49 and 103.57 ppm. In addition, the predictor peaks of isobaric species (Table S2), can be assigned to the measured ^1H -NMR spectrum (Fig. 9B). Importantly, the proposed structures maintain at least one of the amides, suggesting that similar structures of mAbZ would remain bound to part of the protein framework. However, after 8 h photo-irradiated ion with visible light the proteolytic digestion of mAbZ revealed no peptide peak with absorbance around 450 nm (Fig. S5). This may indicate that either the product is not peptide bound, or that a peptide-bound product was not recovered. In Fig. 9, we show a tentative product, **P1**, which is not peptide- or protein-bound. The predicted ^{13}C resonances fit better with the observed ^{13}C -NMR spectrum. However, the ^1H -NMR spectrum does not correlate well with the predicted resonances.

Here, we have reported a chromophoric product of a mAb after exposure to visible light. Using NATA as a model compound for Trp, the structure of the photoproduct was characterized by HPLC-MS/MS spectrum and ^1H - and ^{13}C -NMR. And based on these data we proposed the

structures shown in Chart 1. Among the proposed structures, **P3a** and its isomers fit the NMR spectra best and is likely the prime candidate. Since the UV-Vis spectra of photo-irradiated mAb and NATA have similar absorbance, it is likely the degradation products in mAbZ attributed to modifications to Trp residues resulting in a product similar to P3a and its isomers. Such products are formed after cleavage of an amide bond, which can result in loss of biological activity of the protein as a whole. Since, photo-irradiated NATA in our experimental conditions and the mAb exposed to UV-visible light for 14 days shown by Li *et al.* have exhibited similar brown color, our results may explain one of the factors responsible for the color change of the mAb formulation. Here, the chromophoric product after exposure to visible light was observed from far below the ICH Q1B guideline. The observation of these products indicates that the photosensitive proteins must be protected not only from the UV light, but also from longer exposure to visible light.

3.5. References

1. Reichert, J. M.; Rosensweig, C. J.; Faden, L. B.; Dewitz, M. C., Monoclonal antibody successes in the clinic. *Nat. Biotechnol.* **2005**, *23* (9), 1073-8.
2. Buss, N. A. P. S.; Henderson, S. J.; McFarlane, M.; Shenton, J. M.; de Haan, L., Monoclonal antibody therapeutics: history and future. *Curr. Opin. Pharm.* **2012**, *12* (5), 615-622.
3. Carter, P. J., Potent antibody therapeutics by design. *Nat. Rev. Immunol.* **2006**, *6* (5), 343-357.
4. Li, Y.; Polozova, A.; Gruia, F.; Feng, J., Characterization of the degradation products of a color-changed monoclonal antibody: tryptophan-derived chromophores. *Anal. Chem.* **2014**, *86* (14), 6850-6857.
5. Shire, S. J.; Shahrokh, Z.; Liu, J., Challenges in the development of high protein concentration formulations. *J. Pharm. Sci.* **2004**, *93* (6), 1390-1402.
6. Kanai, S.; Liu, J.; Patapoff, T. W.; Shire, S. J., Reversible self-association of a concentrated monoclonal antibody solution mediated by Fab-Fab interaction that impacts solution viscosity. *J. Pharm. Sci.* **2008**, *97* (10), 4219-4227.
7. Harn, N.; Allan, C.; Oliver, C.; Middaugh, C., Highly concentrated monoclonal antibody solutions: direct analysis of physical structure and thermal stability. *J. Pharm. Sci.* **2007**, *96* (3), 532-546.
8. Dear, B. J.; Hung, J. J.; Truskett, T. M.; Johnston, K. P., Contrasting the influence of cationic amino acids on the viscosity and stability of a highly concentrated monoclonal antibody. *Pharm. Res.* **2017**, *34* (1), 193-207.

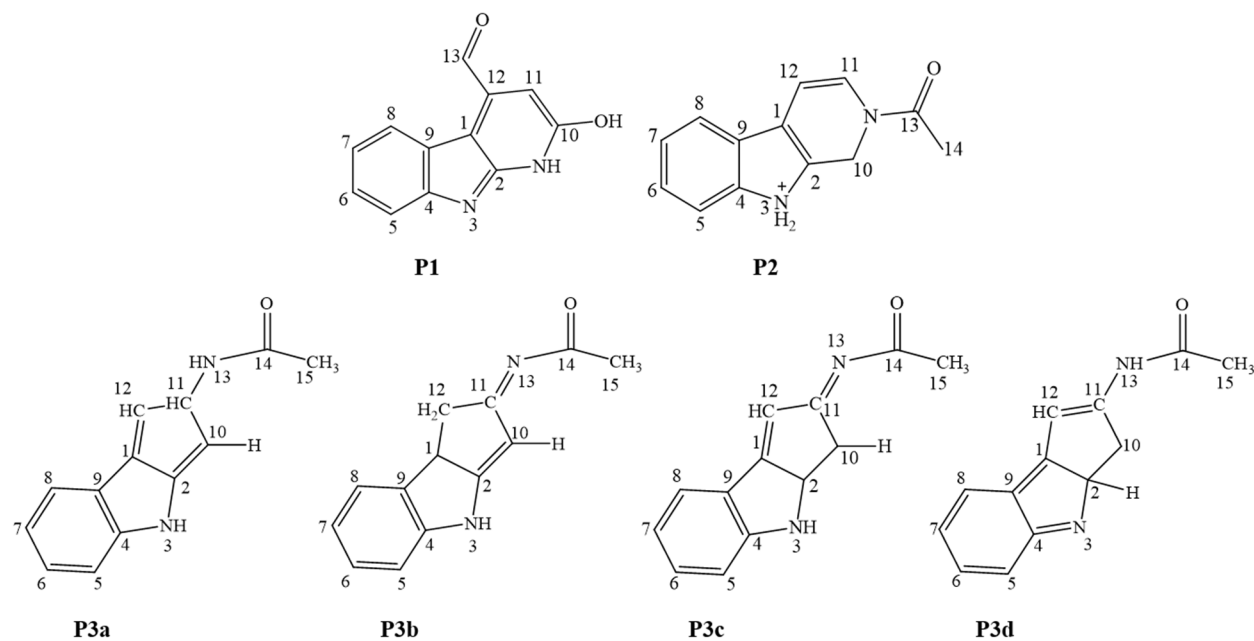
9. Chen, B.; Bautista, R.; Yu, K.; Zapata, G. A.; Mulkerrin, M. G.; Chamow, S. M., Influence of histidine on the stability and physical properties of a fully human antibody in aqueous and solid forms. *Pharm. Res.* **2003**, *20* (12), 1952-1960.
10. Qi, P.; Volkin, D. B.; Zhao, H.; Nedved, M. L.; Hughes, R.; Bass, R.; Yi, S. C.; Panek, M. E.; Wang, D.; DalMonte, P., Characterization of the photodegradation of a human IgG1 monoclonal antibody formulated as a high concentration liquid dosage form. *J. Pharm. Sci.* **2009**, *98* (9), 3117-3130.
11. Guideline, I. H. T., Photostability testing of new drug substance and products. *Fed. Register* **1996**, *62*, 27115-27122.
12. Commission, E. P., European Pharmacopoeia (Ph. Eur). Council of Europe: Strasbourg, France: 2015.
13. Du, C.; Xu, J.; Song, H.; Tao, L.; Lewandowski, A.; Ghose, S.; Borys, M. C.; Li, Z. J., Mechanisms of color formation in drug substance and mitigation strategies for the manufacture and storage of therapeutic proteins produced using mammalian cell culture. *Process Biochem.* **2019**.
14. Quan, C.; Alcala, E.; Petkovska, I.; Matthews, D.; Canova-Davis, E.; Taticek, R.; Ma, S., A study in glycation of a therapeutic recombinant humanized monoclonal antibody: where it is, how it got there, and how it affects charge-based behavior. *Anal. Biochem.* **2008**, *373* (2), 179-191.
15. Butko, M.; Pallat, H.; Cordoba, A.; Yu, X. C., Recombinant Antibody Color Resulting from Advanced Glycation End Product Modifications. *Anal. Chem.* **2014**, *86* (19), 9816-9823.
16. Ahmed, N., Advanced glycation endproducts—role in pathology of diabetic complications. *Diabetes Res. Clin. Pract.* **2005**, *67* (1), 3-21.
17. Xu, J.; Jin, M.; Song, H.; Huang, C.; Xu, X.; Tian, J.; Qian, N.-X.; Steger, K.; Lewen, N. S.; Tao, L., Brown drug substance color investigation in cell culture manufacturing using chemically defined media: A case study. *Process Biochem.* **2014**, *49* (1), 130-139.
18. Song, H.; Xu, J.; Jin, M.; Huang, C.; Bongers, J.; Bai, H.; Wu, W.; Ludwig, R.; Li, Z.; Tao, L., Investigation of color in a fusion protein using advanced analytical techniques: delineating contributions from oxidation products and process related impurities. *Pharm. Res.* **2016**, *33* (4), 932-941.
19. Vijayasankaran, N.; Varma, S.; Yang, Y.; Mun, M.; Arevalo, S.; Gawlitzek, M.; Swartz, T.; Lim, A.; Li, F.; Zhang, B., Effect of cell culture medium components on color of formulated monoclonal antibody drug substance. *Biotechnol. Prog.* **2013**, *29* (5), 1270-1277.
20. Clarizia, L.; Russo, D.; Di Somma, I.; Marotta, R.; Andreozzi, R., Homogeneous photo-Fenton processes at near neutral pH: a review. *Appl. Catal. B* **2017**, *209*, 358-371.
21. Schöneich, C., Photo-Degradation of Therapeutic Proteins: Mechanistic Aspects. *Pharm. Res.* **2020**, *37* (3), 45.
22. Creed, D., The photophysics and photochemistry of the near-UV absorbing amino acids—i. Tryptophan and its simple derivatives. *Photochem. Photobiol.* **1984**, *39* (4), 537-562.

23. Dreaden, T. M.; Chen, J.; Rexroth, S.; Barry, B. A., N-formylkynurenine as a marker of high light stress in photosynthesis. *J. Biol. Chem.* **2011**, *286* (25), 22632-22641.
24. Mizdrak, J.; Hains, P. G.; Truscott, R. J.; Jamie, J. F.; Davies, M. J., Tryptophan-derived ultraviolet filter compounds covalently bound to lens proteins are photosensitizers of oxidative damage. *Free Radic. Biol. Med.* **2008**, *44* (6), 1108-1119.
25. Parker, N. R.; Jamie, J. F.; Davies, M. J.; Truscott, R. J. W., Protein-bound kynurenine is a photosensitizer of oxidative damage. *Free Radic. Biol. Med.* **2004**, *37* (9), 1479-1489.
26. Sreedhara, A.; Yin, J.; Joyce, M.; Lau, K.; Weckler, A. T.; Deperalta, G.; Yi, L.; John Wang, Y.; Kabakoff, B.; Kishore, R. S. K., Effect of ambient light on IgG1 monoclonal antibodies during drug product processing and development. *Eur. J. Pharm. Biopharm.* **2016**, *100*, 38-46.
27. Baptista, M. S.; Cadet, J.; Di Mascio, P.; Ghogare, A. A.; Greer, A.; Hamblin, M. R.; Lorente, C.; Nunez, S. C.; Ribeiro, M. S.; Thomas, A. H.; Vignoni, M.; Yoshimura, T. M., Type I and Type II Photosensitized Oxidation Reactions: Guidelines and Mechanistic Pathways. *Photochem. Photobiol.* **2017**, *93* (4), 912-919.
28. Dyer, J. M.; Bringans, S. D.; Bryson, W. G., Determination of photooxidation products within photoyellowed bleached wool proteins. *Photochem. Photobiol.* **2006**, *82* (2), 551-557.
29. Hood, B. D.; Garner, B.; Truscott, R. J., Human Lens Coloration and Aging EVIDENCE FOR CRYSTALLIN MODIFICATION BY THE MAJOR ULTRAVIOLET FILTER, 3-HYDROXY-KYNURENINE- β -D-GLUCOSIDE. *J. Biol. Chem.* **1999**, *274* (46), 32547-32550.
30. Pirie, A., Formation of N'-formylkynurenine in proteins from lens and other sources by exposure to sunlight. *Biochem. J.* **1971**, *125* (1), 203.
31. Pirie, A., Reaction of tyrosine oxidation products with proteins of the lens. *Biochem. J.* **1968**, *109* (2), 301-305.
32. Hatchard, C.; Parker, C. A., A new sensitive chemical actinometer-II. Potassium ferrioxalate as a standard chemical actinometer. *Proc. R. Soc. London, Ser. A* **1956**, *235* (1203), 518-536.
33. Lee, J.; Seliger, H., Quantum yield of the ferrioxalate actinometer. *J. Chem. Phys.* **1964**, *40* (2), 519-523.
34. Pozdnyakov, I. P.; Kel, O. V.; Plyusnin, V. F.; Grivin, V. P.; Bazhin, N. M., New insight into photochemistry of ferrioxalate. *J. Phys. Chem. A* **2008**, *112* (36), 8316-8322.
35. Prajapati, I.; Peters, B.-H.; Larson, N. R.; Wei, Y.; Choudhary, S.; Kalonia, C.; Hudak, S.; Esfandiary, R.; Middaugh, C. R.; Schöneich, C., Cis/Trans Isomerization of Unsaturated Fatty Acids in Polysorbate 80 During Light Exposure of a Monoclonal Antibody-Containing Formulation. *J. Pharm. Sci.* **2020**, *109* (1), 603-613.
36. Stroop, S. D.; Conca, D. M.; Lundgard, R. P.; Renz, M. E.; Peabody, L. M.; Leigh, S. D., Photosensitizers form in histidine buffer and mediate the photodegradation of a monoclonal antibody. *J. Pharm. Sci.* **2011**, *100* (12), 5142-5155.
37. Inoue, N.; Takai, E.; Arakawa, T.; Shiraki, K., Arginine and lysine reduce the high viscosity of serum albumin solutions for pharmaceutical injection. *J. Biosci. Bioeng.* **2014**, *117* (5), 539-543.

38. Wang, S.; Zhang, N.; Hu, T.; Dai, W.; Feng, X.; Zhang, X.; Qian, F., Viscosity-lowering effect of amino acids and salts on highly concentrated solutions of two IgG1 monoclonal antibodies. *Mol. Pharm.* **2015**, *12* (12), 4478-4487.
39. Wade, A. M.; Tucker, H. N., Antioxidant characteristics of L-histidine 11The work described in this manuscript was partially sponsored and funded by Cytos Pharmaceuticals, LLC. *J. Nutr. Biochem.* **1998**, *9* (6), 308-315.
40. Knox, W. E.; Mehler, A., The conversion of tryptophan to kynurenine in liver. *J. biol. Chem* **1950**, *187*, 419-430.
41. Laws, W. R.; Schwartz, G. P.; Rusinova, E.; Burke, G. T.; Chu, Y.-C.; Katsoyannis, P. G.; Ross, J. A., 5-hydroxytryptophan: an absorption and fluorescence probe which is a conservative replacement for [A14 tyrosine] in insulin. *J. Protein. Chem.* **1995**, *14* (4), 225-232.

3.6. Chart and Figures

Chart 1: Proposed structures of P1, P2, and P3a-d



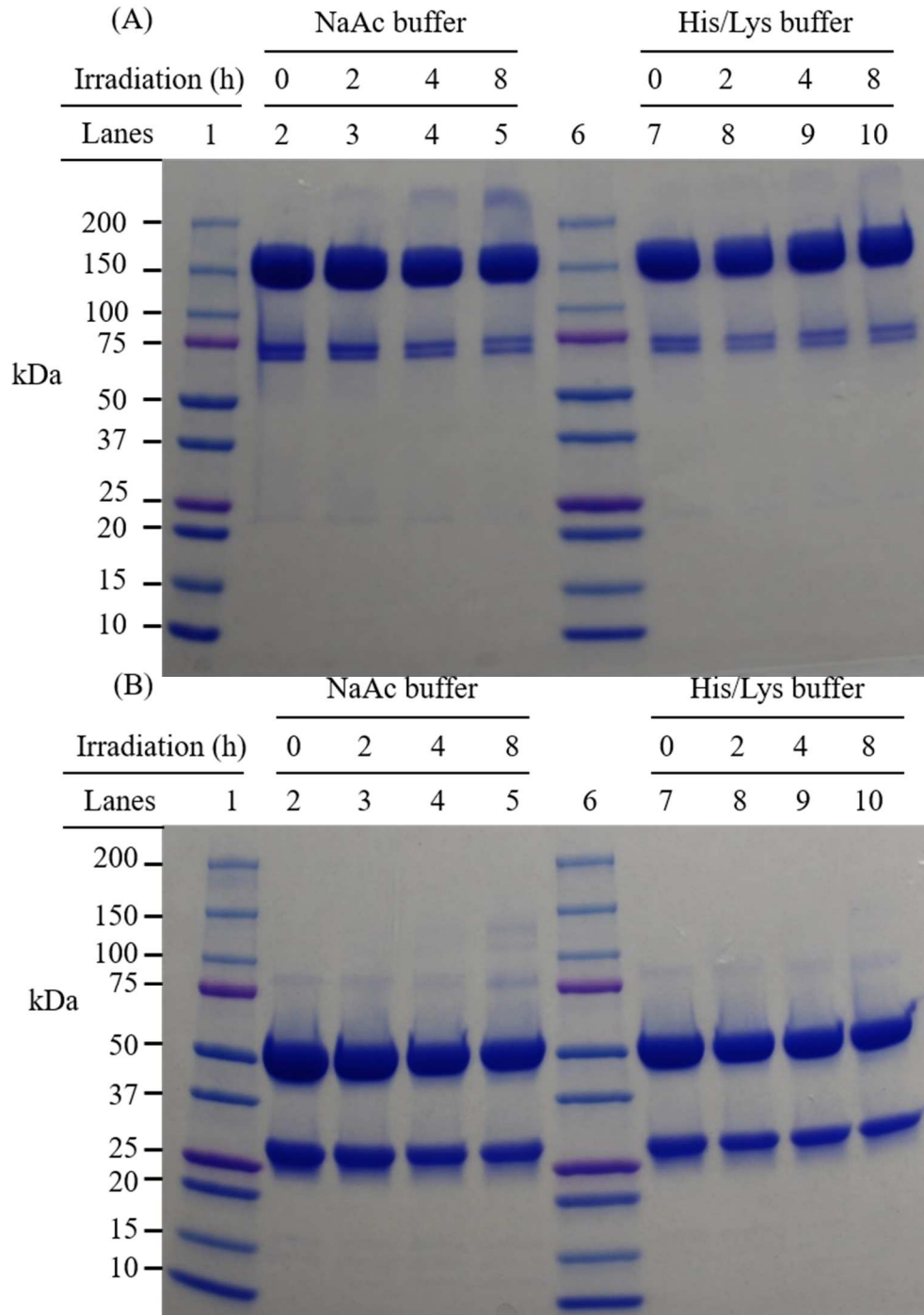


Figure 1: SDS-Page analysis of mAbZ exposed to visible light for 0-8 h in NaAc buffer (lanes 2-5) and in His/Lys buffer (lanes 7-10) Lane 1 and 6 show molecular makers (A) non-reducing gel, (B) reducing gel

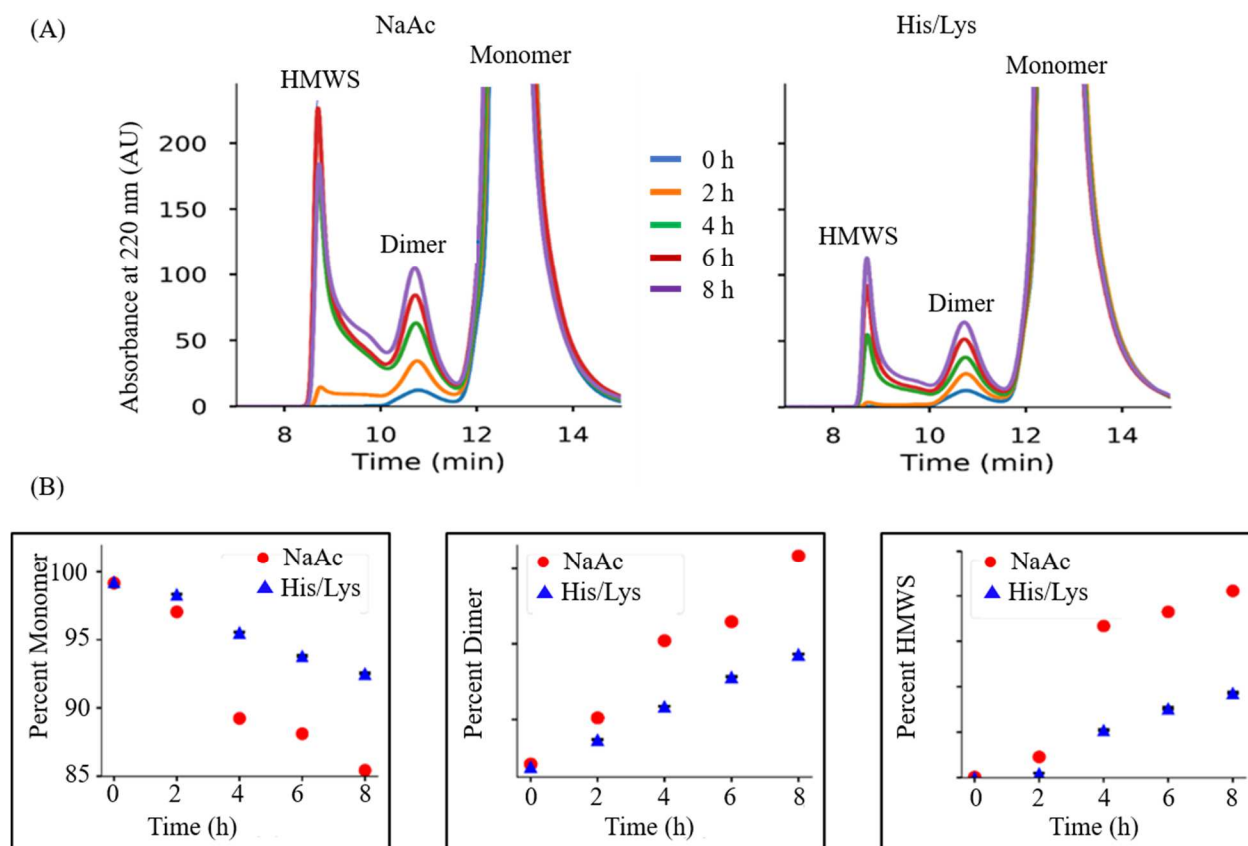


Figure 2: (A) SEC-HPLC of mAbZ in NaAc and His/Lys buffer after photo-irradiation with visible light for 0 h (blue), 2 h (orange trace), 4 h (green trace), 6 h (red trace), and 8 h (purple trace). (B) Quantification of the peak areas of monomer, dimer, and HMWS of mAbZ in NaAc (red circles) and His/Lys (blue triangles).

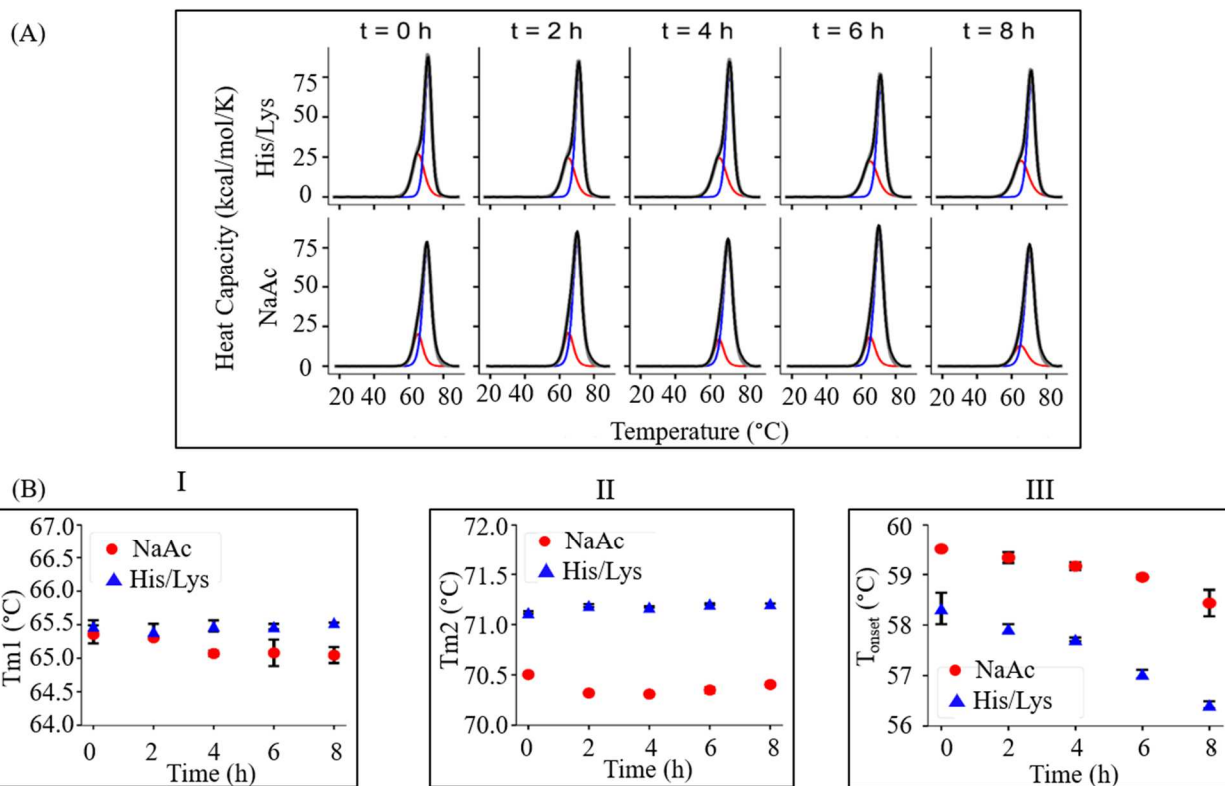
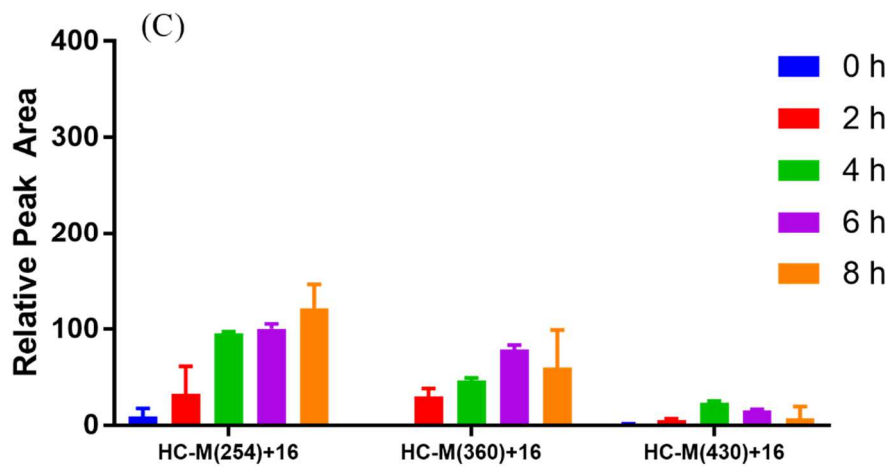
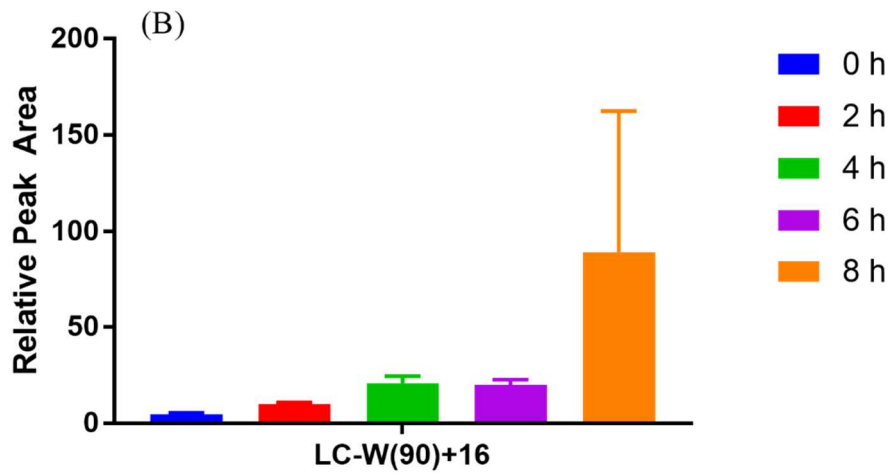
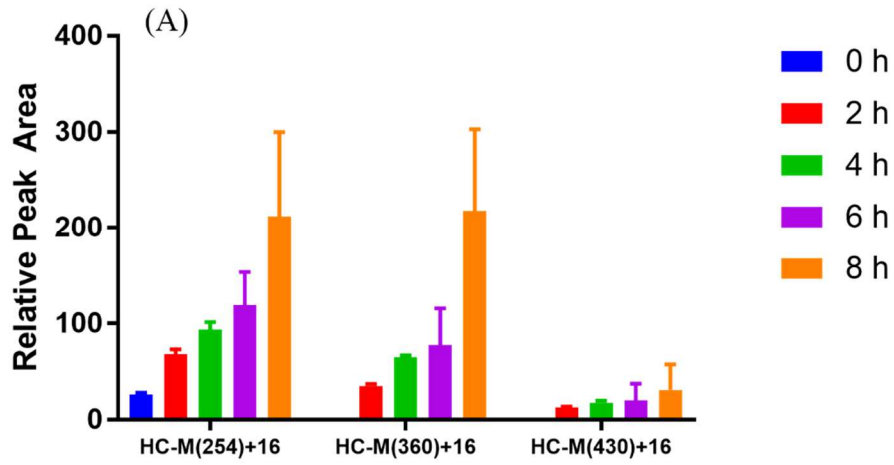


Figure 3: (A) Thermograms measured by DSC of mAbZ in NaAc and His/Lys buffer after photo-irradiation with visible light between 0 and 8 h. (B) T_{m1} (B-I), T_{m2} (B-II), and T_{onset} (B-III) of mAbZ after photo-irradiation with visible light between 0 and 8 h in NaAc (red-circles) and His/Lys buffer (blue-triangles). Samples were run in triplicate and error bars represent the standard deviation of three replicates.



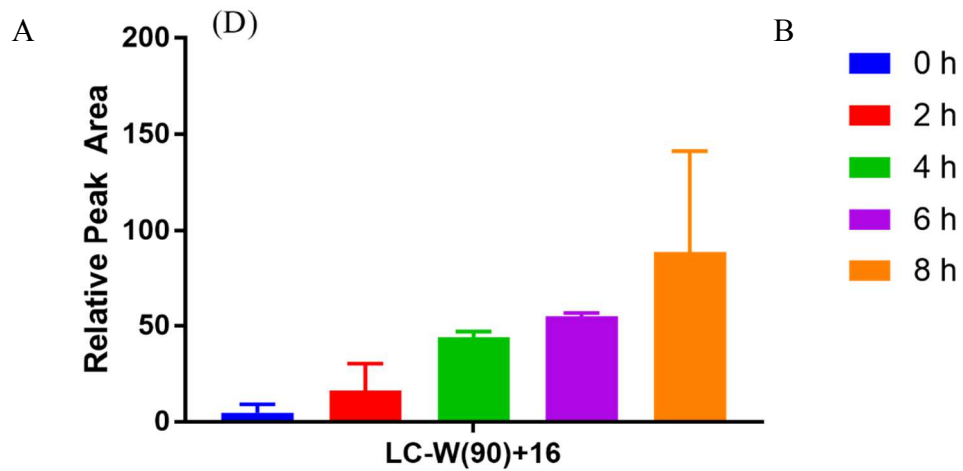


Figure 4: Relative peak areas for MetO-containing peptides (A and C) and OH-Trp-containing peptides (B and D) derived from proteolytic digestion of mAbZ in NaAc buffer (A and B) and His/Lys buffer (C and D) after photo-irradiation for 0 h (blue), 2 h (red), 4 h (green), 6 h (purple), and 8 h (orange).

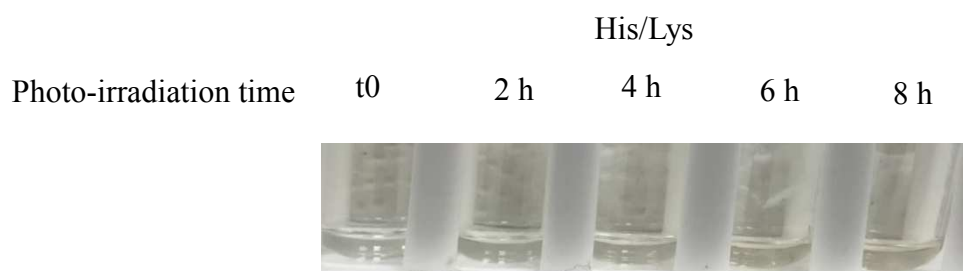
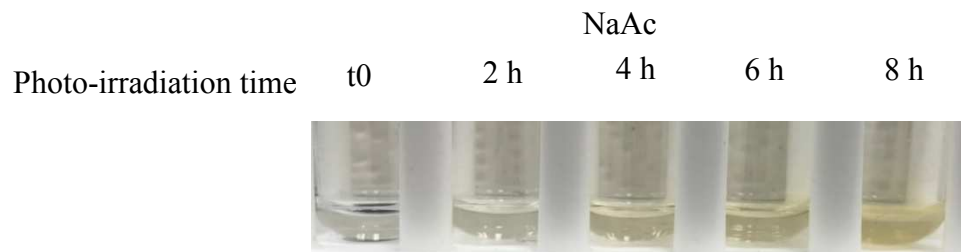
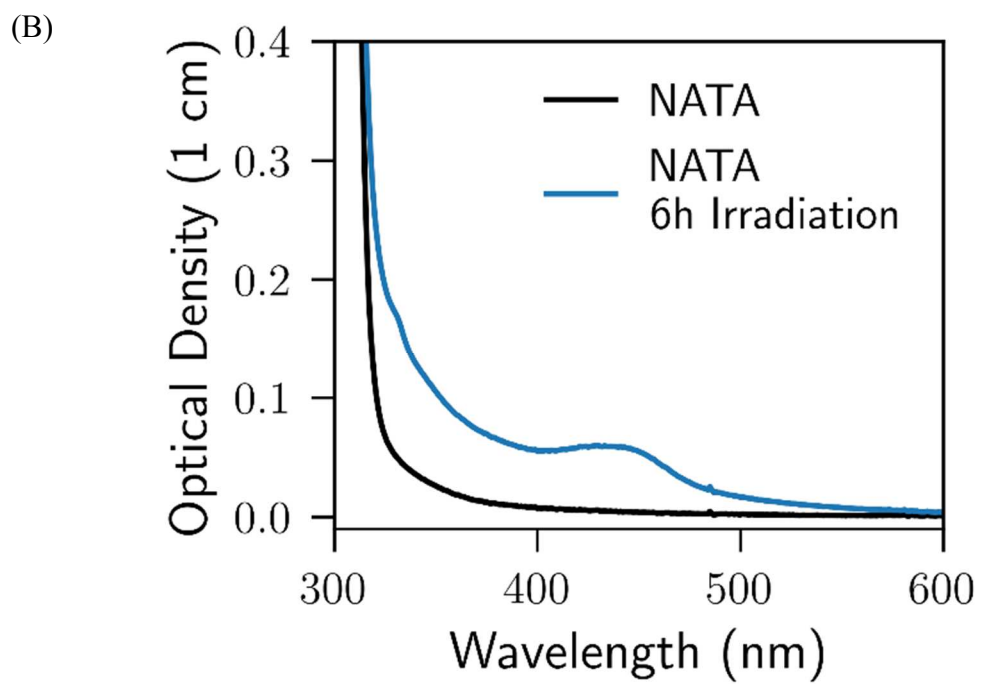
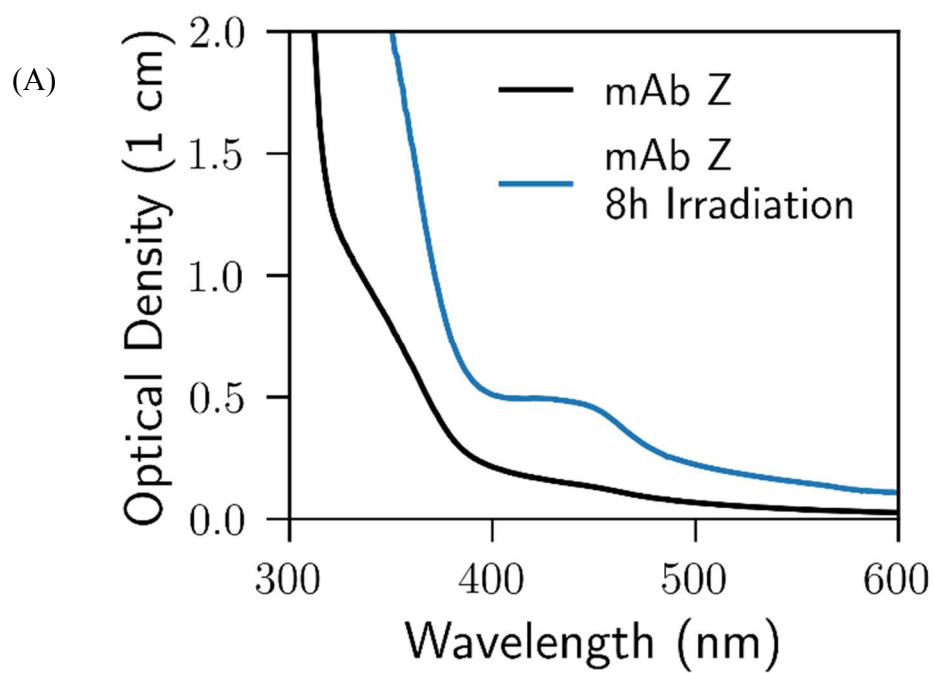


Figure 5: Yellow color observed after mAbZ was photo-irradiated in (A) NaAc and (B) His/Lys buffer.



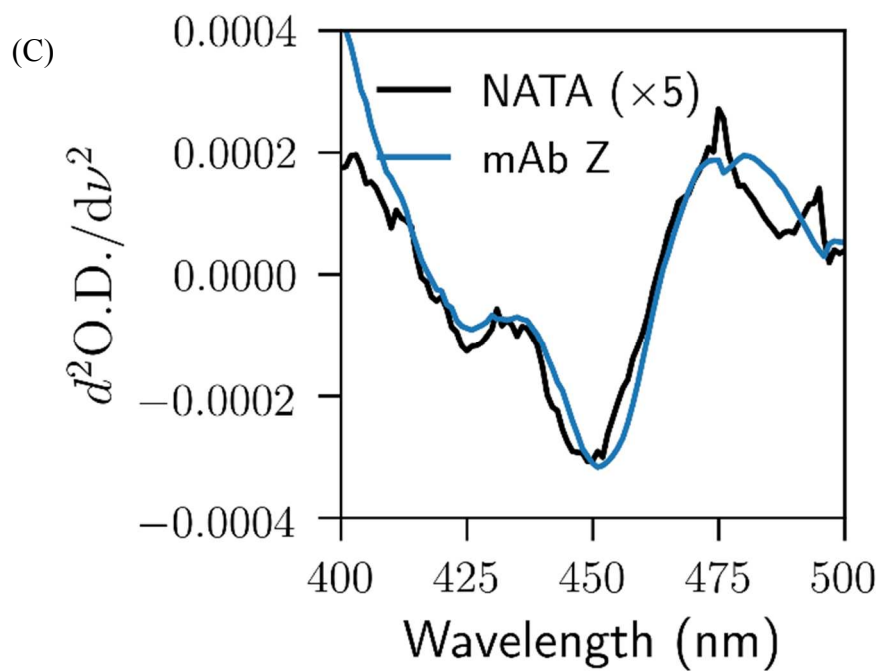


Figure 6: Optical density of (A) mAbZ formulated in 50 mM NaAc buffer, pH 5.5, and (B) 10 mM NATA in 50 mM NaAc buffer, pH 5.5, after photo-irradiation with visible light for 8 h and 6 h, respectively. (C) Second derivative spectra of NATA and mAbZ.

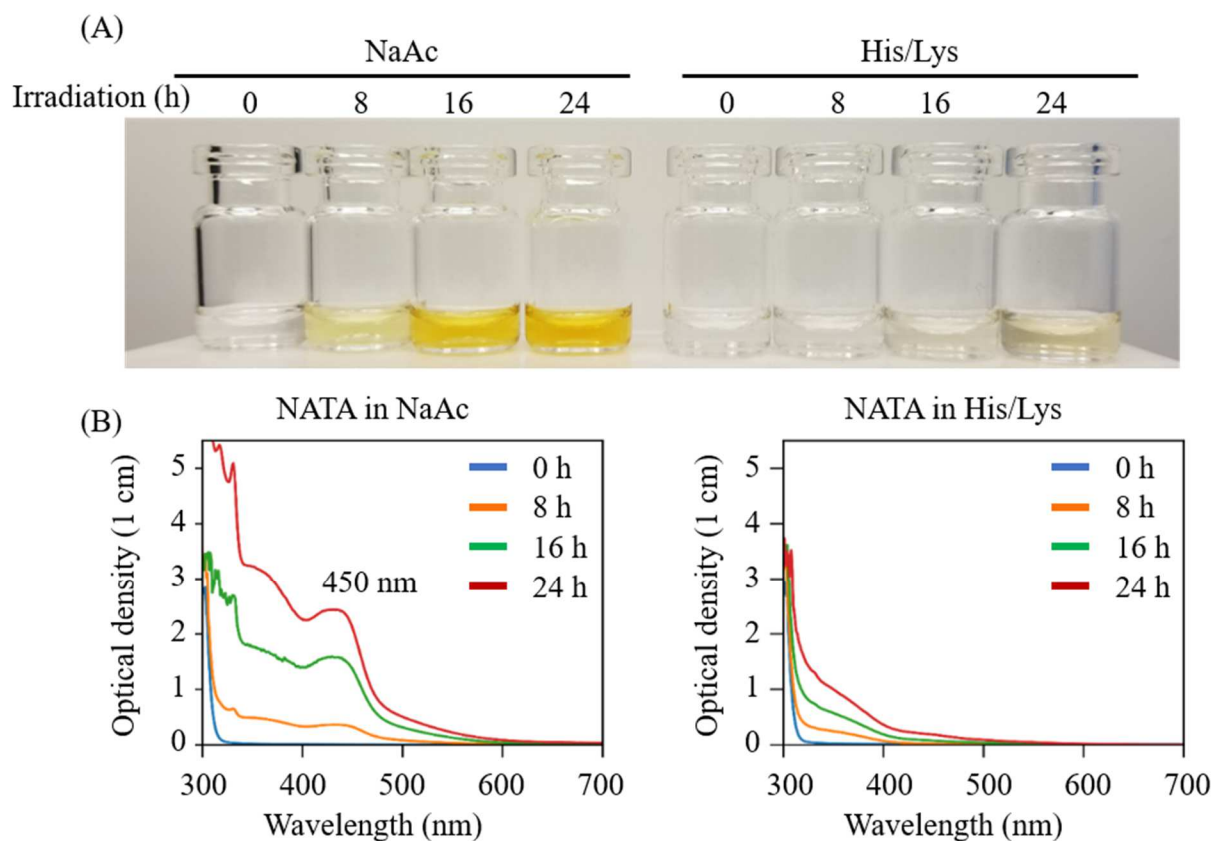


Figure 7: (A) Visible light photo-irradiation of NATA leads to yellow colored solution in NaAc buffer and a brown colored solution in His/Lys. (B) UV-Vis spectra of NATA in NaAc and His/Lys buffer after 0 h (blue trace), 8 h (orange trace), 16 h (green trace), and 24 h (red trace) photo-irradiation. The acetate solution exposed to 24 h photo-irradiation was diluted ten-fold and the displayed spectrum was multiplied by 10.

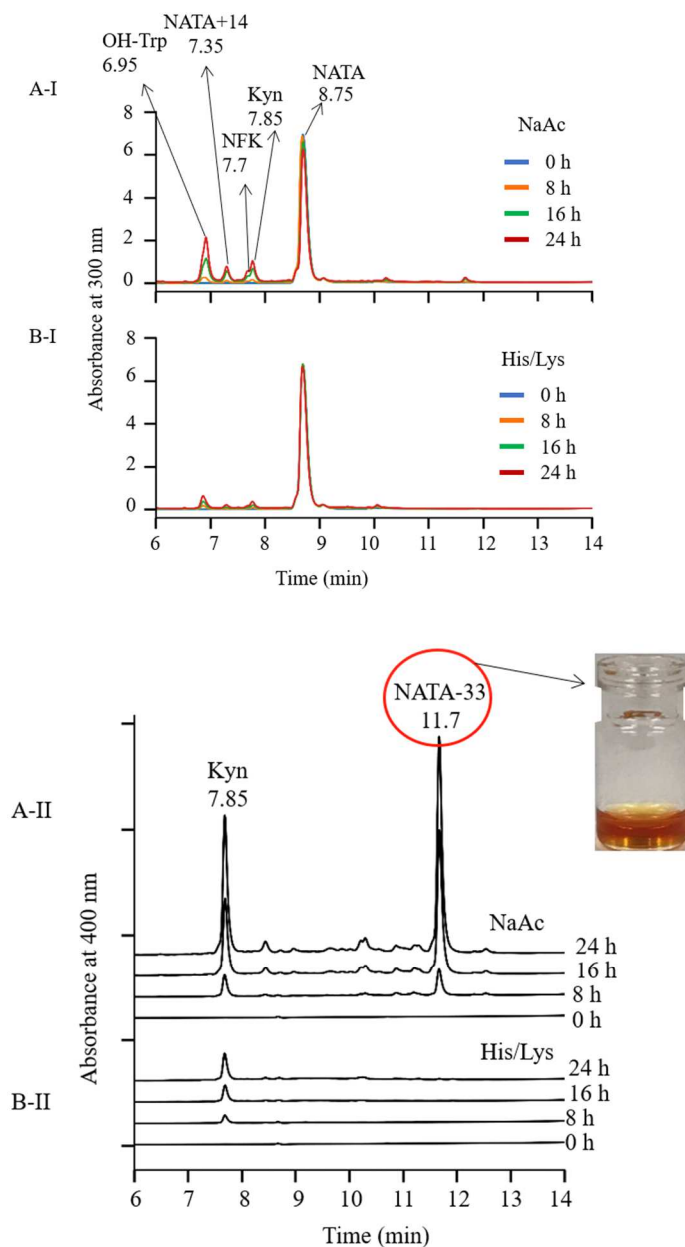


Figure 8: RP-HPLC chromatograms of NATA in NaAc buffer (A-I) monitored at 300 nm and (A-II) at 400 nm, and in His/Lys buffer (B-I) monitored at 300 nm and (B-II) at 400 nm after photoirradiation with visible light for 0 h (blue trace), 8 h (orange trace), 16 h (green trace), and 24 h (red trace). Insert: Picture of NATA-33-containing solution after fraction collection and concentration.

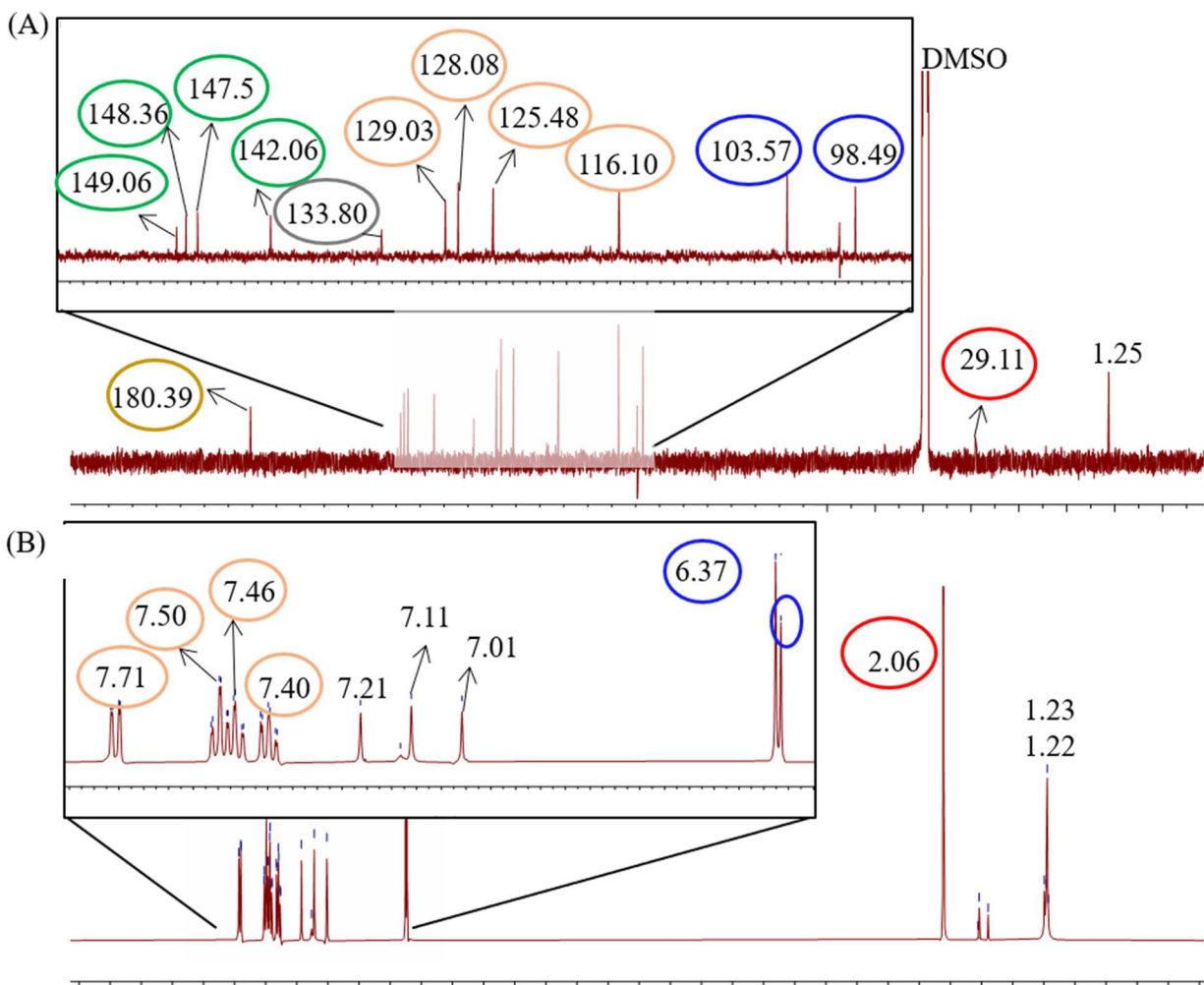
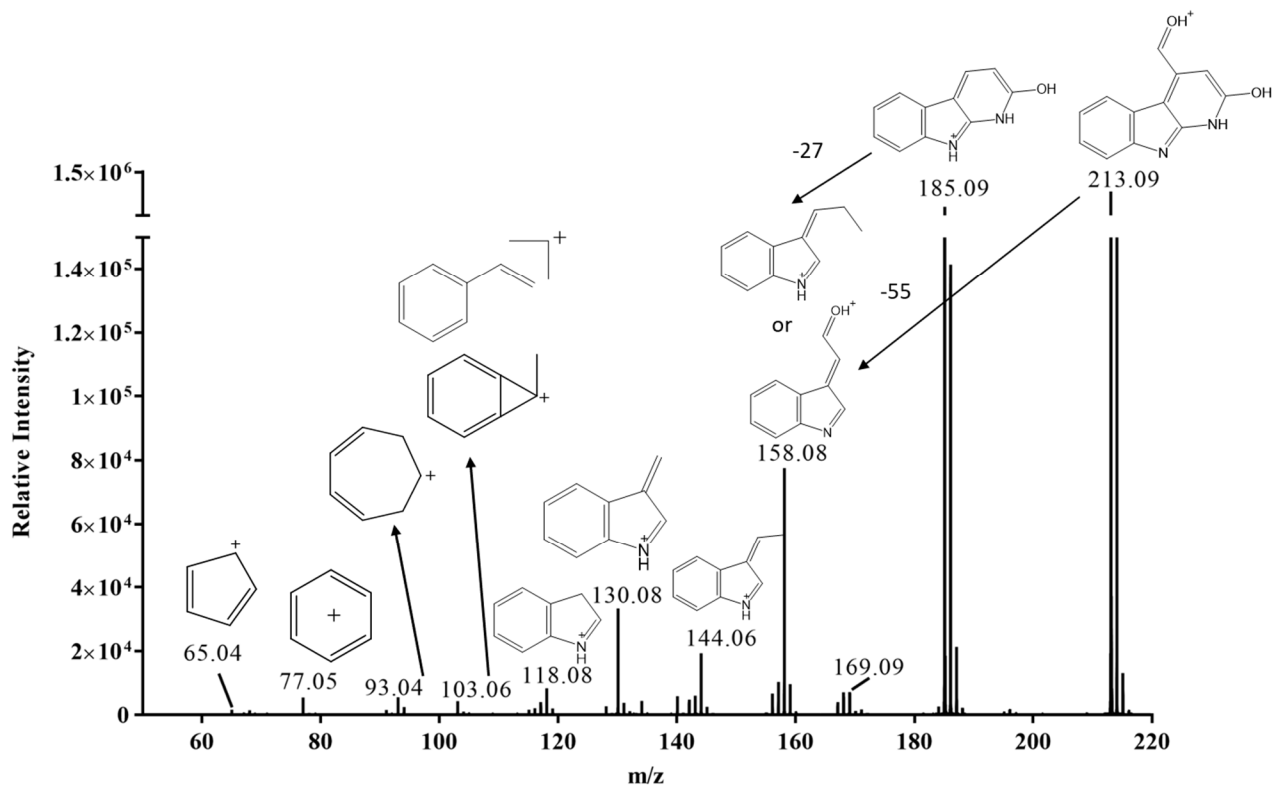


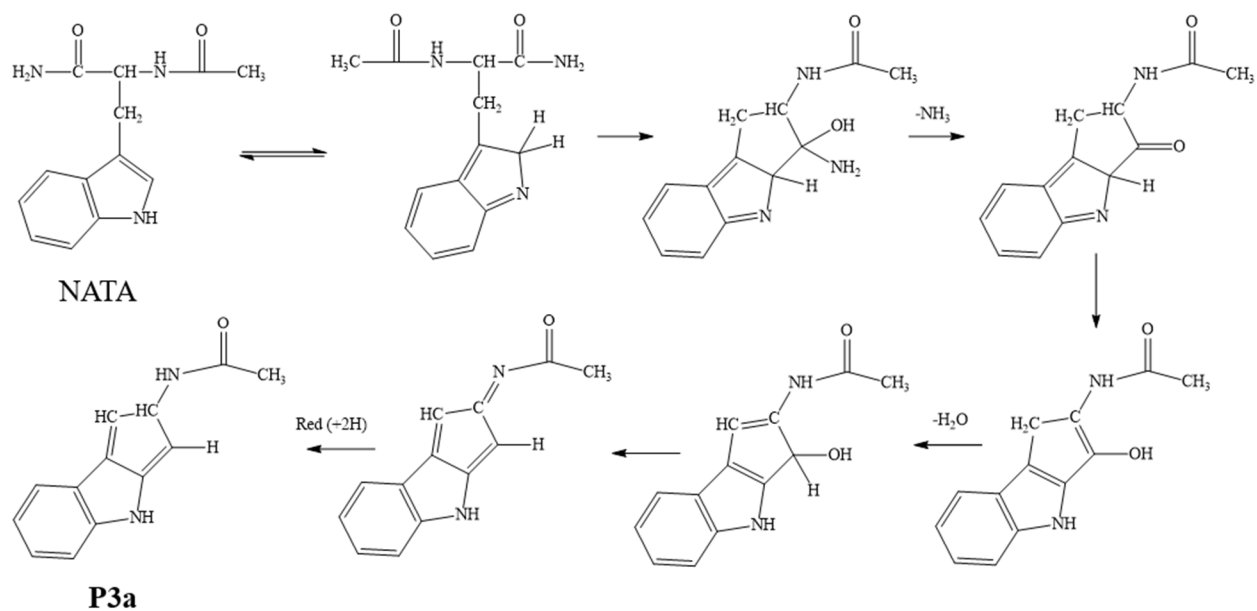
Figure 9: (A) ^{13}C -NMR spectra of NATA-33 and (B) ^1H -NMR spectra of NATA-33, which were correlated with the ^{13}C - and ^1H -NMR predictions of **P1** (refer to structure in Chart 1). See Table 1 for predicted ^1H and ^{13}C peaks of **P1**.



3.7. Table and Scheme

Table 1: Predicted ^{13}C and ^1H spectra of **P1** obtained from MesoNova, nmrd.org, and ChemDraw. The colors are coordinated with spectra in Fig. 9

| | MesoNova | nmrd.org | ChemDraw |
|-----------------|-------------|----------|----------|
| ^{13}C | | | |
| Atoms | Shift (ppm) | | |
| 1 C | 122.8 | 129.2 | 144.3 |
| 2 C | 155.1 | 152.9 | 152.6 |
| 4 C | 151.7 | 156 | 146.7 |
| 5 CH | 117.3 | 120.2 | 126.5 |
| 6 CH | 129.7 | 128.5 | 129.2 |
| 7 CH | 125.3 | 121.8 | 127.1 |
| 8 CH | 126.1 | 120.4 | 127.7 |
| 9 C | 125.1 | 125.6 | 128.4 |
| 11C | 161.6 | 158.3 | 147.4 |
| 12 CH | 98.3 | 119.1 | 73.6 |
| 13 C | 135.5 | 134 | 139.7 |
| 15 CH | 188.1 | 185.2 | 187.5 |
| ^1H | | | |
| | MesoNova | nmrd.org | ChemDraw |
| Atoms | Shift (ppm) | | |
| 5 CH | 7.71 | 8.08 | 7.39 |
| 6 CH | 7.77 | 7.37 | 7.42 |
| 7 CH | 7.51 | 7.54 | 7.32 |
| 8 CH | 7.4 | 7.94 | 7.34 |
| 10 NH | 7.14 | | 5.93 |
| 12 CH | 6.58 | 7.3 | 7.49 |
| 14 OH | 9.82 | | 10.75 |
| 15 CH | 10.77 | 9.98 | 10.35 |



Scheme 1: Proposed mechanism for the formation of **P3a** and its isobaric species shown in Chart 1.

3.8. Supplementary Information

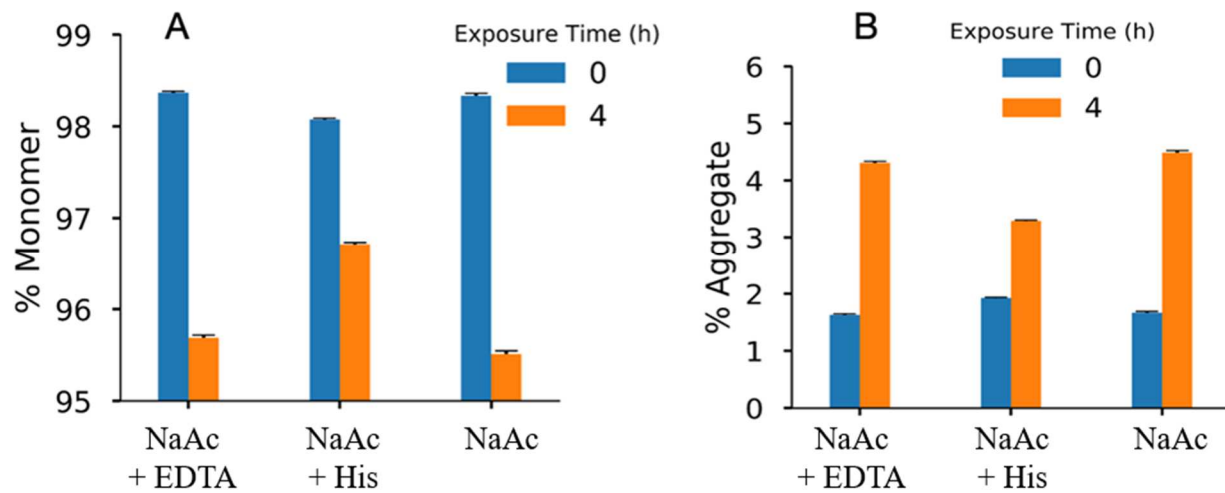


Figure S1: (A) Quantification of loss of monomer and (B) formation of aggregates (contains dimer and HMWS) of mAbZ after exposure to visible light. mAbZ was either formulated in NaAc with EDTA, NaAc with His, or NaAc alone.

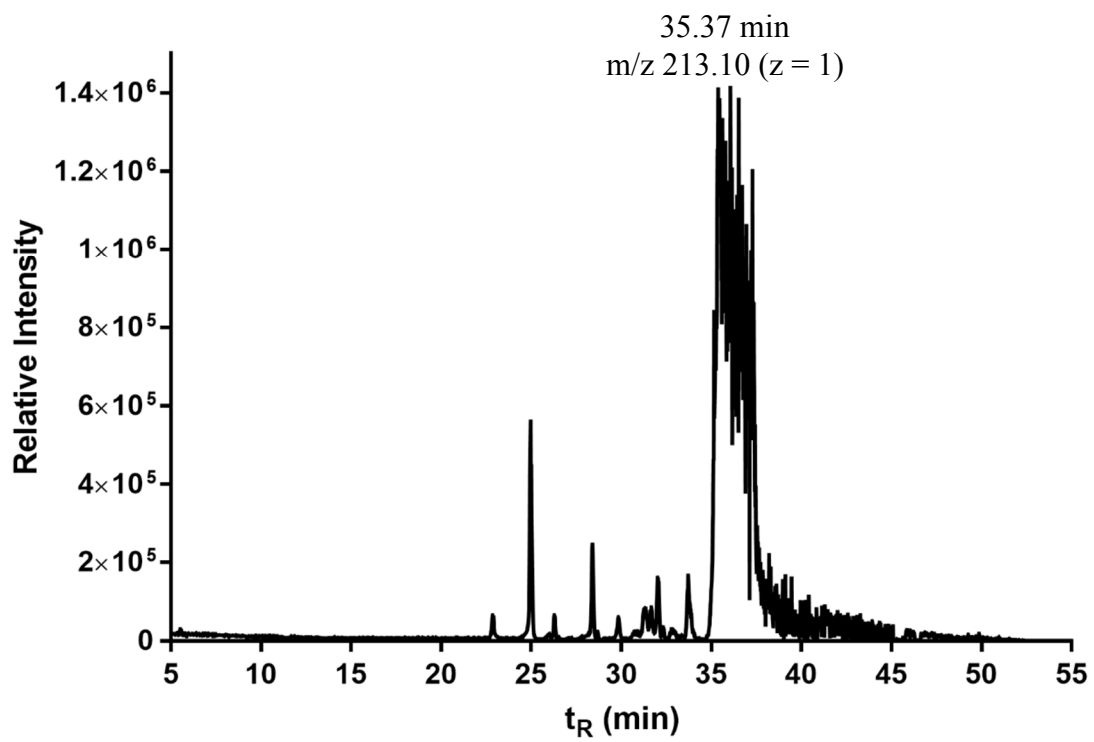


Figure S2: HPLC-MS chromatogram of concentrated NATA-33 photoproduct

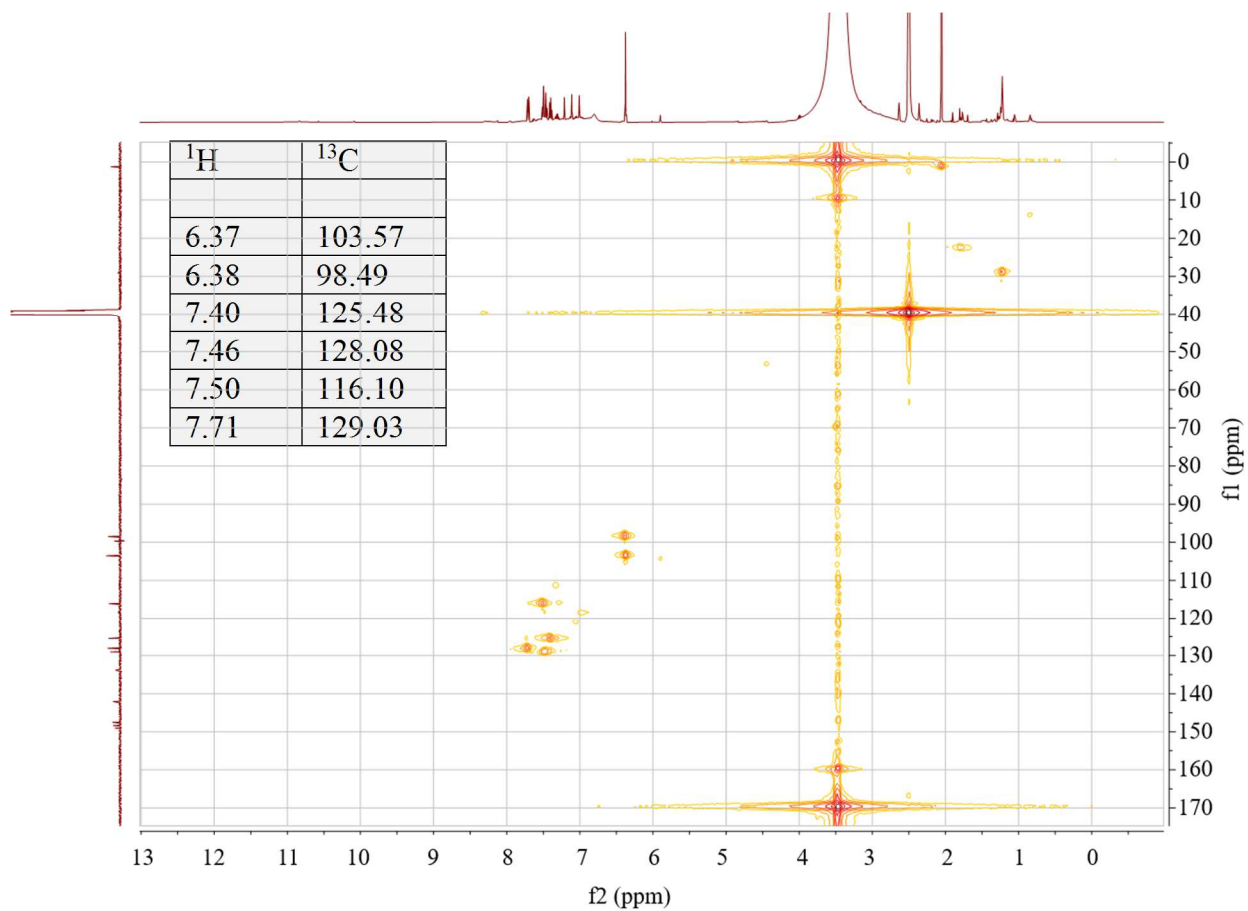


Figure S3: ^1H - ^{13}C HSQC spectrum of NATA-33. Insert: Table with ^1H and ^{13}C HSQC correlation of NATA-33.

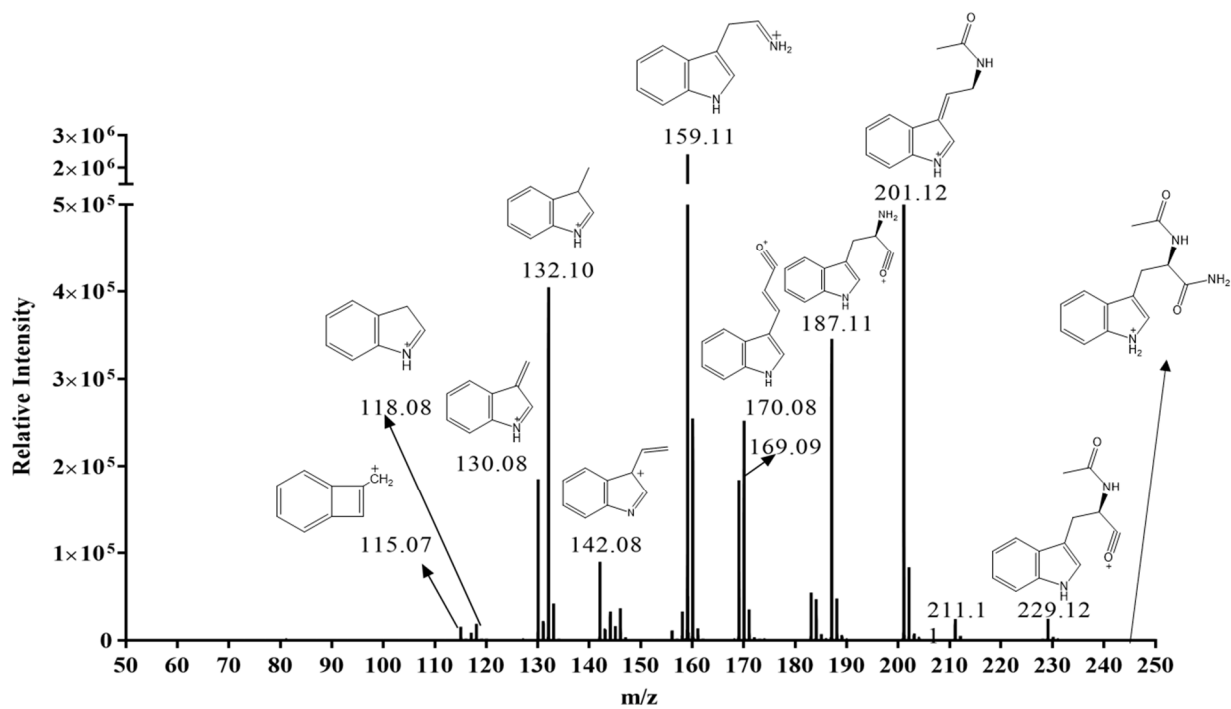


Figure S4: MS/MS spectrum of unmodified NATA

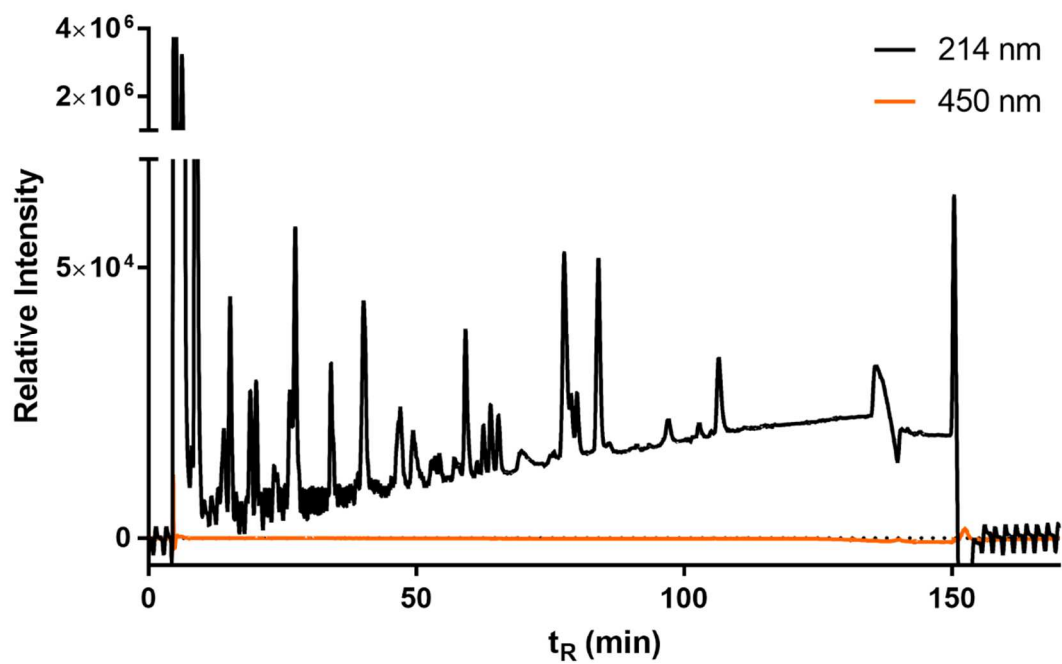
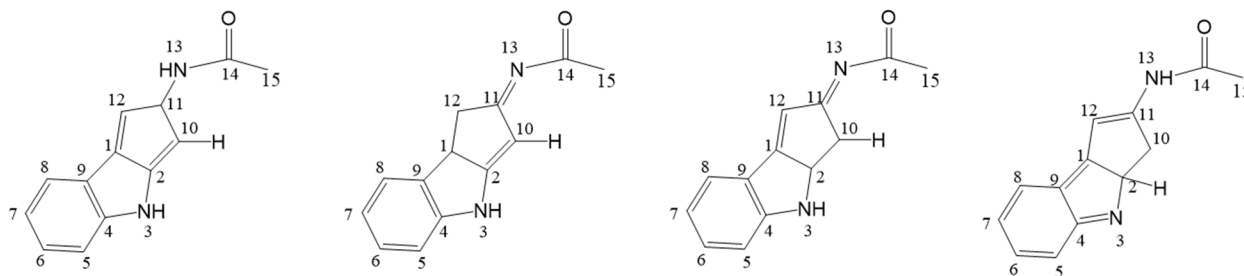


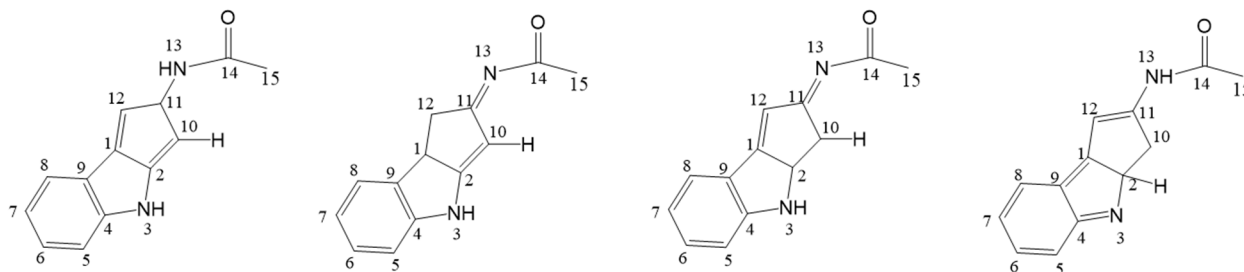
Figure S5: RP-HPLC chromatograms of tryptic peptides of 8 h photo-irradiated mAbZ, monitored at 214 nm (black trace) and 450 nm (orange trace).

Table S1: Predicted ^{13}C spectra of **P3a**, **P3b**, **P3c**, and **P3d** obtained from MesoNova, nmrd.org, and ChemDraw. The colors coordinated with peaks in Fig. 9A.



| P3a | | | | P3b | | | | P3c | | | | P3d | | | |
|-----------------|-------------|----------|-----------|-----------------|-------------|----------|-----------|-----------------|-------------|----------|-----------|-----------------|-------------|----------|-----------|
| | Meso Nova | Nmrd.org | Chem Draw | | Meso Nova | Nmrd.org | Chem Draw | | Meso Nova | Nmrd.org | Chem Draw | | Meso Nova | Nmrd.org | Chem Draw |
| ^{13}C | | | | ^{13}C | | | | ^{13}C | | | | ^{13}C | | | |
| Atom | Shift (ppm) | | | Atom | Shift (ppm) | | | Atom | Shift (ppm) | | | Atom | Shift (ppm) | | |
| 1 C | 131.6 | 129.2 | 141 | 1 CH | 42.9 | 41 | 45.2 | 1 C | 154.7 | 129.2 | 151.5 | 1 C | 170.2 | 129.2 | 141.7 |
| 2 C | 142.6 | 137.5 | 144.9 | 2 C | 162.3 | 137.5 | 153.9 | 2 CH | 59.6 | 58.1 | 54.2 | 2 CH | 68 | 58.1 | 50.9 |
| 4 C | 138.6 | 147.2 | 152.5 | 4 C | 140.5 | 147.2 | 145.1 | 4 C | 152.5 | 147.2 | 158.2 | 4 C | 162.8 | 153.4 | 164.6 |
| 5 CH | 110 | 110.6 | 113.9 | 5 CH | 112.3 | 110.6 | 109.3 | 5 CH | 112.6 | 110.6 | 113.4 | 5 CH | 118.9 | 119.1 | 117.9 |
| 6 CH | 125.3 | 129.6 | 128.7 | 6 CH | 128.5 | 129.6 | 126.7 | 6 CH | 130.7 | 129.6 | 128.7 | 6 CH | 129.5 | 131.3 | 126.5 |
| 7 CH | 120.3 | 122.3 | 118.6 | 7 CH | 122.2 | 122.1 | 118.6 | 7 CH | 118.8 | 122.3 | 117 | 7 CH | 125.5 | 120.8 | 117.9 |
| 8 CH | 121.2 | 124.3 | 123.8 | 8 CH | 123.4 | 122.9 | 126.7 | 8 CH | 124.4 | 124.3 | 125.9 | 8 CH | 126.3 | 132.2 | 126.4 |
| 9 C | 126.1 | 126.7 | 117.3 | 9 C | 129.1 | 130.7 | 118.6 | 9 C | 122.1 | 126.7 | 113.5 | 9 C | 125.8 | 112.6 | 120.8 |
| 10CH | 102 | 119.1 | 97.3 | 10CH | 95.8 | 119.1 | 88 | 10CH2 | 34.2 | 30.5 | 33 | 10CH2 | 37.7 | 30.5 | 41.5 |
| 11CH | 51.9 | 58.1 | 49.8 | 11C | 180.8 | 153.8 | 164.5 | 11C | 169.7 | 153.8 | 164.6 | 11C | 153.3 | 137.5 | 141.9 |
| 12CH | 123.4 | 119.1 | 116.3 | 12CH2 | 39.8 | 30.5 | 27.1 | 12CH | 126.4 | 119.1 | 106.8 | 12CH | 111.1 | 119.1 | 102.9 |
| 14C | 171.1 | 170.6 | 168.6 | 14C | 173.7 | 167.3 | 169 | 14C | 173.7 | 167.3 | 169 | 14C | 170.6 | 168.3 | 169.3 |
| 15CH3 | 22.8 | 22.8 | 23.8 | 15CH3 | 29.2 | 23.3 | 25.1 | 15CH3 | 29.3 | 23.3 | 25.1 | 15CH3 | 23.9 | 23.6 | 23.7 |

Table S2: Predicted ^1H peaks of **P3a**, **P3b**, **P3c**, and **P3d** obtained from MesoNova, nmrdB.org, and ChemDraw. The colors coordinated with peaks in Fig. 9B.



| P2a | | | | P2b | | | | P2c | | | | P2d | | | |
|--------|-------------|-----------|-----------|---------|-------------|-----------|-----------|---------|-------------|-----------|-----------|--------|-------------|-----------|-----------|
| | Meso Nova | nmrdB.org | Chem Draw | | Meso Nova | nmrdB.org | Chem Draw | | Meso Nova | nmrdB.org | Chem Draw | | Meso Nova | nmrdB.org | Chem Draw |
| Atom | Shift (ppm) | | | Atom | Shift (ppm) | | | Atom | Shift (ppm) | | | Atom | Shift (ppm) | | |
| 3 NH | 8.66 | | 10.53 | 1 CH | 4.29 | 4.34 | 3.5 | 2 CH | 4.9 | 5.005 | 3.3 | 2 CH | 4.66 | 4.43 | 2.2 |
| 5 CH | 7.3 | 6.48 | 7.2 | 3 NH | 8.03 | | 10.71 | 3 NH | 4.22 | | 6.91 | 5 CH | 7.46 | 6.19 | 6.2 |
| 6 CH | 7.41 | 7.19 | 7.5 | 5 CH | 6.86 | 7.22 | 6.44 | 5 CH | 7.07 | 6.91 | 6.77 | 6 CH | 7.46 | 6.52 | 7.98 |
| 7 CH | 7.11 | 6.798 | 6.7 | 6 CH | 7.24 | 7.273 | 7.05 | 6 CH | 7.19 | 7.74 | 7.07 | 7 CH | 7.34 | 6.14 | 7.93 |
| 8 CH | 8.16 | 7.3 | 8.49 | 7 CH | 7.05 | 7.12 | 6.41 | 7 CH | 6.97 | 7.31 | 6.79 | 8 CH | 7.76 | 6.89 | 5.84 |
| 11 CH | 6.05 | 4.607 | 5 | 8 CH | 7.46 | 6.57 | 6.98 | 8 CH | 7.44 | 7.79 | 7.24 | 10'CH2 | 2.85 | 3.04 | 2.1 |
| 12 CH | 6.95 | 6.39 | 6.59 | 12' CH2 | 2.91 | 2.59 | 2.59 | 10 CH2' | 2.97 | 2.88 | 2.23 | 10"CH2 | 2.91 | 3.05 | 1.9 |
| 13 NH | 8.25 | | 8.95 | 12" CH2 | 2.96 | 3.07 | 2.34 | 10 CH2" | 3.04 | 3.3 | 2.48 | 12 CH | 7.03 | 6.494 | 5.64 |
| 15 CH3 | 1.96 | 1.91 | 1.92 | 15 CH3 | 2.25 | 2.25 | 2.1 | 12 CH | 6.86 | 6.33 | 5.55 | 13 NH | 8.84 | | 10.45 |
| 10 CH | 6 | 5.32 | 5.87 | 10 CH | 6.91 | 6.04 | 4.59 | 15 CH3 | 2.25 | 2.254 | 2.1 | 15 CH3 | 2.1 | 2.12 | 1.86 |

Chapter 4: Cis/trans isomerization of unsaturated fatty acids in polysorbate 80 during light exposure of a monoclonal antibody-containing formulation

4.1. Introduction

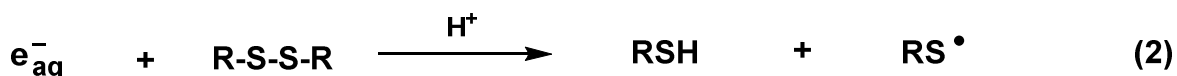
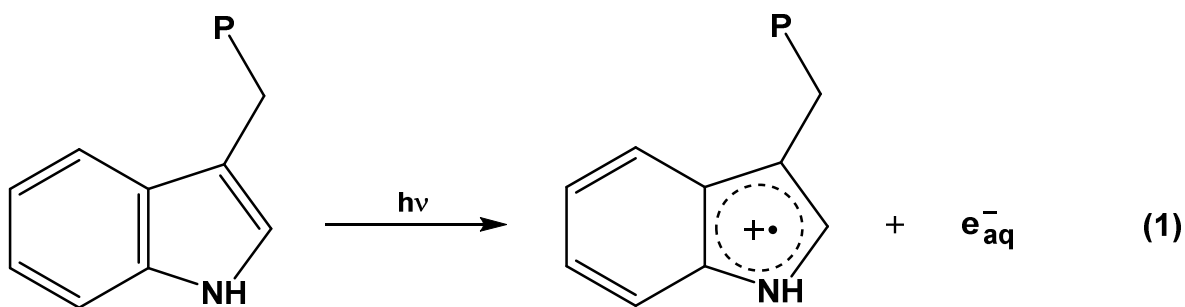
Polysorbates are non-ionic surfactants and are frequently present in protein formulations in order to prevent aggregation or surface adsorption.¹⁻³ They comprise highly heterogeneous mixtures of fatty acid (FA) esters of polyoxyethylene (POE), polyoxyethylated sorbitan and polyoxyethylated isosorbide.¹ The chemical stability of polysorbates is a concern where both oxidation and hydrolysis products can affect the integrity of pharmaceutical formulations.¹⁻⁴ For example, proteins are sensitive to modification by peroxides⁵⁻⁶ and aldehydes/ketones⁷⁻⁸ generated through polysorbate oxidation. Moreover, free fatty acids (FFAs), generated via hydrolysis⁹⁻¹² or oxidation,¹³ can generate particles, which may cause turbidity and/or protein adsorption/aggregation.

A common hypothesis is that polysorbate degradation affects protein stability, i.e. that polysorbate degradation products trigger chemical and/or physical protein degradation. While there is good evidence supporting this hypothesis, recent studies also point to a role for protein in the generation of polysorbate degradation products. For example, it was reported that FFA generation in selected protein formulations can be the result of enzymatic hydrolysis, catalyzed by small levels of residual host cell proteins such as esterases and/or lipases.⁹⁻¹² These results motivated us to evaluate additional potential protein-dependent pathways of polysorbate degradation. Considering the sensitivity of proteins to redox processes, reactive protein intermediates may play a more general role in the oxidative degradation of polysorbate.

Here, we report that the light-exposure of polysorbate 80 (PS80)-containing formulations can induce the cis/trans isomerization of unsaturated FAs in polysorbate esters when proteins are present. These isomerization reactions likely result from reactions of thiyl radicals,¹⁴⁻¹⁹ which can be generated during the light exposure of proteins.²⁰⁻²² Evidence for thiyl radical-mediated

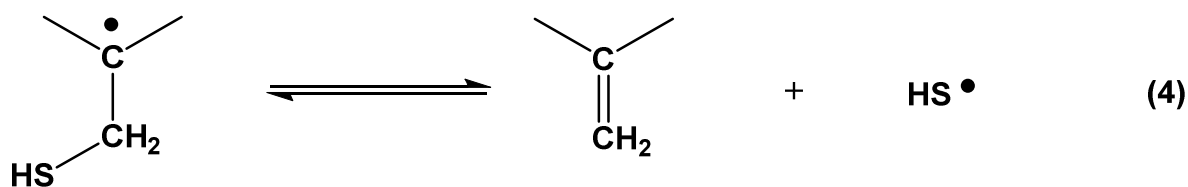
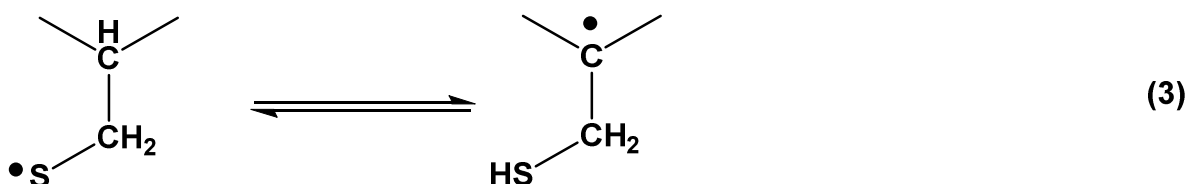
cis/trans isomerization of mono- and polyunsaturated FAs comes from a series of mechanistic studies with isolated FAs and their methyl esters, phospholipids, micelles and vesicles.¹⁴⁻¹⁹

Light exposure of a monoclonal antibody (mAb) can generate thiyl radicals (RS^\bullet) via various different pathways. First, the photo-ionization of a protein tryptophan (Trp) residue²³ can lead to a hydrated electron, which efficiently reduces a protein disulfide bond to yield a protein thiyl radical and thiol (reactions 1 and 2).²² Photo-ionization processes of Trp have been observed at wavelengths > 300 nm,²⁴⁻²⁵ including typical pharmaceutical photostability testing in light chambers.²⁶⁻²⁷



Concomitantly, this photo-ionization generates a tryptophan radical cation ($\text{Trp}^{+\bullet}$), and evidence for the formation of $\text{Trp}^{+\bullet}$ during the light exposure of a mAb was provided by the detection of specific stable reaction products originating from $\text{Trp}^{+\bullet}$ (such as Trp side chain cleavage products).²⁷⁻²⁸ In principle, protein thiyl radicals can react with unsaturated and polyunsaturated FAs to induce cis/trans isomerization. However, in polysorbate-containing solutions such

reactions may be restricted to polysorbate located outside micelles or directly associated with the protein. More efficient at inducing the cis/trans isomerization of unsaturated FAs, especially when located in micelles, would be small, lipophilic thiyl radicals such as e.g. the sulfhydryl radical (HS•)¹⁸. The latter can be generated from cysteine thiyl radicals following 1,3-H-transfer and β-



elimination (reactions 3 and 4; only the side chain of cysteine is shown).²⁹

Because the cis/trans isomerization of mono- and polyunsaturated fatty acids is a chain reaction, even small quantities of thiyl radicals can lead to significant product yields, depending on the chain length of the reaction.³⁰ In the following, we will demonstrate that cis/trans isomerization of unsaturated fatty acids proceeds upon light exposure of a formulation containing PS80 and (i) a monoclonal antibody, or (ii) a combination of N-acetyltryptophan amide (NATA) and glutathione disulfide (GSSG). The latter fact provides additional support for a thiyl radical-mediated mechanism, as the system NATA/GSSG provides the two essential components for thiyl radical formation according to reactions (1) and (2), Trp and a disulfide, and represents a suitable model for Trp/disulfide triads²⁶ in monoclonal antibodies.

4.2. Materials and Methods

4.2.1. Materials

Polysorbate 80 N.F. (J.T. Baker, product #4117-04, batch #0000190001) was purchased from Avantor (Radnor, PA). A monoclonal antibody (mAbZ) was provided by MedImmune (Gaithersburg, MD), formulated at 150 mg/ml mAbZ in the presence of 0.01% (w/w) PS80, sodium chloride, and sodium acetate. Sodium acetate (NaAc, product #S2889), glacial acetic acid (product #A38SI-212), oxidized L-Glutathione (GSSG, product #G4376), N-acetyl-L-tryptophanamide (NATA, product #A6501), poly(ethylene glycol) (PEG, product #92897), linoleic acid (product #L1376), (9Z, 11E)-octadeca-9,11-dienoic acid (product #16413), (9E, 11Z)-octadeca-9,11-dienoic acid (product #90983), (10E, 12Z)-octadeca-10,12-dienoic acid (product #04397), oleic acid (product #75090), elaidic acid (product #45089), and porcine esterase (product #1002633920, batch #SLBM0487V) were from Millipore Sigma (Burlington, MA). Ethyl acetate (product #E195-4) and borosilicate glass tubes (product #1496127) were from Fisher Scientific (Hampton, NH). Quartz glass tubes (product #8683) were from Ace Glass Incorporated (Vineland, NJ). 1,4-Dioxane (product #43167) was from Alfa Aesar (Tewksbury, MA). Ethanol (product #2701) was from Decon Laboratories (King of Prussia, PA). Water of ultra-pure quality (18.2 M Ω) was produced fresh with a WaterPro PS Polishing System (Labconco, Kansas City, MO).

4.2.2. Photo-irradiation

Photo-irradiation was performed in either quartz ($\lambda = 254$ nm) or borosilicate test tubes (all other conditions; wavelength cut off < 295 nm) under air atmosphere in a Rayonet Photoreactor (RPR-200, The Southern New England Ultraviolet Company, Branford, CT) equipped with either of the

following lamps (The Southern New England Ultraviolet Company, Branford, CT): RPR-2537A ($\lambda = 254$ nm), RPR-3000A ($\lambda_{\max} = 305$ nm; emission spectrum between 265 and 340 nm, RPR-3500A ($\lambda_{\max} = 350$ nm, emission spectrum between 305 and 416 nm), or RPR-4190A ($\lambda_{\max} = 419$ nm, emission spectrum between 390 and 475 nm). Actinometry was performed with the iodide/iodate actinometer³¹ for the RPR-2537A lamps, and the ferrioxalate actinometer³²⁻³⁴ for the RPR-3000A, RPR-3500A, and RPR-4190A lamps. In general, photon fluxes for all experimental conditions were $< 4 \times 10^{-8}$ Einstein/s (depending on sample volume). Based on the used sample volumes and test-tube geometries, our conditions correspond to light intensities of < 40 W.h/m² for 1 h photo-irradiations at $\lambda = 254$ nm and < 25 W.h/m² for 1 h photo-irradiations at $\lambda_{\max} = 305, 350$ and 419 nm[§], i.e. $< 20\%$ and $< 12.5\%$, respectively, of the minimal intensity (200 W.h/m²) recommended for UV photostability testing by the ICH guideline ICH Q1B.³⁵ A critical assessment of the ICH Q1B guideline is given in the commentary by Baertschi *et al.*³⁶ The authors provide typical UV-A light intensities for indoor lighting with window-filtered daylight at home and in the clinic (17 W/m²). Our light exposures of < 25 W.h/m² at $\lambda_{\max} = 305, 350$ and 419 nm would correspond to ca. 1-2 h exposure to indoor lighting at home or in the clinic.³⁶

4.2.3. Photo-irradiation of mAbZ formulations containing 0.01% PS80

Aliquots of 500 μ l containing the mAbZ formulations containing 0.01% (w/w) were photo-irradiated for 1 h with 4 lamps using the glassware/lamp type combinations described above. To separate protein from PS80, the protein was precipitated with 900 μ l cold ethanol by incubation at -20 °C for 1 h. The mAbZ pellet was separated from PS80 by centrifugation for 30 min at 14,000 rpm (16,900g) at 4 °C. The supernatant was recovered and dried in a CentriVap (Labconco, Kansas City, MO) for 2 h at room temperature. Each dried sample was then dissolved

in 100 μ l of a 50/50 (v/v) ethanol/water mixture and vortexed to yield a PS80 concentration of 0.01% (w/w) for liquid chromatography-mass spectrometry (LC-MS) analysis. As controls, aliquots of the mAbZ formulations were wrapped in aluminum foil and subsequently subjected to the same procedures of sample preparation.

4.2.4. Photo-irradiation of spiked mAbZ formulations containing 0.2% PS80

PS80 was spiked into the mAbZ formulation (see above) to bring the PS80 concentration to 0.2% (w/w). Aliquots of 200 μ l were photo-irradiated at either $\lambda = 254$ nm or $\lambda_{\text{max}} = 305$ nm as described above for 1 h with 4 lamps, respectively. Precipitation and supernatant drying were performed as described above. Each dried sample was then dissolved in 1 ml of a 50/50 (v/v) ethanol/water solution and vortexed to yield a PS80 concentration of 0.02% (w/w) for LC-MS analysis. As controls, aliquots of the mAbZ formulations were wrapped in aluminum foil and subsequently subjected to the same procedures of sample preparation.

4.2.5. Photo-irradiation of model peptide formulations containing 0.01% and 0.2% PS80

The combination of Trp and disulfide is the basic entity amenable to light-induced generation of thiyl radicals according to reactions 1 and 2, and is a suitable model for Trp/disulfide triads²⁶ in monoclonal antibodies. Stock solutions containing 10 mM GSSG and/or 10 mM NATA were prepared in 20 or 50 mM NaAc buffer (pH 5.5). An initial stock of 10% (w/w) PS80 in water was diluted to 0.02% and 0.4% (w/w) in 20 or 50 mM NaAc buffer (pH 5.5), and mixed 1:1 with the stock solutions containing GSSG, NATA, or both, to bring the final concentration of GSSG and/or NATA to 5 mM, and PS80 to either 0.01% or 0.2% (w/w). Aliquots of 400 μ l were photo-irradiated at $\lambda_{\text{max}} = 305$ nm as described above for 1 h with 4 lamps. To ensure comparability, precipitation and supernatant drying was also performed for model peptide samples as described

above. Each dried sample was then dissolved in 100 μ l (model peptide formulations with 0.01% PS80 (w/w)) or 1 ml (model peptide formulations with 0.2% PS80 (w/w)) of a 50/50 (v/v) ethanol/water solution and vortexed to yield PS80 concentrations of 0.01% and 0.02% (w/w) for LC-MS analysis, respectively. As dark controls, reaction mixtures were wrapped in aluminum foil and exposed to 1 h photo-irradiation in the Rayonet reactor. In addition, we confirmed that the exposure of the reaction mixtures to elevated temperatures (40°C, 2 days) did not result in cis/trans isomerization.

4.2.6. Photo-irradiation of PS80 in the absence of mAbZ and model peptides

A stock solution of 10% PS80 (w/w) was prepared in water. The PS80 stock solution was diluted to either 0.01% or 0.2% (w/w) in either 50 or 20 mM NaAc buffer (pH 5.5). Aliquots of 500 μ l were photo-irradiated separately using the glassware / lamp type combinations described above for 1 h with 4 lamps, respectively. We subsequently subjected these samples to the same precipitation and drying procedures as described above for the removal of mAbZ from samples containing PS80. Each dried sample was then dissolved in 100 μ l (formulations with 0.01% PS80 (w/w)) or 1 ml (formulations with 0.2% PS80 (w/w)) of a 50/50 (v/v) ethanol/water solution and vortexed to yield PS80 concentrations of 0.01% and 0.02% (w/w) for LC-MS analysis, respectively. As dark controls, reaction mixtures were wrapped in aluminum foil and exposed to 1 h photo-irradiation in the Rayonet reactor.

4.2.7. Generation of FFAs from 0.01% and 0.2% PS80 with porcine esterase

FFA generation for analysis from 0.01% (w/w) PS80 solutions required pre-concentration. To concentrate a sample from 0.01% to approximately 0.05% PS80, 100 μ l aliquots from a 500 μ l sample were divided into 5 vials and subjected to precipitation and drying as described above.

Then, 100 μ l of 10 mM phosphate buffer (pH 7.2) was added to the first of the 5 vials, and subsequently transferred from one vial to the next to recover PS80. An aliquot of 2 μ l of porcine esterase (10 units; 24 mg esterase/ml; 208 units/mg protein) was added to this concentrated PS80 solution and incubated at 37 °C for 1 h (during 1 h esterase reaction, ca. 27% free oleic acid was generated, mainly from the hydrolysis of oleic acid monoesters, consistent with earlier data¹⁰). The esterase was precipitated with cold ethanol and the supernatant dried. The dried sample was dissolved in 50 μ l ethanol for LC-MS analysis. The recovery of FFAs was >60%. The dark control samples were wrapped in aluminum, stored at room temperature and subjected to the same procedures to obtain FFAs. No pre-concentration step was required for the generation and analysis of FFAs from 0.2% (w/w) PS80 solutions. They were directly subjected to precipitation and drying. However, two precipitation methods were compared using either borosilicate glass or Eppendorf tubes. Interestingly, higher levels of baseline FFA oxidation products were observed after precipitation in borosilicate glass; therefore, precipitation was conducted in Eppendorf tubes in order to monitor photo-chemically generated FFA oxidation products.

4.2.8. HPLC-MS analysis of PS80

The PS80 components and their degradants were analyzed by electrospray ionization (ESI) mass spectrometry on a Waters Q-TOF Premier mass spectrometer (Milford, MA, USA) coupled to a Waters ACQUITY UPLC system (Milford, MA, USA). The electrospray ionization source was maintained at 120°C, and the capillary voltage set to 2.8 kV. Data were collected in the MS^E mode (first function) at a mass range of 150-2000 Da. The mass spectrometer was operated in the positive ion mode with the Masslynx v.4.1 software, and the data were analyzed with the same software.

All analytes were separated on a Prevail™ C18 column (Grace, Deerfield, IL; 150 mm × 2.1 mm, 300 Å pore-size, 3.0 µm particle size). The column temperature was maintained at 40 °C and either 10 µl of 0.01% (w/w) PS80 or 5 µl of 0.02% (w/w) PS80 (i.e. 1 µg PS80 based on the initial sample concentration) were injected onto the column and eluted at a flow rate of 0.4 ml/min. Four mobile phases, A-D, were used to elute PS80 from the column. Mobile phase A contained 2 mM ammonium formate, and 0.08% formic acid in water, mobile phase B contained a 7:3 (v/v) acetonitrile/methanol solution with 0.08% formic acid, mobile phase C consisted of isopropanol, and mobile phase D contained a 1:9 (v/v) 1,4-dioxane/acetone solution, respectively. Separation of PS80 components was achieved with the following gradient (all changes linear): initially, the mobile phase composition was 40% A and 60% B, within 15 min the composition was changed to 1% A and 99 % B, within the next 5 min the composition was changed to 1% A, 94% B, and 5% C, within the next 1 min the composition was changed to 1% A, 90% B, and 9% C and held for 2 min, within the next 1 min the composition was changed to 1% A and 99% D and held for 3 min (wash phase), within the next 1 min the composition was changed back to 40% A and 60% B and the column was re-equilibrated for 7 min.

4.2.9. HPLC-MS analysis of FFAs

FFAs were analyzed by electrospray ionization mass spectrometry on the same instrument described above. The column, Masslynx software, and instrument settings remained identical except that the instrument was operated in the negative ion mode and data were collected in the MS^E mode (first function) at a mass range of 100-2000 Da. 10 µl aliquots were injected onto the column and eluted at a flow rate of 0.4 ml/min. Three mobile phases, A-C as described above, were used to elute FFAs from the column. Separation of FFAs was achieved with the following gradient (all changes linear): initially, the mobile phase composition was 40% A and 60% B,

within 1 min the composition was changed to 22% A and 78 % B, within the next 11 min the composition was changed to 16% A, 80% B, and 4% C, within the next 1 min the composition was changed to 75% B and 25% C, within the next 2 min the composition was changed to 10% A, 40% B, and 50%C, within the next 1 min the composition was changed back to 40% A and 60% B, and the column was re-equilibrated for 4 min.

4.2.10. Sample preparation for Raman Fourier transform infrared (FTIR) spectroscopy

Two sets of samples were prepared for Raman and FTIR spectroscopy: (i) 5 mM GSSG, 5 mM NATA, 0.2% (w/w) PS80 in 20 mM NaAc (pH 5.5); (ii) 147 mg/ml mAbZ formulated with PS80 and NaAc. A dark control and a photo-irradiated sample were produced for each sample formulation. Aliquots of 3 ml were photo-irradiated at $\lambda_{\max} = 305$ nm as described above for 1h with 4 lamps.

PS80 extraction for each sample was performed using a 50/50 (v/v) ethyl acetate/1,4-dioxane solution (“organic phase”)[§]: equal volumes of sample and organic phase were mixed by pipetting and centrifuged at 4500 rpm and 4 °C for 10 min. The organic phase was then collected into a fresh borosilicate tube and the procedure repeated two more times. The collected organic phases were dried in a CentriVap for 2 h at room temperature. Each dried sample was dissolved in ethanol to yield a 50 mg/ml PS80 solution based on initial PS80 concentrations. Reference substances (oleic acid, elaidic acid, linoleic acid, and the conjugated octadecadienoic acids) were dissolved or diluted in ethanol to yield final concentrations of 50 mg/ml. Except during photo-irradiation, all sample and reference solutions were protected from light and kept on ice at all times.

4.2.11. Raman and FTIR Spectroscopy

Raman spectra of sample and reference solutions were obtained using a Zetasizer Nano ZS Helix (Malvern Panalytical, Malvern, United Kingdom) connected to a Kaiser Raman RxN1 spectrometer (Kaiser Optical Systems, Ann Arbor, MI). The spectrometer includes a 785 nm laser having a maximum power output of 400 mW. For each measurement, 20 replicates of 10 s exposure intervals were recorded from 100 – 1890 cm^{-1} . The sample cell was set to 25 °C. Raman spectra were background subtracted, baseline offset corrected, and normalized. Second derivative spectra were calculated following Savitzky-Golay smoothing with a 13-point 3rd order polynomial.

FTIR spectra of sample and reference solutions were obtained using a Bruker Tensor 27 FTIR spectrometer fitted with a Bio-ATR cell (Bruker, Billerica, MA) set to 25 °C. For each measurement, 256 scans were recorded from 800 – 4000 cm^{-1} at a resolution of 4 cm^{-1} . OPUS 6.5 (Bruker) was used for atmospheric correction and baseline fitting.

4.3. Results

4.3.1. Oleic acid

When we exposed a formulation of 150 mg/mL mAbZ in the presence of 0.01% (w/w) PS80, NaCl, and NaAc to 1 h photo-irradiation at $\lambda_{\text{max}} = 305$ nm, some significant changes in PS80 composition were noted by LC-MS analysis (Figure 1A and 1B). In controls (Figure 1A), the peaks with $t_R = 11.23$ and 12.65 min represent POE sorbitan oleic acid and POE oleic acid, respectively. Notably, photo-irradiation leads to a change in peak shape for POE sorbitan oleic acid (Figure 1B; peak I), and a new peak with $t_R = 12.84$ min (Figure 1B; peak IIb), eluting directly after POE oleic acid (Figure 1B; peak IIa). MS analysis reveals that the new peak with t_R

= 12.84 min contains a product which is isobaric with POE oleic acid, suggesting the generation of isomers. None of these changes appear when 0.01% (w/w) PS80 in either 20 mM or 50 mM NaAc (pH 5.5) is photo-irradiated in the absence of mAbZ (not shown). Figure 2 compares the LC-MS peaks representatively for the extracted signal of m/z 828.60 ($z = +1$, $[M+NH_4]$) of a control formulation (Figure 2A) and a formulation photo-irradiated for 1 h at $\lambda = 254$ nm (Figure 2B) and $\lambda_{\max} = 305$ nm (Figure 2C) to further illustrate the formation of such isobaric species. Here, m/z 828.60 represents a POE oleic acid containing 12 ethylene oxide (EO) units, POE (12) oleic acid. Analogous analyses were made for POE oleic acid components; these contain between 6 and 22 EO units and make up the envelope of all POE oleic acid species present in the peaks eluting with $t_R = 12.56$ and 12.84 min. The isobaric species with m/z 828.60 forms during photo-irradiation for 1h at either $\lambda = 254$ nm and $\lambda_{\max} = 305$ nm, but not $\lambda_{\max} = 350$ nm (Figure 2D). However, during longer photo-irradiation times (up to 8 h; equivalent to < 200 W.h/m²) at $\lambda_{\max} = 350$ nm, the isobaric species with m/z 828.60 is generated (Figure S1), indicating that near UV light is able to trigger the reactions leading to the formation of the isobaric species. In contrast, visible light photo-irradiation at $\lambda_{\max} = 419$ nm for up to 12 h did not generate significant yields of the isobaric reaction product. A similar analysis was also made for POE sorbitan oleic acid components, where photo-irradiation at $\lambda_{\max} = 305$ nm resulted in the generation of isobaric species. This is shown representatively for POE (26) sorbitan oleic acid in Figure S2, where the signal of m/z 804.56 ($z = +2$, $[M+2NH_4]$) revealed a shoulder after photo-irradiation.

The formation of a reaction product isobaric with POE oleic acid suggests that oleic acid may undergo cis/trans isomerization to elaidic acid. In order to evaluate this possibility, we subjected reaction mixtures to porcine esterase to liberate FFAs. Figure 3 compares formulations containing no (panel A) or 150 mg/ml mAbZ (panel B), after esterase treatment following 1h photo-

irradiation at $\lambda_{\max} = 305$ nm. Clearly, elaidic acid is generated during photo-irradiation only in the presence of mAbZ, confirmed by spiking (0.01 mg/mL) with an authentic standard of elaidic acid (Figure S3).

The conversion of oleic into elaidic acid is likely caused by intermediary thiyl radicals, which can be generated by photo-induced electron transfer from Trp to protein disulfide bonds²². In fact, mAbs contain Cys-Cys-Trp triads, which are exquisitely sensitive to photo-degradation²⁶. Further experimental support for a role of photo-induced electron transfer from Trp to disulfides in the formation of elaidic acid was, therefore, acquired in a model system where final concentrations of 5 mM NATA and 5 mM GSSG were added to 0.01% (w/w) PS80 in 20 mM NaAc (pH 5.5). Photo-irradiation of this reaction mixture for 1h at $\lambda_{\max} = 305$ nm resulted in the generation of elaidic acid (Figure 3, panels C and D) when both GSSG and NATA were present but not in absence of either NATA or GSSG (Figure S4). Hence, thiyl radicals generated by the NATA/GSSG model system were able to induce cis/trans isomerization of oleic acid. This was confirmed by positive ion mode ESI-LC-MS showing the formation of isobaric products, e.g. representatively of POE (12) oleic acid. No isobaric species of POE (12) oleic acid was formed in the absence of either NATA or GSSG (Figure S5). Quantitation of the extent of cis/trans isomerization was achieved by two ways. First, POE oleic acid is reasonably well resolved from POE elaidic acid during HPLC-MS analysis, which allows for quantitation of ca. 70% POE oleic acid and 30 % POE elaidic acid after 1h photo-irradiation (with $\lambda_{\max} = 305$ nm) of PS80 formulations containing mAbZ. POE sorbitan oleic acid and POE isosorbide oleic acid are less well resolved from their elaidic acid isomers, so that direct quantitation of cis/trans isomerization for these species by HPLC-MS analysis could not be achieved. However, the relative contents of oleic and elaidic acid were quantified by HPLC-MS analysis after esterase hydrolysis, revealing

ca. 90% oleic acid and 10% elaidic acid after 1h photo-irradiation (with $\lambda_{\max} = 305$ nm) of PS80 formulations containing mAbZ. These data suggest that POE oleic acid is somehow more sensitive to cis/trans isomerization compared to POE sorbitan oleic acid and POE isosorbide oleic acid.

4.3.2. Linoleic acid

PS80 contains a significant fraction of linoleic acid, specified as < 18% by the European, the US, and the Japanese Pharmacopoeia³. While this content of <18% is lower compared to that of oleic acid ($\geq 58\%$), the higher reactivity of linoleic acid as well as all polyunsaturated FAs towards oxidizing radicals³⁷ makes linoleic acid a prominent target for oxidative degradation. With two isolated double bonds, separated by a bisallylic methylene group, linoleic acid is also a *bona fide* target for radical-induced isomerization¹⁶. By mass spectrometry analysis of marker ions for oleic and linoleic acid, we quantified the content of oleic acid as 75.1% in PS80 obtained directly from J.T.Baker (see Materials) and 64.6% in PS80 present in the MedImmune formulation of mAbZ. The content of linoleic acid was 14.4% in PS80 directly obtained from J.T. Baker and 7.3%, in PS80 present in the MedImmune formulation of mAbZ.

The photo-irradiation (1 h at $\lambda_{\max} = 305$ nm) of a formulation containing 150 mg/mL mAbZ, 0.01% (w/w) PS80, NaCl and NaAc generated isobaric species from linoleic acid. This is shown in Figure 4, where peaks IIa and IIb, contain isobaric species, representing POE sorbitan linoleic acid with 26 EO units, POE (26) sorbitan linoleate (m/z 803.56, $z = +2$, $[M+2NH_4]$). Similar observations were made for POE (20-32) sorbitan linoleate. In Figure 4, peak V elutes closer to the diester species and represents most likely POE (20) sorbitan oleate/linoleate or POE (21) isosorbide palmitate/linoleate (peaks I, II, and IV do not represent monoisotopic masses).

This is confirmed by the analysis of FFAs, shown in Figure 5A, where photo-irradiation of the formulation containing 150 mg/mL mAbZ resulted in a change of the relative intensities of three isobaric peaks with m/z 279.22 ($z = -1$, [M-H]), representing linoleic acid and isomers of linoleic acid. Additional experiments were performed with 0.2% (w/w) of PS80, in order to increase the sensitivity of our analysis and relate our LC-MS data to Raman and FTIR spectroscopy (*vide infra*) which required higher PS80 concentrations. For these experiments, we purchased PS80 and spiked it into the original mAbZ formulation obtained from MedImmune. Figure 5B[‡] compares non-irradiated controls with photo-irradiated (1 h at either $\lambda = 254$ nm or $\lambda_{\text{max}} = 305$ nm) formulations after esterase digestion of the reaction mixtures. Again, extraction of the signal with m/z 279.22 ($z = -1$, [M-H]) resulted in three isobaric species, similar to the data in Figure 5A[#]. Specifically, photo-irradiation with $\lambda_{\text{max}} = 305$ nm revealed an increased intensity of peaks eluting with $t_R = 8.44$ min and $t_R = 9.66$ min. Spiking with authentic standards (0.01 mg/mL) of (9Z, 12Z)-octadeca-9,12-dienoic acid (linoleic acid), and conjugated linoleic acids (CLA), specifically (9Z, 11E)-octadeca-9,11-dienoic acid (rumenic acid), (9E, 11E)-octadeca-9,11-dienoic acid, and (10E, 12Z)-octadeca-10,12-dienoic acid, was performed to get a general idea on the elution times of geometric isomers of linoleic acid. To our surprise, linoleic acid ((9Z, 12Z)-octadeca-9,12-dienoic acid; $t_R = 8.44$ min) clearly represented only a minor component in the PS80 we purchased to spike into the MedImmune formulations. Instead a peak eluting with $t_R = 8.78$ min, co-eluting with (9Z, 11E)-octadeca-9,11-dienoic acid (rumenic acid) and (10E, 12Z)-octadeca-10,12-dienoic acid, represented the major component of PS80. Both, (9Z, 11E)-octadeca-9,11-dienoic acid (rumenic acid) and (10E, 12Z)-octadeca-10,12-dienoic acid can be generated from (9Z, 12Z)-octadeca-9,12-dienoic acid (linoleic acid) by hydrogen abstraction from the bisallylic methylene group, generating an intermediary carbon-centered radical at C-11. The latter usually converts

into carbon-centered radicals at C-13 or C-9, hydrogen addition to which would yield (9Z, 11E)-octadeca-9,11-dienoic acid (rumenic acid) and (10E, 12Z)-octadeca-10,12-dienoic acid, respectively (we note, that oxygen addition would yield peroxy radicals and hydroperoxides, generating oxidation products; see below). Photo-irradiation with both $\lambda = 254$ nm and $\lambda_{\max} = 305$ nm resulted in a slight increase of the peak representing linoleic acid but in significant growth of a peak with $t_R = 9.66$ min, co-eluting with (9E, 11E)-octadeca-9,11-dienoic acid. A quantitative comparison of the changes of relative peak areas of the respective FA isomers during photo-irradiation at $\lambda_{\max} = 305$ nm is shown in Figure 6. Noteworthy, in formulations containing 0.2% PS80 small changes are even observed during photo-irradiation in the absence of mAbZ; however, a significantly higher conversion of cis/trans or trans/cis conjugated FAs into trans/trans conjugated FAs is observed in the presence of mAbZ.

4.3.3. Oxidation products

The light exposure of formulations containing 150 mg/ml mAbZ, 0.01% (w/w) PS80, NaCl and NaAc, leads not only to cis/trans isomerization but also to the formation of oxidation products. Figure 7 shows data (m/z 313.24 (281.24+32); $z = -1$, [M-H]) representative for oleic acid with an addition of +32 atomic mass units (amu), consistent with hydroperoxide formation, and observed during FFA analysis after photo-irradiation and esterase hydrolysis of PS80. Figure 7A displays a baseline level of the signal with m/z 313.24 even in control PS80, where at least three isobaric components can be distinguished, eluting with $t_R = 2.74$, 3.08 and 3.12 min. Considering that radical processes can theoretically introduce hydroperoxide groups at positions C-8, C-9, C-10, and C-11, the chromatographic resolution of isobaric hydroperoxide products is expected. The photo-irradiation of the formulations at $\lambda = 254$ nm, $\lambda_{\max} = 305$ nm, and $\lambda_{\max} = 350$ nm revealed

a pronounced increase in the intensities of the isobaric signals with m/z 313.24, and thus is consistent with the photo-induced generation of radicals from oleic acid followed by the formation of hydroperoxides.

4.3.4. The model system containing PS80, GSSG, and NATA

Reactions 1 and 2 provide a facile mechanism for the generation of mAbZ thiyl radicals which can then induce the cis/trans isomerization and/or oxidation of unsaturated fatty acids. In order to further confirm the feasibility of this mechanism, a formulation containing 0.01% (w/w) PS80, 5 mM GSSG, and 5 mM NATA in either 20 mM or 50 mM NaAc buffer (pH 5.5), was photo-irradiated for 1 h at $\lambda_{\max} = 305$ nm. Under these conditions, we observed the conversion of oleic acid into elaidic acid (Figures 3C, 3D, and S2; see above) analogous to our results in the presence of mAbZ (Figures 3A and 3B). Furthermore, a significant loss of the signal representing (9Z, 11E)-octadeca-9,11-dienoic acid (rumenic acid) and (10E, 12Z)-octadeca-10,12-dienoic acid was only in part accounted for by an increase in the signal for (9E, 11E)-octadeca-9,11-dienoic acid (Figure 8A and B). These unaccounted products are likely oxidation products. Consistent with this expectation, the photo-irradiation of 0.01% (w/w) PS80, 5 mM GSSG, and 5 mM NATA in 20 mM NaAc buffer (pH 5.5) for 1 h at $\lambda_{\max} = 305$ nm yielded significant quantities of several oxidation products isobaric with linoleic acid +16 amu (Figure 8C) and a product isobaric with linoleic acid +32 amu, likely linoleic acid hydroperoxide (Figure 8D).

4.3.5. Raman and FTIR Spectroscopy

Second derivative Raman spectra of FFA reference solutions are displayed in Figure 9A. In general, due to the conjugated dienes, CLAs showed significantly stronger Raman scattering than FAs containing isolated cis or trans bonds. (9E, 11E)-octadeca-9,11-dienoic acid revealed a peak

at 1659.5 cm^{-1} while (9Z, 11E)-octadeca-9,11-dienoic acid and (10E, 12Z)-octadeca-10,12-dienoic acid both revealed a peak at 1653.0 cm^{-1} . Linoleic, oleic, and elaidic acids showed broad peaks at 1658.0 cm^{-1} , 1655.0 cm^{-1} , and 1669.0 cm^{-1} , respectively.

Second derivative Raman spectra of solutions containing either individual formulation components or complete formulations (control and photo-irradiated) are displayed in in Figure 9B. All non-irradiated solutions (controls) containing PS80 showed a peak at 1653.5 cm^{-1} . This peak clearly indicated the presence of (9Z, 11E)-octadeca-9,11-dienoic acid and/or (10E, 12Z)-octadeca-10,12-dienoic acid; the shift to a slightly higher wavenumber with respect to the FFA reference solutions is possibly related to the presence of oleic and linoleic acid. Photo-irradiation of PS80 in presence GSSG and NATA or in presence of mAbZ had a strong effect on the FA composition. In both cases, a relative reduction of the peak intensity for (9Z, 11E)-octadeca-9,11-dienoic acid and/or (10E, 12Z)-octadeca-10,12-dienoic acid and a relative increase of peak intensity for (9E, 11E)-octadeca-9,11-dienoic acid was observed. In contrast, photo-irradiation of PS80 alone resulted only in a minor loss of peak intensity at 1653.5 cm^{-1} and no additional peaks were observed. The peak at $\sim 1620\text{ cm}^{-1}$ was attributed to the presence of NATA. Raman spectroscopy was found advantageous when analyzing CLAs in PS80 because the POE segment of a polysorbate molecule, which can be represented by PEG, displays no spectral features in the range from 1700 cm^{-1} to 1600 cm^{-1} (Figure 10C). No difference between a freshly prepared 5% PS80 (Figure 9C) solution in ethanol and the processed PS80 control (Figure 9B) was observed.

FTIR spectra of FFA reference solutions are displayed in Figure 10A. (9E, 11E)-octadeca-9,11-dienoic acid showed a peak at 988 cm^{-1} and elaidic acid, containing an isolated trans double bond, showed a peak at 968 cm^{-1} . (9Z, 11E)-octadeca-9,11-dienoic acid (rumenic acid) and (10E, 12Z)-octadeca-10,12-dienoic acid both revealed two peaks at $\sim 984\text{ cm}^{-1}$ and $\sim 948\text{ cm}^{-1}$. Linoleic acid

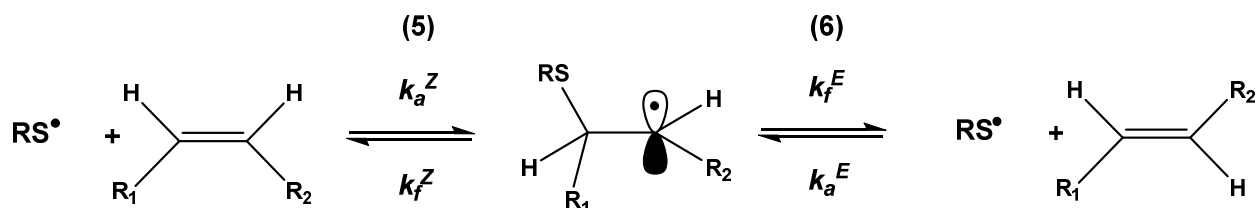
((9Z, 12Z)-octadeca-9,12-dienoic acid) showed a broad peak at $\sim 913\text{ cm}^{-1}$, while no characteristic peak was identified for oleic acid. These reference spectra are in good agreement with earlier reports³⁸. FTIR spectra of solutions containing either individual formulation components or complete formulations (control and photo-irradiated) are displayed in Figure 10B. All solutions, except the ones prepared from buffer solutions in the absence of PS80, revealed peaks at $\sim 986\text{ cm}^{-1}$, $\sim 950\text{ cm}^{-1}$, and $\sim 915\text{ cm}^{-1}$. The peaks at $\sim 986\text{ cm}^{-1}$ and $\sim 950\text{ cm}^{-1}$ indicated a mixture of CLAs: The peak at $\sim 986\text{ cm}^{-1}$ is located in between the reference peaks for (9E, 11E)-octadeca-9,11-dienoic acid, and (9Z, 11E)-octadeca-9,11-dienoic acid and (10E, 12Z)-octadeca-10,12-dienoic acid (984 cm^{-1}). The peak at $\sim 950\text{ cm}^{-1}$ indicated the presence of (9Z, 11E)-octadeca-9,11-dienoic acid and (10E, 12Z)-octadeca-10,12-dienoic acid. The peak at $\sim 915\text{ cm}^{-1}$ indicated the presence of linoleic acid. However, the use of FTIR to assess PS80 has several limitations not encountered when using Raman spectroscopy as described above. First, FTIR assessment of a 5% solution of PS80 in ethanol showed very similar spectral features when compared to a saturated solution of PEG, representing the POE segment of PS80 (Figure 10C). The spectral features of the fatty acids are only observed after PS80 extraction, drying, and dissolution of the dried sample. One possible explanation is the limited solubility of PEG in ethanol when compared to PS80, meaning that extracted PS80 but not free POE readily dissolves after drying. In addition, the overlapping signals of the CLAs as well as signals from NATA and linoleic acid complicate a definite assignment beyond the statement that various CLA species are present.

4.4. Discussion

The oxidative degradation of polysorbate is a well-known phenomenon, usually attributed to oxidation processes induced by transition metal catalysis, reactive oxygen species, and/or light exposure¹⁻⁴. In general, pharmaceutical formulators are concerned with the consequences of

polysorbate degradation for the chemical and physical integrity of APIs such as therapeutic proteins. These include chemical modifications, e.g. the potential reactions of peroxides and aldehydes/ketones with proteins, and physical alterations, e.g. the generation of protein aggregates and/or particles^{1-3, 5-11, 39-40}. In this chapter, we show that light-exposure of PS80-containing formulations leads to cis/trans-isomerization of unsaturated FA components of PS80 when a mAb is present, but not in its absence. This pathway likely involves the reductive cleavage of disulfide bonds by photo-induced electron transfer from Trp, generating thiyl radicals (reactions 1-4). This pathway was independently confirmed by light exposure of PS80 in the presence of the model system NATA/GSSG, which caused cis/trans isomerization of unsaturated fatty acids. Importantly, the photo-induced cis/trans isomerization occurred at wavelengths including near UV light, i.e. at wavelengths present in indoor fluorescent lighting.

In 1959, Walling and Helmreich reported on the isomerization of olefins by thiyl radicals⁴¹. About 40 years later, Chatgililoglu, Ferreri and coworkers initiated a series of mechanistic studies on thiyl radical-induced isomerization of double bonds in mono- and polyunsaturated FAs¹⁴⁻¹⁹, proceeding according to equilibria 5 and 6, where in *tert*-butanol at room temperature $k_a^Z = 1.6 \times 10^5 \text{ M}^{-1}\text{s}^{-1}$, $k_a^E = 2.9 \times 10^{-1}\text{s}^{-1}$, $k_f^Z = 1.7 \times 10^7 \text{ M}^{-1}\text{s}^{-1}$, and $k_f^E = 1.6 \times 10^8 \text{ M}^{-1}\text{s}^{-1}$ ($\text{RS}^\bullet = \text{HOCH}_2\text{CH}_2\text{S}^\bullet$)⁴².



This cis/trans isomerization proceeds via a chain reaction, which is subject to retardation by several pathways³⁰. First, retardation may proceed via hydrogen abstraction from allylic or

bisallylic methylene groups such as present in mono- and polyunsaturated FAs. Such reactions lead to intermediary carbon-centered radicals, which, in the presence of oxygen, will convert into peroxy radicals and ultimately FA hydroperoxides. Figure 7 shows representative data for the formation of oleic acid-derived products, which are +32 amu higher in mass, consistent with the formation of oleic acid hydroperoxides from PS80. Second, retardation can be achieved by the reaction of thiyl radicals with conjugated double bonds, such as shown by Graham *et al.*⁴³ for the cis/trans isomerization of 2-butene in the presence of 1,3-butadiene. The latter observation is relevant for our formulations, as our analysis of FFAs (Figures 5 and 6) shows that PS80 can contain significant amounts of FAs with conjugated double bonds such as e.g. (9Z, 11E)-octadeca-9,11-dienoic acid (rumenic acid) and/or (10E, 12Z)-octadeca-10,12-dienoic acid. This observation, also confirmed by Raman spectroscopy, is consistent with earlier NMR data presented by Hvattum *et al.*⁴⁴, which suggested that the majority of the C18:2 fatty acids in PS80 contain conjugated double bonds. Photo-irradiation of formulations containing 150 mg/mL mAbZ together with PS80, NaCl and NaAc generated a product co-eluting with (9E, 11E)-octadeca-9,11-dienoic acid (Figure 5), and it would be feasible to assume that thiyl radicals could convert (9Z, 11E)-octadeca-9,11-dienoic acid (rumenic acid) into (9E, 11E)-octadeca-9,11-dienoic acid. We note that different batches of PS80 can contain different amounts of linoleic acid and conjugated linoleic acids, as we observed when comparing PS80 obtained from J.T. Baker and PS80 present in the formulations containing mAbZ. We do not know to what extent these differences are caused by batch-to-batch variability or aging of PS80.

The presence of fatty acids with conjugated double bonds has likely an inhibitory effect³⁰ on the cis/trans isomerization reactions induced by light exposure of mAbZ and NATA/GSSG under our experimental conditions. However, in general fatty acids with conjugated double bonds are

expected to be rather sensitive to oxidation. Kitaguchi *et al.* reported a linear relationship of rate constants for hydrogen abstraction by peroxy radicals from polyunsaturated fatty acids depending on the number of bisallylic methylene groups⁴⁵. Hydrogen abstraction from the bisallylic methylene groups leads to the formation of pentadienyl radicals. Linoleic acid contains two non-conjugated double bonds and one bisallylic methylene group. However, CLAs contain methylene groups on each site of the conjugated double bond system, where hydrogen abstraction would lead to the generation of pentadienyl radicals. Consequently, we expect that CLAs exhibit oxidation sensitivities comparable to that of linolenic acid, a highly oxidation-sensitive polyunsaturated fatty acid. Hence, despite their potential to retard cis/trans isomerization reactions, CLAs represent prominent targets for radical formation, and origins for oxidation reactions.

The potential for radical-induced cis/trans isomerization of mono- and polyunsaturated fatty acids in PS80 is significant for the following reasons. First, the appearance of trans-FAs in formulations, either in polysorbate esters or FFAs, may serve as a probe for the intermediary generation of free radicals during manufacturing and/or storage. Second, the chemical and physical properties of PS80 may change following the formation of trans-FAs. This is concluded from a series of studies focusing on FFAs, but also focusing on lipids, synthetic model surfactants, or FAs physically incorporated into micelles or inverted micelles, as outlined in the following. For example, the critical micelle concentration (cmc) of sodium elaidate (2.5×10^{-3} M) is slightly below that of sodium oleate (2.7×10^{-3} M), consistent with a greater tendency for association of elaidic acid as compared to oleic acid, measured in non-polar solvents⁴⁶. When the physical properties of elaidyltrimethyl ammonium chloride and oleyltrimethyl ammonium chloride surfactants were examined, the presence of a trans vs. cis double bond in these synthetic

surfactants led to differences in drag-reduction, micellar structure, and shear viscosities⁴⁷. Likewise, differential scanning calorimetry experiments of lipids show that the cis/trans isomerization of 1-palmitoyl-2-oleyl L- α -phosphatidylcholine (POPC) to 1-palmitoyl-2-elaidyl L- α -phosphatidylcholine (PEPC) changes the phase transition temperature⁴⁸. The incorporation of increasing concentrations of elaidic acid into inverted micelles generated from monoolein-oleic acid reduces the sphericity of these micelles⁴⁹. Lennox and McClelland studied the chemical bromination of elaidic and oleic acid⁵⁰. They reported that physical incorporation into micelles significantly changed the relative reactivities of the cis and trans double bonds as compared to bromination in homogenous solution⁵⁰.

In conclusion, the light-exposure of a PS80-containing formulation containing a monoclonal antibody resulted in the cis/trans isomerization of unsaturated fatty acids (oleic acid, linoleic and conjugated linoleic acids). The presence of trans fatty acids may modulate the physico-chemical properties of PS80 micelles. In addition, the presence of trans fatty acids may serve as a probe for free radical formation and reactions within formulations. It will be interesting to evaluate whether free trans fatty acids behave similar or different compared to free cis fatty acids in the formation of particles.

4.5. Footnotes

§ For photo-irradiations at $\lambda_{\text{max}} = 305, 350$ and 419 nm, light intensities were integrated over the entire emission spectra of the respective lamps, which are available from The Southern New England Ultraviolet Company.

§ We compared extraction by ethanol, acetonitrile and ethyl acetate/1,4-dioxane (50/50, v/v), and found no significant differences in extraction efficiency.

‡ We observed that over the lifetime of the column, absolute retention times of the components were subject to shift, while the relative elution order remained constant. This is the reason for the different retention times in Figures 6A and 6B.

We note that PS80 (J.T. Baker) originally present in the MedImmune formulation, and PS80 (J.T. Baker), which we purchased later and spiked into the MedImmune formulation appear to vary in the relative content of the three isobaric species prior to photo-irradiation. At this point, we do not know whether this is due to batch-to-batch variability or due to the age of the MedImmune formulations.

4.6. References

1. Kerwin, B. A., Polysorbates 20 and 80 used in the formulation of protein biotherapeutics: structure and degradation pathways. *J. Pharm. Sci.* **2008**, *97* (8), 2924-35.
2. Jones, M. T.; Mahler, H. C.; Yadav, S.; Bindra, D.; Corvari, V.; Fesinmeyer, R. M.; Gupta, K.; Harmon, A. M.; Hinds, K. D.; Koulov, A.; Liu, W.; Maloney, K.; Wang, J.; Yeh, P. Y.; Singh, S. K., Considerations for the Use of Polysorbates in Biopharmaceuticals. *Pharm Res-Dordr* **2018**, *35* (8).
3. Dwivedi, M.; Blech, M.; Presser, I.; Garidel, P., Polysorbate degradation in biotherapeutic formulations: Identification and discussion of current root causes. *Int J Pharmaceut* **2018**, *552* (1-2), 422-436.
4. Singh, S. R.; Zhang, J.; O'Dell, C.; Hsieh, M. C.; Goldstein, J.; Liu, J.; Srivastava, A., Effect of polysorbate 80 quality on photostability of a monoclonal antibody. *AAPS Pharm.Sci.Tech.* **2012**, *13* (2), 422-30.
5. Ha, E.; Wang, W.; Wang, Y. J., Peroxide formation in polysorbate 80 and protein stability. *J Pharm Sci-Us* **2002**, *91* (10), 2252-2264.
6. Lam, X. M.; Lai, W. G.; Chan, E. K.; Ling, V.; Hsu, C. C., Site-Specific Tryptophan Oxidation Induced by Autocatalytic Reaction of Polysorbate 20 in Protein Formulation. *Pharm Res-Dordr* **2011**, *28* (10), 2543-2555.
7. Kishore, R. S. K.; Kiese, S.; Fischer, S.; Pappenberger, A.; Grauschopf, U.; Mahler, H. C., The Degradation of Polysorbates 20 and 80 and its Potential Impact on the Stability of Biotherapeutics. *Pharm Res-Dordr* **2011**, *28* (5), 1194-1210.
8. Kishore, R. S. K.; Pappenberger, A.; Dauphin, I. B.; Ross, A.; Buergi, B.; Staempfli, A.; Mahler, H. C., Degradation of Polysorbates 20 and 80: Studies on Thermal Autoxidation and Hydrolysis. *J Pharm Sci-Us* **2011**, *100* (2), 721-731.
9. LaBrenz, S. R., Ester Hydrolysis of Polysorbate 80 in mAb Drug Product: Evidence in Support of the Hypothesized Risk After the Observation of Visible Particulate in mAb Formulations. *J Pharm Sci-Us* **2014**, *103* (8), 2268-2277.
10. McShan, A. C.; Kei, P.; Ji, J. A.; Kim, D. C.; Wang, Y. J., Hydrolysis of Polysorbate 20 and 80 by a Range of Carboxylester Hydrolases. *PDA J Pharm Sci Technol* **2016**, *70* (4), 332-45.
11. Dixit, N.; Salamat-Miller, N.; Salinas, P. A.; Taylor, K. D.; Basu, S. K., Residual Host Cell Protein Promotes Polysorbate 20 Degradation in a Sulfatase Drug Product Leading to Free Fatty Acid Particles. *J Pharm Sci-Us* **2016**, *105* (5), 1657-1666.
12. Hall, T.; Sandefur, S. L.; Frye, C. C.; Tuley, T. L.; Huang, L. H., Polysorbates 20 and 80 Degradation by Group XV Lysosomal Phospholipase A(2) Isomer X1 in Monoclonal Antibody Formulations. *J Pharm Sci-Us* **2016**, *105* (5), 1633-1642.
13. Zhang, L.; Yadav, S.; Demeule, B.; Wang, Y. J.; Mozziconacci, O.; Schöneich, C., Degradation Mechanisms of Polysorbate 20 Differentiated by 18O-labeling and Mass Spectrometry. *Pharm Res* **2017**, *34* (1), 84-100.

14. Chatgililoglu, C.; Ferreri, C.; Ballestri, M.; Mulazzani, Q. G.; Landi, L., cis-trans isomerization of monounsaturated fatty acid residues in phospholipids by thiyl radicals. *J Am Chem Soc* **2000**, *122* (19), 4593-4601.
15. Chatgililoglu, C.; Ferreri, C.; Guerra, M.; Samadi, A.; Bowry, V. W., The Reaction of Thiyl Radical with Methyl Linoleate: Completing the Picture. *J Am Chem Soc* **2017**, *139* (13), 4704-4714.
16. Chatgililoglu, C.; Ferreri, C.; Melchiorre, M.; Sansone, A.; Torreggiani, A., Lipid Geometrical Isomerism: From Chemistry to Biology and Diagnostics. *Chem Rev* **2014**, *114* (1), 255-284.
17. Ferreri, C.; Costantino, C.; Landi, L.; Mulazzani, Q. G.; Chatgililoglu, C., The thiyl radical-mediated isomerization of cis-monounsaturated fatty acid residues in phospholipids: a novel path of membrane damage? *Chem Commun* **1999**, (5), 407-408.
18. Lykakis, I. N.; Ferreri, C.; Chatgililoglu, C., The sulfhydryl radical (HS center dot/S center dot-): A contender for the isomerization of double bonds in membrane lipids. *Angew Chem Int Edit* **2007**, *46* (11), 1914-1916.
19. Mihaljevic, B.; Tartaro, I.; Ferreri, C.; Chatgililoglu, C., Linoleic acid peroxidation vs. isomerization: a biomimetic model of free radical reactivity in the presence of thiols. *Org Biomol Chem* **2011**, *9* (9), 3541-3548.
20. Mozziconacci, O.; Kerwin, B. A.; Schöneich, C., Exposure of a monoclonal antibody, IgG1, to UV-light leads to protein dithiohemiacetal and thioether cross-links: a role for thiyl radicals? *Chem Res Toxicol* **2010**, *23* (8), 1310-1312.
21. Mozziconacci, O.; Williams, T. D.; Kerwin, B. A.; Schöneich, C., Reversible intramolecular hydrogen transfer between protein cysteine thiyl radicals and alpha C-H bonds in insulin: control of selectivity by secondary structure. *J Phys Chem B* **2008**, *112* (49), 15921-32.
22. Vanhooren, A.; Devreese, B.; Vanhee, K.; Van Beeumen, J.; Hanssens, I. A., Photoexcitation of tryptophan groups induces reduction of two disulfide bonds in goat alpha-lactalbumin. *Biochemistry-Us* **2002**, *41* (36), 11035-11043.
23. Creed, D., The Photophysics and Photochemistry of the near-Uv Absorbing Amino-Acids .1. Tryptophan and Its Simple Derivatives. *Photochem Photobiol* **1984**, *39* (4), 537-562.
24. Truong, T. B., Charge-Transfer to a Solvent State .5. Effect of Solute-Solvent Interaction on the Ionization-Potential of the Solute - Mechanism for Photo-Ionization. *J Phys Chem-Us* **1980**, *84* (9), 964-970.
25. Mossoba, M. M.; Makino, K.; Riesz, P., Photo-Ionization of Aromatic-Amino-Acids in Aqueous-Solutions - a Spin-Trapping and Electron-Spin Resonance Study. *J Phys Chem-Us* **1982**, *86* (17), 3478-3483.
26. Weckler, A. T.; Yin, J.; Tao, P. L.; Kabakoff, B.; Sreedhara, A.; Deperalta, G., Photodisruption of the Structurally Conserved Cys-Cys-Trp Triads Leads to Reduction-Resistant Scrambled Intrachain Disulfides in an IgG1 Monoclonal Antibody. *Mol Pharmaceut* **2018**, *15* (4), 1598-1606.

27. Bane, J.; Mozziconacci, O.; Yi, L.; Wang, Y. J.; Sreedhara, A.; Schöneich, C., Photo-oxidation of IgG1 and Model Peptides: Detection and Analysis of Triply Oxidized His and Trp Side Chain Cleavage Products. *Pharm Res-Dordr* **2017**, *34* (1), 229-242.
28. Haywood, J.; Mozziconacci, O.; Allegre, K. M.; Kerwin, B. A.; Schöneich, C., Light-induced conversion of Trp to Gly and Gly hydroperoxide in IgG1. *Mol Pharm* **2013**, *10* (3), 1146-50.
29. Nauser, T.; Koppenol, W. H.; Schöneich, C., Reversible Hydrogen Transfer Reactions in Thiyl Radicals From Cysteine and Related Molecules: Absolute Kinetics and Equilibrium Constants Determined by Pulse Radiolysis. *J Phys Chem B* **2012**, *116* (18), 5329-5341.
30. Chatgililoglu, C.; Bowry, V. W., Why Not Trans? Inhibited Radical isomerization Cycles and Coupling Chains of Lipids and Alkenes with Alkane-thiols. *J Org Chem* **2018**, *83* (16), 9178-9189.
31. Rahn, R. O., Potassium iodide as a chemical actinometer for 254 nm radiation: Use of iodate as an electron scavenger (vol. 66, pg. 450, 1997). *Photochem Photobiol* **1997**, *66* (6), 885-885.
32. Hatchard, C. G.; Parker, C. A., A New Sensitive Chemical Actinometer .2. Potassium Ferrioxalate as a Standard Chemical Actinometer. *Proc R Soc Lon Ser-A* **1956**, *235* (1203), 518-536.
33. Lee, J.; Seliger, H. H., Quantum Yield of Ferrioxalate Actinometer. *J Chem Phys* **1964**, *40* (2), 519-&.
34. Pozdnyakov, I. P.; Kel, O. V.; Plyusnin, V. F.; Grivin, V. P.; Bazhin, N. M., New insight into photochemistry of ferrioxalate. *J Phys Chem A* **2008**, *112* (36), 8316-8322.
35. Photostability testing of new drug substances and products. *Fed Reg* **1997**, *62*, 27115-27122.
36. Baertschi, S. W.; Alsante, K. M.; Tonnesen, H. H., A Critical Assessment of the ICH Guideline on Photostability Testing of New Drug Substances and Products (Q1B): Recommendation for Revision. *J Pharm Sci-Us* **2010**, *99* (7), 2934-2940.
37. Yao, J.; Dokuru, D. K.; Noestheden, M.; Park, S. S.; Kerwin, B. A.; Jona, J.; Ostovic, D.; Reid, D. L., A Quantitative Kinetic Study of Polysorbate Autoxidation: The Role of Unsaturated Fatty Acid Ester Substituents. *Pharm Res-Dordr* **2009**, *26* (10), 2303-2313.
38. Jackson, J. E.; Paschke, R. F.; Tolberg, W.; Boyd, H. M.; Wheeler, D. H., Isomers of Linoleic Acid - Infrared and Ultraviolet Properties of Methyl Esters. *J Am Oil Chem Soc* **1952**, *29* (6), 229-234.
39. Tomlinson, A.; Demeule, B.; Lin, B. W.; Yadav, S., Polysorbate 20 Degradation in Biopharmaceutical Formulations: Quantification of Free Fatty Acids, Characterization of Particulates, and Insights into the Degradation Mechanism. *Mol Pharmaceut* **2015**, *12* (11), 3805-3815.
40. Dahotre, S.; Tomlinson, A.; Lin, B. W.; Yadav, S., Novel markers to track oxidative polysorbate degradation in pharmaceutical formulations. *J Pharmaceut Biomed* **2018**, *157*, 201-207.
41. Walling, C.; Helmreich, W., Reactivity and Reversibility in the Reaction of Thiyl Radicals with Olefins. *J Am Chem Soc* **1959**, *81* (5), 1144-1148.

42. Chatgililoglu, C.; Samadi, A.; Guerra, M.; Fischer, H., The kinetics of Z/E isomerization of methyl oleate catalyzed by photogenerated thiyl radicals. *Chemphyschem* **2005**, *6* (2), 286-291.
43. Graham, D. M.; Mieville, R. L.; Sivertz, C., Photo-Initiated Reactions of Thiols and Olefins .I. Thiyl Radical Catalyzed Isomerization of Butene-2 and 1,2-Ethylene-D2. *Can J Chem* **1964**, *42* (10), 2239-&.
44. Hvattum, E.; Yip, W. L.; Grace, D.; Dyrstad, K., Characterization of polysorbate 80 with liquid chromatography mass spectrometry and nuclear magnetic resonance spectroscopy: Specific determination of oxidation products of thermally oxidized polysorbate 80. *J Pharmaceut Biomed* **2012**, *62*, 7-16.
45. Kitaguchi, H.; Ohkubo, K.; Ogo, S.; Fukuzumi, S., Additivity rule holds in the hydrogen transfer reactivity of unsaturated fatty acids with a peroxy radical: mechanistic insight into lipoygenase. *Chem Commun* **2006**, (9), 979-981.
46. Tamamushi, B.; Shirai, M.; Tamaki, K., A Study on the Micellar Solutions of Sodium Oleate and Elaidate. *B Chem Soc Jpn* **1958**, *31* (4), 467-472.
47. Qi, Y. Y.; Kesselman, E.; Hart, D. J.; Talmon, Y.; Mateo, A.; Zakin, J. L., Comparison of oleyl and elaidyl isomer surfactant-counterion systems in drag reduction, rheological properties and nanostructure. *J Colloid Interf Sci* **2011**, *354* (2), 691-699.
48. Ferreri, C.; Pierotti, S.; Barbieri, A.; Zambonin, L.; Landi, L.; Rasi, S.; Luisi, P. L.; Barigelletti, F.; Chatgililoglu, C., Comparison of phosphatidylcholine vesicle properties related to geometrical isomerism. *Photochem Photobiol* **2006**, *82* (1), 274-280.
49. Rappolt, M.; Cacho-Nerin, F.; Morello, C.; Yaghmur, A., How the chain configuration governs the packing of inverted micelles in the cubic Fd3m-phase. *Soft Matter* **2013**, *9* (27), 6291-6300.
50. Lennox, R. B.; McClelland, R. A., Electrophilic Bromination of Micelle-Associated Alkenes as a Probe of Micelle Structure. *J Am Chem Soc* **1986**, *108* (13), 3771-3781.

4.7. Figures

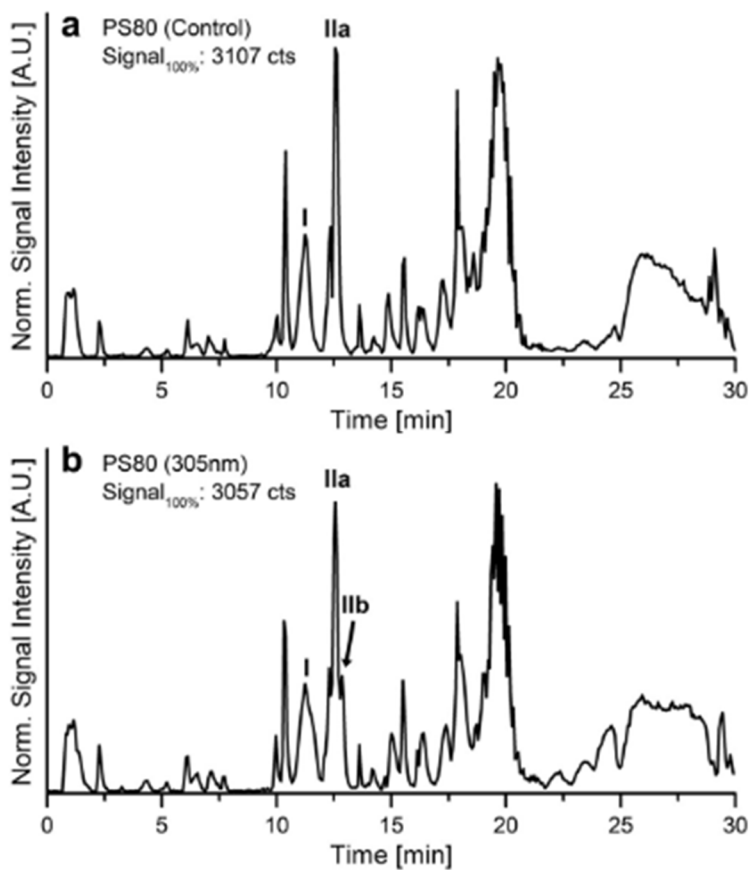


Figure 1: Positive-mode LC-MS chromatograms of PS80 after extraction from the mAbZ formulation: Dark control sample (a) and samples photoirradiated (1 h) with $\lambda_{\text{max}} = 305 \text{ nm}$ (b); peak I: POE sorbitan oleic acid, peak IIa: POE oleic acid, peak IIb: isobaric product to IIa; y-axis scaling: scaling of each subplot is normalized to its own respective maximum signal intensity.

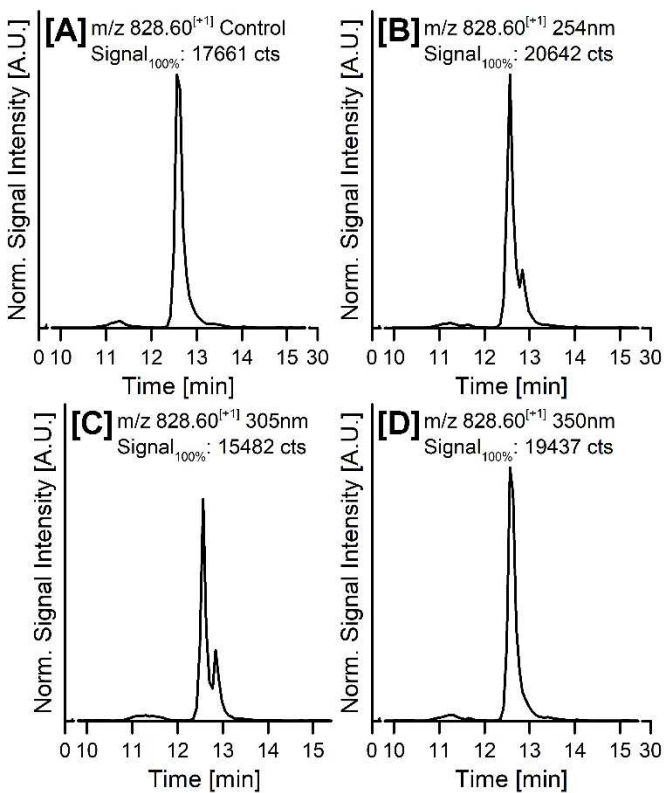


Figure 2: Figure 2. Positive-mode LC-MS chromatogram of the POE (12) oleic acid ammonium adduct (m/z 828.60, $z = 1$; $[M + NH_4]^{+1}$) after PS80 extraction from the mAbZ formulation: Dark control sample (a) and samples photoirradiated (1 h) with $\lambda = 254$ nm (b), $\lambda_{\max} = 305$ nm (c), and $\lambda_{\max} = 350$ nm (d); y-axis scaling: scaling of each subplot is normalized to the maximum signal intensity of subplot (b).

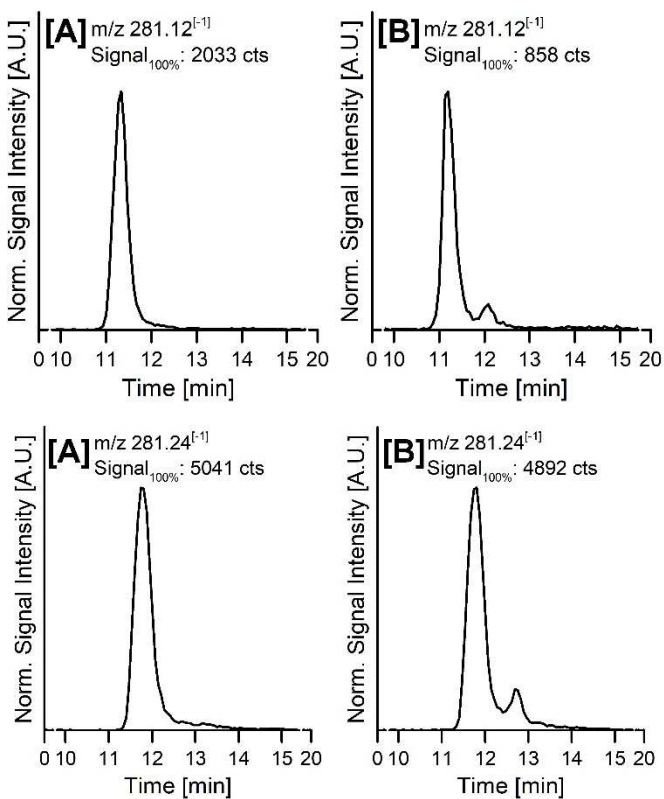


Figure 3: Negative-mode LC-MS chromatogram of oleic acid (m/z 281.24, $[M-H]^{-1}$) after FFA extraction. PS80 photoirradiated (1 h) with $\lambda_{\text{max}} = 305$ nm in the absence (a) or presence (b) of mAbZ. PS80 in the presence of NATA and GSSG: dark control sample (c) and sample photoirradiated (1 h) with $\lambda_{\text{max}} = 305$ nm (d); y-axis scaling: scaling of each subplot is normalized to its own respective maximum signal intensity.

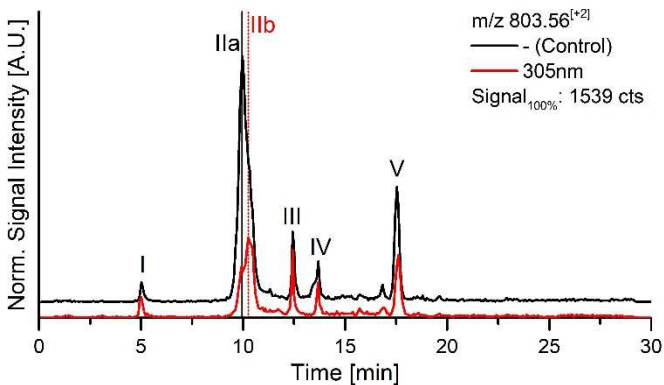


Figure 4: Positive-mode LC-MS chromatogram of the POE (26) sorbitan linoleic acid bis-ammonium adduct (m/z 803.56, $[M + 2NH_4]^{+2}$) after PS80 extraction from the mAbZ formulation: Dark control sample (black line) and sample photoirradiated (1 h) with $\lambda_{max} = 305$ nm (blue line); peaks IIa and IIb: isobaric species of the POE (26) sorbitan linoleic acid ammonium adduct, peaks I, III, IV, and V belong to isotopic envelopes of other PS80 species; y-axis scaling: scaling is normalized to the maximum signal intensity of the dark control sample; stacked presentation.

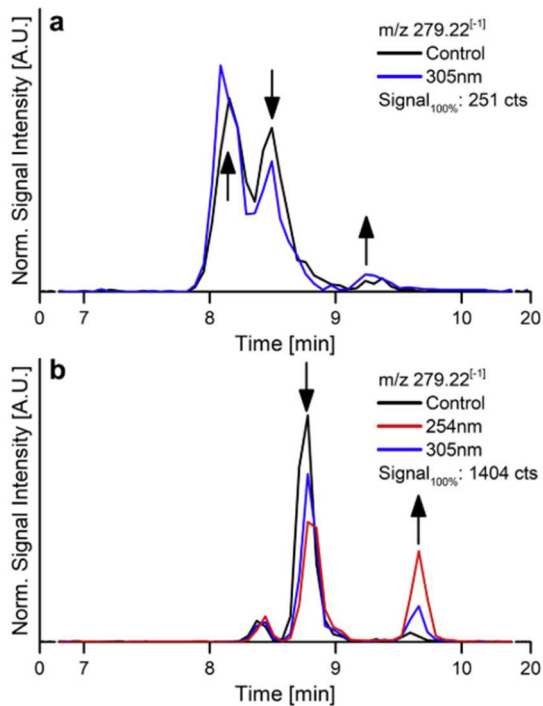


Figure 5: Negative-mode LC-MS chromatogram of linoleic acid and its isobaric species (m/z 279.22, $[M-H]^{-1}$) after FFA extraction from (a) PS80 present in the mAbZ formulation and (b) PS80 spiked into the mAbZ formulation (We observed that over the lifetime of the column, absolute retention times of the components were subject to shift, whereas the relative elution order remained constant. This is the reason for the different retention times in Figures 6a and 6b; We note that PS80 (J.T. Baker) originally present in the MedImmune formulation and PS80 (J.T. Baker), which we purchased later and spiked into the MedImmune formulation, appear to vary in the relative content of the 3 isobaric species before photoirradiation. At this point, we do not know whether this is due to batch-to-batch variability or due to the age of the MedImmune formulations): Dark control sample (black line) and photoirradiated samples (1 h) with $\lambda = 254$ nm (red line, B only) and $\lambda_{\text{max}} = 305$ nm (blue line); y-axis scaling: scaling of each subplot is normalized to the maximum signal intensity presented in the respective subplot.

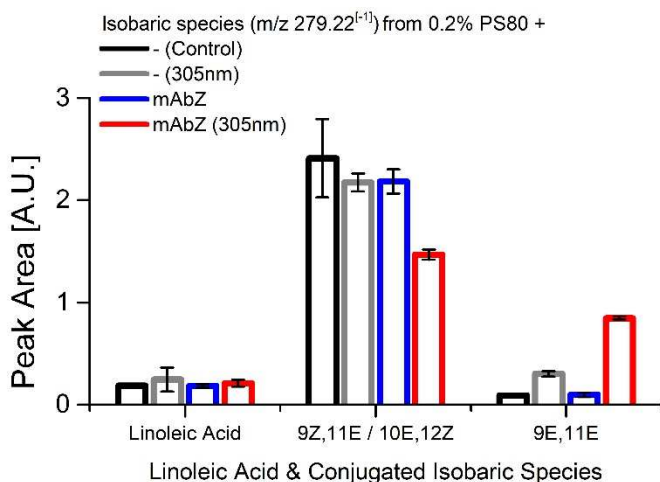


Figure 6: Quantitative comparison of linoleic acid and its isobaric species (m/z 279.22, $[M-H]^{-1}$) after FFA extraction from PS80 alone and from PS80 spiked into the mAbZ formulation: Dark control samples (black and blue lines, respectively) and photoirradiated samples (1 h) with $\lambda_{\max} = 305\text{nm}$ (gray and red lines, respectively); ‘9Z, 11E’ refers to (9Z, 11E)-octadeca-9,11-dienoic acid, ‘10E, 12Z’ refers to (10E, 12Z)-octadeca-10,12-dienoic acid, and ‘9E, 11E’ refers to (9E, 11E)-octadeca-9,11-dienoic acid.

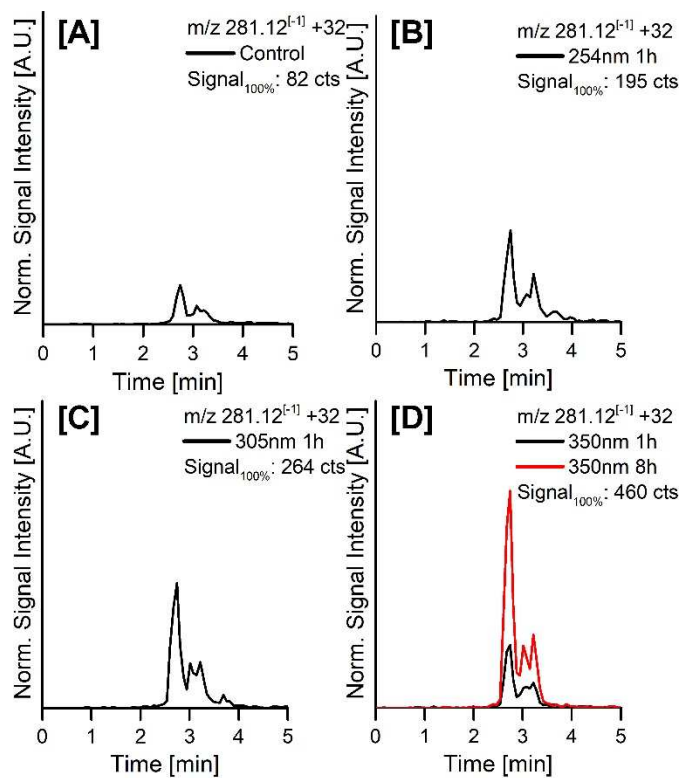


Figure 7: Negative-mode LC-MS chromatogram of oleic acid oxidation products (m/z 281.24 + 32, $[M-H]^{-1}$) after FFA extraction from PS80 present in the mAbZ formulation: Dark control sample (a) and samples photoirradiated for 1 h with $\lambda = 254$ nm (b), $\lambda_{\text{max}} = 305$ nm (c), $\lambda_{\text{max}} = 350$ nm (d, black line), and for 8 h with $\lambda_{\text{max}} = 350$ nm (d, red line); y-axis scaling: scaling of each subplot is normalized to the maximum signal intensity of subplot (d).

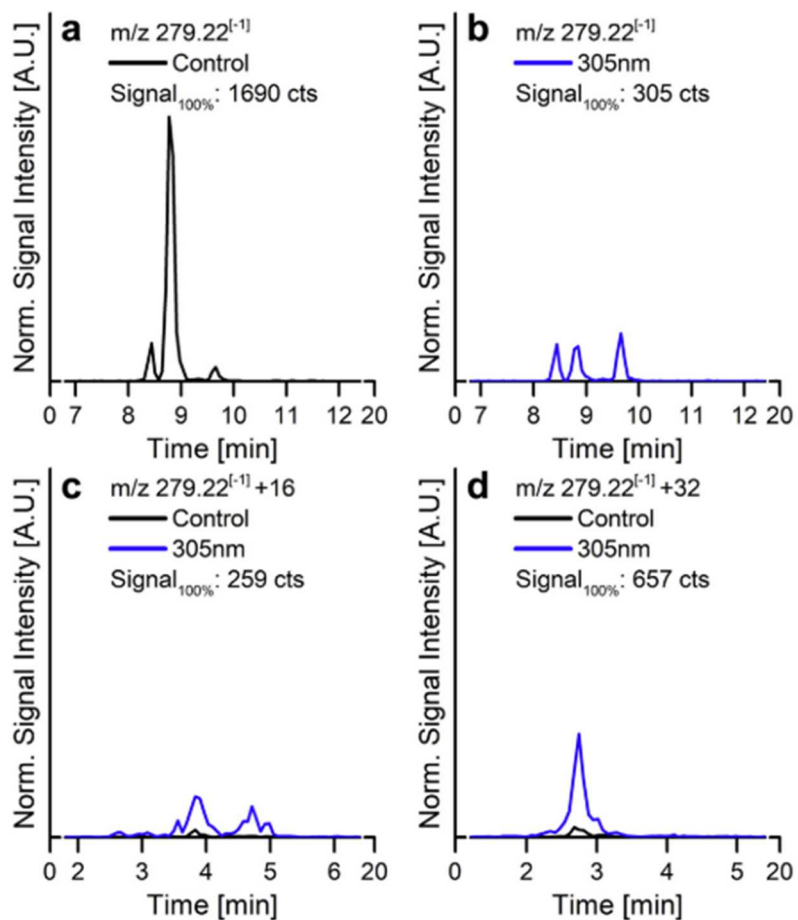


Figure 8: Negative-mode LC-MS chromatogram of linoleic acid and its isobaric species (m/z 279.22, $[M-H]^{-1}$), and linoleic acid oxidation products (m/z 279.22 + 16 and + 32, both $[M-H]^{-1}$) after FFA extraction from PS80 mixed with NATA and GSSG: Dark control samples (a, c, d, black lines) and photoirradiated samples (1 h) with $\lambda_{\text{max}} = 305$ nm (b, c, d, blue lines); y-axis scaling: scaling of each subplot is normalized to the maximum signal intensity of subplot (a).

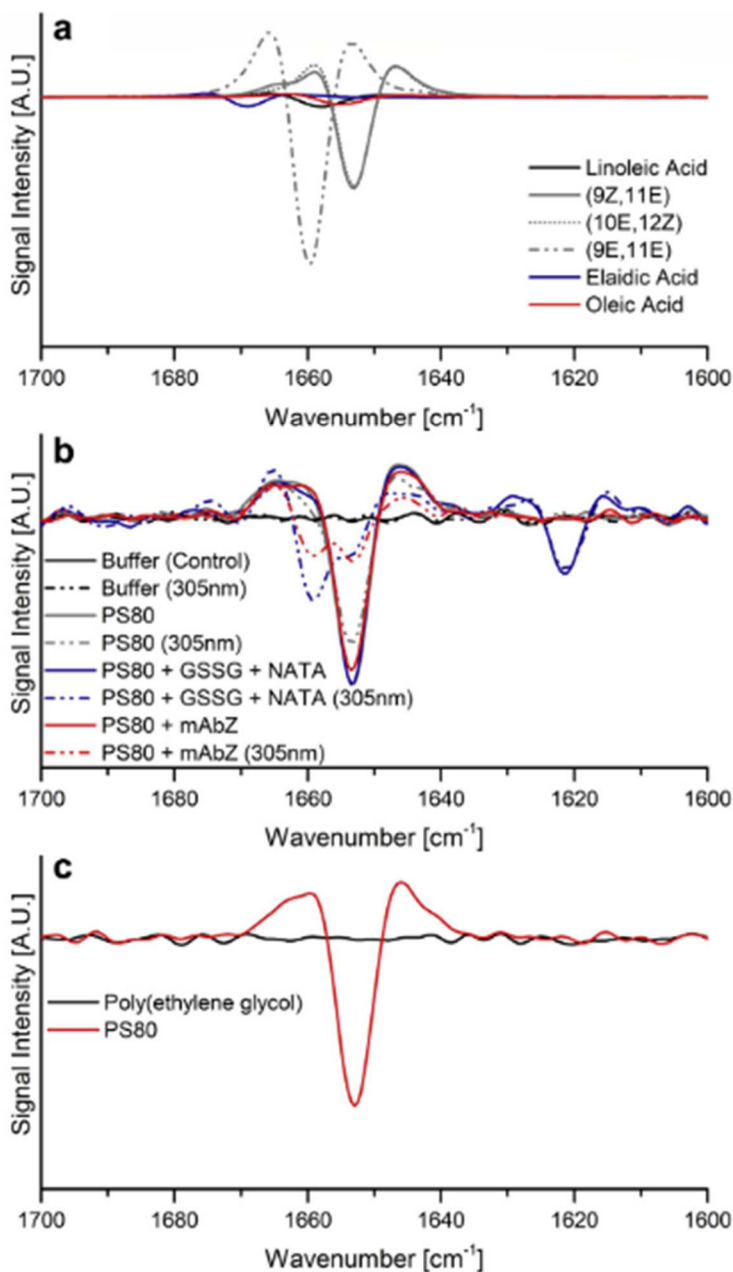


Figure 9: (a) Raman spectra of FA references in ethanol, (b) Raman spectra of samples after biphasic 1,4-dioxane/ethyl acetate extraction, drying, and dissolution in ethanol, (c) Raman spectra of PEG and PS80 directly dissolved in ethanol; ‘9Z, 11E’ refers to (9Z, 11E)-octadeca-9,11-dienoic acid, ‘10E, 12Z’ refers to (10E, 12Z)-octadeca-10,12-dienoic acid, and ‘9E, 11E’ refers to (9E, 11E)-octadeca-9,11-dienoic acid; y-axis scaling: scaling of each subplot is normalized to the maximum signal intensity presented in the respective subplot.

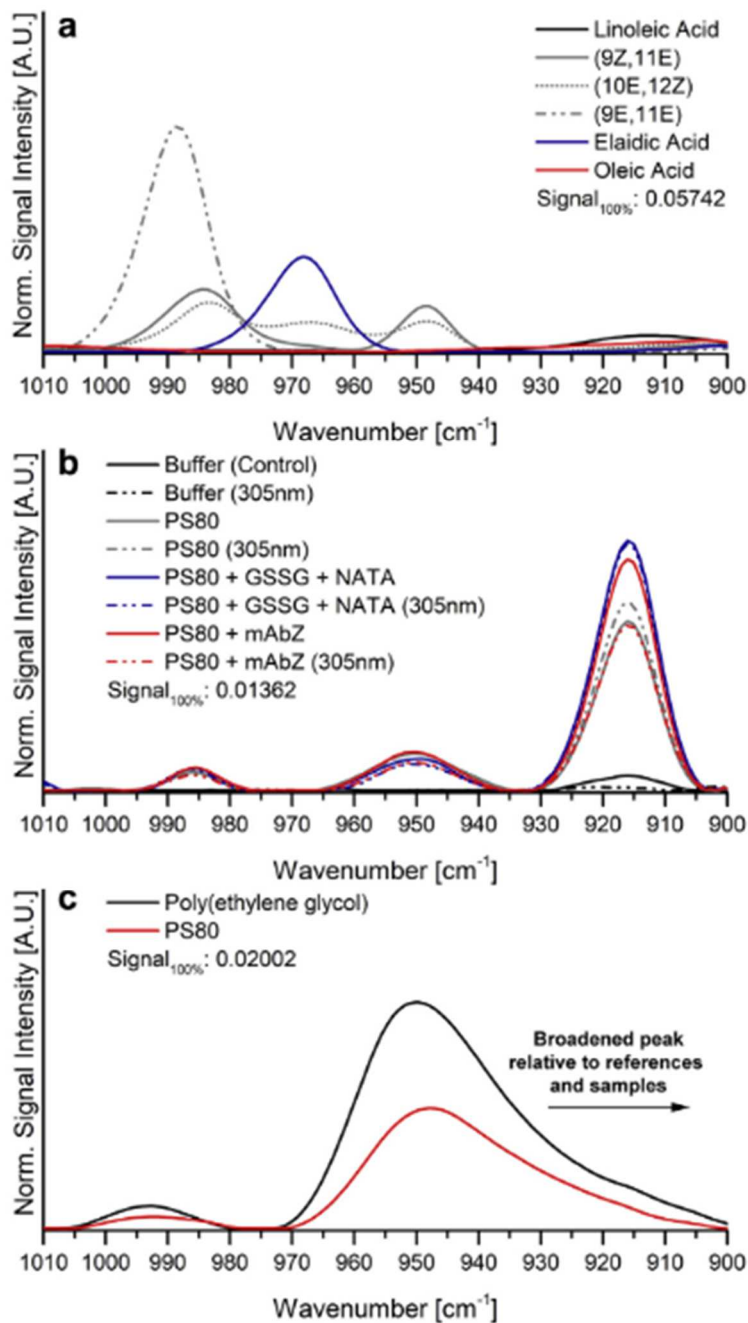


Figure 10: (a) FTIR spectra of FA references in ethanol, (b) FTIR spectra of samples after biphasic 1,4-dioxane/ethyl acetate extraction, drying, and dissolution in ethanol, (c) FTIR spectra of PEG and PS80 directly dissolved in ethanol; ‘9Z, 11E’ refers to (9Z, 11E)octadeca-9,11-dienoic acid, ‘10E, 12Z’ refers to (10E, 12Z)-octadeca-10,12-dienoic acid, and ‘9E, 11E’ refers to (9E, 11E)-octadeca-9,11-dienoic acid; y-axis scaling: scaling of each subplot is normalized to the maximum signal intensity presented in the respective subplot.

4.8. Supplementary Figures

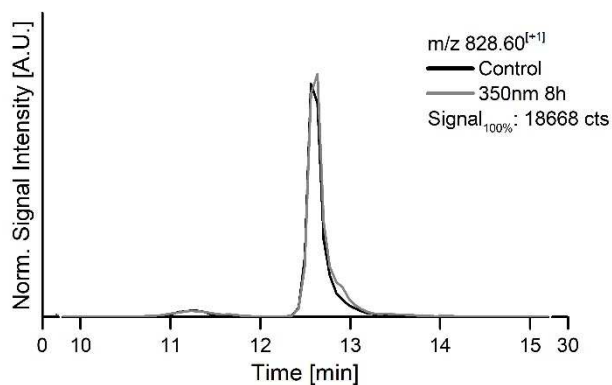


Figure S1: Positive mode LC-MS chromatogram of the POE (12) oleic acid ammonium adduct (m/z 828.60, $[M+NH_4]^{+1}$) after PS80 extraction from the mAbZ formulation: Dark control sample (black line) and sample photo-irradiated (8 h) with $\lambda_{\max} = 350$ nm (gray line); **y-axis scaling:** scaling is normalized to the maximum signal intensity of the photo-irradiated sample. (For a reference to color in this figure legend please see the online version)

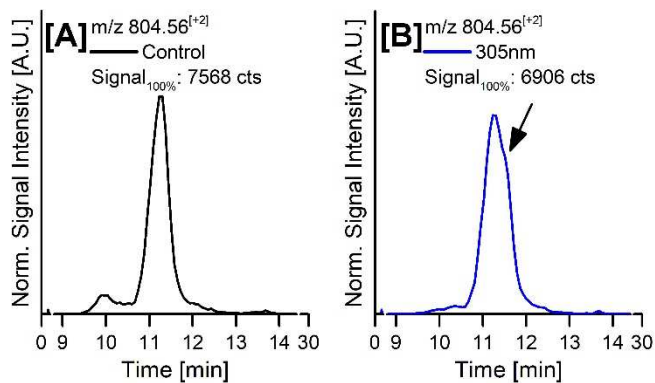


Figure S2: Positive mode LC-MS chromatogram of the POE (26) sorbitan oleic acid bis-ammonium adduct (m/z 804.56, $[M+2NH_4]^{2+}$) after PS80 extraction from the mAbZ formulation: Dark control sample (A) and sample photo-irradiated (1hr) with $\lambda_{max} = 305$ nm (B); **y-axis scaling:** scaling of each sub-plot is normalized to the maximum signal intensity of sub-plot A.

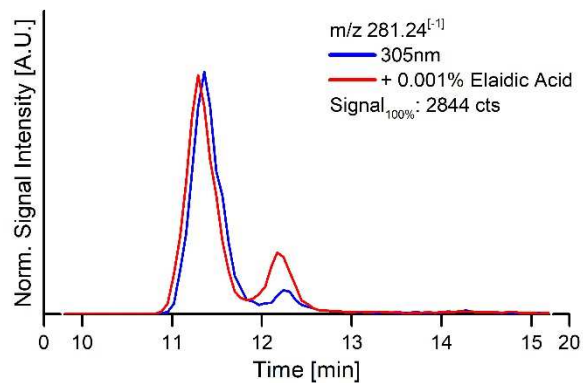


Figure S3: Negative mode LC-MS chromatogram of oleic acid and its isobaric species (m/z 281.24, $[M-H]^{-1}$) after FFA extraction from PS80 present in the mAbZ formulation: samples photo-irradiated (1hr) with $\lambda_{\max} = 305$ nm (blue line) and spiked with elaidic acid (red line); **y-axis scaling**: scaling is normalized to the maximum signal intensity of the photo-irradiated sample (blue line). (For a reference to color in this figure legend please see the online version)

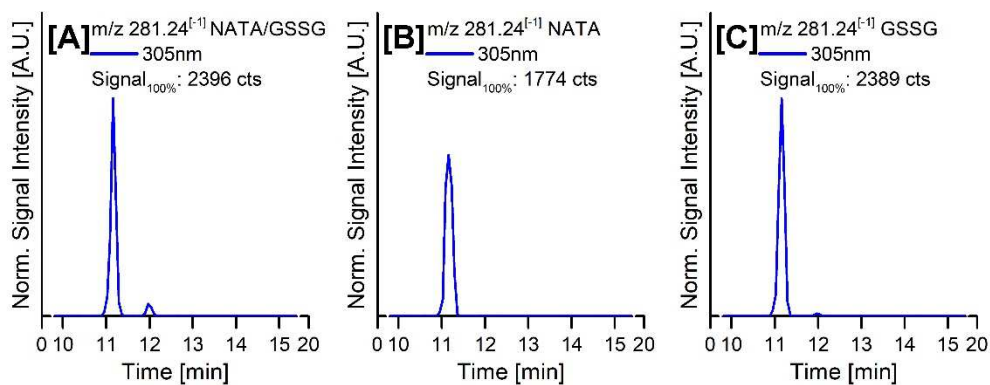


Figure S4: Negative mode LC-MS chromatogram of oleic acid and its isobaric species (m/z 281.24, $[M-H]^{-1}$) after FFA extraction from PS80 mixed with (A) NATA and GSSG, (B) NATA only, and (C) GSSG only; all samples photo-irradiated (1hr) with $\lambda_{\max} = 305$ nm; **y-axis scaling:** scaling of each sub-plot is normalized to the maximum signal intensity of sub-plot A.

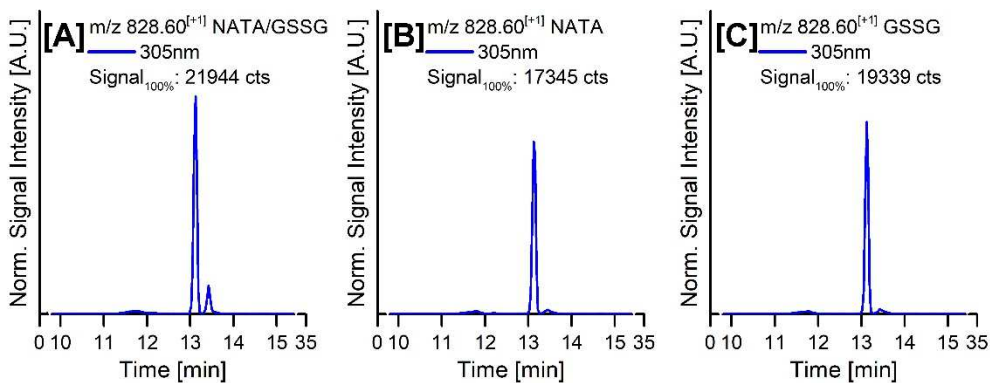


Figure S5: Positive mode LC-MS chromatogram of the POE (12) oleic acid ammonium adduct (m/z 828.60, $[M+NH_4]^{+1}$) from PS80 mixed with (A) NATA and GSSG, (B) NATA only, and (C) GSSG only; all samples photo-irradiated (1hr) with $\lambda_{max} = 305$ nm; **y-axis scaling:** scaling of each sub-plot is normalized to the maximum signal intensity of sub-plot A.

**Chapter 5: Oxidation and Cis/trans Isomerization
of Unsaturated Fatty Acids in Polysorbate 80 via
photo-induced degradation of citrate buffer**

5.1. Introduction

The development of protein therapeutics involves the use of various excipients to keep them stable for long shelf lives.¹⁻² One of the criteria is to maintain the pH of these therapeutics to ensure the physical and chemical stability. Therefore, a wide variety of buffers such as citrate, acetate, histidine and phosphate buffers are used.³ Citrate is a polyprotic buffer that has four pKa values, 3.13, 4.75, 5.80, and 14.40,³ and as a result it can buffer over a wide range of pHs. Citrate is known to have dual effect on proteins; some studies show that citrate accumulates on protein surfaces, leading to reduced colloidal stability,⁴⁻⁹ while others show that citrate can bind to the native state of proteins resulting in net stabilization.¹⁰⁻¹³ For γ D-crystalline, citrate buffer in the formulation inhibits unfolding and aggregation via ligand binding, and retains the conformational stability of the protein.¹⁴⁻¹⁵ In addition, degradation products of citrate can react with the N-terminus or lysine.¹⁶⁻¹⁷ For example, citrate-derived products formed covalent adducts of acetone and aldimine to a monoclonal antibody that was formulated in citrate buffer in presence of iron after light exposure.¹⁷

Although Fe^{3+} is rather insoluble in water, it becomes soluble through chelation with citrate.¹⁸⁻¹⁹ Depending on the ratio of citrate: Fe^{3+} , pH, temperature, and solvent, a variety of Fe^{3+} -citrate complexes may be formed.²⁰ These complexes absorb UV and visible light, eventually generating reactive oxygen species (ROS), which can modify the ingredient of formulation.¹⁷ Due to the generation of ROS, these complexes have also found their use in degrading poorly biodegradable pollutants in water under UV-A or sunlight.²¹⁻²³ Even though drug products may not be exposed to sunlight, the fluorescence lamps in the laboratory settings emit UV-A light and visible light,²⁴ where the Fe^{3+} -citrate complexes absorb. In addition, trace amounts of Fe^{3+} are present in formulations as contaminants from excipients.²⁵ Iron may also leach from stainless steel

bioreactors,²⁶⁻²⁷ glass vials²⁷ and/or rubber stoppers.²⁸ As shown in Scheme 1, reactions 1-4, when a citrate-Fe³⁺ is exposed to the UV-A light, Fe²⁺ is generated by a ligand-to-metal charge transfer (LMCT). Ferrous iron readily reduces oxygen to superoxide (O₂^{•-}), which can undergo further dismutation to hydrogen peroxide (H₂O₂). The combination of Fe²⁺ and H₂O₂ promotes the Fenton reaction ($k_4 = 1.10 \times 10^6 \text{ M}^{-1}\text{s}^{-1}$) to form •OH,²⁹ which is a strong oxidant that can oxidize proteins and surfactants. Therefore, the entire reaction is referred to as photo-Fenton reaction. An important aspect of photo-Fenton reaction is the formation of radicals originating from citrate. Carboxyl radical (R-COO•) (Scheme 1, reaction 1) are formed from citrate after LMCT and transforms into 3-hydroxy-glurate radical (3-HGA^{•2-}) (Scheme 1, reaction 5) after loss of carbon dioxide, which in the presence of oxygen converts 3-HGA^{•2-} to 3-oxo-glutarate (3-OGA²⁻) (Scheme 1, reaction 6).³⁰⁻³¹ In terms of R-COO•, it can also degrade to form a carbon dioxide radical anion (•CO₂⁻) after multiple steps (Scheme 1, reaction 7).³² This radical anion is a one-electron reductant that can reduce the disulfide bond forming a thiyl radical and a thiol.³³

Here, we report on the photo-induced oxidation and cis/trans isomerization of polysorbate (PS80) by ROS and one-electron reductants such as •CO₂⁻ and 3-HGA^{•2-}, respectively. These radicals are generated by photo-irradiation of citrate in the presence of Fe³⁺, present as a contaminant in protein formulations. We have investigated the roles of •CO₂⁻ and 3-HGA^{•2-} in generating thiyl radicals in a model peptide containing a disulfide bond, oxidized glutathione (GSSG), and inducing cis/trans isomerization of unsaturated fatty acids of PS80. It is pharmaceutically relevant as some of the marketed protein biotherapeutics such as Brentuximab Vedotin (Adcetris), Belimumab (Benlysta), Adalimumab (Humira), and Rituximab (Rituxan) are formulated in citrate buffer and PS80.

5.2. Materials and Methods

PS80 N.F. (J.T. Baker) was purchased from Avantor (Radnor, PA). Sodium acetate, phosphate monobasic, phosphate dibasic, GSSG, and ferric chloride were purchased from Sigma-Aldrich Corporation (St. Louis, MO). Citric acid monohydrate was purchased from Fisher Scientific (Hampton, NH). All the solutions were prepared using fresh water of ultra-pure quality (18.2 MΩ) using a WaterPro PS Polishing System (Labconco, Kansas City, MO).

5.2.1. Photo-irradiation

The solutions were photo-irradiated under air using 4 ml borosilicate glass vials (cut-off of <295 nm), using four RPR-3500A lamps, emitting wavelengths between 305 nm and 416 nm ($\lambda_{\max} = 350$ nm), placed in a Rayonet Photoreactor (RPR-200, The Southern New England Ultraviolet Company, Branford, CT). These four lamps gave a photon flux of $\sim 3 \times 10^{-8}$ Einstein/s and an irradiance of 6.3 W.h/m² quantified by ferrioxalate actinometer.³⁴⁻³⁶ Our experimental conditions used up to 42 W.h/m², which is well below the ICH Q1B guideline of the International Conference of Harmonization (ICH) recommendation of 200 W.h/m² of UV-A light for the photo-stability testing of drug product and drug substance.³⁷

5.2.2. Sample preparation

An initial stock of 10% PS80 (w/v) was prepared and diluted to 0.2% (w/v) in water. Similarly, initial stocks of 100 mM buffers (citrate, phosphate and acetate) at pH 6.0, 200 μ M Fe³⁺ and 50 mM GSSG (pH adjusted to 6.0) were prepared in water. The final desired concentrations of 0.02% PS80, 10 mM buffers, 1 μ M Fe³⁺, and 5 mM GSSG were achieved by adding 40 μ l of 0.2% PS80, 40 μ l of 100 mM buffer, 2 μ l of 200 μ M Fe³⁺, and 40 μ l of 50 mM GSSG; the final volume was adjusted to 400 μ l by the addition of 278 μ l of water. The solutions were vortexed and photo-

irradiated in borosilicate test tubes under the conditions mentioned above. Some experimental conditions required either different concentration of Fe^{3+} (0-50 μM), different concentration of buffers (10-50 mM), or no GSSG. In these cases, the volumes of the solutions were adjusted accordingly, and water was added as needed to adjust the final volumes to 400 μl .

In case of Ar-saturated solutions, the solutions were capped with rubber septa and saturated with Ar for 30 min. During Ar-saturation, the solutions were wrapped in an aluminum foil to prevent light exposure. After Ar-saturation, the solutions were photo-irradiated as described above. The photo-irradiated solutions were stored at $-80\text{ }^{\circ}\text{C}$ until further analysis by HPLC-mass spectrometry (MS). Control solutions under air or Ar were either wrapped in an aluminum foil and placed into the Rayonet Photoreactor during photo-irradiation or were placed in the dark.

5.2.3. Mass spectrometry

Control and photo-irradiated solutions were analyzed by HPLC-electrospray MS in the positive mode, using a Q-ToF PremierTM (Waters Corporation, Milford, MA) connected to a Waters ACQUITY UPLC system (Waters Corporation, Milford, MA). The solutions were introduced into the mass analyzer in the ESI source. The desolvation temperature and source temperature were maintained at $250\text{ }^{\circ}\text{C}$ and at $120\text{ }^{\circ}\text{C}$, respectively, and the capillary voltage was set at 2.8 kV. The mass spectrometer was operated in the MS^{E} mode, collecting fragmentation patterns of PS80, which give unique fragmentation ions of fatty acids.³⁸ The analyzed mass range was 150-2000 Da. The mass spectrometer settings, UPLC settings, and data analysis were achieved with the Masslynx v.4.1 software version.

The resolution of PS80 species and its degradation products was achieved by a PrevailTM C18 column (Grace, Deerfield, IL) with dimensions of 150 mm X 2.1 mm, 300 Å pore size, and 3.0

mm particle size. For better separation, the column heater was maintained at 40 °C. Five μl of 0.02% PS80 was run at the flow rate of 0.4 ml/min. Four mobile phases were employed for the separation of the solutions and to clean the column. Mobile phase A contained water, 2 mM ammonium formate, and 0.08% formic acid, mobile phase B contained 30% methanol, 70% acetonitrile, and 0.08% formic acid, mobile phase C contained 100% isopropanol, and mobile phase D contained 10% 1,4-dioxane and 90% acetone. The solvent gradient started with 60% A and 40% B, and the organic phase gradually increased linearly to 1% A and 99% B within 15 min. The composition was then changed to 1% A, 90% B, and 9% C, and held for 2 min. The column was then washed using 1% A and 99% D for 3 min and was re-equilibrated for 7 min before the next run.

5.3. Results

5.3.1. Oxidation products

PS80 is prone to oxidation when exposed to reactive oxygen species, contaminants (such as metals and peroxides), heat, and light.³⁹ Here, we monitored the degradation of PS80 in the presence of Fe^{3+} -citrate during exposure to UV-A light. MS chromatogram of a control solution containing 0.02% PS80 and 10 μM Fe^{3+} in 10 mM citrate buffer shows PS80 species, which were eluted in the following order; at $t_{\text{R}} = 10.32$ min POE sorbitan monolinoleate, at $t_{\text{R}} = 11.74$ min POE sorbitan monooleate, at $t_{\text{R}} = 13.22$ min POE oleate, at $t_{\text{R}} = 17.82$ min POE sorbitan oleate-linoleate, at $t_{\text{R}} = 18.64$ min POE sorbitan dioleate, and at $t_{\text{R}} = 20.80$ min higher order esters were eluted. A photo-irradiated solution containing 0.02% PS80 and 10 μM Fe^{3+} in 10 mM citrate buffer (Fig. 1, red trace) was compared with a photo-irradiated solution of 0.02% PS80 in 10 mM citrate buffer without Fe^{3+} (Fig. 2, blue trace) and a control solution. Photo-irradiation in presence of Fe^{3+} revealed the reduction of the peaks at $t_{\text{R}} = 10.32$ min displaying the m/z of POE sorbitan

monolinoleate, at $t_R = 17.82$ min displaying the m/z of POE sorbitan oleate-linoleate, and increase of the peak at $t_R = 13.90$ min displaying the m/z of POE oleate with an increase of 30 Da. In contrast, photo-irradiation of solutions without Fe^{3+} did not reveal in significant changes in the peak intensities compared to the control sample. These observations suggest the involvement of Fe^{3+} -citrate in the degradation of PS80 via a photo-Fenton reaction. The oxidation products of PS80 in citrate buffer were quantified after exposure to UV-A light in increased concentration of Fe^{3+} and increased photo-irradiation time shown in section 4.1.1 and 4.1.2, respectively.

5.3.1.1. Effect of Fe^{3+} concentration

The degradation profile of 0.02% PS80 in 10 mM citrate buffer, pH 6.0, was monitored in the presence of various concentration of Fe^{3+} between 0 and 50 μM Fe^{3+} (Fig. 2). The peak areas of POE (25) sorbitan linoleate (Fig. 2, black trace) display a rapid degradation of this species when the PS80 solution in 10 mM citrate buffer contained 5 μM Fe^{3+} and almost all of this species degraded in the solutions containing ≥ 10 μM Fe^{3+} after photo-irradiation. POE (25) sorbitan monooleate degraded gradually as the Fe^{3+} concentration increased (Fig. 2, blue trace), indicated by its peak areas. Among the PS80 species quantified, POE(11) oleate (Fig. 2, red trace) decreased at a slower rate.

The degradation products of PS80 were monitored by analyzing the peak areas of oxidation products, specially of products displaying an increase of 16 Da, corresponding to the addition/insertion of an oxygen atom. These species indicate the formation of hydroxylation products (Fig. 3). The oxidation product, POE(11) hydroxy-oleate ($m/z = 784.57$, $z = 1$) showed gradual increase in peak area when the Fe^{3+} concentration was increased from 0 to 50 μM Fe^{3+} . A similar pattern was observed for POE(25) sorbitan hydroxy-monooleate ($m/z = 782.54$, $z = 2$)

and POE(25) sorbitan hydroxy-monolinoleate ($m/z = 781.54$, $z = 2$) except for the solution containing $5 \mu\text{M Fe}^{3+}$.

5.3.1.2. Duration of light exposure

The solutions containing 0.02% PS80 and $1 \mu\text{M Fe}^{3+}$ in 10 mM citrate buffer, pH 6.0, were exposed to UV-A light for various time between 0 and 200 min (Fig. 3). As in section 4.1.1, the oxidation products were evaluated by extraction of a desired m/z and calculation of relative peak areas. The relative peak areas of the oxidation products, such as POE (11) hydroxy-oleate, POE (25) sorbitan hydroxy-monooleate, POE (25) sorbitan hydroxy-monolinoleate increased on the light exposure extended to 175 min, but did not change further when the solutions were exposed for 200 min. A small amount of POE (25) sorbitan hydroxy-monooleate was present in the control solution as well.

5.3.2. Cis/trans isomerization

5.3.2.1. Cis/trans isomerization of unsaturated fatty acids of PS80 under air

In presence of Fe^{3+} , a citrate-derived radical is $\cdot\text{CO}_2^-$ is formed after exposure to UV-A light. This radical anion is a reductant and can transfer an electron to a disulfide bond, which subsequently breaks the bond forming a thiol and a thiyl radical. Our previous study on cis/trans isomerization of unsaturated fatty acids of PS80 was mediated by thiyl radical after an electron was transferred to a disulfide bond from a photoionization of tryptophan (Trp).⁴⁰ Therefore, we employed a model peptide containing a disulfide bond, GSSG, to accept an electron from $\cdot\text{CO}_2^-$, reduce to a thiyl radical, and induce cis/trans isomerization of unsaturated fatty acids of PS80. Therefore, to confirm this hypothesis, 400 μl of solutions containing 0.02% PS80 (w/v), $10 \mu\text{M Fe}^{3+}$, 5 mM GSSG complex prepared in 10-50 mM citrate buffer, at pH 6.0, were exposed to UV-

A light for 1 h (Fig. 5). Significant changes in the extracted ion chromatogram (XIC) peaks of POE(11) oleate and POE(25) sorbitan monooleate were observed for all the light exposed solutions in comparison to the control sample that was wrapped in aluminum foil during photo-irradiation. For photo-irradiated solution containing 10, 20, and 50 mM citrate, the extracted ion chromatograms (XICs) of POE(11) oleate, eluting at $t_R = 13.22$ min, with m/z 784.59 ($z = 1$) (Fig. 5A), revealed an isobaric peak eluting directly after POE(11) oleate at $t_R = 13.46$ min. The obtained isobaric peaks have slight increase in peak areas with increase in buffer concentration. Similarly, XICs of POE(25) sorbitan monooleate displaying a molecular ion with m/z 782.52 ($z = 2$) resulted in an unresolved isobaric peak, which was absent in the control sample (Fig. 5B). The peak areas of these isobaric species indicated that the increase in citrate buffer concentration has very little effect on their formation. This is because 10 mM citrate was already 1000-fold higher than $10 \mu\text{M Fe}^{3+}$ and all the complexing sites of iron are occupied so increasing the concentration further had little effect.

Next, we investigated the role of increasing concentration of iron on the formation of isobaric species. Solutions containing 0.02% PS80 (w/v) and 5 mM GSSG prepared in 10 citrate buffer, pH 6.0, with Fe^{3+} concentration ranging from 0 to $10 \mu\text{M}$ iron were exposed to UV-A light for 1 h (Fig. 6). Representatively, XICs of POE(11) oleate displaying a molecular ion with m/z 784.59 ($z = 1$) resulted in higher yield of isobaric species in $10 \mu\text{M Fe}^{3+}$ compared to $2.5 \mu\text{M Fe}^{3+}$ containing photo-irradiated sample and control sample (Fig. 6A). Likewise, XICs of POE(25) sorbitan monooleate displaying a molecular ion with m/z 782.52 ($z = 2$) resulted in a new unresolved peak, which is absent in both $2.5 \mu\text{M Fe}^{3+}$ containing photo-irradiated sample and control sample (Fig. 6B). These data suggest with increasing Fe^{3+} concentration more citrate bind

to iron, giving higher yield of $\cdot\text{CO}_2^-$ that reduces disulfide bonds to thiyl radicals. These thiyl radicals then induces cis/trans isomerization of the unsaturated fatty acids of PS80.

5.3.2.2. Cis/trans isomerization of unsaturated fatty acids of PS80 under Ar

Since photo-irradiation of citrate- Fe^{3+} in the UV-A region also generate 3-HGA \cdot^{2-} , a reductant, in absence of oxygen, we investigated the role of such radical anion in reducing disulfide bond of GSSG and generating thiyl radicals, which can induce cis/trans isomerization of unsaturated fatty acids in PS80 under Ar-saturation. Therefore, Ar-saturated solutions containing 0.02% PS80, 5 mM GSSG, and 10 μM Fe^{3+} were prepared in either 10, 20, or 50 mM citrate buffer and exposed to UV-A light for 1 h.(Fig. 7). XICs of POE(11) oleate displaying a molecular ion with m/z 784.59 ($z = 1$) resulted in an isobaric species, eluting directly after POE(11) oleate, and XICs of POE(25) sorbitan monooleate displaying a molecular ion with m/z 782.52 ($z = 2$) resulted in a new unresolved peak, which were observed only in the photo-irradiated samples, and not in control sample. Ar-saturated photo-irradiated solution showed a very little effect of increased citrate buffer concentration on the yields of these isobaric species. By comparison to the air-saturated solution (Fig. 5), in Ar-saturated solution, the yields of isobaric species of both POE(11) oleate and POE(25) sorbitan monooleate were lower. Next, concentration of Fe^{3+} from 0 to 10 μM was used in solutions containing 0.02% PS80 and 5 mM GSSG prepared in 10 mM citrate buffer, pH 6.0, and exposed to UV-A light. XICs of POE(11) oleate with m/z 784.59 ($z = 1$) resulted in isobaric species eluting at $t_R = 13.46$ min in the photo-irradiated samples, but not in the control sample. Photo-irradiated solution with 10 μM Fe^{3+} is in higher yield compared to the photo-irradiated solution with 2.5 μM Fe^{3+} , which is similar observation made in air-saturated solution; however, by comparison Ar-saturated solutions have lower yield of isobaric species of POE(11) oleate. Similarly, XICs of POE(25) sorbitan oleate with m/z 782.52 ($z = 2$) revealed a smaller

shoulder peak in the solution containing $2.5 \mu\text{M Fe}^{3+}$ compared to $10 \mu\text{M Fe}^{3+}$. Thus, these citrate buffer and iron concentration dependent experiments were similar in both air and Ar-saturated solutions; however, yields of these isobaric species were higher in air-saturated solution.

5.3.2.3. Cis/trans isomerization of unsaturated fatty acids in different buffers under Ar

Apart from citrate, other buffers such as acetate and phosphate are used frequently in the biotherapeutic formulations.³ Additionally, disulfides can directly absorb UV light and form thiyl radicals, so we investigated the abilities of acetate and phosphate buffers, and disulfide without buffers in inducing cis/trans isomerization of unsaturated fatty acids of PS80 via thiyl radicals. Hence, Ar-saturated solutions containing 0.02% PS80, $1 \mu\text{M Fe}^{3+}$, and 5 mM GSSG that were prepared either in no buffer, 10 mM phosphate buffer, 10 mM sodium acetate buffer, or in 10 mM citrate buffer at pH 6.0 and were exposed to UV-A light for 1 h. XICs of POE(11) oleate displaying a molecular ion with m/z 784.59 ($z = 1$), showed a small peak, eluting next to all the samples, but the yield was higher in citrate buffer. Likewise, XICs of POE(25) sorbitan monooleate displaying a molecular ion with m/z 782.52 ($z = 2$) revealed shoulder peaks in all the samples, but citrate buffer had a prominent shoulder peak. These results suggest that disulfide bonds without buffers can absorb some UV-A and generate thiyl radicals, which can prompt cis/trans isomerization. Since, acetate and phosphate buffers did not increase the yield of isobaric species, they suggest little to no effect on cis/trans isomerization. On the other hand, among the buffers tested, citrate can form citrate-derived radical ions, which reduce the disulfide bonds to thiyl radicals and promote cis/trans isomerization of unsaturated fatty acids of PS80.

5.4. Discussion

We observed oxidation of PS80 in solutions containing citrate and Fe^{3+} after exposure to UV-A light. In addition, when GSSG, a model system for disulfide bonds in proteins, was added to

solutions containing PS80 and Fe^{3+} in citrate buffer, isobaric species of unsaturated fatty acids of PS80 species were observed. Therefore, we hypothesized that the oxidation of PS80 species is initiated by the ROS generated during photo-irradiation and the cis/trans isomerization is carried out by radical ions, one-electron reductants, which reduce GSSG to give thiyl radicals after one-electron transfer. These reductants are generated from citrate after LMCT, followed by multiple steps discussed in section 5.2 and shown in Scheme 1.

5.4.1. Oxidation products

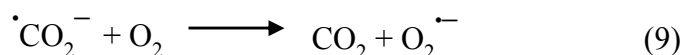
In order to determine the role of ROS in the formation of PS80 oxidation products via the photo-Fenton reaction, we focused on two experimental conditions (i) different ratios of Fe^{3+} and citrate (Fig. 3) and (ii) duration of light exposure (Fig. 4). Our observations indicate that PS80 oxidation depends both on the concentration of Fe^{3+} and the duration of light exposure. The effect of an increasing Fe^{3+} concentration was most pronounced for oxidation products derived from linoleic acid (Fig. 2) suggested by rapid decline of POE(25) sorbitan monolinoleate. Our previous studies showed that a large fraction of linoleic acid is in conjugated forms (CLAs).⁴⁰ In general, we also observed an increase in peak areas of the hydroxy products of PS80 species, such as POE(11) hydroxy-oleate, POE(25) sorbitan hydroxy-oleate, and POE(25) sorbitan hydroxy-linoleate, as we increased the concentration of Fe^{3+} (Fig. 3) and with longer UV-A light exposure (Fig. 4). The formation of ROS such as hydroxyl radical ($\cdot\text{OH}$), a strong oxidant, promotes oxidation of PS80. Formation of $\cdot\text{OH}$ is dependent on the generation and stability of $\text{O}_2^{\cdot-}$, H_2O_2 , and Fe^{2+} (Scheme 1, reactions 2-3, 6). The formation of these intermediates depends on the ratio of Fe^{3+} and citrate concentration. Feng *et al.* have illustrated that an increase in citrate concentration from 50 μM to 200 μM with a constant concentration of iron (10 μM) increases the initial rate of $\cdot\text{OH}$ formation; however, beyond 200 μM citrate the initial rate of $\cdot\text{OH}$ formation did not change significantly.⁴¹

In our experimental conditions, we have used 10 mM citrate, which is in excess to carry out the photo-Fenton reaction. Additionally, in the same study, increasing the concentration of Fe^{3+} from 10 μM to 100 μM with constant concentration of citrate (300 μM) showed an increase in the initial rate of $\cdot\text{OH}$ formation. This result also supports our results as we observed increased PS80 oxidation product with increasing iron concentration; however, the oxidation product does not increase linearly with iron concentration because citrate is a quencher of $\cdot\text{OH}$ radical.⁴² The reaction rate of $\cdot\text{OH}$ with citrate is $2.4 \times 10^8 \text{ M}^{-1}\text{s}^{-1}$ ⁴³ and with unsaturated hydrocarbons, such as cis-butene, is $3.68 \times 10^{10} \text{ M}^{-1}\text{s}^{-1}$,⁴⁴ suggesting that the unsaturated hydrocarbon fatty acids in PS80 have higher reactivity with $\cdot\text{OH}$ radical. An $\cdot\text{OH}$ radical can either abstract a hydrogen atom from allylic carbon (dehydrogenation), generating a carbon-centered radical which can readily react with oxygen at the diffusion-limited reaction, or it can add to the unsaturated bond forming hydroxy radicals (hydroxylation) (Scheme 2).⁴⁵⁻⁴⁷ Such intermediates can lead to peroxy, hydroxy, keto, and epoxy product formation.⁴⁸ The unsaturated fatty acids such as oleic acid and linoleic acid were reported as common targets in PS80.^{39, 48-49} These PS80 oxidation products can react with proteins and oxidize labile amino acids such as Met,⁵⁰⁻⁵¹ affecting the efficacy of proteins.

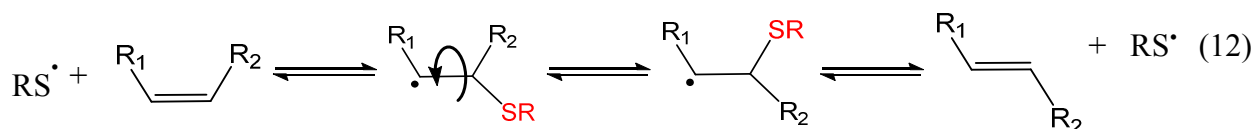
5.4.2. Cis/trans isomerization

Our previous work on PS80 demonstrated the role of thiyl radicals in cis/trans isomerization of unsaturated fatty acids of PS80.⁴⁰ A thiyl radical was generated after an electron transfer from photoionized Trp to a disulfide bond after exposure to UV-B light, which was confirmed by using a model Trp-containing compound, NATA and GSSG. Namely, we observed increase in the concentration of elaidic acid (cis-oleic acid) in MS negative mode. In our present work, we generated a citrate-derived one-electron reductant, $\cdot\text{CO}_2^-$, in presence of Fe^{3+} after exposure to

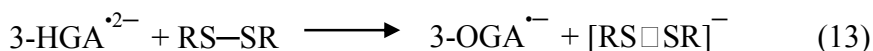
UV-A light under air. $\cdot\text{CO}_2^-$ can react either with H_2O_2 , reduce oxygen, or reduce disulfide bonds. $\cdot\text{CO}_2^-$ reacts with H_2O_2 at $k_8 = 7.3 \times 10^5 \text{ M}^{-1}\text{s}^{-1}$ and undergoes a Fenton-like reaction to give $\cdot\text{OH}$ radical (reaction 8).⁵² On the other hand, $\cdot\text{CO}_2^-$ reduces O_2 to give $\text{O}_2^{\cdot-}$ at $k_9 = 1 \times 10^9 \text{ M}^{-1}\text{s}^{-1}$ (reaction 9).⁵³ These ROS generated via $\cdot\text{CO}_2^-$ are also responsible for PS80 oxidation.



Instead, in the presence of a disulfide bond, $\cdot\text{CO}_2^-$ reduces a disulfide bond to an intermediate $2\sigma/1\sigma^*$ three electron bonded disulfide radical anion $[\text{RS}\cdot\text{SR}]^-$,⁵⁴ which dissociates into a thiyl radical and thiolate within 1 μsec (reactions 10 and 11).⁵⁵ A series of studies have indicated that thiyl radicals promote cis/trans isomerization of mono- and poly-unsaturated fatty acids (reactions 12).⁵⁶⁻⁶¹



It is noteworthy that in our present study, we also observed isobaric species of unsaturated fatty acids of PS80 under Ar (Fig. 7 and 8). Since $\cdot\text{CO}_2^-$ formation requires O_2 , it is unlikely that $\cdot\text{CO}_2^-$ is responsible for thiyl radical formation under Ar. Another citrate-derived reductant, 3-HGA \cdot^{2-} , readily oxidizes to 3-OGA $^{2-}$ under air, but may have longer half-life under Ar. As such, 3-HGA \cdot^{2-} can reduce disulfide bond (reaction 13), forming a thiyl radical (reaction 11) and promoting cis/trans isomerization. This is suggested by the formation of isobaric species under Ar.



Our results revealed the formation of isobaric species of PS80 in photo-irradiated solutions containing GSSG, which suggested the role of thiyl radicals in cis/trans isomerization of unsaturated fatty acids of PS80. Such reactions can also occur in protein biotherapeutics as they are commonly formulated in citrate buffer and PS80. Additionally, thiyl radicals can lead to cross-linking, react with Tyr residue to form tyrosyl radical, and induce free thiol deactivation.³³ The presence of trans instead of cis fatty acids in surfactants have shown to change the phase transition temperature,⁶² structures of micelles,⁶³⁻⁶⁴ drag reduction, and shear viscosities.⁶³ As such, changes in micellar structure and other properties of surfactants can reduce its ability to protect proteins from aggregation.

In conclusion, the photo-Fenton reaction resulted in oxidation and cis/trans isomerization of unsaturated fatty acids of PS80 species (in the presence of disulfides). The ROS and one-electron reductants ($\cdot\text{CO}_2^-$ and 3-HGA \cdot^{2-}) are generated in the solutions containing citrate and Fe^{3+} after exposure to UV-A light. These radical ions can initiate secondary radicals such as thiyl radicals in proteins and subsequently generate radical-induced products that can challenge the efficacy and safety of the drugs. Further work on the physicochemical properties of trans fatty acids and cis fatty acids will help in understanding their influence on stability of the biotherapeutics.

5.5. References

1. Rayaprolu, B. M.; Strawser, J. J.; Anyarambhatla, G., Excipients in parenteral formulations: selection considerations and effective utilization with small molecules and biologics. *Drug Dev. Ind. Pharm.* **2018**, *44* (10), 1565-1571.
2. Zhang, Y.; Williams III, R. O.; Tucker, H. O., Formulation strategies in immunotherapeutic pharmaceutical products. *World J. Clin. Oncol.* **2020**, *11* (5), 275-282.
3. Zbacnik, T. J.; Holcomb, R. E.; Katayama, D. S.; Murphy, B. M.; Payne, R. W.; Coccaro, R. C.; Evans, G. J.; Matsuura, J. E.; Henry, C. S.; Manning, M. C., Role of Buffers in Protein Formulations. *J. Pharm. Sci.* **2017**, *106* (3), 713-733.
4. Joshi, V.; Shivach, T.; Kumar, V.; Yadav, N.; Rathore, A., Avoiding antibody aggregation during processing: establishing hold times. *Biotechnol. J.* **2014**, *9* (9), 1195-1205.
5. Peterson, S. E.; Wang, S.; Ranheim, T.; Owen, K. E., Citrate-mediated disaggregation of rotavirus particles in RotaTeq® vaccine. *Antiviral Res.* **2006**, *69* (2), 107-115.
6. Roberts, C. J.; Nesta, D. P.; Kim, N., Effects of Temperature and Osmolytes on Competing Degradation Routes for an IgG1 Antibody. *J. Pharm. Sci.* **2013**, *102* (10), 3556-3566.
7. Roberts, D.; Keeling, R.; Tracka, M.; van der Walle, C. F.; Uddin, S.; Warwicker, J.; Curtis, R., Specific Ion and Buffer Effects on Protein-Protein Interactions of a Monoclonal Antibody. *Mol. Pharm.* **2015**, *12* (1), 179-193.
8. Barnett, G. V.; Razinkov, V. I.; Kerwin, B. A.; Hillsley, A.; Roberts, C. J., Acetate- and Citrate-Specific Ion Effects on Unfolding and Temperature-Dependent Aggregation Rates of Anti-Streptavidin IgG1. *J. Pharm. Sci.* **2016**, *105* (3), 1066-1073.
9. Barnett, G. V.; Razinkov, V. I.; Kerwin, B. A.; Laue, T. M.; Woodka, A. H.; Butler, P. D.; Perevozchikova, T.; Roberts, C. J., Specific-Ion Effects on the Aggregation Mechanisms and Protein-Protein Interactions for Anti-streptavidin Immunoglobulin Gamma-1. *J. Phys. Chem. B* **2015**, *119* (18), 5793-5804.
10. White, M. C.; Doyle, A. G.; Jacobsen, E. N., A synthetically useful, self-assembling MMO mimic system for catalytic alkene epoxidation with aqueous H₂O₂. *J. Am. Chem. Soc.* **2001**, *123* (29), 7194-7195.
11. Kaushik, J. K.; Bhat, R., A mechanistic analysis of the increase in the thermal stability of proteins in aqueous carboxylic acid salt solutions. *Protein Sci.* **1999**, *8* (1), 222-233.
12. Harinarayan, C.; Skidmore, K.; Kao, Y.; Zydney, A.; Van Reis, R., Small molecule clearance in ultrafiltration/diafiltration in relation to protein interactions: Study of citrate binding to a Fab. *Biotechnol. Bioeng.* **2009**, *102* (6), 1718-1722.
13. Kochany, J.; Lipczynska-Kochany, E., Application of the EPR spin-trapping technique for the investigation of the reactions of carbonate, bicarbonate, and phosphate anions with hydroxyl radicals generated by the photolysis of H₂O₂. *Chemosphere* **1992**, *25* (12), 1769-1782.
14. Goulet, D. R.; Knee, K. M.; King, J. A., Inhibition of unfolding and aggregation of lens protein human gamma D crystallin by sodium citrate. *Exp. Eye Res.* **2011**, *93* (4), 371-381.

15. Ohishi, S. i.; Shimizu, N.; Mihara, K. i.; Imamoto, Y.; Kataoka, M., Light induces destabilization of photoactive yellow protein. *Biochemistry* **2001**, *40* (9), 2854-2859.
16. Chumsae, C.; Zhou, L. L.; Shen, Y.; Wohlgemuth, J.; Fung, E.; Burton, R.; Radziejewski, C.; Zhou, Z. S., Discovery of a chemical modification by citric acid in a recombinant monoclonal antibody. *Anal. Chem.* **2014**, *86* (18), 8932-6.
17. Valliere-Douglass, J. F.; Connell-Crowley, L.; Jensen, R.; Schnier, P. D.; Trilisky, E.; Leith, M.; Follstad, B. D.; Kerr, J.; Lewis, N.; Vunnum, S.; Treuheit, M. J.; Balland, A.; Wallace, A., Photochemical degradation of citrate buffers leads to covalent acetonation of recombinant protein therapeutics. *Protein Sci.* **2010**, *19* (11), 2152-63.
18. Gutteridge, J. M. C., Hydroxyl radical formation from the auto-reduction of a ferric citrate complex. *Free Radic. Biol. Med.* **1991**, *11* (4), 401-406.
19. Neilands, J., Evolution of biological iron binding centers. In *Structure and Bonding, Volume 11*, Springer: 1972; pp 145-170.
20. Gautier-Luneau, I.; Merle, C.; Phanon, D.; Lebrun, C.; Biaso, F.; Serratrice, G.; Pierre, J. L., New trends in the chemistry of iron (III) citrate complexes: Correlations between X-ray structures and solution species probed by electrospray mass spectrometry and kinetics of iron uptake from citrate by iron chelators. *Chem. Eur. J.* **2005**, *11* (7), 2207-2219.
21. Rodríguez, E. M.; Núñez, B.; Fernández, G.; Beltrán, F. J., Effects of some carboxylic acids on the Fe (III)/UVA photocatalytic oxidation of muconic acid in water. *Appl. Catal. B* **2009**, *89* (1-2), 214-222.
22. Ou, X.; Quan, X.; Chen, S.; Zhang, F.; Zhao, Y., Photocatalytic reaction by Fe(III)-citrate complex and its effect on the photodegradation of atrazine in aqueous solution. *J. Photochem. Photobiol. A: Chem.* **2008**, *197* (2), 382-388.
23. Seraghni, N.; Belattar, S.; Mameri, Y.; Debbache, N.; Sehili, T., Fe (III)-citrate-complex-induced photooxidation of 3-methylphenol in aqueous solution. *Int. J. Photoenergy* **2012**, *2012*.
24. Nicole, W., Ultraviolet Leaks from CFLs. National Institute of Environmental Health Sciences: 2012.
25. Buettner, G. R.; Jurkiewicz, B. A., Catalytic metals, ascorbate and free radicals: combinations to avoid. *Radiat. Res.* **1996**, *145* (5), 532-41.
26. Zhou, S.; Evans, B.; Schöneich, C.; Singh, S. K., Biotherapeutic formulation factors affecting metal leachables from stainless steel studied by design of experiments. *AAPS PharmSciTech* **2012**, *13* (1), 284-294.
27. Zhou, S.; Schöneich, C.; Singh, S. K., Biologics formulation factors affecting metal leachables from stainless steel. *AAPS PharmSciTech* **2011**, *12* (1), 411-421.
28. Li, X.; Qian, P., Identification of an exposure risk to heavy metals from pharmaceutical-grade rubber stoppers. *J. Food Drug Anal.* **2017**, *25* (3), 723-730.
29. Millero, F. J.; Sotolongo, S., The oxidation of Fe(II) with H₂O₂ in seawater. *J. Geochim. Cosmochim. Acta* **1989**, *53* (8), 1867-1873.

30. Quici, N.; Litter, M. I.; Braun, A. M.; Oliveros, E., Vacuum-UV-photolysis of aqueous solutions of citric and gallic acids. *J. Photochem. Photobiol. A: Chem.* **2008**, *197* (2-3), 306-312.
31. Gautier-Luneau, I.; Bertet, P.; Jeunet, A.; Serratrice, G.; Pierre, J.-L., Iron-citrate complexes and free radicals generation: Is citric acid an innocent additive in foods and drinks? *BioMetals* **2007**, *20* (5), 793-796.
32. Subelzu, N.; Schoneich, C., Near UV and visible light induce iron-dependent photo-degradation reactions in pharmaceutical buffers: mechanistic and product studies. (*unpublished*)
33. Favaudon, V.; Tourbez, H.; Houee-Levin, C.; Lhoste, J. M., Carboxyl radical induced cleavage of disulfide bonds in proteins. A γ -ray and pulse radiolysis mechanistic investigation. *Biochemistry* **1990**, *29* (49), 10978-10989.
34. Pozdnyakov, I. P.; Kel, O. V.; Plyusnin, V. F.; Grivin, V. P.; Bazhin, N. M., New insight into photochemistry of ferrioxalate. *J. Phys. Chem. A* **2008**, *112* (36), 8316-8322.
35. Lee, J.; Seliger, H., Quantum yield of the ferrioxalate actinometer. *J. Chem. Phys.* **1964**, *40* (2), 519-523.
36. Hatchard, C.; Parker, C. A., A new sensitive chemical actinometer-II. Potassium ferrioxalate as a standard chemical actinometer. *Proc. R. Soc. London, Ser. A* **1956**, *235* (1203), 518-536.
37. Guideline, I. H. T., Photostability testing of new drug substance and products. *Fed. Register* **1996**, *62*, 27115-27122.
38. Borisov, O. V.; Ji, J. A.; Wang, Y. J.; Vega, F.; Ling, V. T., Toward understanding molecular heterogeneity of polysorbates by application of liquid chromatography–mass spectrometry with computer-aided data analysis. *Anal. Chem.* **2011**, *83* (10), 3934-3942.
39. Kerwin, B. A., Polysorbates 20 and 80 used in the formulation of protein biotherapeutics: structure and degradation pathways. *J. Pharm. Sci.* **2008**, *97* (8), 2924-35.
40. Prajapati, I.; Peters, B.-H.; Larson, N. R.; Wei, Y.; Choudhary, S.; Kalonia, C.; Hudak, S.; Esfandiary, R.; Middaugh, C. R.; Schöneich, C., Cis/Trans Isomerization of Unsaturated Fatty Acids in Polysorbate 80 During Light Exposure of a Monoclonal Antibody–Containing Formulation. *J. Pharm. Sci.* **2020**, *109* (1), 603-613.
41. Feng, X.; Wang, Z.; Chen, Y.; Tao, T.; Wu, F.; Zuo, Y., Effect of Fe(III)/Citrate Concentrations and Ratio on the Photoproduction of Hydroxyl Radicals: Application on the Degradation of Diphenhydramine. *Ind. Eng. Chem. Res.* **2012**, *51* (20), 7007-7012.
42. Bektaşoğlu, B.; Celik, S. E.; Özyürek, M.; Güçlü, K.; Apak, R., Novel hydroxyl radical scavenging antioxidant activity assay for water-soluble antioxidants using a modified CUPRAC method. *Biochem. Biophys. Res. Chem.* **2006**, *345* (3), 1194-1200.
43. Zepp, R. G.; Faust, B. C.; Hoigne, J., Hydroxyl radical formation in aqueous reactions (pH 3-8) of iron (II) with hydrogen peroxide: the photo-Fenton reaction. *Environ. Sci. Technol.* **1992**, *26* (2), 313-319.
44. Morris, E. D.; Niki, H., Reactivity of hydroxyl radicals with olefins. *J. of Phys. Chem.* **1971**, *75* (23), 3640-3641.

45. Dorfman, L. M.; Adams, G. E. *Reactivity of the hydroxyl radical in aqueous solutions*; National Standard Reference Data System: 1973.
46. Mousset, E.; Oturan, N.; Oturan, M. A., An unprecedented route of OH radical reactivity evidenced by an electrocatalytical process: Ipso-substitution with perhalogenocarbon compounds. *Appl. Catal. B* **2018**, *226*, 135-146.
47. Oturan, M. A.; Aaron, J.-J., Advanced oxidation processes in water/wastewater treatment: principles and applications. A review. *Crit. Rev. Environ. Sci. Technol.* **2014**, *44* (23), 2577-2641.
48. Borisov, O. V.; Ji, J. A.; John Wang, Y., Oxidative Degradation of Polysorbate Surfactants Studied by Liquid Chromatography–Mass Spectrometry. *J. Pharm. Sci.* **2015**, *104* (3), 1005-1018.
49. Yao, J.; Dokuru, D. K.; Noestheden, M.; Park, S. S.; Kerwin, B. A.; Jona, J.; Ostovic, D.; Reid, D. L., A Quantitative Kinetic Study of Polysorbate Autoxidation: The Role of Unsaturated Fatty Acid Ester Substituents. *Pharm. Res.* **2009**, *26* (10), 2303-2313.
50. Wang, W.; Wang, Y. J.; Wang, D. Q., Dual effects of Tween 80 on protein stability. *Int. J. Pharm.* **2008**, *347* (1), 31-38.
51. Ha, E.; Wang, W.; Wang, Y. J., Peroxide formation in polysorbate 80 and protein stability. *J. Pharm. Sci.* **2002**, *91* (10), 2252-64.
52. Kishore, K.; Moorthy, P.; Rao, K., Reactivity of H₂O₂ with radiation produced free radicals: steady state radiolysis methods for estimating the rate constants. *Int. J. Rad. Appl. C* **1987**, *29* (4), 309-313.
53. Packer, J.; Mahood, J.; Mora-Arellano, V.; Slater, T.; Willson, R.; Wolfenden, B., Free radicals and singlet oxygen scavengers: reaction of a peroxy-radical with β -carotene, diphenyl furan and 1, 4-diazobicyclo (2, 2, 2)-octane. *Biochem. Biophys. Res. Chem* **1981**, *98* (4), 901-906.
54. Asmus, K.-D., Sulfur-centered three-electron bonded radical species. In *Sulfur-centered reactive intermediates in chemistry and biology*, Springer: 1990; pp 155-172.
55. Asmus, K.-D., [15] Sulfur-centered free radicals. In *Methods Enzymol.*, Elsevier: 1990; Vol. 186, pp 168-180.
56. Chatgililoglu, C.; Ferreri, C.; Ballestri, M.; Mulazzani, Q. G.; Landi, L., Cis– trans isomerization of monounsaturated fatty acid residues in phospholipids by thiyl radicals. *J. Am. Chem. Soc.* **2000**, *122* (19), 4593-4601.
57. Chatgililoglu, C.; Ferreri, C.; Guerra, M.; Samadi, A.; Bowry, V. W., The reaction of thiyl radical with methyl linoleate: completing the Picture. *J. Am. Chem. Soc.* **2017**, *139* (13), 4704-4714.
58. Chatgililoglu, C.; Ferreri, C.; Melchiorre, M.; Sansone, A.; Torreggiani, A., Lipid geometrical isomerism: from chemistry to biology and diagnostics. *Chem. Rev.* **2014**, *114* (1), 255-284.

59. Ferreri, C.; Costantino, C.; Chatgililoglu, C.; Landi, L.; Mulazzani, Q. G., The thiyl radical-mediated isomerization of cis-monounsaturated fatty acid residues in phospholipids: a novel path of membrane damage? *Chem. Commun.* **1999**, (5), 407-408.
60. Lykakis, I. N.; Ferreri, C.; Chatgililoglu, C., The sulfhydryl radical (HS./S.-): A contender for the isomerization of double Bonds in membrane lipids. *Angew. Chem. Int. Ed.* **2007**, 46 (11), 1914-1916.
61. Mihaljević, B.; Tartaro, I.; Ferreri, C.; Chatgililoglu, C., Linoleic acid peroxidation vs. isomerization: a biomimetic model of free radical reactivity in the presence of thiols. *Org. Biomol. Chem.* **2011**, 9 (9), 3541-3548.
62. Ferreri, C.; Pierotti, S.; Barbieri, A.; Zamboni, L.; Landi, L.; Rasl, S.; Luisi, P. L.; Barigelletti, F.; Chatgililoglu, C., Comparison of phosphatidylcholine vesicle properties related to geometrical isomerism. *Photochem. Photobiol.* **2006**, 82 (1), 274-280.
63. Qi, Y.; Kesselman, E.; Hart, D. J.; Talmon, Y.; Mateo, A.; Zakin, J. L., Comparison of oleyl and elaidyl isomer surfactant-counterion systems in drag reduction, rheological properties and nanostructure. *J. Colloid Interface Sci.* **2011**, 354 (2), 691-699.
64. Rappolt, M.; Cacho-Nerin, F.; Morello, C.; Yagmur, A., How the chain configuration governs the packing of inverted micelles in the cubic Fd 3 m-phase. *Soft Matter* **2013**, 9 (27), 6291-6300.

5.6. Charts and Figures

Chart 1: Structures of Citric acid and its derivatives

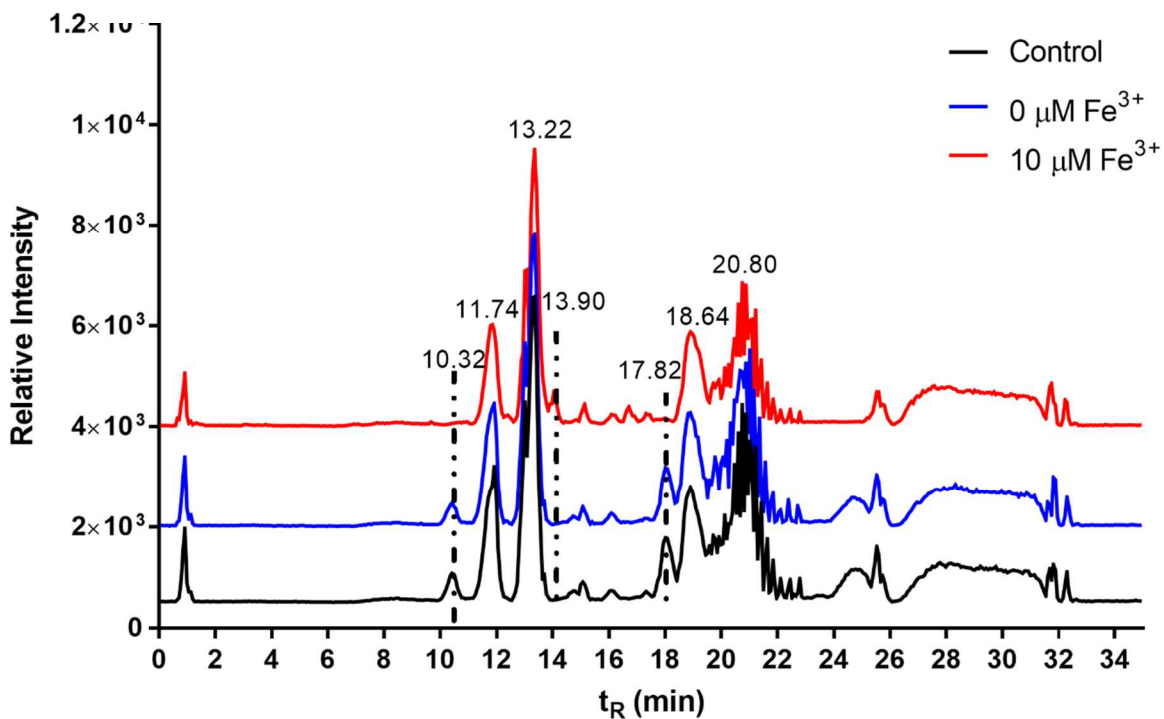
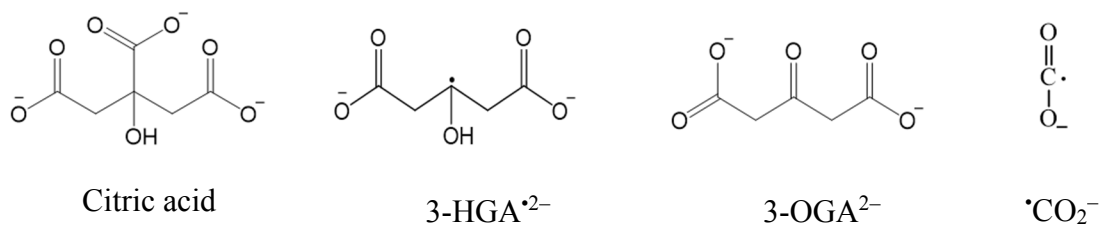


Figure 1: MS chromatograms of 0.02% PS80 in 10 mM citrate buffer, pH 6.0; Control: samples placed in dark (black trace), photo-irradiated at $\lambda_{\text{max}} = 350$ nm for 1 h with 0 $\mu\text{M Fe}^{3+}$ (blue trace) and with 10 $\mu\text{M Fe}^{3+}$ (red trace). For color, refer to the online version.

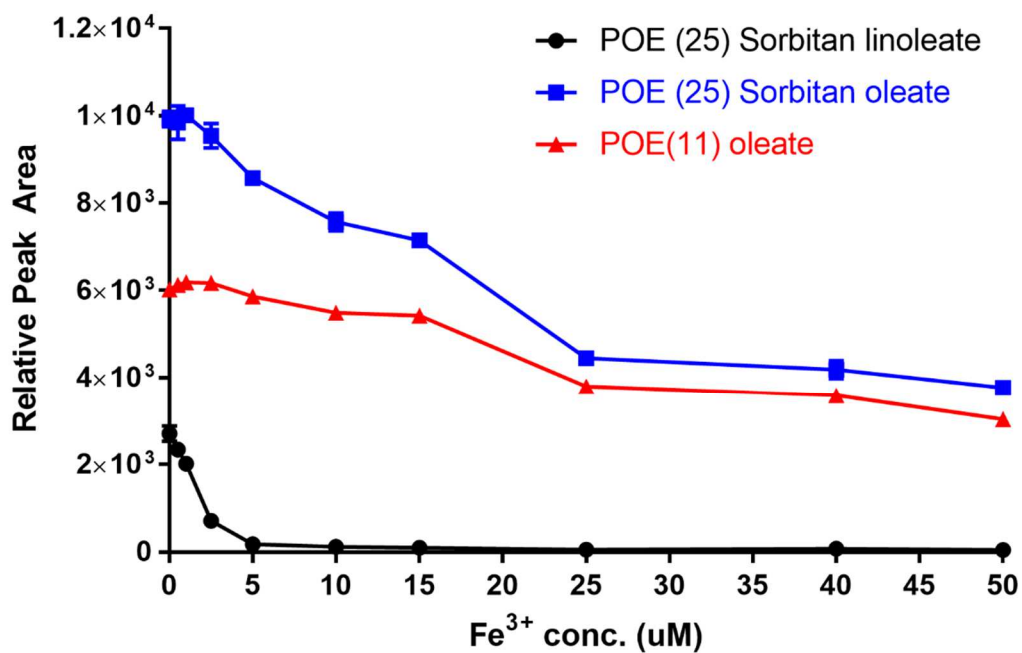


Figure 2: Quantification of loss of PS80 species based on relative peak area using LC-MS representing POE (25) sorbitan monolinoleate ($m/z = 781.57$, $z = 2$) (black trace), POE (25) sorbitan oleate ($m/z = 782.57$, $z = 2$) (blue trace), and POE (11) monooleate ($m/z = 784.59$, $z = 1$). For color, refer to the online version.

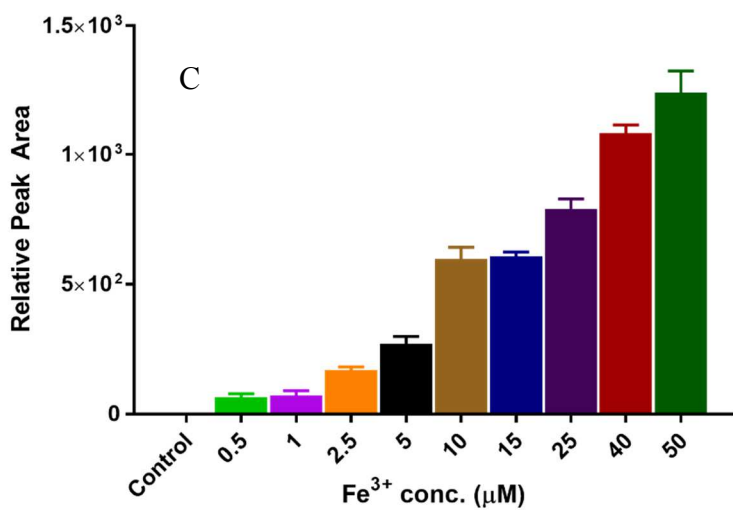
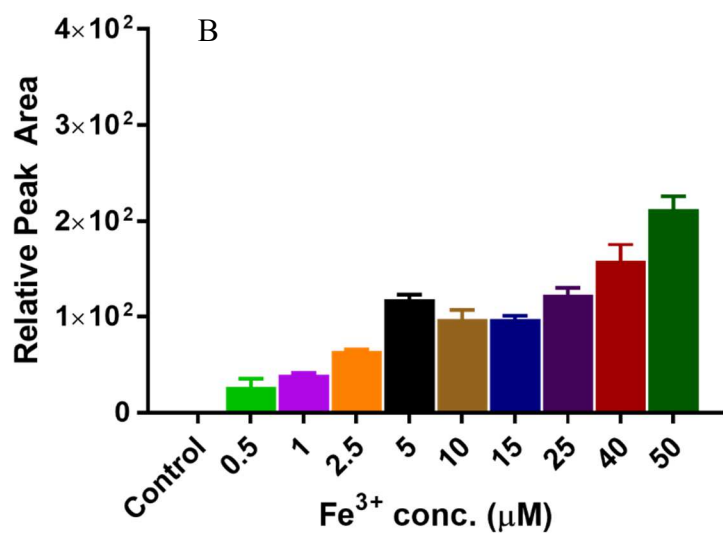
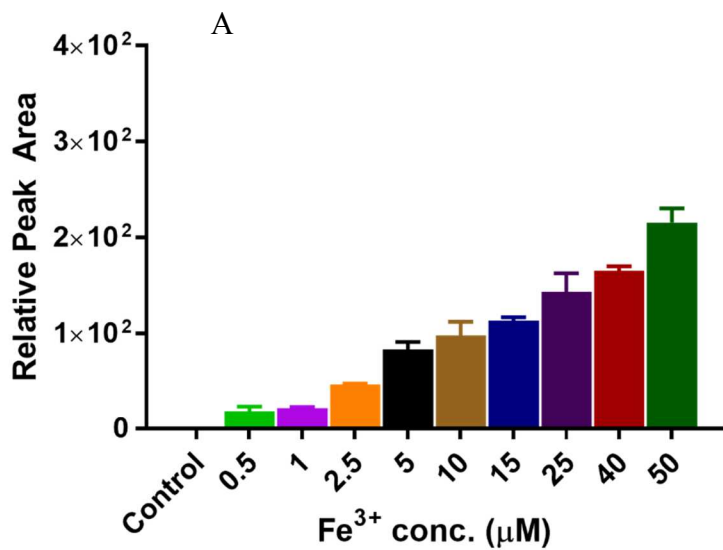


Figure 3: Quantification of PS80 degradation products based on relative peak area using LC-MS obtained after photo-irradiation of 0.02% PS80 with increasing concentration of Fe^{3+} (0-50 μM) in 10 mM citrate buffer, pH 6.0, representing (A) POE (11) hydroxy-oleate, (B) POE (25) sorbitan hydroxy-oleate, and (C) POE (25) sorbitan hydroxy-linoleate.

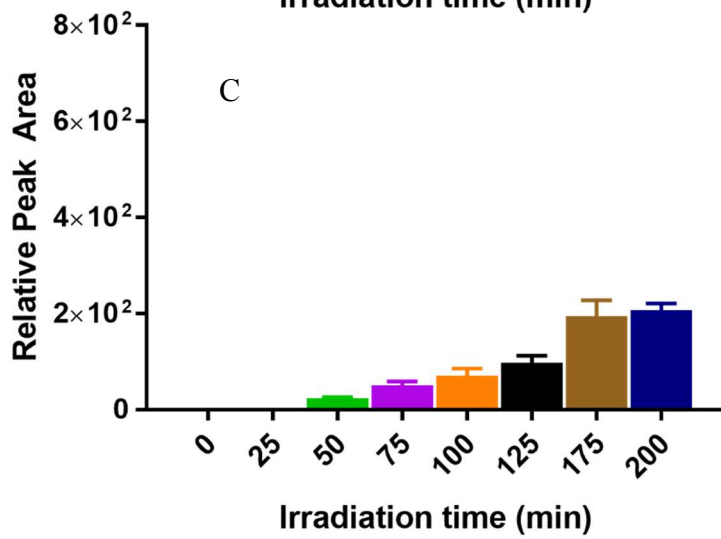
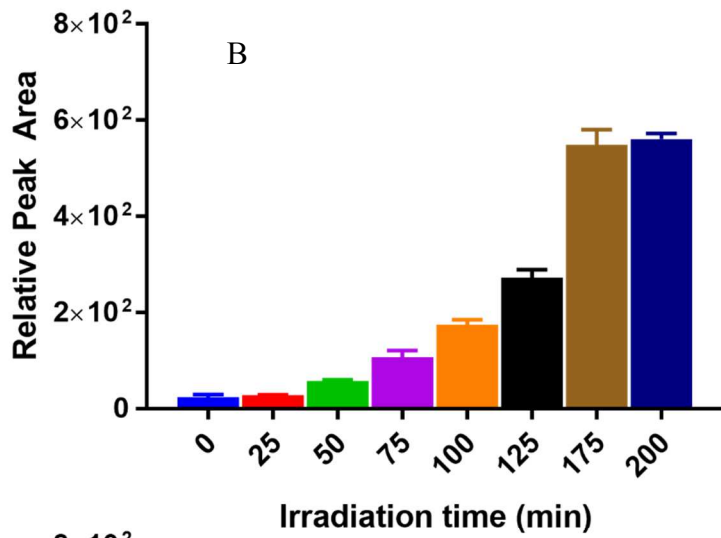
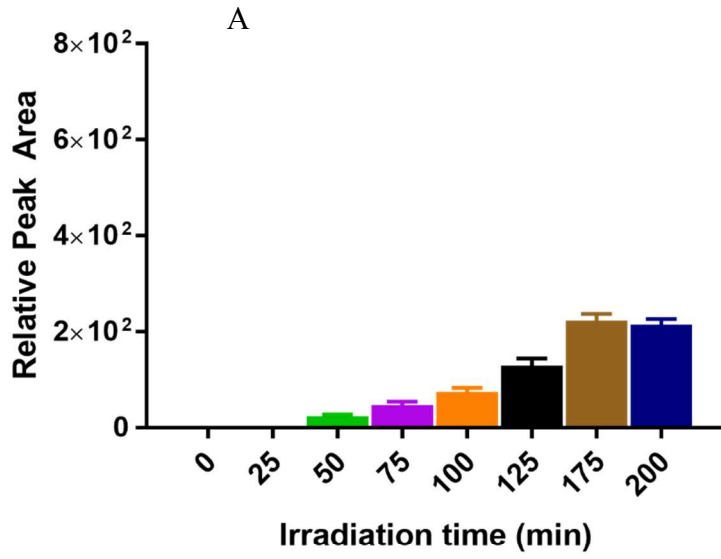


Figure 4: Quantification of PS80 hydroxylation products based on relative peak area using LC-MS obtained after photo-irradiation (up to 200 min) of 0.02% PS80 with 1 μM Fe^{3+} in 10 mM citrate buffer, pH 6.0, representing (A) POE (11) hydroxy-oleate, (B) POE (25) sorbitan hydroxy-oleate, and (C) POE (25) sorbitan hydroxy-linoleate.

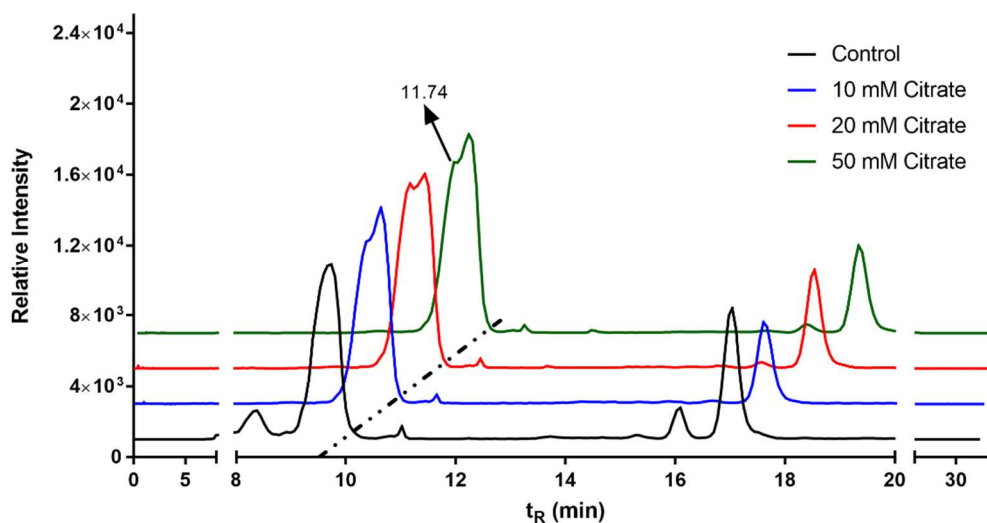
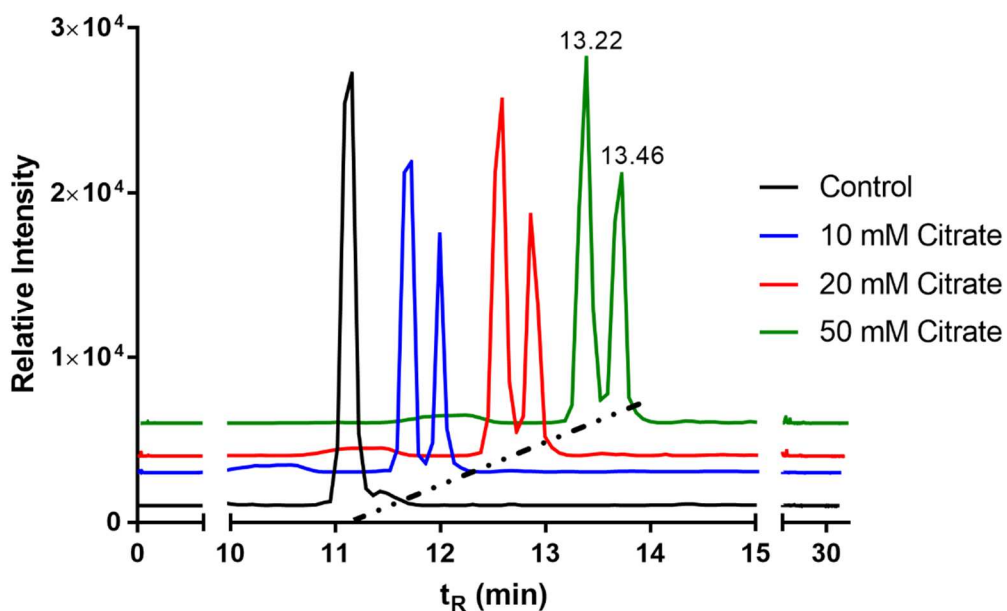


Figure 5: (A) XIC chromatograms of POE(11) oleate and (B) XIC chromatograms of POE(25) sorbitan oleate placed in dark-Control (black trace) and after photo-irradiation of 0.02% PS80 with $10 \mu\text{M Fe}^{3+}$ and 5mM GSSG in 10 mM citrate buffer (blue trace), 20 mM citrate buffer (red trace), and 50 mM citrate buffer (green trace) at pH 6.0.

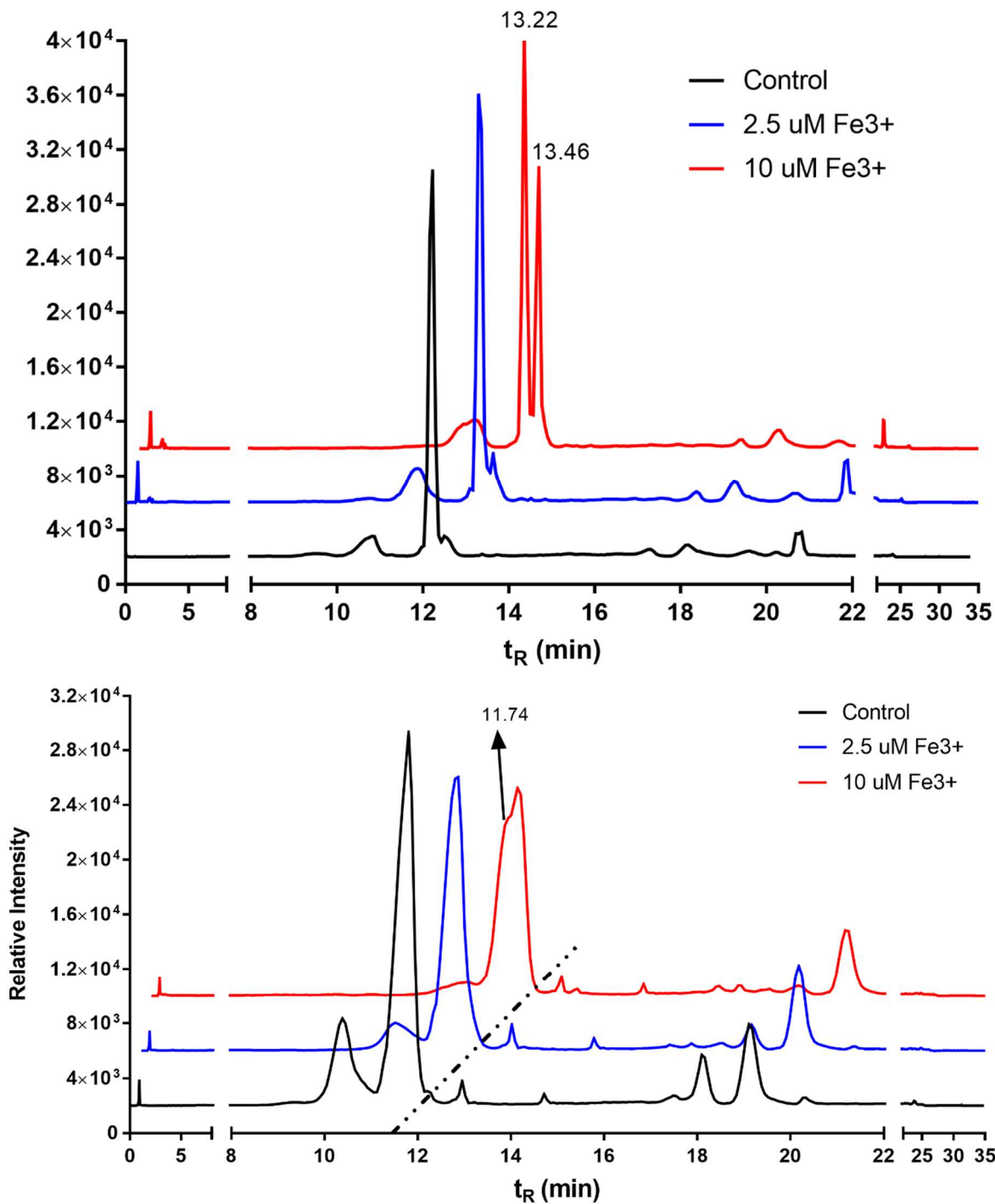


Figure 6: (A) XIC chromatograms of POE(11) oleate and (B) XIC chromatograms of POE(25) sorbitan oleate placed in dark-Control (black trace) and after photo-irradiation of 0.02% PS80 with 5mM GSSG in 10 mM citrate buffer and 1 μM Fe^{3+} (blue trace), 10 μM Fe^{3+} (red trace), or 50 μM Fe^{3+} (green trace) at pH 6.0.

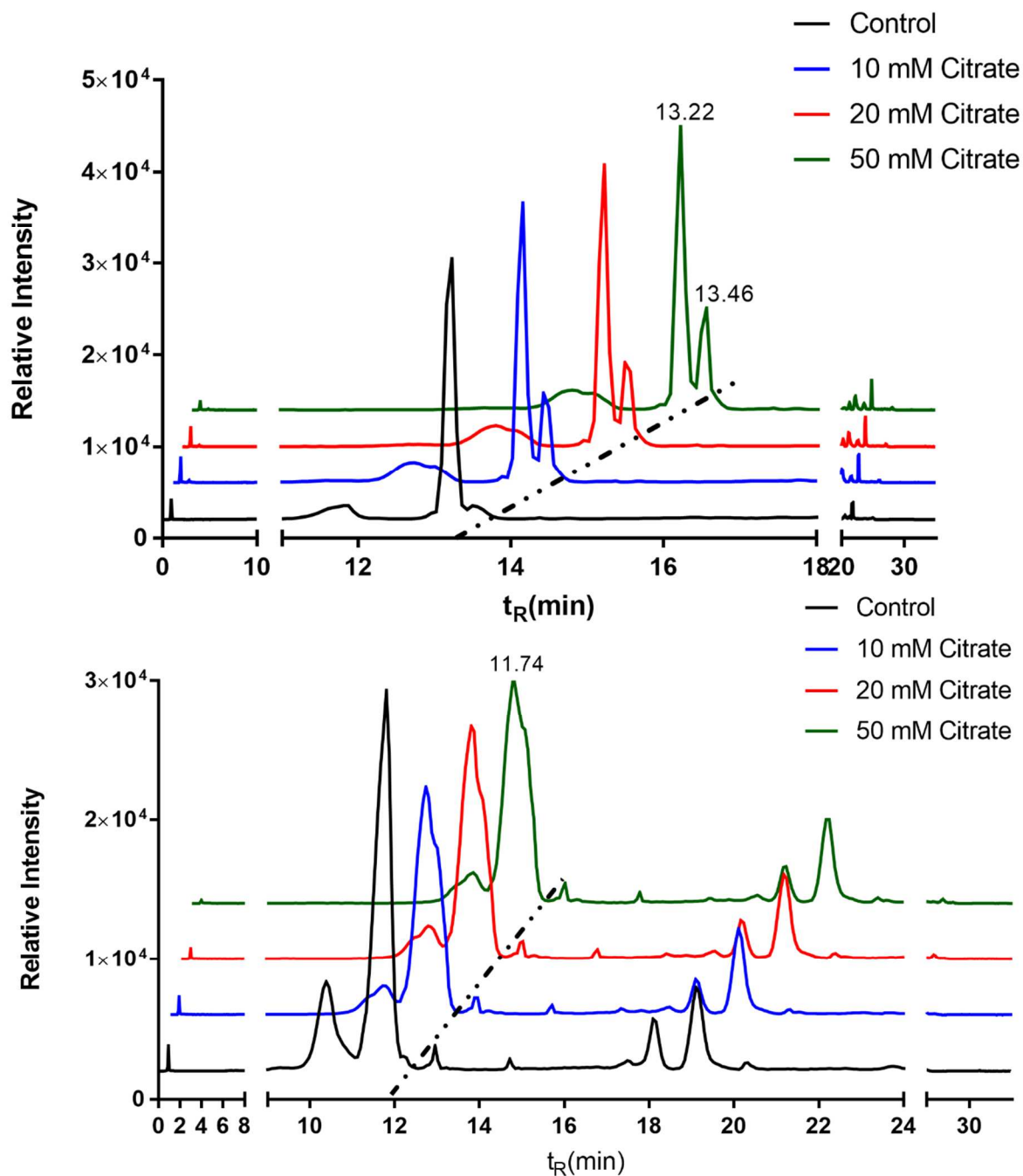


Figure 7: (A) XIC chromatograms of POE(11) oleate and (B) XIC chromatograms of POE(25) sorbitan oleate placed in dark-Control (black trace) and after photo-irradiation of 0.02% PS80 with $10 \mu\text{M Fe}^{3+}$ and 5mM GSSG in 10 mM citrate buffer (blue trace), 20 mM citrate buffer (red trace), and 50 mM citrate buffer (green trace) at pH 6.0 under Ar.

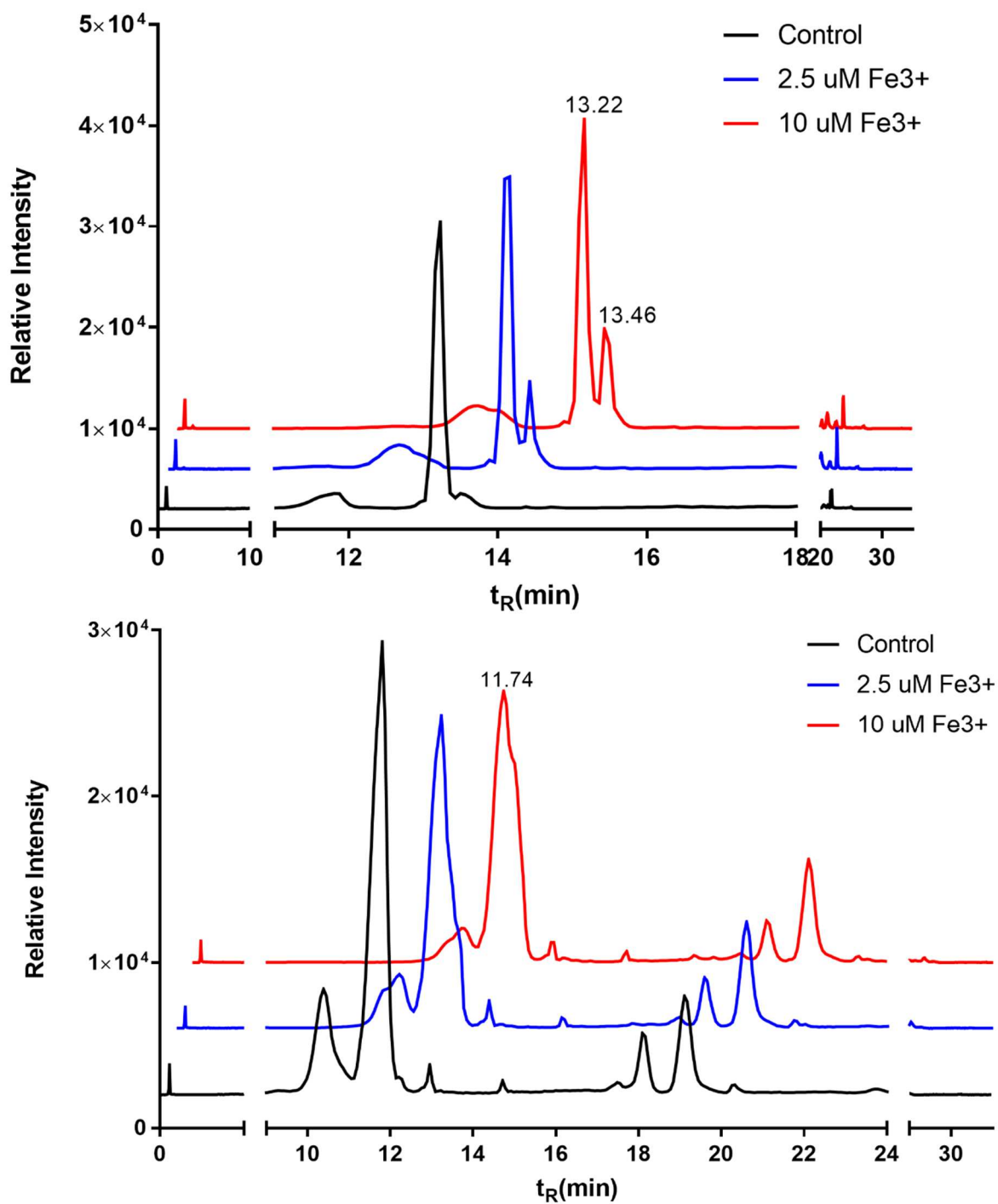


Figure 8: XIC chromatograms of POE(11) oleate and placed in dark-Control (black trace) and after photo-irradiation of 0.02% PS80 with 5mM GSSG in 10 mM citrate buffer and 1 μM Fe^{3+} (blue trace), 10 μM Fe^{3+} (red trace), or 50 μM Fe^{3+} (green trace) at pH 6.0 under Ar.

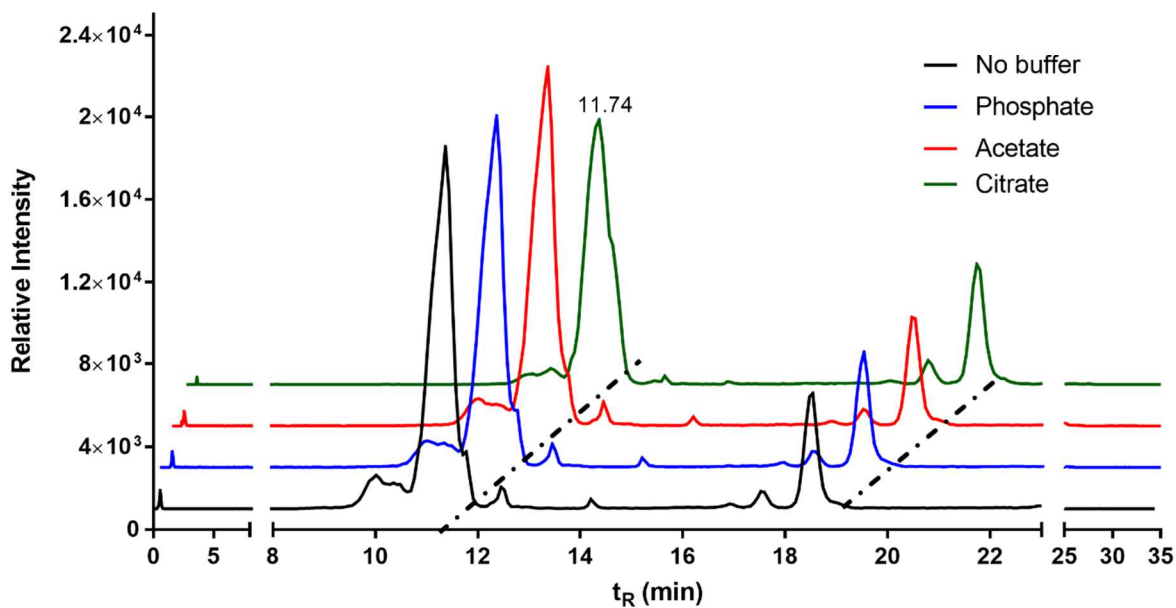
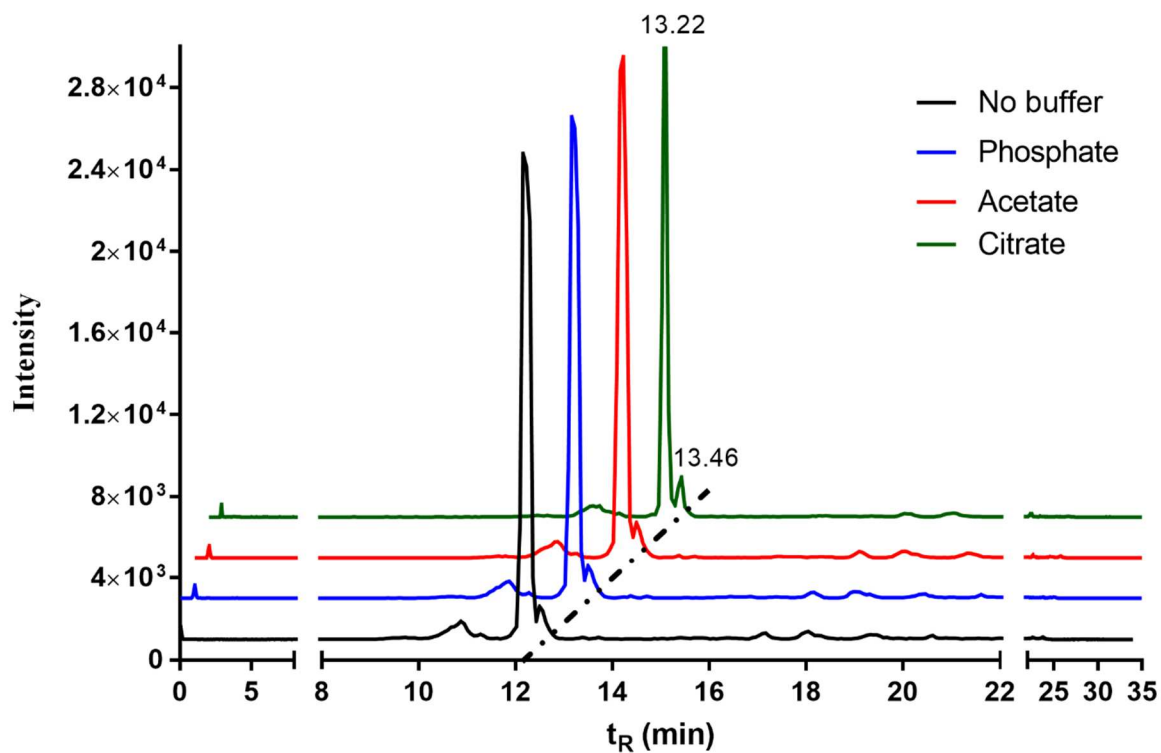
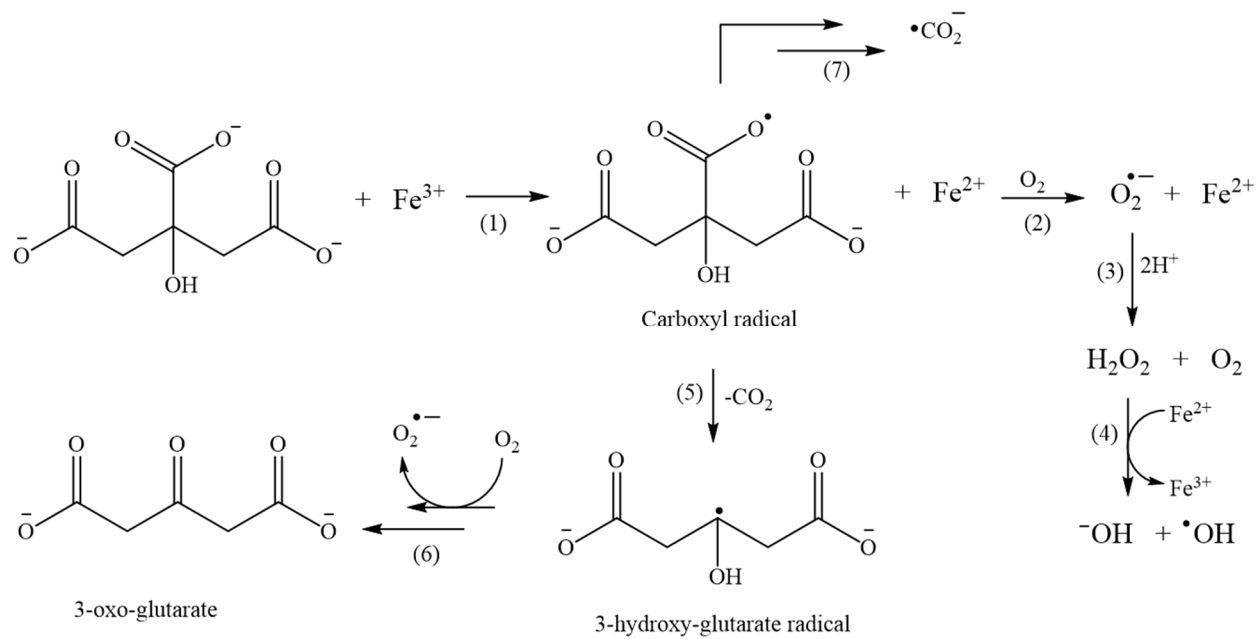
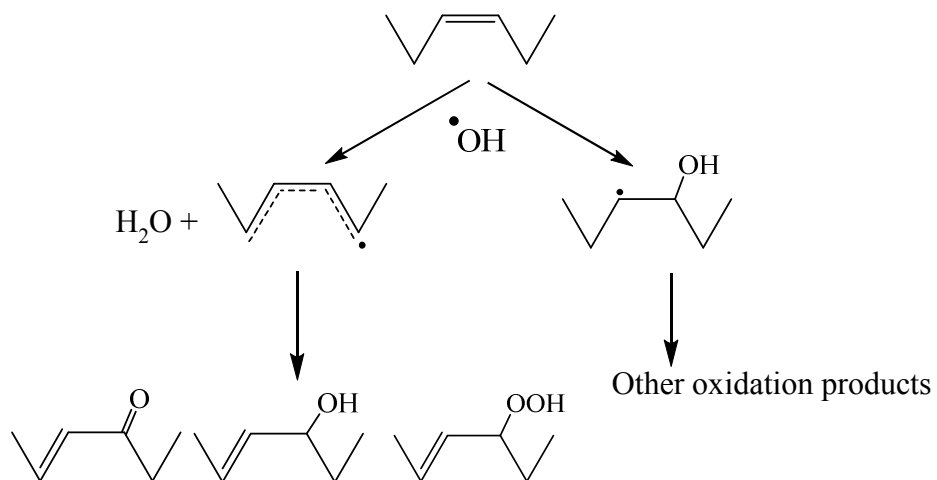


Figure 9: (A) XIC chromatograms of POE(11) oleate after photo-irradiation of 0.02% PS80 with 1 μM Fe^3 in GSSG alone (black trace), with GSSG in 10 mM acetate buffer (blue trace), with GSSG in 10 mM phosphate buffer (red trace), and with GSSG in 10 mM citrate buffer (green trace) at pH 6.0.

5.7. Schemes



Scheme 1: Generation of carboxyl radical (R-COO \bullet), hydroxyl radical ($\bullet\text{OH}$), 3-hydroxy-glutarate radical (3-HGA $^{2\bullet}$), 3-oxo-glutarate (3-OGA $^{2-}$), and carbon dioxide radical anion ($\bullet\text{CO}_2^-$) via photo-Fenton reaction.



Scheme 2: Degradation of unsaturated fatty acid of PS80 species by hydroxyl radical

Chapter 6: Conclusions and Future Directions

6.1. Summary and conclusions

The ingredients in drug products are prone to oxidation upon light exposure. Interactions between active pharmaceutical ingredients and excipients play a major role in the stability and efficacy of the drug products and determine their shelf-lives. It is important to monitor any chemical and physical instabilities that may occur during manufacturing, storage, and delivery of these drug products. Therefore, the aim of this dissertation is to understand the effect of photo-induced radicals and radical ions on physical and chemical instabilities of ingredients in the peptide and protein formulations.

Chapter 2 investigates a role of $\text{Met}^{\bullet+}$ on the peptides containing Met-Xn-His sequences, which are present in protein biotherapeutics such as mAbs and hPTH. A series of novel photoproducts including a covalent cross-link between Met oxidation product(s) and a neighboring histidine residue was observed, which is possibly related to a carbon-centered radical generated via deprotonation of $\text{Met}^{\bullet+}$. A Gly or Gly-Gly bridging Met and His also resulted in the cross-link product, revealing the possibility of these cross-links formation even when Met and His are not linked by an amide bond. These products were identified by HPLC-MS/MS, by reduction with NaBH_4 , derivatization with GRT, and/or alkylation with NEM. The formation of such a cross-link may lead to nonreducible aggregates and loss in biological efficacy as it changes the Met residues irreversibly.

Chapter 3 compares the photostability of mAbZ in NaAc and His/Lys buffer when exposed to visible light. mAbZ formulated in His/Lys buffer is superior to NaAc buffer as less aggregation and color change were observed in His/Lys buffer. A chromophoric photoproduct responsible for the color change in mAbZ was characterized by using a model Trp-containing compound, NATA. The chromophoric product was identified as NATA-33 (loss of 33 Da) by HPLC-MS/MS and the

tentative structure of the product was proposed based on ^1H -, ^{13}C -, and HSQC NMR spectra. The proposed structures have three conjugated rings, which are formed with breakage of an amide bond; such products, if formed in CDR region of a mAb, can affect its binding ability and can result in a loss of efficacy. Thus, the photo-sensitive proteins should be protected from long exposure to visible light in addition to UV light.

Chapter 4 identified light-induced cis/trans isomerization of unsaturated fatty acids of PS80 (oleic and linoleic acid) in the presence of mAbZ under UV-B light. The mechanistic study was carried out with NATA and disulfide bonds (GSSG), which indicated the role of thiyl radical in cis/trans isomerization. The trans fatty acids, as revealed by negative mode in MS, were confirmed by spiking of commercially available free fatty acid standards. The presence of trans fatty acid may impact the physicochemical properties of PS80 micelles. Furthermore, together with linoleic acid, we detected conjugated linoleic acids in PS80, which also underwent light-induced cis/trans isomerization. The conjugated fatty acids are susceptible to radical formation, which can propagate other reactions within the formulation.

Chapter 5 revealed key roles of UV-A light exposed solutions containing citrate and Fe^{3+} in the oxidation and cis/trans isomerization of unsaturated fatty acids of PS80. After generation of light-induced ROS, oxidation products such as hydroxylation products in PS80 were quantified, which increased with increasing iron concentration and longer duration of light exposure. On the other hand, citrate-derived one-electron reductants transfer electrons to disulfide bonds (GSSG), leading to the formation of thiols and thiyl radicals, which can induce cis/trans isomerization of unsaturated fatty acids of PS80, suggested by the formation of isobaric products in oleic acids containing species. The presence of trans-fatty acids in modified PS80 may change the structure of PS80 micelles. Moreover, the radicals and radical ions generated in the photo-irradiated solutions

containing citrate and Fe^{3+} can also directly react with proteins. Subsequently, these radicals and radical ions can generate secondary protein-bound radicals, which can drive unwanted reactions and generate oxidation products that can affect their stability and efficacy.

6.2. Future works

The formation of photo-induced cross-links in Met- X_n -His sequence ($n = 0-2$) of model peptides is of importance in protein biotherapeutics containing the Met- X_n -His sequence such as mAbs and hPTH. Further investigations can be carried out to identify such cross-link between Met oxidation product and His in protein biotherapeutics. Changes in the side chain of amino acids can affect their function, especially in case of mAb, Met and His play role in receptor binding. Likewise, identification of chromophoric species leading to color change in mAbs can give insights into degradation of Trp residue, which is one of the important amino acids in CDR region responsible for antigen binding.

Our studies on PS80 degradation suggested that both proteins and other excipients such as citrate buffer (with iron) can lead to oxidation and cis/trans isomerization of PS80. Conversion of cis-unsaturated fatty acids into trans-unsaturated fatty acids may change the micellar structures of PS80, so the effect of trans-unsaturated fatty acid on micellar structure and stability of proteins in liquid formulation can be carried out.